PROPERTIES OF MORPHOLOGICAL FILTERS AND THEIR APPLICATIONS IN ULTRASONIC IMAGING

BY

MOTAZ ABDEL-LATIF MOHAMED

Submitted in partial fulfillment of the
requirements for the degree of
Doctor of Philosophy in Electrical and Computer Engineering
in the Graduate School of the
Illinois Institute of Technology

Approved _____
Advisor

Chicago, Illinois
December, 1992

ACKNOWLEDGEMENT

The author wishes to express his sincere gratitude and appreciation to his major professor, Dr. J. Saniie, for his guidance and assistance through all phases of this research. The author also would like to thank Dr. B. Heller, Dr. P. Clarkson, and Dr. G. Atkin for serving on his thesis committee. The author is also appreciative of the financial assistance provided by a fellowship from the Egyptian Government, Electric Power Research Institute, and the Office of Naval Research.

Finally, the author would like to thank his parents and wife for their continual encouragement and unwaivering support for everything.

M.A.M.

TABLE OF CONTENTS

Page

ACKNOWLEDGMENT iii

LIST OF TABLES vi

LIST OF FIGURES vii

ABSTRACT xiv

CHAPTER

I. INTRODUCTION 1

II. THEORETICAL BACKGROUND AND LITERATURE SURVEY 4

2.1 Introduction 4
2.2 Set Morphological Operations 5
2.2.1 Dilation and Erosion 5
2.2.2 Opening and Closing 6
2.2.3 Properties of Set Morphological Operators 13
2.3 Multilevel Morphology 13
2.3.1 Multilevel Dilation and Erosion 14
2.3.2 Multilevel Opening and Closing 15
2.4 Clos-Opening and Open-Closing Filters 18

III. STATISTICAL PROPERTIES OF MORPHOLOGICAL FILTERS 20

3.1 Calculation of Dilation Density Function 20
3.2 Calculation of Erosion Density Function 26
3.3 Calculation of Closing Density Function 32

IV. MONTE CARLO SIMULATION OF MORPHOLOGICAL FILTERS 51

4.1 Simulation Results 51
4.1.1 Results using Flat Structuring Element 52
4.1.2 Results using Triangular Structuring Element 57
4.2 Conclusion 98

CHAPTER Page

V. DETERMINISTIC PROPERTIES OF MORPHOLOGICAL FILTERS 99

5.1 Noise Suppression using Morphological Filters 99
5.2 Filter Classification 107

VI. MORPHOLOGICAL FILTERS FOR ULTRASONIC FLAW DETECTION 118

6.1 Introduction 118
6.2 Experimental Results for Noise Suppression and Flaw Detection 118
6.3 Comparison of Morphological and Median Filters 128
6.4 Comparison of Morphogical and Rank Order Filters 132
6.5 Morphological Processing of Ultrasonic Images 136

VII. MORPHOLOGICAL FILTERS AND DECONVOLUTION 145

7.1 Introduction 145
7.2 Deconvolution 145
7.3 Simulation Results 147
7.4 Experimental Results 149
7.5 Conclusion 155

VIII. CONCLUSION 158

REFERENCES 161

LIST OF TABLES

Table		Page
3.1	The Relationship between Input and Processed Sets	38
7.1	Comparison of SNR for Simulation Signals using Different Types of Processing	152
7.2	Comparison of SNR for Experimental Signals using Different Types of Processing	156

LIST OF FIGURES

Figure		Page
2.1	Examples of Dilation	7
2.2	Examples of Erosion	9
2.3	Examples of Opening	11
2.4	Examples of Closing	12
2.5	Examples of Multilevel Dilation	16
2.6	Examples of Multilevel Erosion	17
3.1	Dilation Density Function when the Input Signal has a Uniform Density Function and the Structuring Element is Flat with a Height A: (a) A=0.0 and (b) A=0.6	23
3.2	Triangular Structuring Element with a Width M=5 and a Height A	25
3.3	Dilation Density Function when the Input Signal has a Uniform Density Function and the Structuring Element is Triangular with a Width M: (a) M=3 and (b) M=5	27
3.4	Erosion Density Function when the Input Signal has a Uniform Density Function and the Structuring Element is Flat with a Height A: (a) A=0.0 and (b) A=0.6	30
3.5	Erosion Density Function when the Input Signal has a Uniform Density Function and the Structuring Element is Triangular with a Width M: (a) M=3 and (b) M=5	33
3.6	Input and Processed Sets using a Closing Operation with a Flat Structuring Element	37
3.7	Set Structure of Negative Constant Sets	37
3.8	Closing Density Function when the Input Signal has a Uniform Density Function and the Structuring Element is Flat	40

Figure Page

3.9 Closing Density Function when the Input Signal has a Rayleigh Density Function and the Structuring Element is Flat 42

3.10 Closing Density Function when the Input Signal has a Gaussian Density Function and the Structuring Element is Flat 43

3.11 Mean, Variance and Skewness of the Closing Density Function when the Input Signal has a Uniform Density Function using a Flat Structuring Element 45

3.12 Mean, Variance and Skewness of Closing Density Function when the Input Signal has a Rayleigh Density Function using a Flat Structuring Element 47

3.13 Mean, Variance and Skewness of the Closing Density Function when the Input Signal has a Gaussian Density Function using a Flat Structuring Element 49

4.1 Output Density Function for a Flat Structuring Element when the Input Signal has Uniform Density Function for:
(a) Dilation Operation (b) Closing Operation
(c) Clos-Erosion Operation (d) Clos-Opening Operation..... 53

4.2 Mean, Normalized Variance and Skewness of Dilation, Closing, Clos-Erosion and Clos-Opening when the Input Signal has a Uniform Density Function using a Flat Structuring Element..... 55

4.3 Output Density Function for a Flat Structuring Element when the Input Signal has a Gaussian Density Function for:
(a) Dilation Operation (b) Closing Operation
(c) Clos-Erosion Operation (d) Clos-Opening Operation..... 58

4.4 Output Density Function for a Flat Structuring Element when the Input Signal has a Rayleigh Density Function for:
(a) Dilation Operation (b) Closing Operation
(c) Clos-Erosion Operation (d) Clos-Opening Operation..... 60

4.5 Mean, Normalized Variance and Skewness of Dilation, Closing, Clos-Erosion and Clos-Opening when the Input Signal has a Gaussian Density Function using a Flat Structuring Element..... 62

Figure Page

4.6 Mean, Normalized Variance and Skewness of Dilation, Closing, Clos-Erosion and Clos-Opening when the Input Signal has a Rayleigh Density Function using a Flat Structuring Element 64

4.7 Output Density Function when the Input Signal has a Uniform Density Function for a Triangular Structuring Element with a Height A=20% of the Dynamic Range of The Input Signal for:
(a) Dilation Operation (b) Closing Operation
(c) Clos-Erosion Operation (d) Clos-Opening Operation.... 67

4.8 Mean of Dilation, Closing, Clos-Erosion and Clos-Opening when the Input Signal has a Uniform Density Function using a Triangular Structuring Element with a Height A:
(a) A=0.2 (b) A=0.4
(c) A=0.6 (d) A=0.8..... 69

4.9 Normalized Variance of Dilation, Closing, Clos-Erosion and Clos-Opening when the Input Signal has a Uniform Density Function using a Triangular Structuring Element with a Height A:
(a) A=0.2 (b) A=0.4
(c) A=0.6 (d) A=0.8..... 71

4.10 Skewness of Dilation, Closing, Clos-Erosion and Clos-Opening when the Input Signal has a Uniform Density Function using a Triangular Structuring Element with a Height A :
(a) A=0.2 (b) A=0.4
(c) A=0.6 (d) A=0.8..... 73

4.11 (a) Input Signal with a Uniform Density Function
(b) The Dilated Signal using Triangular Structuring Element
(c) The Closed Signal using Triangular Structuring Element 76

4.12 A Comparison Between Dilation, Closing, Clos-Erosion, and Clos-Opening for:
(a) Flat Structuring Element with a Width M=7
(b) Triangular Structuring Element with a Width M=7 and a Height A=0.2..... 78

4.13 A Comparison between the Variance of a Closing Density Function for Signals with a Uniform Density Function using Flat and Triangular Structuring Elements 79

Figure Page

4.14 Output Density Function when the Input Signal has a Gaussian Density Function using a Triangular Structuring Element with a Height A=20% of the Dynamic Range of the Input Signal for:
(a) Dilation Operation (b) Closing Operation
(c) Clos-Erosion Operation (d) Clos-Opening Operation..... 81

4.15 Output Density Function when the Input Signal has a Rayleigh Density Function using a Triangular Structuring Element with a Height A=20% of the Dynamic Range of the Input Signal for:
(a) Dilation Operation (b) Closing Operation
(c) Clos-Erosion Operation (d) Clos-Opening Operation..... 83

4.16 Mean of Dilation, Closing, Clos-Erosion and Clos-Opening when the Input Signal has a Gaussian Density Function using a Triangular Structuring Element with a Height A :
(a) A=0.2 (b) A=0.4
(c) A=0.6 (c) A=0.8..... 85

4.17 Normalized Variance of Dilation, Closing, Clos-Erosion and Clos-Opening when the Input Signal has a Gaussian Density Function using a Triangular Structuring Element with a Height A :
(a) A=0.2 (b) A=0.4
(c) A=0.6 (d) A=0.8..... 87

4.18 Skewness of dilation, closing, clos-erosion and clos-opening when the Input Signal has a Gaussian Density Function using a Triangular Structuring Element with a Height A :
(a) A=0.2 (b) A=0.4
(c) A=0.6 (d) A=0.8..... 89

4.19 Mean of Dilation, Closing, Clos-Erosion and Clos-Opening when the Input Signal has a Rayleigh Density Function using a Triangular Structuring Element with a Height A :
(a) A=0.2 (b) A=0.4
(c) A=0.6 (d) A=0.8..... 91

4.20 Normalized Variance of Dilation, Closing, Clos-Erosion and Clos-Opening when the Input Signal has a Rayleigh Density Function using a Triangular Structuring Element with a Height A :
(a) A=0.2 (b) A=0.4
(c) A=0.6 (d) A=0.8..... 93

Figure Page

4.21 Skewness of Dilation, Closing, Clos-Erosion and Clos-Opening when the Input Signal has a Rayleigh Density Function using a Triangular Structuring Element with Height A :
(a) A=0.2 (b) A=0.4
(c) A=0.6 (d) A=0.8 95

4.22 A Comparison between Clos-Opening Density Functions when the Input Signal has a Gaussian Density Function using Flat and Triangular Structuring Elements with Different Heights
(a) A=0.2 (b) A=0.4
(c) A=0.6 (d) A=0.8 97

5.1 Impulsive Noise Suppression using Morphological Open-Closing
(a) Simulated Ultrasonic Echo
(b) Echo Contaminated by Random Impulsive Noise
(c) Recovered Signal using Open-Closing Operation
(d) Error Signal 101

5.2 Block Diagram of Morphological Operations for Noise Suppression 103

5.3 Noise Suppression and Echo Detection using a Morphological Filter 104

5.4 A Sinusoidal Structuring Element with a Width M=7 and a Height A=1 105

5.5 (a) A Comparison between the Input Echo Signal and Recovered Echo
(b) The Error Signal 106

5.6 The Output Echo using a Flat Structuring Element 108

5.7 The Output Echo using a Sinusoidal Structuring Element 109

5.8 The Effect of Height when using a Sinusoidal Structuring Element 111

5.9 Block Diagram of a Highpass Morphological Filter 112

5.10 Block Diagram of a Bandpass Morphological Filter 113

5.11 Examples of Lowpass Characteristics of Morphological Filters 114

Figure		Page
5.12	Examples of Highpass Characteristics of Morphological Filters	115
5.13	Examples of Bandpass Characteristics of Morphological Filters	116
6.1	(a) An Ultrasonic Backscattered Flaw Signal (b) Amplitude Spectrum of the Signal	120
6.2	Flaw Echo Detection and Clutter Suppression using Morphological Filters with Flat Structuring Elements. The Flat Structuring Elements have Different Widths (M). Figure (a) is the Original Measured Signal	121
6.3	Flaw-to-Clutter Ratio of the Output Signal as a Function of the Width of the Flat Structuring Element	123
6.4	Zero Crossing of the Output Signal as a Function of the Width	124
6.5	The Effect of Structuring Elements on the Processed Ultrasonic Signals using (a) Flat Structuring Element with a Width M=5. (b) Sinusoidal Structuring Element	126
6.6	Flaw-to-Clutter Ratio of the Output Signal as a Function of the Width using (a) Flat Structuring Element (b) Sinusoidal Structuring Element with a Height A=2.0	127
6.7	Processed Backscattered Flaw Signal using a Morphological Bandpass Filter	129
6.8	(a) A Typical Measured Ultrasonic Echo with Poor Flaw-to-Clutter Ratio (b) The Processed Echo using Morphological Filter (c) Ensemble Averaging of the Echo using 500 Measurements	130
6.9	Flaw Echo Detection and Clutter Suppression using Recursive Median Filters with Different Widths. Figure (a) is the Original Measured Signal	133
6.10	Split-Spectrum Processor Coupled with Rank Order Filters	135

Figure		Page
6.11	Ranked Outputs of Order Statistic Filters for 0-12.8 MHz Frequency Information	137
6.12	Ranked Outputs of Order Statistic Filters for 0-6.8 MHz Frequency Information	139
6.13	An Experimental B-Scan Image	141
6.14	The Processed B-Scan Image using a Lowpass Morphological Filter	143
6.15	Processed B-Scan Image using The Bandpass Morphological Filter	144
7.1	(a) Simulated Ultrasonic Echo (b) Echo Contaminated by Uniformly Distributed Noise	148
7.2	(a) Processed Echo using a Morphological Filter (b) Processed Echo using a Morphological Filter Followed by Deconvolution	150
7.3	(a) Processed Echo using Deconvolution (b) Processed Echo using Deconvolution Followed by a Morphological Filter	151
7.4	(a) Processed Backscattered Flaw Signal using a Morphological Filter (b) Processed Backscattered Flaw Signal using a Morphological Filter Followed by Deconvolution	153
7.5	(a) Processed Backscattered Flaw Signal using Deconvolution (b) Processed Backscattered Flaw Signal using Deconvolution Followed by a Morphological Filter	154
7.6	(a) Processed Backscattered Flaw Signal using a Morphological Filter (b) Processed Backscattered Flaw Signal using a Morphological Filter Followed by a Bandpass Filter	157

ABSTRACT

Morphological filters are a class of nonlinear operations based on set theory. Recently, these filters have found numerous applications in signal and image processing. In this thesis, the deterministic and stochastic properties of morphological filters have been studied in the context of utilizing different structuring elements. The structuring elements are characterized by their shape, width, and height.

From a deterministic point of view, it has been shown that the filtering process depends on the input signal as well as the parameters of the structuring elements. From a stochastic point of view, a mathematical expression for the dilation and erosion density function of independent and identically distributed (iid) inputs is derived for any shape of structuring element. Also, a general statistical expression for closing density function is derived when inputs are iid for any density function, but limited to flat structuring elements since the main tool of analysis is threshold decomposition. Furthermore, the statistical properties of sequential morphological operations (i.e., dilation, closing, clos-erosion and clos-opening) using different shapes of structuring elements (triangular or flat) applied to signals with different density functions are examined using Monte Carlo simulation. In particular, the output density function of sequential morphological operations has been presented when input signals have uniform, Gaussian and Rayleigh distributions. The simulated results and their statistics (mean, variance and skewness) present an interpretation of the noise suppression capability of morphological filters and their biasing effects.

As an application, morphological filters have been used to detect flaw in ultrasonic signals contaminated by grain scattering echoes (i.e., clutters or speckles) with random amplitudes and phases. These interfering echoes become significant to the point where detection of flaw echoes becomes very difficult. In particular, the performance of morphological filters is evaluated using different

shapes of structuring elements, and the information content of ultrasonic signals has been used to design a suitable structuring element with optimal performance. The processed experimental results show that morphological filters can improve flaw visibility by suppressing grain scattering noise. To further improve flaw-to-clutter ratio (FCR), the bandpass morphological filtering has been presented.

In this study, a recursive median filter has been introduced in a novel application to detect flaw and enhance the features of ultrasonic signals (such as echoes representing targets or bounders in the materials). Morphological and recursive median filters have been compared with the split-spectrum technique combined with rank order statistic filters. The results indicate that morphological filters have better performance in preserving the geometrical structure of the signal because of their flexibility in changing the shape of the structuring elements to preserve certain patterns of the original signal.

The performance of morphological filters combined with deconvolution also has been evaluated. The results presented indicate that by combining morphological operations and deconvolution filtering, microstructure noise is reduced and resolution is improved. Also, morphological filters can replace ensemble averaging which required numerous measurements. It has been shown that coupling bandpass filtering with morphological filtering provides the best performance in regard to FCR and resolution. Finally, the evaluation of morphological filtering for flaw detection has been extended from A-Scans (one dimension) to B-Scans (two dimensions). The results indicate the ability of morphological filters for reducing background noise and improving ultrasonic imaging resolution.

CHAPTER I

INTRODUCTION

Insonification of the microstructure of materials results in a backscattered signal consisting of multiple interfering echoes with random amplitudes and phases. In general, the intensity of the microstructure echoes are sensitive to change in frequency. In addition to the microstructure echoes, an additive impulsive noise is caused by the instruments. The measurement noise often becomes significant to the point where the detection of flaw echoes (target) in ultrasonic signals or images becomes very difficult. An effective solution to the above problems is introduced by utilizing morphological filters. Morphological filters [1, 2], a class of nonlinear operations, are capable of eliminating impulsive noise, moderately reducing microstructure echoes and improving the overall signals or image quality while selectively preserving certain signal or image features. These filters are based on mathematical morphology [2, 3] that incorporates the shape information of a signal. Shape information is extracted by using another signal often referred to as a structuring element, which is simpler in nature than the signal under processing. In mathematical morphology, a signal is operated on by several morphological operations using structuring elements. The basic morphological operations are erosion, dilation, opening and closing.

To sufficiently understand the performance of morphological filters and capitalize on their applications, both statistical and deterministic analyses are needed. This thesis deals with an analysis of morphological filters as well as their applications in ultrasonic imaging, and is organized as follows: Chapter II provides a survey of the fundamental morphological operations and their properties as well as applications in digital signal processing. The statistical properties of morphological operations are examined in Chapter III, using structuring elements with different shapes. In particular, the statistical expression for the dilation and erosion operations for a general shape structuring element is derived utilizing the

relationship between morphological and order statistic filters. Also, the closing density function is derived for a class of morphological filters for which threshold decomposition [3] is applicable. In Chapter IV, the Monte Carlo technique is used to extend the statistical properties of morphological operations to other sequential stages such as clos-erosion and clos-opening. The above operations are applied to signals with different density functions using structuring elements with different shapes. The Monte Carlo technique describes the statistical characteristics of the processed signal overcoming the complexity that often arises in direct analysis due to statistical dependency of the results at different stages of morphological operations.

In order to evaluate the geometric behavior of morphological filters in the time domain, their deterministic properties are also examined using different structuring elements. By varying the structuring element, different types of signal patterns can be extracted from the signal. The structuring element is characterized by its width (length), height and shape. In Chapter V, the effect of these parameters on the output signal is investigated through a sequence of opening and closing operations. Also, different types of filters are constructed using a sequence of morphological operations in parallel and series.

Ultrasonic flaw detection is an important application of morphological filters. The goal in detection is to isolate the flaw echoes from background noise (e.g, speckles or microstructure scattering echoes) and to estimate flaw location. Chapter VI focuses upon the selection of morphological filters to detect flaw (i.e., target) in ultrasonic signals (A-Scan or B-Scan) of complex structures with high scattering noise (clutter) and illustrates the effectiveness of the parameters of the structuring element in improving the detection resolution and flaw to clutter ratio FCR). Also in Chapter VI, the performance of morphological filters for flaw detection has been compared with the performance of recursive median filters and the split-spectrum technique combined with rank order statistic filters.

The performance of morphological filters combined with deconvolution to

improve FCR and detection resolution of flaw echoes has been evaluated in Chapter VII. Finally, a summary of research achievements and conclusions along with suggestions for future research is presented in Chapter VIII.

CHAPTER II

THEORETICAL BACKGROUND AND LITERATURE SURVEY

Morphological filters are a class of nonlinear filters which have recently become popular in signal and image processing. These filters are attractive because they are simple to implement and can suppress impulsive noise while preserving certain features of the signal such as edges and lines. Morphological filters are based on geometrical concepts and have a desirable syntactical performance. This chapter reviews the theoretical background and the basic concepts of morphological filters and discusses their properties.

2.1 Introduction

The word morphology refers to the study of forms and structures [1]. Mathematical morphology has evolved in Europe since the 1960s, motivated mainly by problems in quantitative microscopy. The theoretical foundations of mathematical morphology and a wide range of its applications were introduced systematically by Matheron [2] and Serra [3]. Many applications of morphological filters are found in biomedical image processing, metallography, geology, geography, remote sensing, astronomy, and automated industrial inspection. Recently, mathematical morphology has been applied to image processing/analysis such as edge detection, noise suppression, shape representation, smoothing, recognition, skeletonization, and coding [3 - 17].

Mathematical morphology [17 - 20] provides an approach to signal processing and shape analysis utilizing a set theoretic concepts. In mathematical morphology, a signal is viewed as a set in Euclidean space and is operated on by several set-processing morphological operations. The primitives of morphological operations are erosion and dilation. All other morphological operations are sequences of combining erosions and dilations. These operations use a structuring element to interact with the signal and extract information. A structuring element [17, 21,

22] is another signal of a somewhat simpler nature than the signal under processing. It is similar to the kernel in a convolution operation. The structuring element interacts with the signal under study and transforms it into a new signal which is more expressive in some way than the original. By varying the structuring element, different types of information can be extracted from the signal. Morphological operations are attractive for their relatively simple computational demands. The computation is made up of addition, subtraction and logical comparison. It has been shown that these types of operations can be implemented in VLSI for real-time processing [23].

In general, signals or images can be represented either by sets (binary) or functions (multilevel). This classification of signals induces a similar classification for morphological filters into set processing and function processing filters. A set processing (SP) filter is a transformation of a set by a set (binary signals and binary structuring elements). A function processing (FP) filter is a transformation of a function by a function (multilevel signal and multilevel structuring element). A subclass of FP filters is called function and set processing (FSP) filters which are a transformation of a function by a set [22, 24]. Therefore, we begin our discussion with set morphological operations then extend it to the more general function (multilevel) morphological operations.

2.2 Set Morphological Operations

There are two fundamental morphological operators: erosion and dilation. Other operations such opening and closing are derived operations defined in terms of erosion and dilation [25]. In this section, we briefly review the set morphological operators and summerize their properties.

2.2.1 Dilation and Erosion. Dilation is the morphological transformation which combines two sets using vector addition of set elements. If A and B are sets in N-space (E^N) with elements a and b, respectively, where a = (a_1, ..., a_N) and b = (b_1, ..., b_N) being N-tuples of element coordinates, then the dilation of A by

B is the set of all possible vector sums of pairs of elements, one coming from A and one coming from B.

$$A \oplus B = c \in E^N \mid c = a + b \text{ for } some\ a \in A \text{ and } b \in B \tag{2.1}$$

Erosion is the morphological dual to dilation. It is the morphological transformation which combines two sets using the vector subtraction of set elements. If A and B are sets in Euclidean N space, then the erosion of A by B is the set of all elements x for which x + b ϵ A for every b ϵ B. The erosion of A by B is denoted by $A \ominus B$ and is defined by :

$$A \ominus B = x \in E^N \mid x + b \in A \text{ for } every\ b \in B \tag{2.2}$$

Examples of dilation and erosion operations [7, 26, 27] are shown in Figures 2.1 and 2.2 respectively. These figures show that dilation expands the image whereas erosion shrinks it. The manner in which a dilation (erosion) operation expands (shrinks) set A is dependent upon the shape of the structuring element B. Thus by designing B appropriately, certain shape features can be filled in or eroded away from A [24].

2.2.2 Opening and Closing. Both erosion and dilation operations are generally noninvertible [7]. For example, if A is eroded by B, it is generally not possible to recover A completely by dilating the eroded set by B. Instead, a new set is recovered which is a somewhat simplified and less detailed version of A [22]. This transformation described is known as the opening operation. The opening of image A by structuring element B is denoted by A o B and is defined as:

$$A\ o\ B = (A \ominus B) \oplus B \tag{2.3}$$

The dual operation to opening is known as closing. The closing of image A by structuring element B is denoted by A • B and is defined as:

$$A \bullet B = (A \oplus B) \ominus B \tag{2.4}$$

Examples of opening and closing operations [9, 26, 27] are shown in Figures 2.3 and 2.4 respectively.

$A = \{ (0, 1), (1, 1), (2, 1), (2, 2), (3, 0) \}$

$B = \{ (0, 0), (0, 1) \}$

B

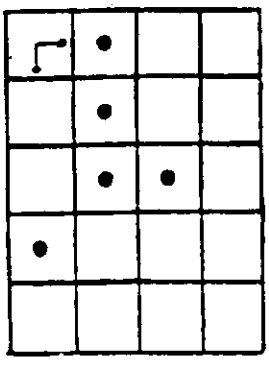

A

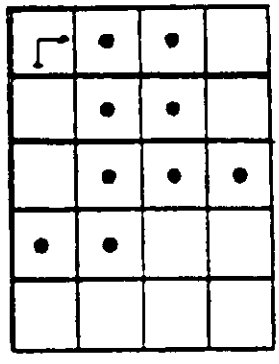

$A \oplus B$

$$A \oplus B = \{ (0, 1), (1, 1), (2, 1), (2, 2), (3, 0), (0, 2), (1, 2), (2, 2), (2, 3), (3, 1)\}$$

(a)

Figure 2.1 Examples of Dilation

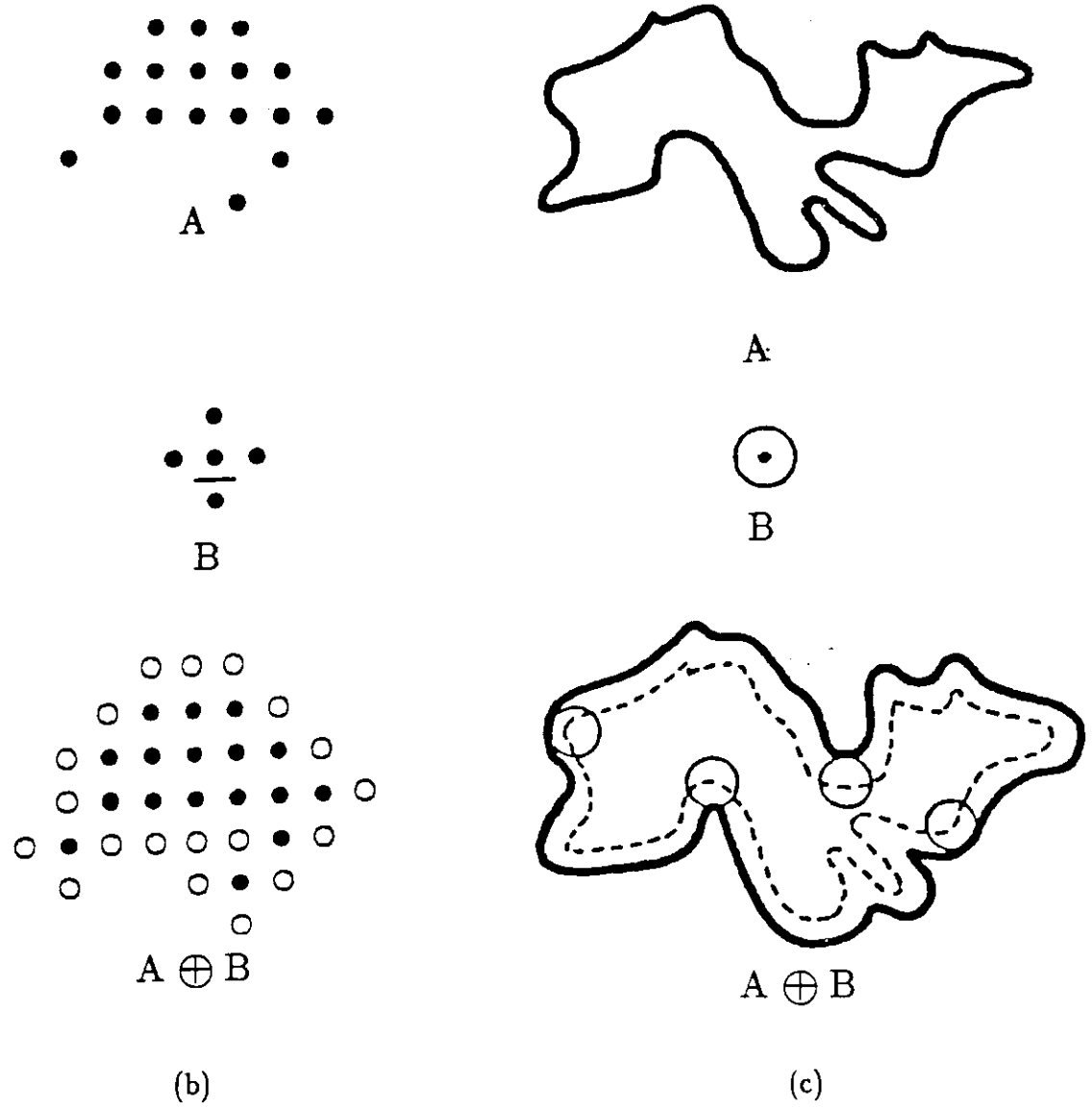

Figure 2.1 (Continued)

$$A = \{ (1, 0), (1, 1), (1, 2), (1, 3), (1, 4), (1, 5), (2, 1), (3, 1), (4, 1), (5, 1) \}$$

$$B = \{ (0, 0), (0, 1) \}$$

B

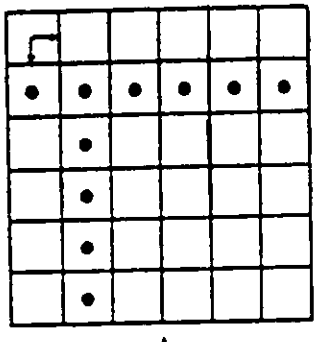

A

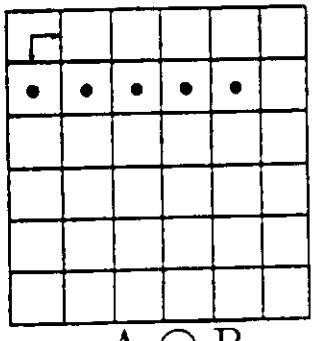

$A \ominus B$

$$A \ominus B = \{ (1, 0), (1, 1), (1, 2), (1, 3), (1, 4) \}$$

(a)

Figure 2.2 Examples of Erosion

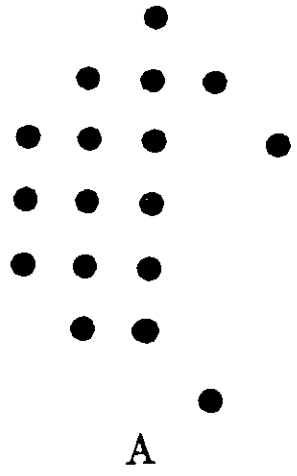

A

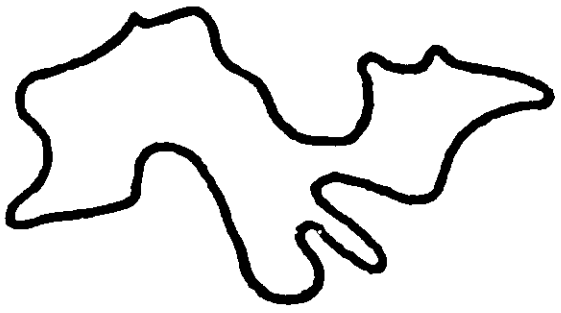

A

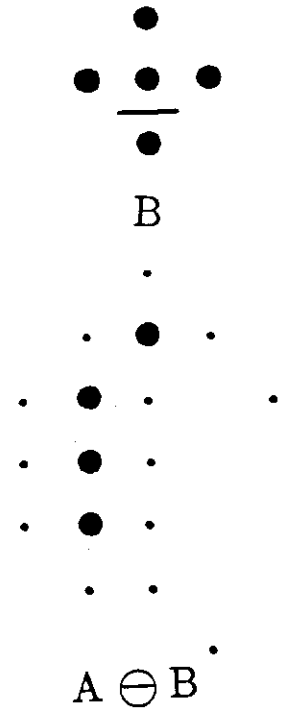

B

$A \ominus B$

B

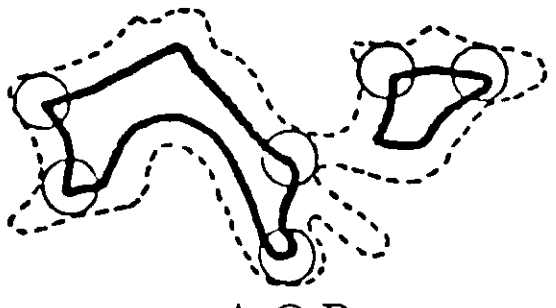

$A \ominus B$

(b)

(c)

Figure 2.2 (Continued)

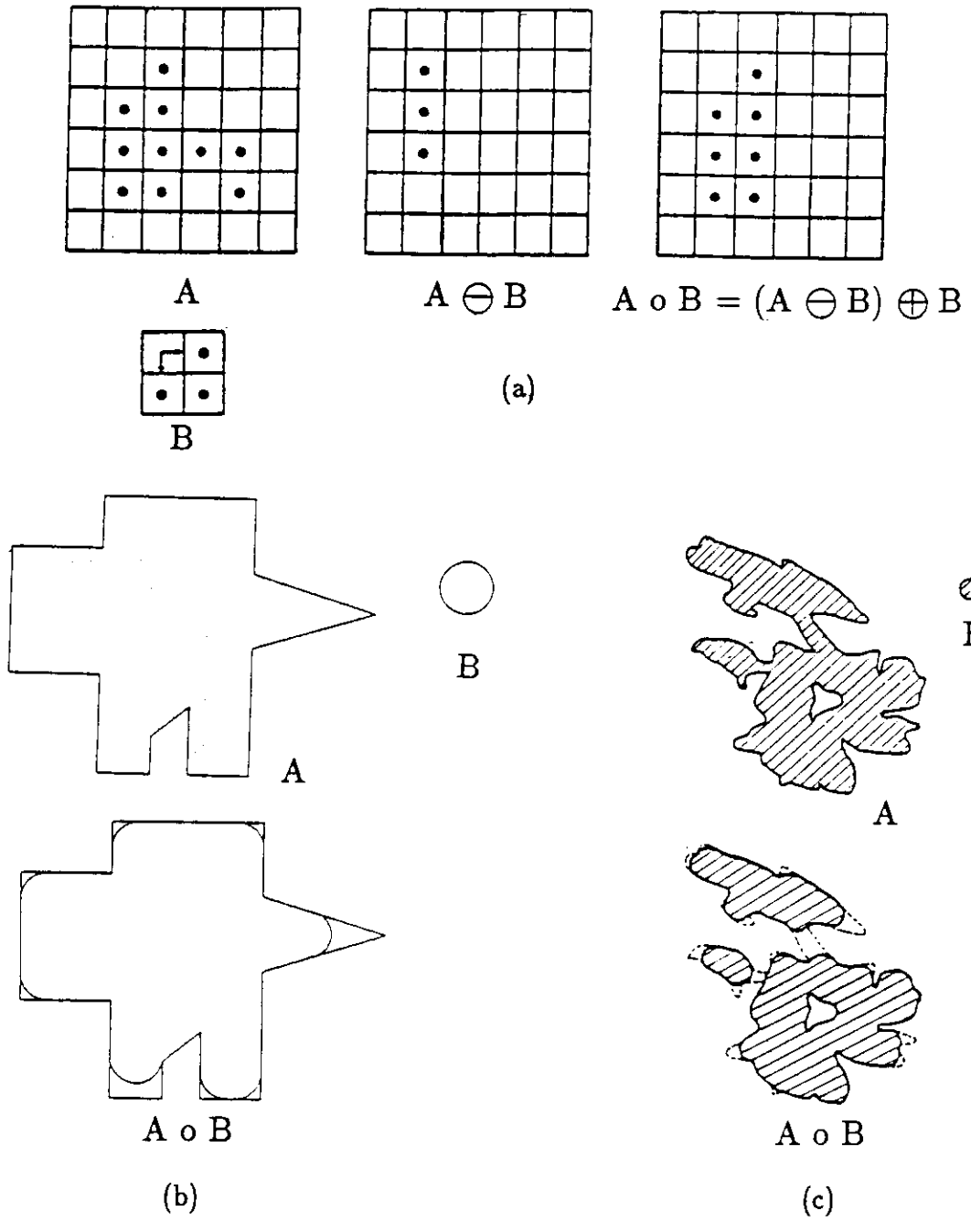

Figure 2.3 Examples of Opening

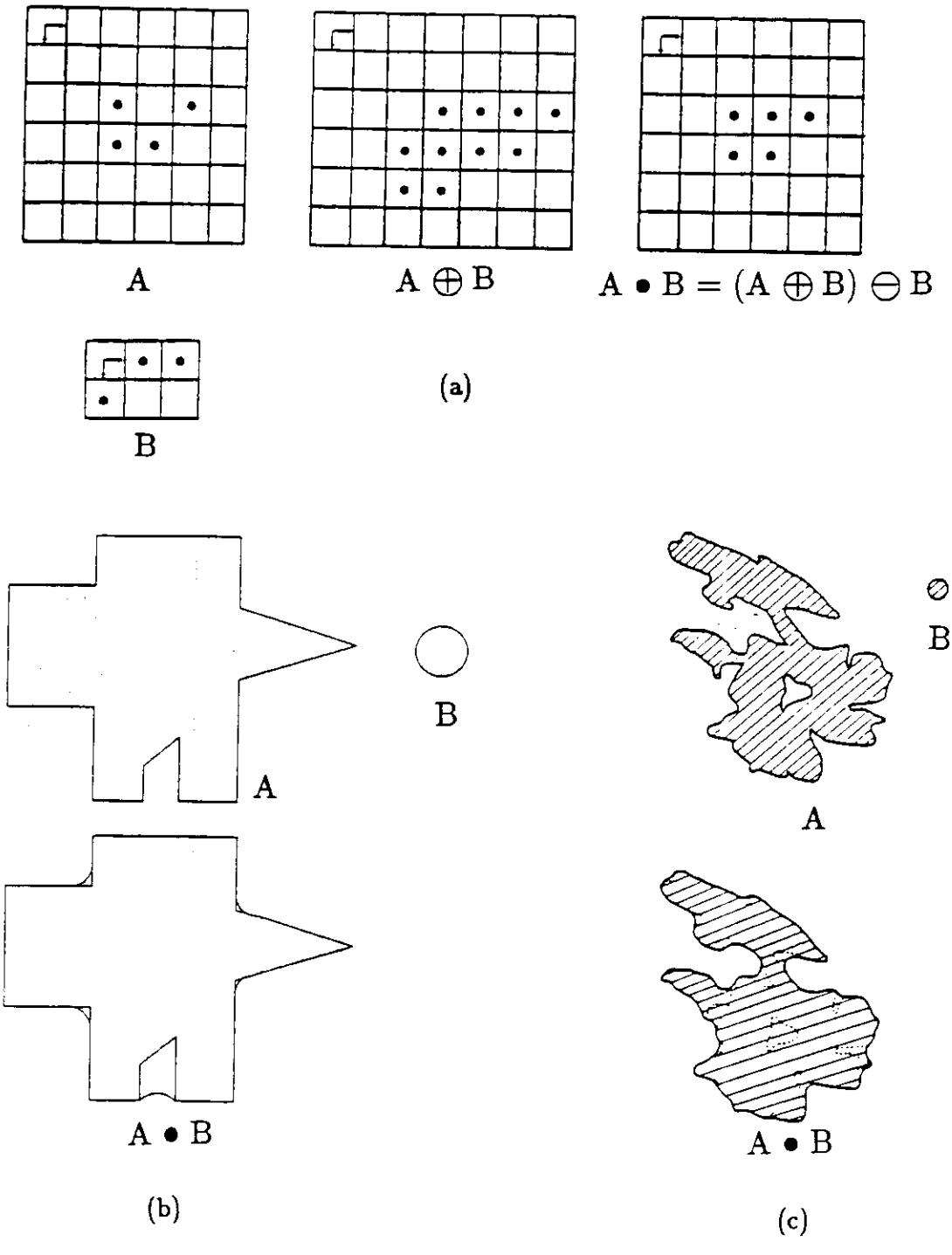

Figure 2.4 Examples of Closing

The result of opening and closing is an elimination of specific image detail smaller than the structuring element without the global geometric distortion of unsuppressed features. For example, opening an image with a disk structuring element smooths the contour, eliminates narrow isthmuses, and discards small islands and sharp peaks or capes (Figure 2.3c). Closing an image with a disk structuring element smooths the contours, and eliminates gaps, small holes and long thin gulfs (Figure 2.4c).

2.2.3 Properties of Set Morphological Operators. The goal of any morphological treatment is to manage the loss of information through successive transformations. In order to do this, we must consider the properties of morphological set operations which are the key to any morphological analysis. Among many properties associated with the above morphological operators, several are worth mentioning in this review [28].

(1) Increasing: dilation, erosion, opening and closing operations are increasing. That is, they preserve the order between sets. For example, given sets A and B with order $A \supseteq B$, opening A and B each with structuring element K will preserve the order, that is, $A \circ K \supseteq B \circ K$.

(2) Anti-extensivity: the opening operation is anti-extensive, i.e., the output of the opening operation is always contained in the original signal. As a dual operation of opening, the closing operation is extensive. That is, the output of the closing operation always contains the original signal.

(3) Idempotence: it is an invariance property for iterations of the operators. That is, the output of the operation remains unchanged if we reapply the operation. For example, given a set A and a structuring element K, let $B=A \circ K$, then $B=B \circ K$.

2.3 Multilevel Morphology

The extension from a set (binary) signal to a function (multilevel) signal was introduced by Serra and Sternberg using different but equivalent approaches. The

first approach is based on threshold decomposition [3, 29] and the other approach is derived using the concept of umbra [26, 30]. In the first approach, the input function can be represented by a collection of sets by thresholding the input at different levels. These sets are operated on by a morphological set transformation, creating a new family of transformed sets. The new sets represent the output function by "piling" the transformed sets. In the second approach, the multilevel operations can be defined as algebraic operations using the concepts of the umbra. In particular, the multilevel dilation is defined as the surface of dilation of the umbra. From this definition, multilevel dilation can be computed in terms of a maximum operation and a set of addition operations. Using the same method, the erosion can be evaluated in terms of a minimum operation and a set of subtraction operations. The details of this approach can be found in [26].

2.3.1 Multilevel Dilation and Erosion. In this section, the definitions of multilevel dilation and multilevel erosion will be given. The multilevel dilation of function f by a multilevel structuring element s

$$(f \oplus s)(x) = MAX\ [f(x-z) + s(z)] \quad \text{for } all\ z \in S \text{ and } x-z \in F \tag{2.5}$$

where F and S are the domain of functions f and s, respectively. Alternately, the dilation of f by s, f $\oplus$ s, can be written as

$$(f \oplus s)(m) = MAX_{n=m-M+1,\ldots,m}\ [f(n)+s(m-n)], \quad \text{for } m=M-1,M,\ldots,N-1 \tag{2.6}$$

Note that the dilation operation is an "expansion" operation in that the values of f $\oplus$ s are always greater than those of f.

The procedure to determine the value of f $\oplus$ s at m is to

(1) left-right reverse the structuring element s,

(2) translate the reversed structuring element to m,

(3) add the reversed structuring element to the input signal, and

(4) find the maximum value of the sums.

The above definition of multilevel dilation shows that multilevel dilation has

the same complexity as convolution. However, instead of doing the summation of products as in convolution, a maximum of sums is performed. Examples of multilevel dilation [31] are shown in Figure 2.5. In Figure 2.5b the structuring element is flat with a width equal to 8. This figure shows that dilation enlarges its maxima.

The multilevel erosion of a function f by a multilevel structuring element s is denoted by f $\ominus$ s, and is defined by

$$(f \ominus s)(x) = MIN\,[f\,(x+z) - s\,(z)] \quad \text{for } all\ z \in S \text{ and } x+z \in F \tag{2.7}$$

where F and S are the domain of functions f and s respectively. Alternatively, the erosion of a function f by another function s can also be written as

$$(f \ominus s)(m) = MIN_{n=0,\ldots,M-1}\,[f\,(m+n) - s\,(n)], \quad \text{for } m=0,\ldots\ldots,N-M \tag{2.8}$$

The erosion is a "shrinking" operator in that values of f $\ominus$ s are always less than those of f. To determine the values of f $\ominus$ s at a point m, the procedure is to

(1) translate the structuring element to m,

(2) subtract the structuring element from the input signal, and

(3) find the minimum value of the differences.

The multilevel erosion is like correlation with the summation of correlation replaced by a minimum operation and the product of correlation replaced by a subtraction operation. Examples of multilevel erosion [31] are shown in Figure 2.6. In Figure 2.6b the structuring element is flat with a width equal to 8. This figure shows that erosion enlarges its minima.

2.3.2 Multilevel Opening and Closing. Multilevel opening and closing are defined in an analogous way to opening and closing in binary morphology and have similar properties. The multilevel opening of f, by structuring element s, is denoted by f o s and is defined by

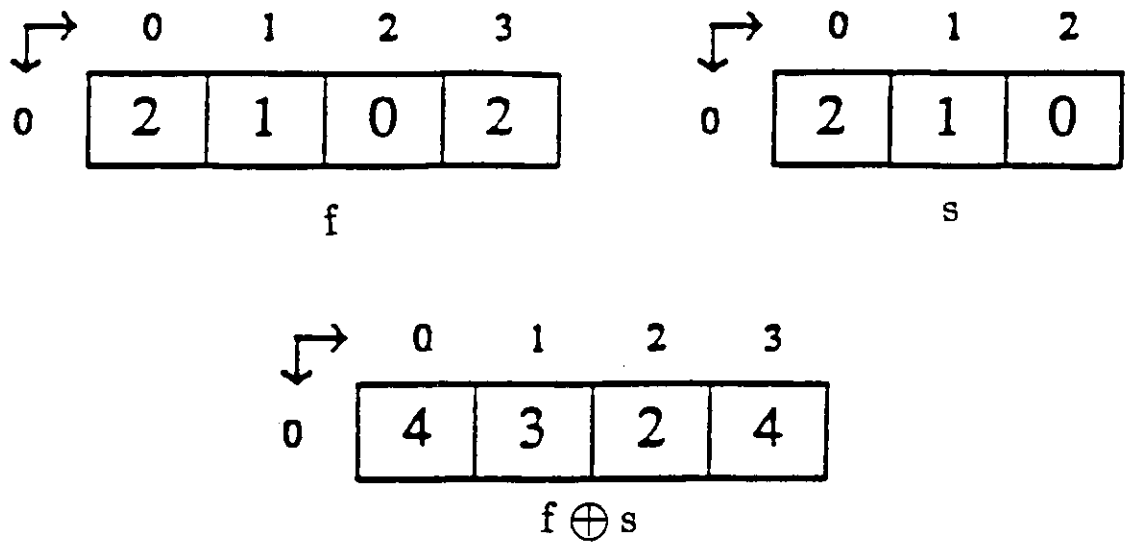

(a)

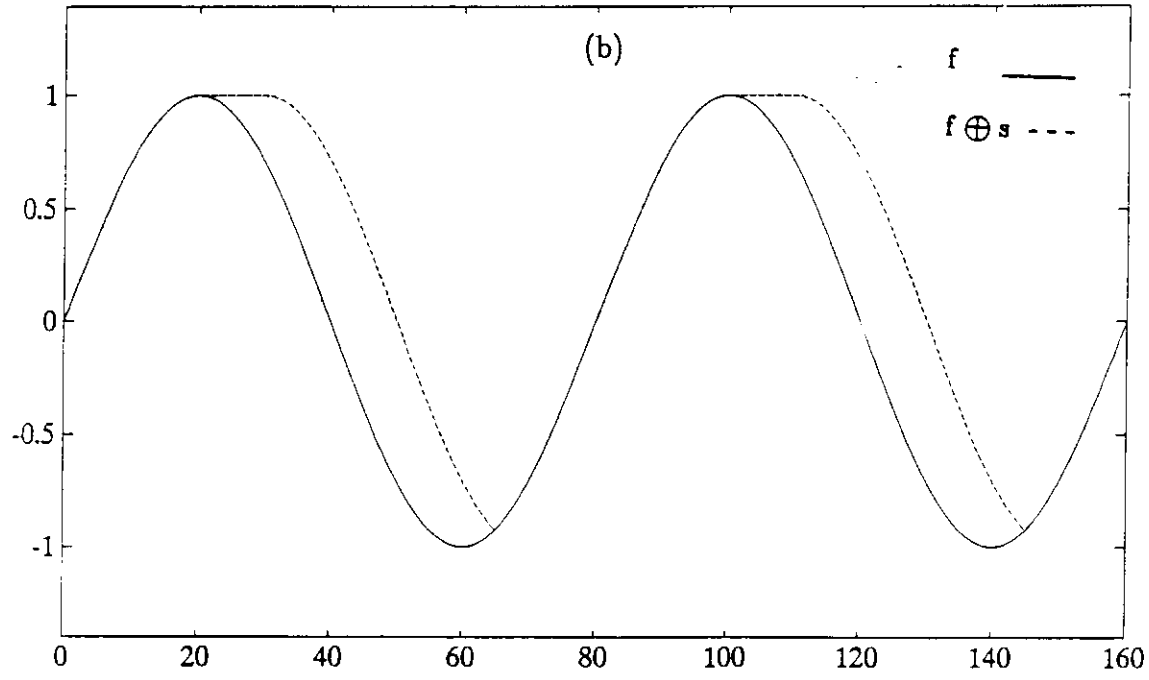

Figure 2.5 Examples of Multilevel Dilation

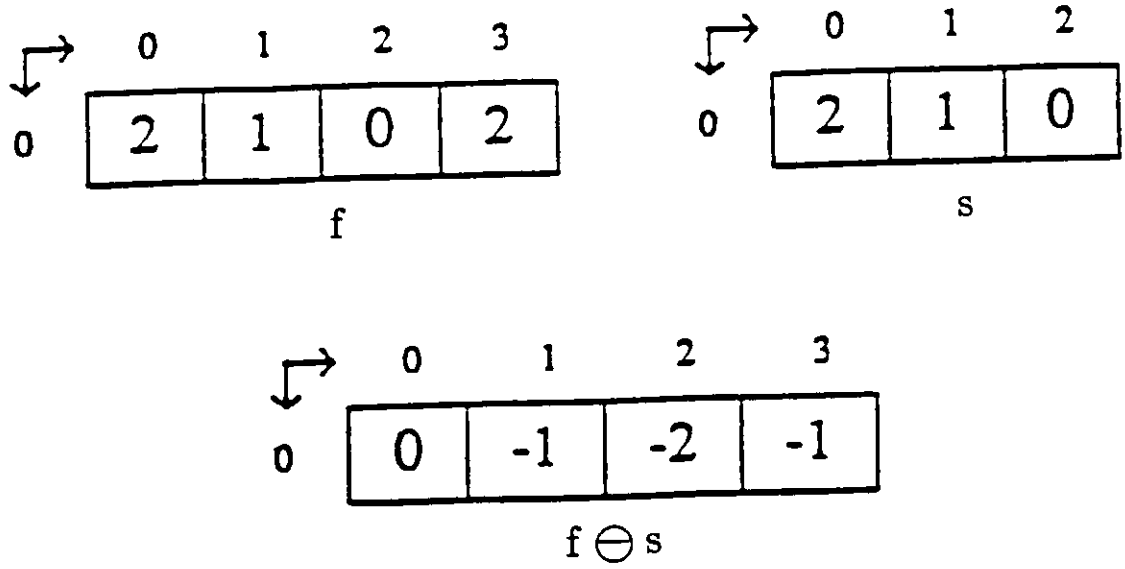

(a)

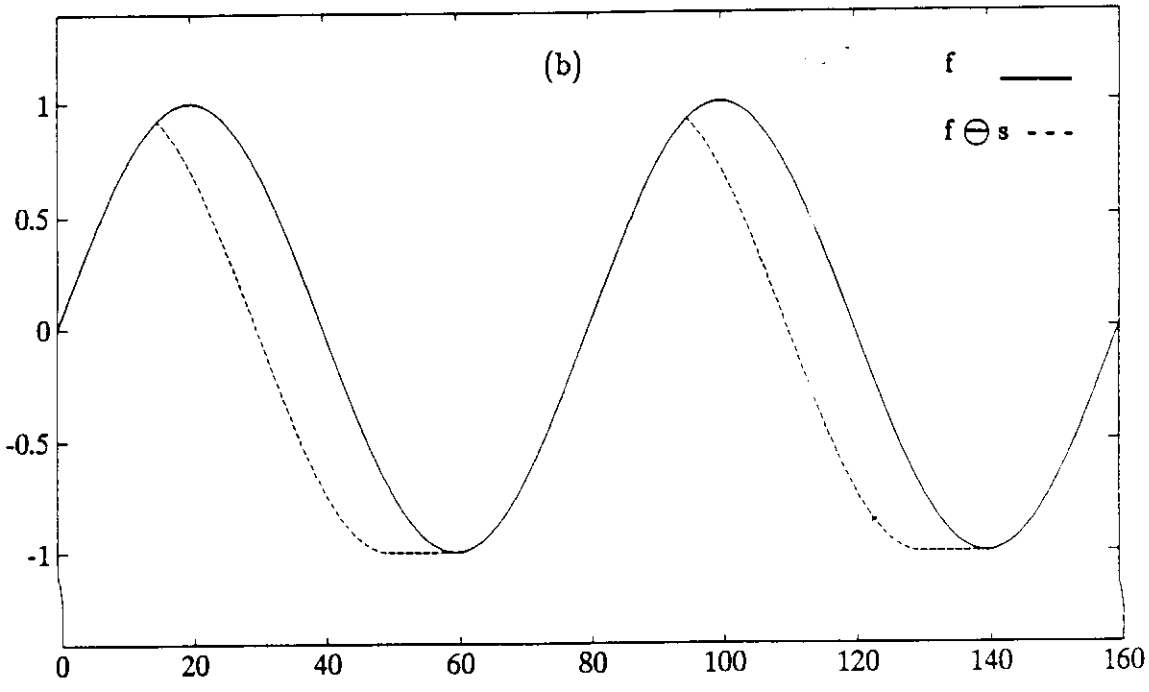

Figure 2.6 Examples of Multilevel Erosion

$$f o s = (f \ominus s) \oplus s \tag{2.9}$$

The multilevel closing of f, by structuring element s, is denoted by f • s and is defined by

$$f \bullet s = (f \oplus s) \ominus s \tag{2.10}$$

It has been shown that an opening is used to suppress peaks (i.e., positive pulses) while a closing is used to suppress bits (i.e., negative pulses). In general, opening any sequence with a structuring element that is flat and has the length M will contain no peaks with an interval of length M-1 or less. Also closing any sequence with such a structuring element will contain no pits with an interval of length M-1 or less [25]. Note that the shape of the output of either opening or closing is affected by the shape of the structuring element. Depending on the shape characteristics of the signal that is to be preserved, a specific structuring element has to be designed for processing the signal.

There is a geometric interpretation to the multilevel opening and to the multilevel closing in the same manner that there is a geometric meaning to the binary morphological opening and closing. The opening of a multilevel signal can be visualized as sliding the structuring element along the surface of the signal from beneath. The result is a mapping of the highest points reached by any part of the structuring element [26, 32]. Similarly, the closing of a multilevel signal can be interpreted as sliding a "flipped-over" version of the structuring element along the surface of the signal from above which results in the lowest points reached by any part of the structuring element [25].

2.4 Clos-Opening and Open-Closing Filters

A general morphological filter consists of several morphological operators performed with various structuring elements. Morphological operators are usually applied in tandem. It is important to point out that the order of the operations is critical because different results are obtained depending on whether an opening or

closing is done first. Open-closing (OC) and clos-opening (CO) [33] are two types of morphological filters used for impulsive noise suppression [25] and edge preservation [34].

The open-closing filter consists of opening followed by closing using the same structuring element. The clos-opening filter consists of closing followed by opening using the same structuring element. By using these filters we can obtain smoothed versions of the original image. These filters have some interesting properties in relation to median filters [29, 35]. In particular, the open-closing and clos-opening give us median roots in a single pass, smooth signals similar to the median, although they have some advantages over the median, i.e., the open-closing or clos-opening is computationally less complex than the median filter. In addition it can discriminate between positive and negative spikes, i.e., opening suppresses the positive noise impulses, and closing suppresses the negative noise impulses, whereas the median cannot.

An important connection between median filters and morphological operations has been made by Maragos [36, 37]. In particular, he proved that a signal is a median root if it is a root of both the opening and closing. Also, medians and their iterations are bounded below by openings and above by closings while the median root is bounded below by the open-closing and above by clos-opening.

CHAPTER III

STATISTICAL PROPERTIES OF MORPHOLOGICAL FILTERS

In order to properly apply morphological filters to random signals, their statistical properties have been examined using different structuring elements. The structuring elements have been characterized by their shape, width and height. In this chapter, the effect of these parameters on random input signals is presented and mathematical expressions for the output density function of morphological filters are derived. This study will provide insights to nonlinear behavior of morphological filters.

3.1 Calculation of Dilation Density Function

To understand the performance of morphological filters and capitalize on their applications, the statistical properties of morphological filters have been investigated. In particular, statistical expressions for the density functions of dilation and erosion operations have been derived (Sections 3.1 and 3.2) utilizing the relationship between morphological filters and order statistic filters (OS). In Section 3.3, the statistical properties of dilation and erosion have been extended to the closing density function by utilizing probabilistic mappings between input and output signals.

Stevenson and Arce [34] derived an expression for the output distribution function of the open-closing and clos-opening for a class of morphological filters for which threshold decomposition is applicable. Neuvo [38, 39] derived an expression for the output distribution function of opening and open-closing utilizing the relationship between morphological and stack filters. It should be noted that they have restricted their expression to function and set processing (FSP), i.e, they have limited their expression to a flat shape (set) structuring element. Maragos and Schafer [36] introduced a unified approach for representing a large class of linear and nonlinear filters (including order statistic (OS) filters) as a supremum

of erosions or infimum of dilations. They analyzed OS filters and related them to function and set processing morphological (FSP) filters that commute with thresholding.

Let f and s denote two discrete functions defined on F = {0, 1, ..., N-1} and S = {0, 1, ..., M-1}, respectively. It is further assumed that N>M. The dilation of the function f by structuring element s is defined as

$$(f \oplus s)(m) = MAX_{n=m-M+1,\ldots,m} \quad [f(n) + s(m-n)] \qquad (3.1)$$
$$\text{for } m = M-1,\ M,\ \ldots\ldots,\ N-1$$

If, the structuring element s has a width M and a constant value zero, then

$$(f \oplus s)(m) = MAX_{n=m-M+1,\ldots,m} \quad [f(n)] \qquad (3.2)$$
$$\text{for } m = M-1,\ M,\ \ldots,\ N-1$$

The above equation can be related to OS filters. Let f be a set of N real numbers. Suppose we sort M numbers in ascending order with respect to their algebraic value within a window size of length M. The Mth OS, is equal to the local maximum of f inside the window M. By combining the definition of OS with the definition of dilation (Equation 3.2), the Mth OS of any signal by window M coincides with dilation by a structuring element with a width M and a constant value zero.

Now, an expression for the distribution function of dilation can be derived using the statistical property of Mth OS [40]. Let's assume that X_1, X_2, ..., X_M are M independent and identically distributed (iid) variates, each with cumulative distribution function (cdf) F(x). Let F_j(x) (j=1, 2, ..., M) denotes the cdf of the jth order statistic X_j. Then the cdf of the largest OS (Mth OS), $X_{(M)}$, is given by

$$F_M(x) = Pr[\ X_{(M)} \leq x] = Pr[\ all\ X_i \leq x] = F^M(x) \qquad (3.3)$$

Using the above relation, the distribution function of dilation by a flat structuring element with a width M and a constant value zero becomes

$$F_d(x) = F^M(x) \qquad (3.4)$$

The dilation density function $p_d(x)$ can be found by taking the derivative of Equation (3.4) with respect to x

$$p_d(x) = M\ F^{M-1}(x)\ p(x) \tag{3.5}$$

where p(x) is the density function of the input X_i.

If a flat structuring element s has a width M and a constant value A, then Equation (3.1) becomes

$$(\ f \oplus s\ )(m) = MAX_{n=m-M+1,\ldots,m}\ [\ f(n) + A\ ] \quad \text{for } m = M-1,\ M,\ \ldots\ldots,\ N-1 \tag{3.6}$$

Equation (3.6) indicates that a constant value A is added to each element of the function f. Therefore, the dilation density function is equal to the shifted density function of the Mth OS by a constant A, i.e.,

$$p_d(x) = M\ F^{M-1}(x-A)\ p(x-A) \tag{3.7}$$

For uniform, independent and identically distributed inputs, the dilation density function is plotted in Figure 3.1 for M=(2, 3, 4, and 5) and A = (0.0, and 0.6). This figure shows that the output signal is biased toward upper values and the signal become more smoothed (i.e., signal variance is reduced).

Calculation of the dilation density function for independent and identically distributed inputs can be generalized to any structuring element by modifying the density function of the variates of the input signal. The modification is performed by shifting each density function to the right by a value depending on the values of the structuring element. Therefore, the density function of dilation can be calculated using the statistical property of the Mth OS density function for independent and non-identically distributed variates. The density function of the Mth order statistics for X_1, X_2, ..., X_M independent and non-identically distributed variates is given by [40]

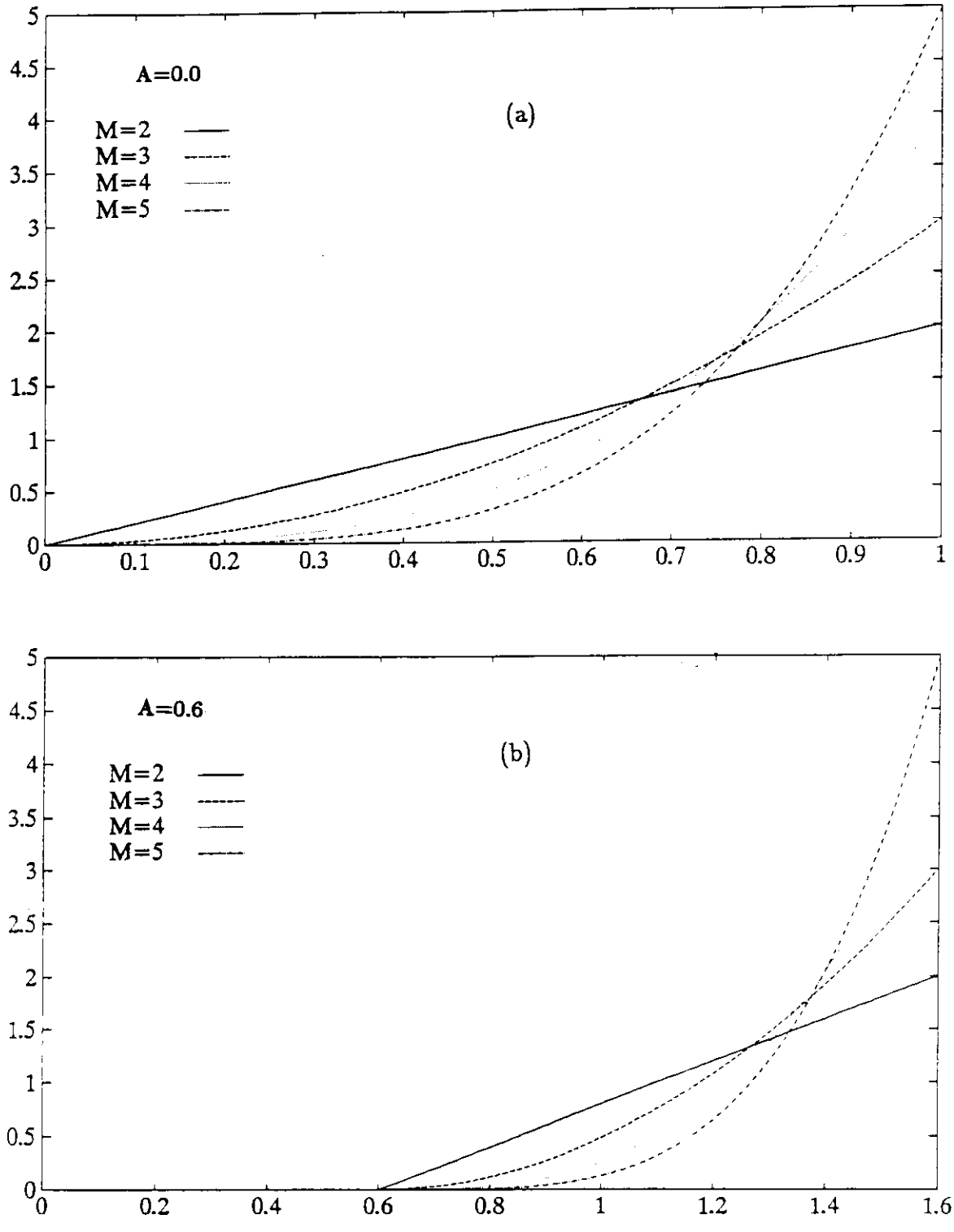

Figure 3.1 Dilation Density Function when the Input Signal has a Uniform Density Function and the Structuring Element is Flat with a Height A:
(a) A=0.0 (b) A=0.6

$$p_M(x)=[\prod_{i=1}^{M} F_i(x)]\sum_{i=1}^{M}(\frac{p_i(x)}{F_i(x)}) \tag{3.8}$$

where $p_i(x)$ and $F_i(x)$ are the density function and distribution function of X_i respectively. Then, the dilation density function by any structuring element becomes

$$p_d(x) = [\prod_{i=1}^{M} F_i(x)]\sum_{i=1}^{M}(\frac{p_i(x)}{F_i(x)}) \tag{3.9}$$

where $p_i(x)$ and $F_i(x)$ are the modifying density function and distribution function by the values of the structuring element.

As an example, let's assume that the structuring element s has a triangular shape with a width M= 5 and a height A as shown in Figure 3.2. Also, the inputs will be considered as independent and identically distributed. Then the first and fifth inputs have the same density function as the input density functions p(x), [i.e., $p_1(x)= p_5(x)=$ p(x)]. The second and the fourth input density functions are shifted by A/2 to the right, [i.e., $p_2(x)= p_4(x)=$ p(x-A/2)] and the third input density function shifted by A to the right, [i.e., $p_3(x)=$ p(x-A)]. Then, using Equation (3.9), the dilation density function of uniform distribution inputs, for M=5, is given by

$$p_d(x)=\begin{cases} 0 & 0\le x\le A \\ x(x-A/2)(5x^2-5.5Ax+A^2) & A\le x\le 1 \\ (x-A/2)(3x-2.5A) & 1\le x\le 1+A/2 \\ 1 & 1+A/2\le x\le 1+A \\ 0 & x\ge 1+A \end{cases} \tag{3.10}$$

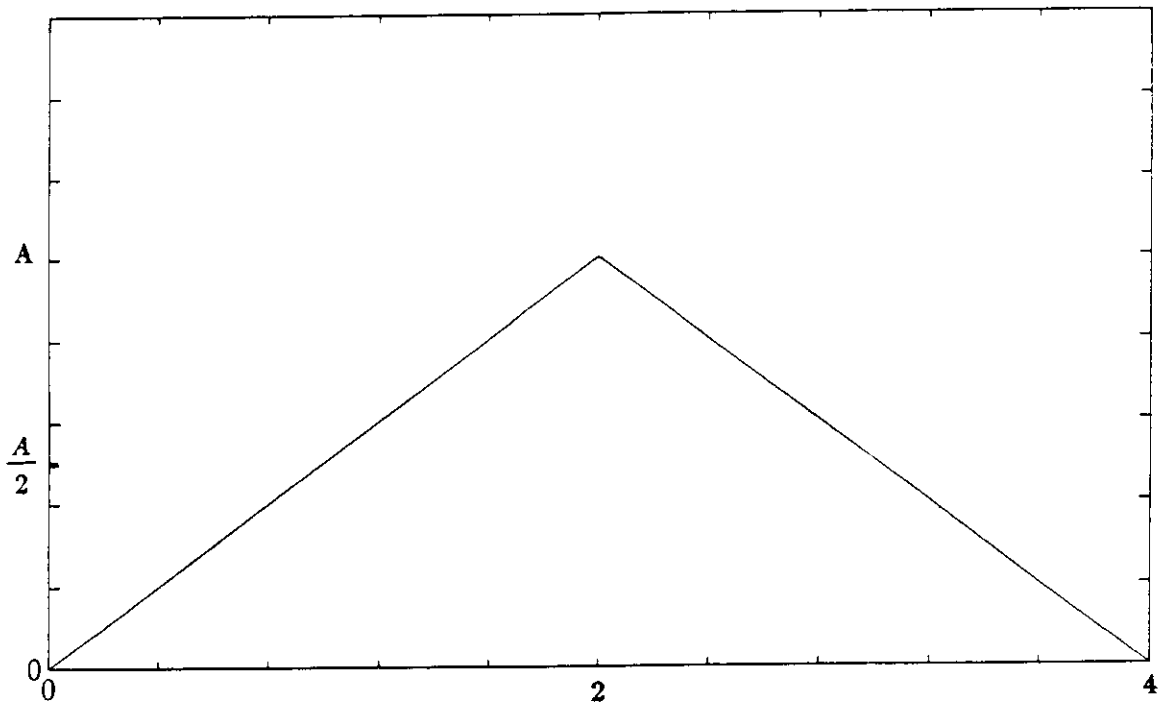

Figure 3.2 Triangular Structuring Element with a Width M=5 and a Height A

If M=3, then

$$p_d(x)=\begin{cases}0 & 0\le x\le A\\ x(3x-2A) & A\le x\le 1\\ 1 & 1\le x\le 1+A\\ 0 & x\ge 1+A\end{cases} \tag{3.11}$$

A comparison of the dilation density functions of uniformly distributed inputs for two different widths (M=3, and 5) and four heights (A=0.2, 0.4, 0.6 and 0.8) of triangular structuring elements are shown in Figure 3.3 indicating that the dilation density function depends on the density of the input signal, the shape, height and width of the structuring element. The effect of these parameters on the output density function can be summerized as follows:

1) The output density function is shifted to the right and the shift increases when the height of the structuring element (A) increases.

2) For the same width (M), the change in the shape of the input density function due to dilation is less affected by increasing the height of the structuring element. This observation coincides with the deterministic properties of morphological filters (see Chapter V).

3) For the same height of structuring element (A), the peak of the density function increases and the variance of the output density function decreases as window width (M) increases.

3.2 Calculation of Erosion Density Function

In this section, we derive an expression for the erosion density function. This expression is derived using a similar method applied to the derivation of the dilation density function.

The erosion of the function f by the structuring element s is defined as

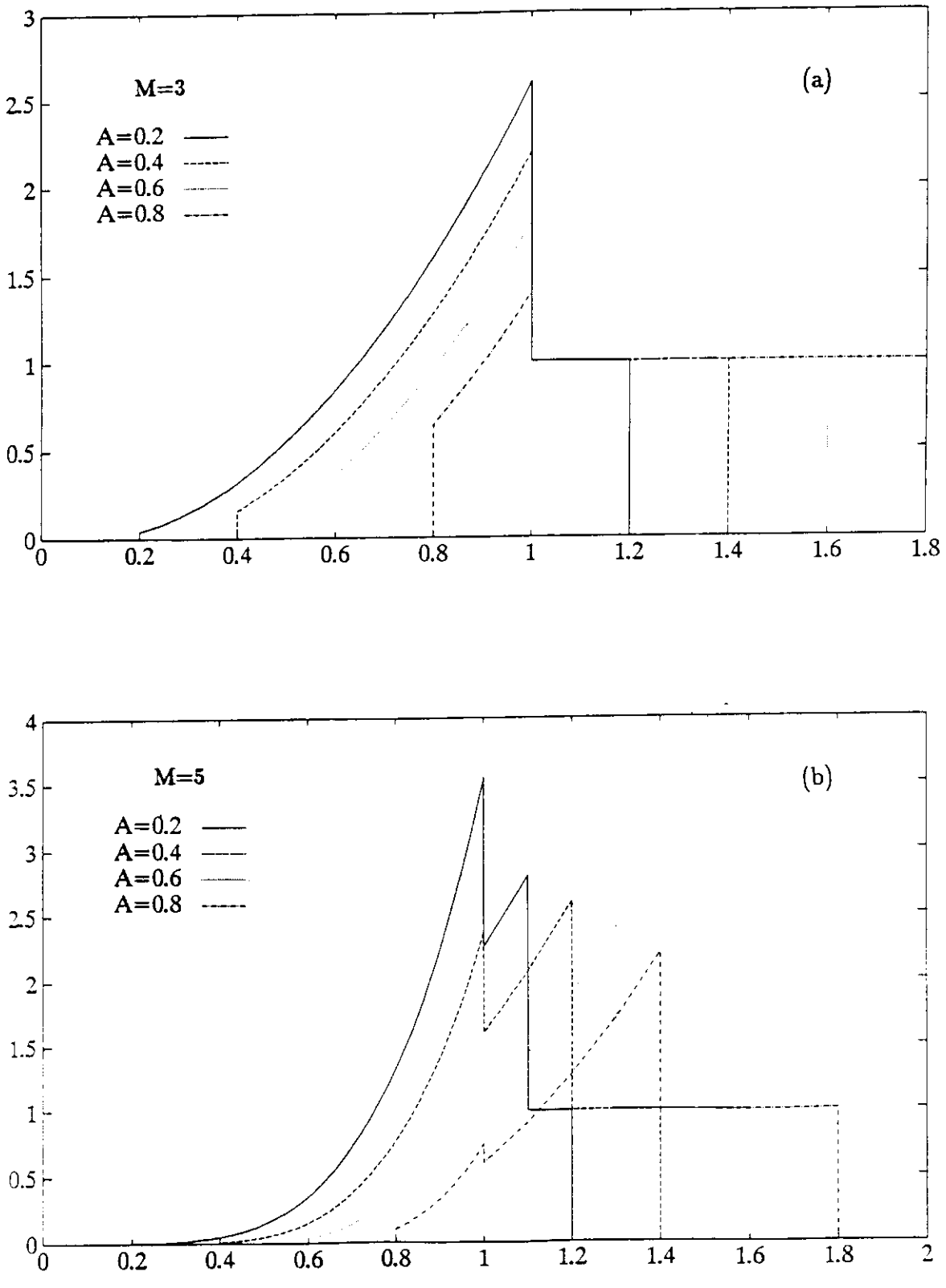

Figure 3.3 Dilation Density Function when the Input Signal has a Uniform Density Function and the Structuring Element is Triangular with a Width M:
(a) M=3 (b) M=5

$$(f \ominus s)(m) = \underset{\text{for } m=0,\ \ldots,\ N-M}{MIN_{n=0,\ldots,M-1}} \ [f(m+n) - s(n)] \tag{3.12}$$

If, the flat structuring element has a width M and a constant value zero, then

$$(f \ominus s)(m) = \underset{\text{for } m=0,\ldots,N-M}{MIN_{n=0,\ldots,M-1}} \ [f(m+n)] \tag{3.13}$$

The above equation can be related to OS filters indicating that the first order statistic (1st OS) of any signal by window M coincides with erosion by structuring element s has a width M and a constant value zero.

Now, an expression for the distribution function of erosion is derived using the statistical property of the 1st OS [40]. Let's assume that X_1, X_2, ..., X_M are M independent and identically distributed (iid) variates, each with a cumulative distributed function F(x). Let $F_j(x)$ (j= 1, 2, ..., M) denote the cdf of the jth order statistic. Then the cdf of the 1st OS is given by

$$F_1(x) = Pr[\ X_{(1)} \leq x] = 1 - Pr[X_{(1)} > x]$$

$$= 1 - Pr[\ all\ X_i > x] = 1 - (1 - F(x))^M \tag{3.14}$$

Using the above relation, the distribution function of erosion by a flat structuring element with a width M and a constant value zero becomes

$$F_e(x) = 1 - (\ 1 - F(x))^M \tag{3.15}$$

The erosion density function $p_e(x)$ can be found by taking the derivative of Equation (3.15) with respect to x,

$$p_e(x) = M(1-F(x))^{M-1}\ p(x) \tag{3.16}$$

where p(x) is the density function of the input X_i.

If a flat structuring element s has a width M and a constant value A, then Equation (3.12) becomes

$$(f \ominus s)(m) = MIN_{n=0,\ldots,M-1} \; [f(m+n) - A] \qquad \text{for } m = 0, \ldots, N-M \tag{3.17}$$

Equation (3.17) indicates that a constant value A is subtracted from each element of the function f. Therefore, the erosion density function is equal to the left-shifted density function of the 1st OS by a constant A, i.e.,

$$p_e(x) = M[1-F(x+A)]^{M-1} \; p(x+A) \tag{3.18}$$

For uniform, independent and identically distributed inputs, the erosion density function is plotted in Figure 3.4 for M=(2, 3, 4, and 5) and A=(0.0, and 0.6).

Calculation of the erosion density function for independent and identically distributed inputs can be generalized to any structuring element by modifying the density function of the input signal. The modification is performed by shifting each density function to the left by a value depending on the values of the structuring element. Then, the erosion density function can be calculated using the statistical property of the 1st OS of independent and nonidentically distributed variates.

In general, the density function of the jth order statistics for X_1, X_2, ..., X_M, independent and non-identically distributed variates, is given by [41]

$$f_{(j)}(x) = \frac{1}{(M-j)!(j-1)!} \left\| \begin{array}{cccc} F_1(x) & F_2(x) & \cdots & F_M(x) \\ \cdot & \cdot & \cdot & \cdot \\ \cdot & \cdot & \cdot & \cdot \\ F_1(x) & F_2(x) & \cdots & F_M(x) \\ f_1(x) & f_2(x) & \cdots & f_M(x) \\ 1-F_1(x) & 1-F_2(x) & \cdots & 1-F_M(x) \\ \cdots & \cdots & \cdots & \cdots \\ 1-F_1(x) & 1-F_2(x) & \cdots & 1-F_M(x) \end{array} \right\| \begin{array}{l} \} \; j-1 \text{ rows} \\ \\ \\ \\ \} \; M-j \text{ rows} \end{array} \tag{3.19}$$

where $\| \; \|$ is the permanent of a square matrix and is defined [42] like the determinant of the matrix, except that all signs are positive.

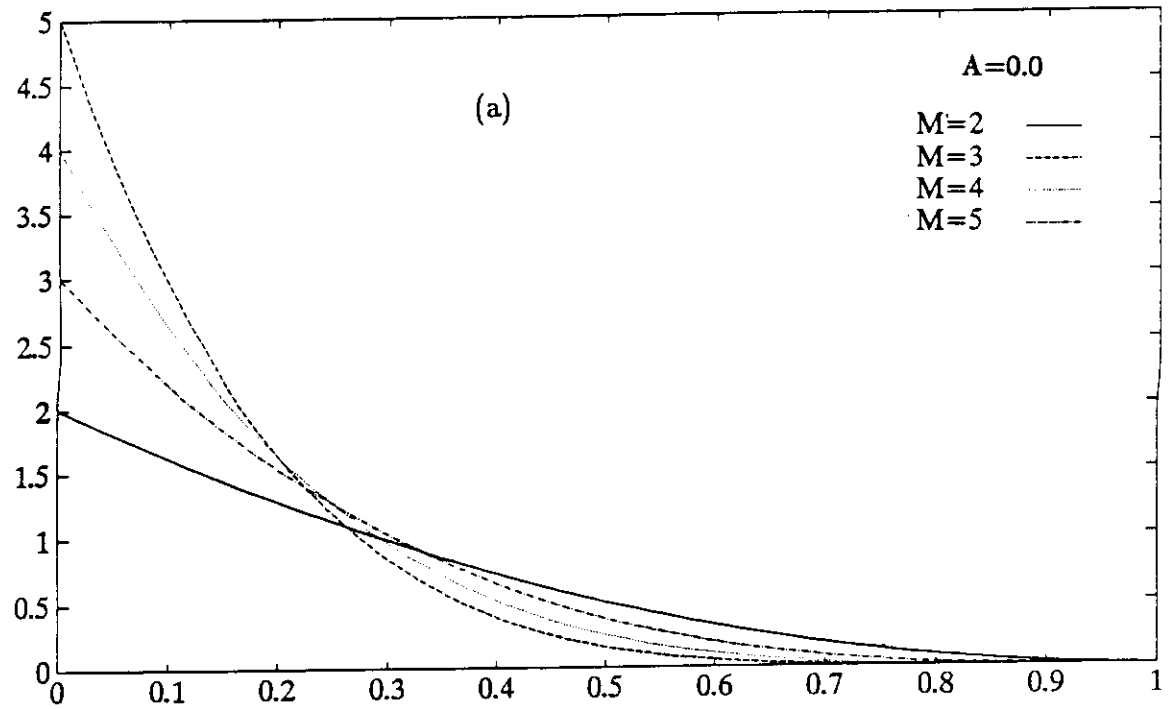

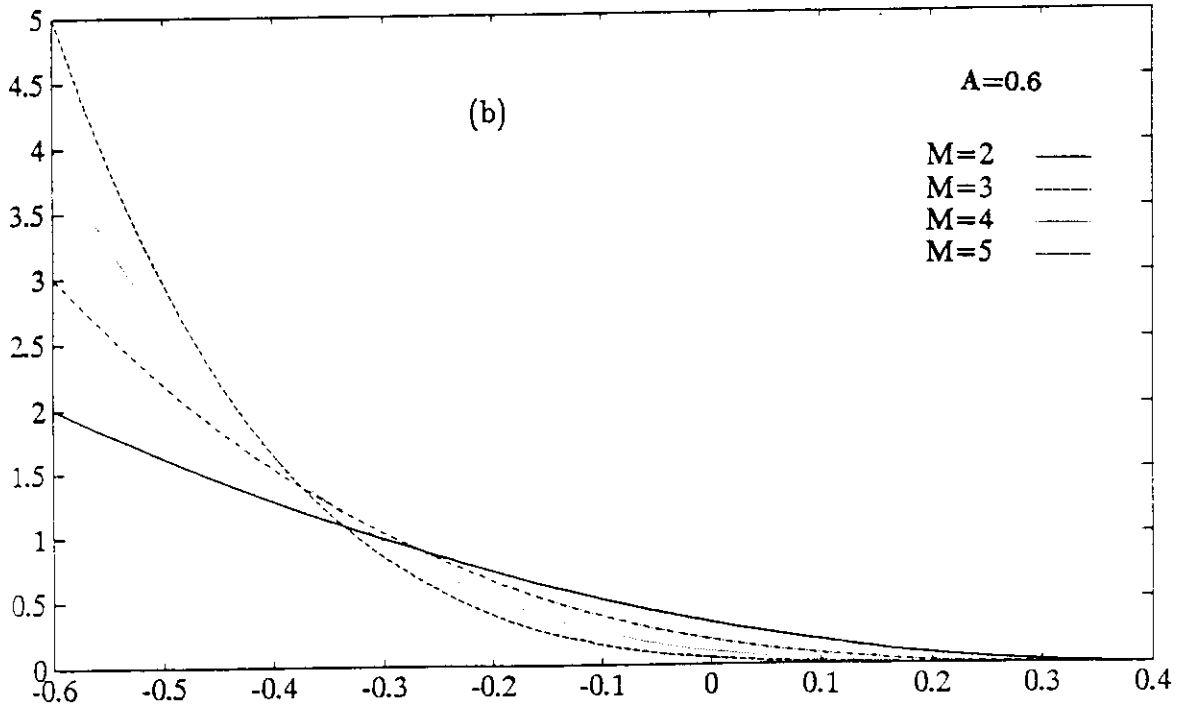

Figure 3.4 Erosion Density Function when the Input Signal has a Uniform Density Function and the Structuring Element is Flat with a Height A:
(a) A=0.0 (b) A=0.6

Using Equation (3.19) for (j=1), the erosion density function for any structuring element is given by

$$f_e(x)=\frac{1}{(M-1)!}\begin{array}{c} \begin{array}{cccc} + & & & + \end{array} \\ \left|\begin{array}{cccc} f_1(x) & f_2(x) & \cdots & f_M(x) \\ 1-F_1(x) & 1-F_2(x) & \cdots & 1-F_M(x) \\ \cdot & \cdot & \cdot & \cdot \\ \cdot & \cdot & \cdot & \cdot \\ \cdot & \cdot & \cdot & \cdot \\ 1-F_1(x) & 1-F_2(x) & \cdots & 1-F_M(x) \end{array}\right| \end{array} \left.\begin{array}{c} \\ \\ \\ \\ \\ \end{array}\right\} \begin{array}{l} M-1 \\ rows \end{array} \tag{3.20}$$

Suppose that the structuring element s has a width M and a triangular shape with a height A. Then using the above equation, the erosion density function of uniform, independent and identically distributed inputs for M=3 is given by

$$f_e(x)=\begin{cases} 0 & x\leq -A \\ 1 & -A\leq x\leq 0 \\ 3(1-x)^2-2A(1-x) & 0\leq x\leq 1-A \\ 0 & x\geq 1-A \end{cases} \tag{3.21}$$

and for M=5

$$f_e(x)=\begin{cases} 0 & x\leq -A \\ 1 & -A\leq x\leq -A/2 \\ 3(1-x)^2-4A(1-x)+5A^2/4 & -A/2\leq x\leq 0 \\ (1-x)(1-x-A/2)[5(1-x)^2-5.5A(1-x)+A^2] & 0\leq x\leq 1-A \\ 0 & x\geq 1-A \end{cases} \tag{3.22}$$

By substituting $(1-x)$ for x in Equations (3.21) and (3.22), it can be shown that the expression of the erosion and dilation density function is symmetrical with respect to x=0.5. A comparison of the erosion density function of uniformly distributed inputs for different widths (M=3, and 5) and heights (A=0.2, 0.4, 0.6

and 0.8) of triangular structuring elements is shown in Figure 3.5. These results reveal that the erosion density function depends on the input density function, the shape, height and width of the structuring element. Note that the effect of the parameters of the structuring element on the erosion density function of uniform and identically distributed variates is the same as that of the dilation density function due to the symmetry of their expressions.

3.3 Calculation of Closing Density Function

In this Section, the statistical properties of dilation and erosion are extended to other sequential stages. In particular, a general statistical expression for a closing density function is derived when inputs are independent and identically distributed. The closing density function is derived by utilizing probabilistic mappings between input and output signals [34]. This expression is restricted to FSP morphological filters (i.e., flat structuring elements) since the main tool of analysis is threshold decomposition. The threshold decomposition property is used so that binary (set) signals can be examined to obtain results for the multilevel signals.

In order to investigate the effect of the closing operation on a multilevel signal, a collection of binary set structures is defined. By understanding the effect of the closing operation on these set structures, results can then be obtained through the threshold decomposition property, for an arbitrary multilevel signal. The set structures are defined as follows [34]:

- The constant set, (ω_n), contains all the points that have at least M adjacent identically valued point.
- The oscillation set (A_n), is made up of all points that do not belong to the constant set. A subset of the oscillation set that needs special definition is the impulse set. An impulse set contains those points which have no more than M-1 adjacent identically valued points and also belong to the oscillation set.

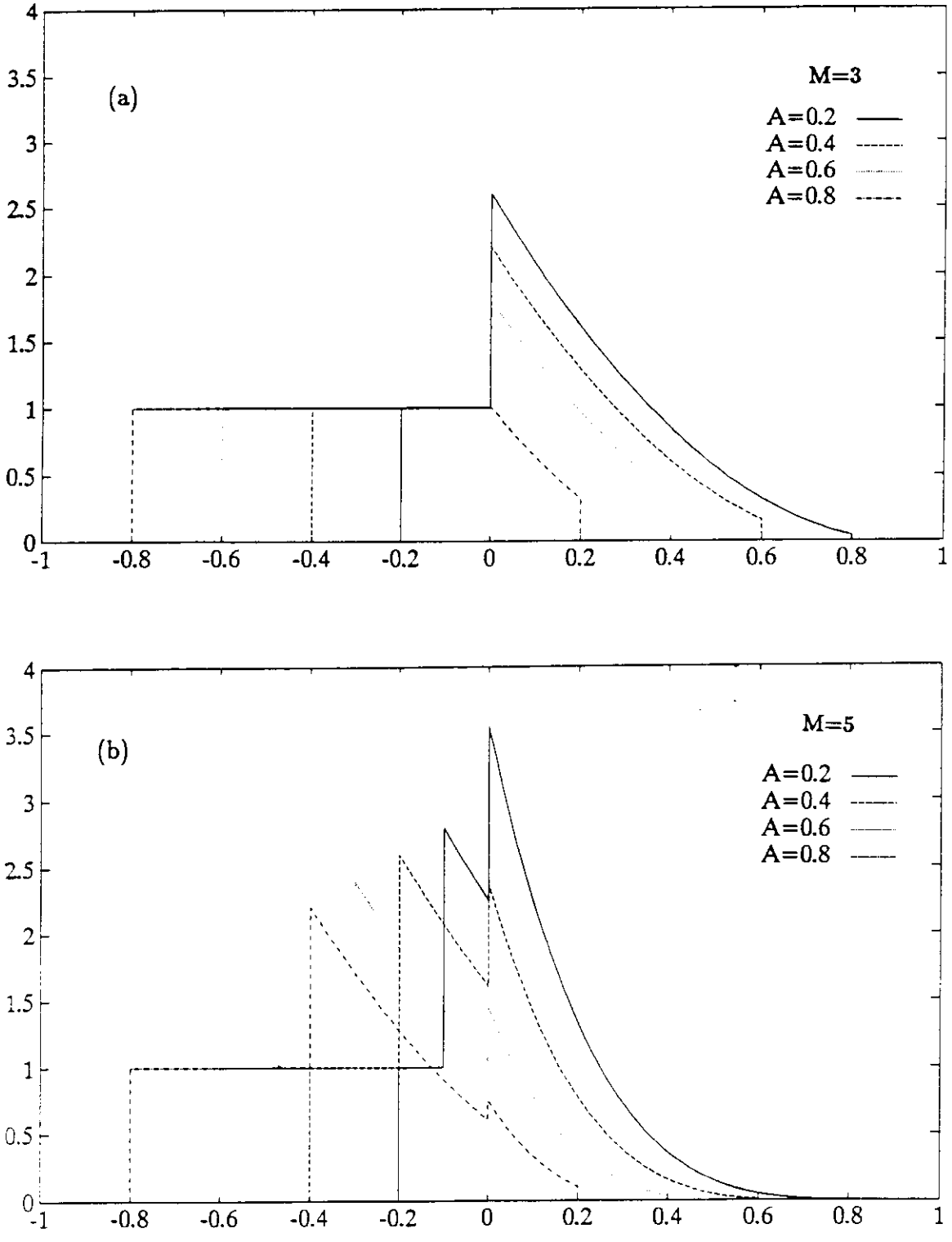

Figure 3.5 Erosion Density Function when the Input Signal has a Uniform Density Function and the Structuring Element is Triangular With a Width M:
(a) M=3 (b) M=5

In general, any arbitrary binary input signal can be split into five independent sets, i.e., no two sets contain the same point. These sets are the positive constant set (ω_n^1), negative constant set (ω_n^0), positive impulse set (T_n^1), negative impulse set (T_n^0). The fifth set ($A_n \cap T_n^c$), is an oscillation set that does not belong to any of the previous four sets. An example of an arbitrary binary input set is given in Figure 3.6a. Now, to determine how each particular set structure will be affected by the closing operation, an example is shown in Figure 3.6b using a flat structuring element with a width M=3 and a height A=0. The relationship between structure input and processed sets is shown in Table 3.1. The results indicate that if a point belongs to the constant set (i.e., positive or negative) or positive impulsive set, then that point is unchanged by the closing operation. However, since all negative impulse points are bounded on both sides by elements of the positive constant set, the negative impulses themselves will become members of the positive constant set. Also, the oscillation set structure ($A_n \cap T_n^c$) becomes part of the positive constant set after the closing operation. Note that the positive impulse points do not become part of the constant set after the closing operation because these points are bounded on both sides by elements of the negative constant set.

Knowing how each possible set structure is transformed by a closing operation will allow us to derive the output statistics of the multilevel signal. For multilevel signals we define some important signal structures, these structures are similar to those defined for median filter [35]:

- A constant neighborhood is a region of at least M consecutive points, all of which are identically valued.
- An edge is a monotonically rising or falling set of points surrounded on both sides by a constant neighborhood.
- An oscillation is a sequence of points that is not part of a constant neighborhood or an edge.

An arbitrary input signal will be entirely composed of a constant neighborhood, edges and oscillations. When thresholded, the points of constant neighborhoods and edges will become members of the constant set, and oscillation points will become members of the oscillation set. It is known that when transformed, the constant set or positive impulse set remains unchanged. The negative impulse set (T_n^1) and the oscillation set ($A_n \cap T_n^c$) become members of the positive constant set (ω_n^1). Thus constant neighborhoods and edges will be preserved exactly by the transformation.

Now, the statistical analysis of the closing density function can be performed in two steps. First, the output statistics of the binary (set) signal can be derived by a probabilistic mapping of set structure transformations. Then, by applying Serra' theorem [3] which establishes the connection from sets to functions, the multilevel closing density function can be evaluated for the signal with samples which are independent and identically distributed.

To obtain the collection of sets that represent a function, the multilevel function f(z) is thresholded at a level t to obtain sets X_t. Once the family of thresholded sets is obtained they can be operated on by a morphological binary set) operations, $\Psi(.)$, to generate a new family of sets. These sets represent the transformed function. As long as $\Psi(.)$ is increasing [3] and uses the family of transformed sets, $Y_t = \Psi[X_t]$, the multilevel transformed function $y(z) = \psi[f(z)]$ is given by

$$y(z) = \psi[f(z)] = Sup[t : z \in Y_t] \tag{3.23}$$

where Sup is the supremum " largest" of t's such that $y(z) \geq t$.

Now, if we let ω_n^1, ω_n^o, $A_n \cap T_n^c$, T_n^1 and T_n^o denote the input binary sets of the thresholding sets X_t, then if $z \in \omega_n^o$ then $z \notin Y_t$. If we let the probability of an event be denoted by Pr[.], this can be written as

$$Pr[z \notin Y_t] = Pr[z \in \omega_n^o] \tag{3.24}$$

Let Pr[z $\not\in$ X_t] = α_t, then the output probability Pr[z $\not\in$ Y_t] can be found in terms of the input probability using the following property:

$$P[z \in \omega_n^o]=M\,\alpha_t^M-(M-1)\,\alpha_t^{M+1} \tag{3.25}$$

where M is the width of the structuring element.

The proof of Equation (3.25) is as follows. For z ϵ ω_n^o it must be adjacent to at least (M-1) other points belonging to ω_n^o. If we define the set ω_L to be any subset of X_t with two members, $|\omega_L|$=2, that bound exactly L adjacent members of ω_n^o, then ω_L will be of the structure illustrated in Figure 3.7. The probability of a structure such as ω_L will be

$$Pr[\,\omega_L \subseteq X_t]=(1-\alpha_t)^2\alpha_t^L \tag{3.26}$$

Since there are L points in the structure that belong to ω_n^o

$$Pr[z \in \omega_n^o \textit{ bounded by } \omega_L] = L(1-\alpha_t)^2\alpha_t^L \tag{3.27}$$

Since z ϵ ω_n^o —> z is bounded by a ω_L for some L$\geq$ M, the probability that z ϵ ω_n^o will be the sum over all $L \geq M$,

$$Pr[z \in \omega_n^o\,] = \sum_{L=M}^{\infty} L\,(1-\alpha_t)^2\alpha_t^L = M\alpha_t^M - (M-1)\alpha_t^{(M+1)} \tag{3.28}$$

The above property describes the statistics of the processed binary sets. By using Serra's Theorem, we can now find the distribution function of multilevel signal for the closing operation.

• Let a(z) and y(z) be the multilevel iid input and output signals, respectively. Then the output distribution function is given by

$$F_{y(t)} = M\,F(t)^M-(M-1)F(t)^{M+1} \tag{3.29}$$

where F(t) is the input distribution function.

The proof of Equation (3.29) is as follows. From the definition of the threshold

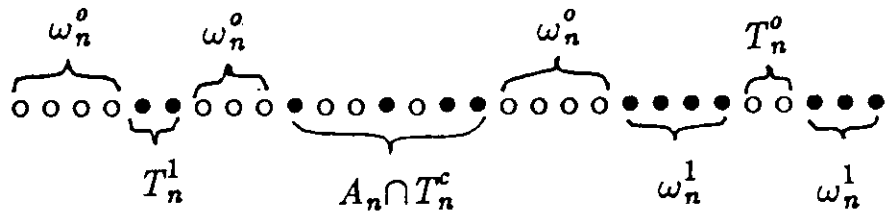

Input Sets

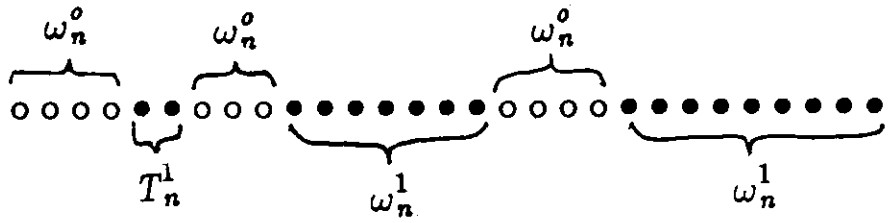

Processed Sets

Figure 3.6 Input Set Structures and Processed Sets using a Closing Operation with a Flat Structuring Element

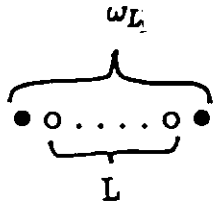

Figure 3.7 Set Structure of Negative Constant Sets

Table 3.1 The Relationship between Structure Input and Processed Sets

Input Structures	Output Set
ω_n^1	ω_n^1
ω_n^o	ω_n^o
T_n^1	T_n^1
T_n^o	ω_n^1
$A_n \cap T_n^c$	ω_n^1

sets X_t = [z: a(z)≥t], thus, z $\not\in$ X_t if a(z)<t. The input distribution function :

$$F(t) = Pr[a(z)<t] = Pr[z \not\in X_t] = \alpha_t \tag{3.30}$$

and similarly,

$$F_{y(t)} = Pr[y(z)<t] = Pr[z \not\in Y_t] \tag{3.31}$$

Substituting Equations (3.24), (3.28) and (3.30) into (3.31) yields (3.29).

The closing density function $p_c(t)$ can be found by taking the derivative of Equation (3.29) with respect to t,

$$p_c(t) = [\, M^2 F(t)^{M-1} - (M^2-1)\, F^M(t)\,]\, p(t) \tag{3.32}$$

where p(t) is the density function of the input.

To investigate the effect of the width (M) of a flat structuring element due to the closing operation, the closing density function when input signals have uniform, Rayleigh and Gaussian distributions and their moments (mean, variance and skewness) is presented throughout the rest of this section. The mean (E[.]), variance (E[.]=σ^2) and skewness (SK[.]) of the closing density function are defined as follows:

$$E[p_c(t)] = \int_{-\infty}^{\infty} t p_c(t)\, dt \tag{3.33}$$

$$\sigma^2[p_c(t)] = \int_{-\infty}^{\infty} (t - E[p_c(t)])^2 p_c(t)\, dt \tag{3.34}$$

and

$$SK[p_c(t)] = \int_{-\infty}^{\infty} (t - E[p_c(t)])^3 p_c(t)\, dt \tag{3.35}$$

For uniform, independent and identically distributed inputs (ranging between zero and one), the closing density function is plotted in Figure 3.8 for M = (2, 3, 4

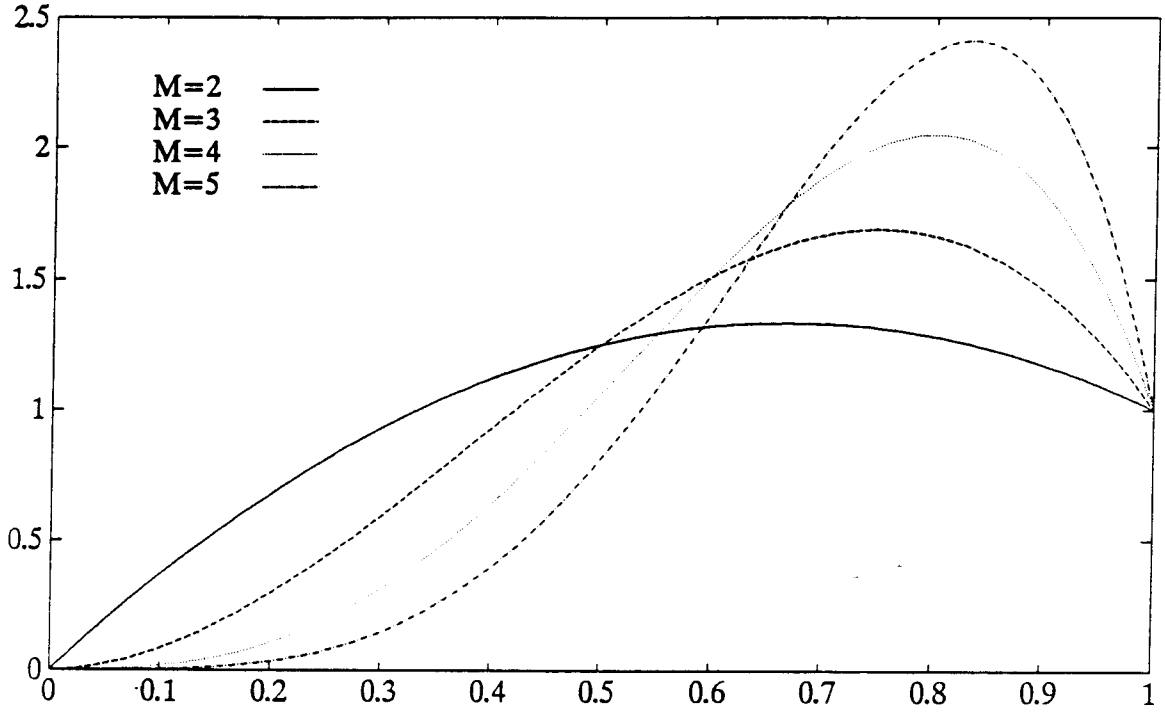

Figure 3.8 Closing Density Function when the Input Signal has a Uniform Density Function and the Structuring Element is Flat

and 5). In this case, the mean, variance and skewness (the third central moment) of the closing density function when input signals have a uniform density function are given by:

$$E[p_c(t)\ ]=\frac{(M^2+M+1)}{(M+1)(M+2)} \tag{3.36}$$

$$\sigma^2[p_c(t)\ ]=\frac{2\ M^3\ +4\ M^2\ +5M+1}{(M+1)^2\ (M+2)^2\ (M+3)} \tag{3.37}$$

and

$$SK[p_c(t)\ ]=\frac{(M^2+M+3)}{(M+3)(M+4)}-3\frac{(M^2+M+2)(M^2+M+1)}{(M+1)(M+2)^2(M+3)} +2\frac{(M^2+M+1)^3}{(M+1)^3(M+2)^3} \tag{3.38}$$

For Rayleigh density function (with mean equal to $\sqrt{\pi/2}$ and variance equal to $2(1 - \pi/4)$), the closing density function is plotted in Figure 3.9 for M=3, 7, 13, and 21). In this case, the mean, variance and skewness are:

$$E[p_c(t)]=\sqrt{\frac{\pi}{2}}\ +\ [\ \sum_{n=1}^{M-1}(-1)^n\frac{(M)!}{(M-n)!(n)!}\frac{(1-nM)}{(n+1)}\sqrt{\frac{\pi}{2(n+1)}}\ ] -(-1)^M(M-1)\sqrt{\frac{\pi}{2(M+1)}} \tag{3.39}$$

$$\sigma^2[p_c(t)\ ]=2\ +\ [\ \sum_{n=1}^{M-1}2(-1)^n\frac{(M)!}{(M-n)!(n)!}\frac{(1-nM)}{(n+1)^2}\ ]\ -\ 2(-1)^M\frac{(M-1)}{(M+1)} \tag{3.40}$$

and

$$SK[p_c(t)\ ]=3\ \sqrt{\frac{\pi}{2}}\ +\ [\ \sum_{n=1}^{M-1}3(-1)^n\frac{(M)!}{(M-n)!(n)!}\ \frac{(1-Mn)}{(n+1)^2}\sqrt{\frac{\pi}{2(n+1)}}\ ] -3(-1)^M\frac{(M-1)}{(M+1)}\sqrt{\frac{\pi}{2(M+1)}} \tag{3.41}$$

For the Gaussian density function (with mean equal to zero and variance equal to , the closing density function is plotted in Figure 3.10 for M=(3, 7, 13, and . Since, closed form expression for mean, variance and skewness can not be

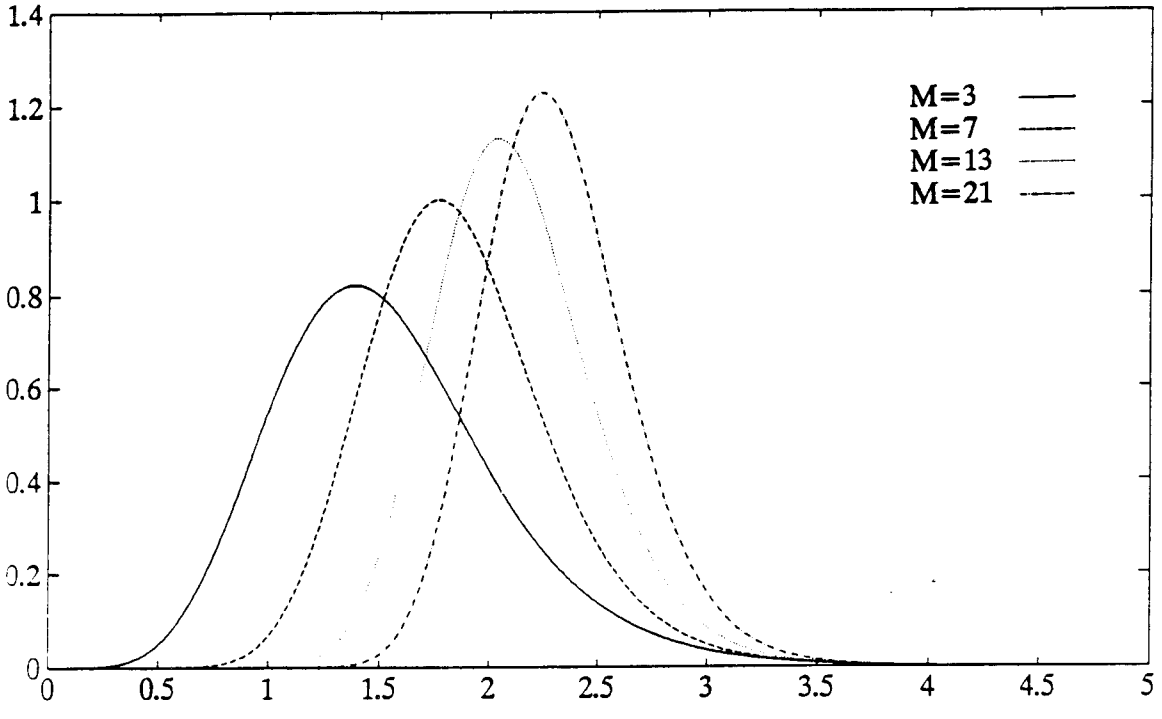

Figure 3.9 Closing Density Function when the Input Signal has a Rayleigh Density Function and the Structuring Element is Flat

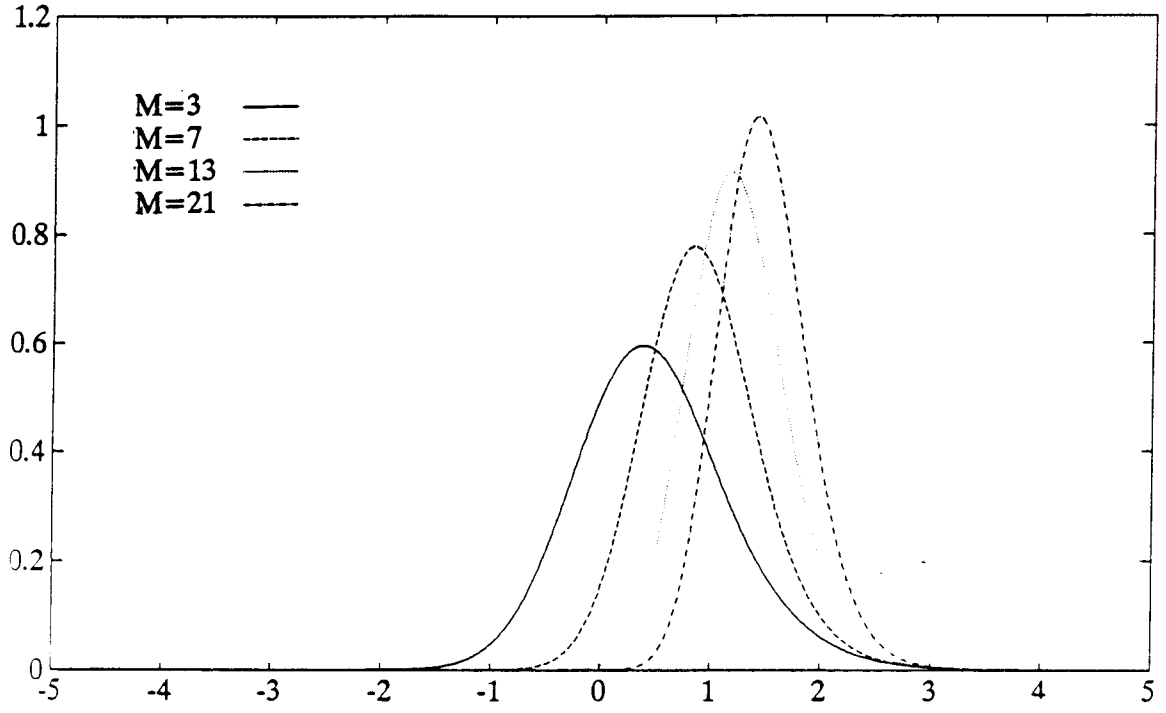

Figure 3.10 Closing Density Function when the Input Signal has a Gaussian Density Function and Structuring Element is Flat

obtained, numerical techniques are used to solve Equations (3.33) - (3.35) [43]. The mean, variance and skewness of the closing density functions for uniform, Rayleigh and Gaussian functions are shown in Figures 3.11 - 3.13 respectively.

In general, these results indicate that the mean (bias) of the closing density function is increased by increasing the width of the flat structuring element, while variance and skewness are decreased.

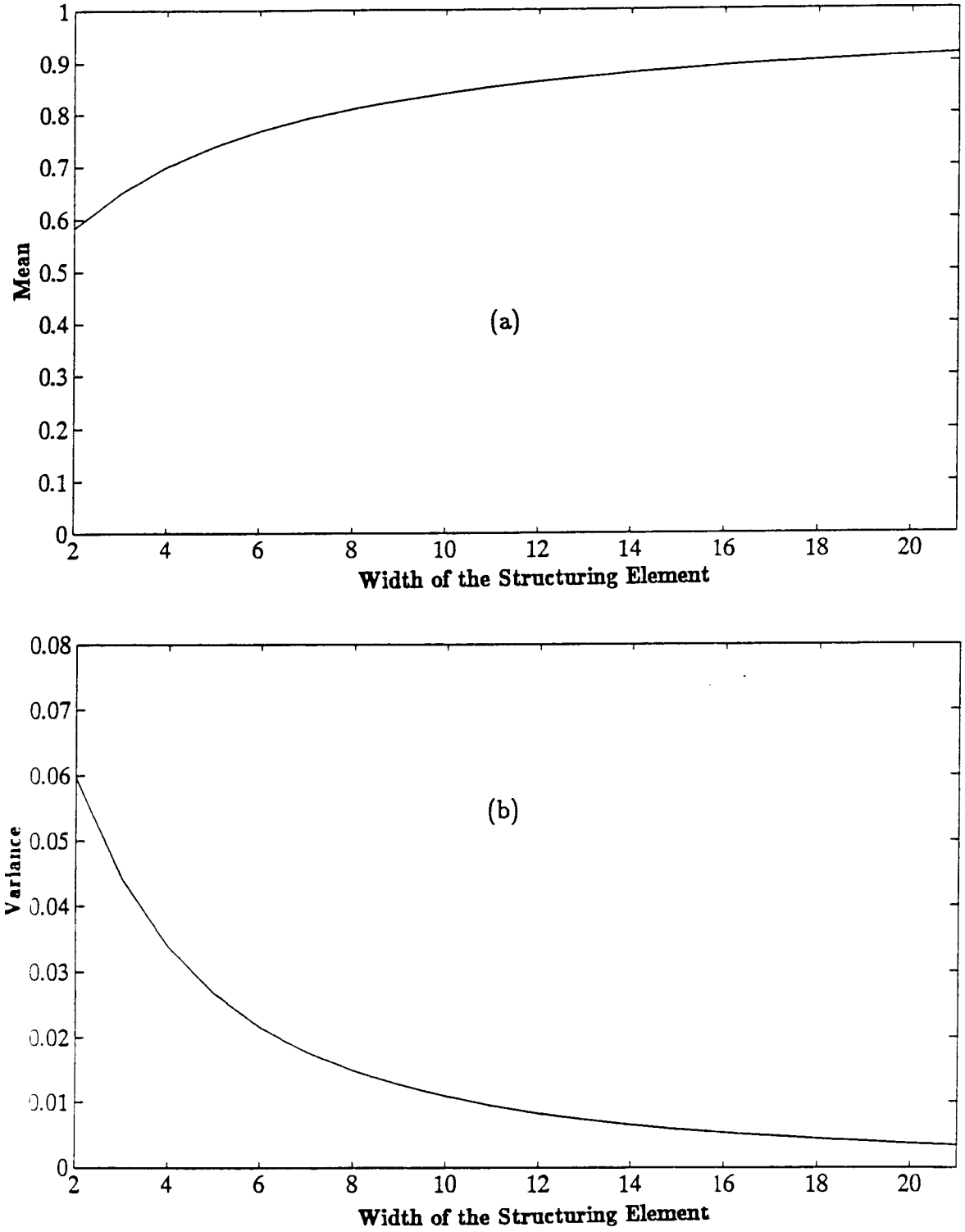

Figure 3.11 Mean, Variance and Skewness of the Closing Density Function when the Input Signal has a Uniform Density Function using a Flat Structuring Element

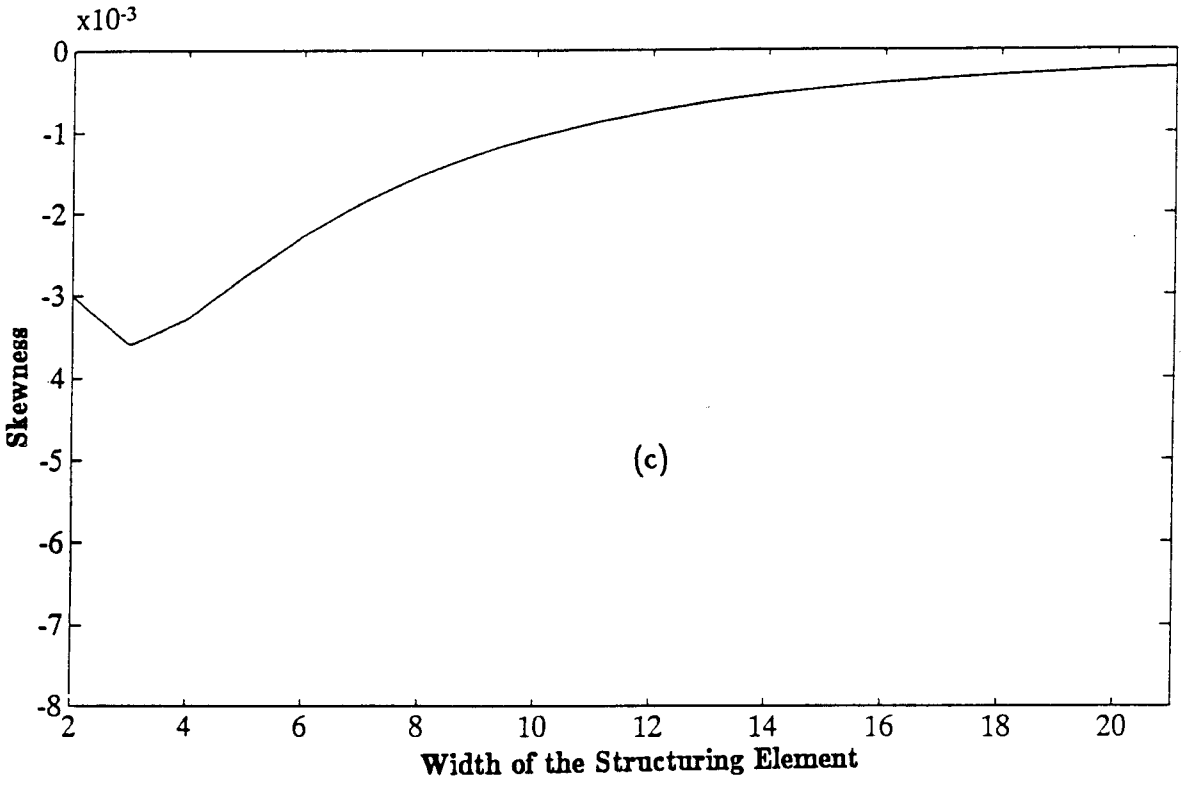

Figure 3.11 (Continued)

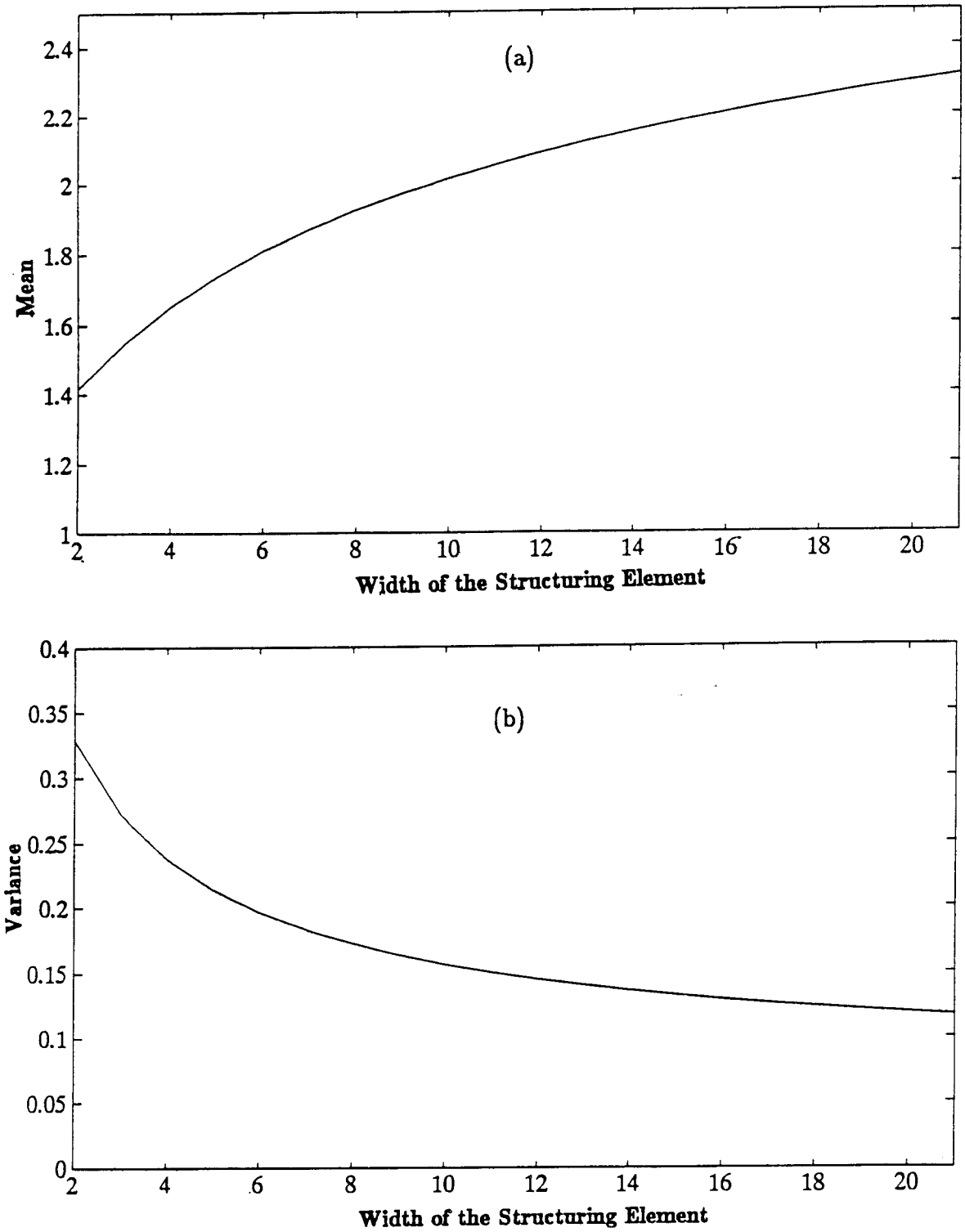

Figure 3.12 Mean, Variance and Skewness of the Closing Density Function when the Input Signal has a Rayleigh Density Function using a Flat Structuring Element

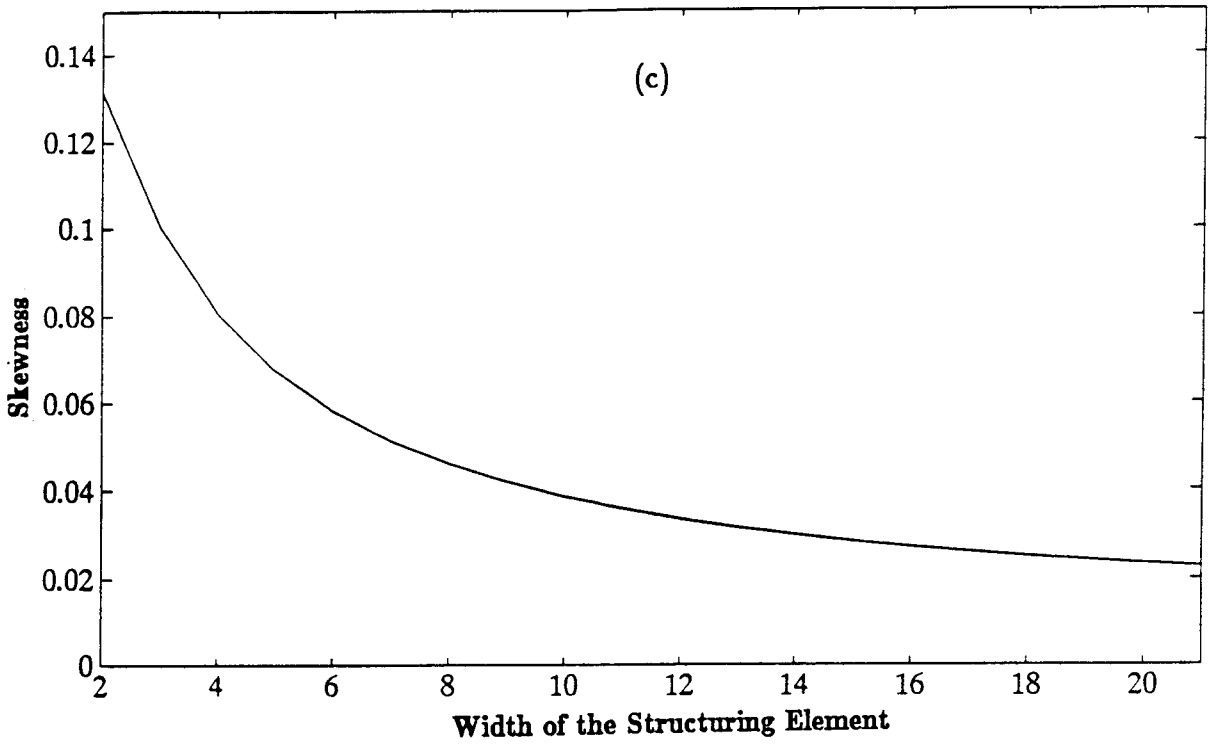

Figure 3.12 (Continued)

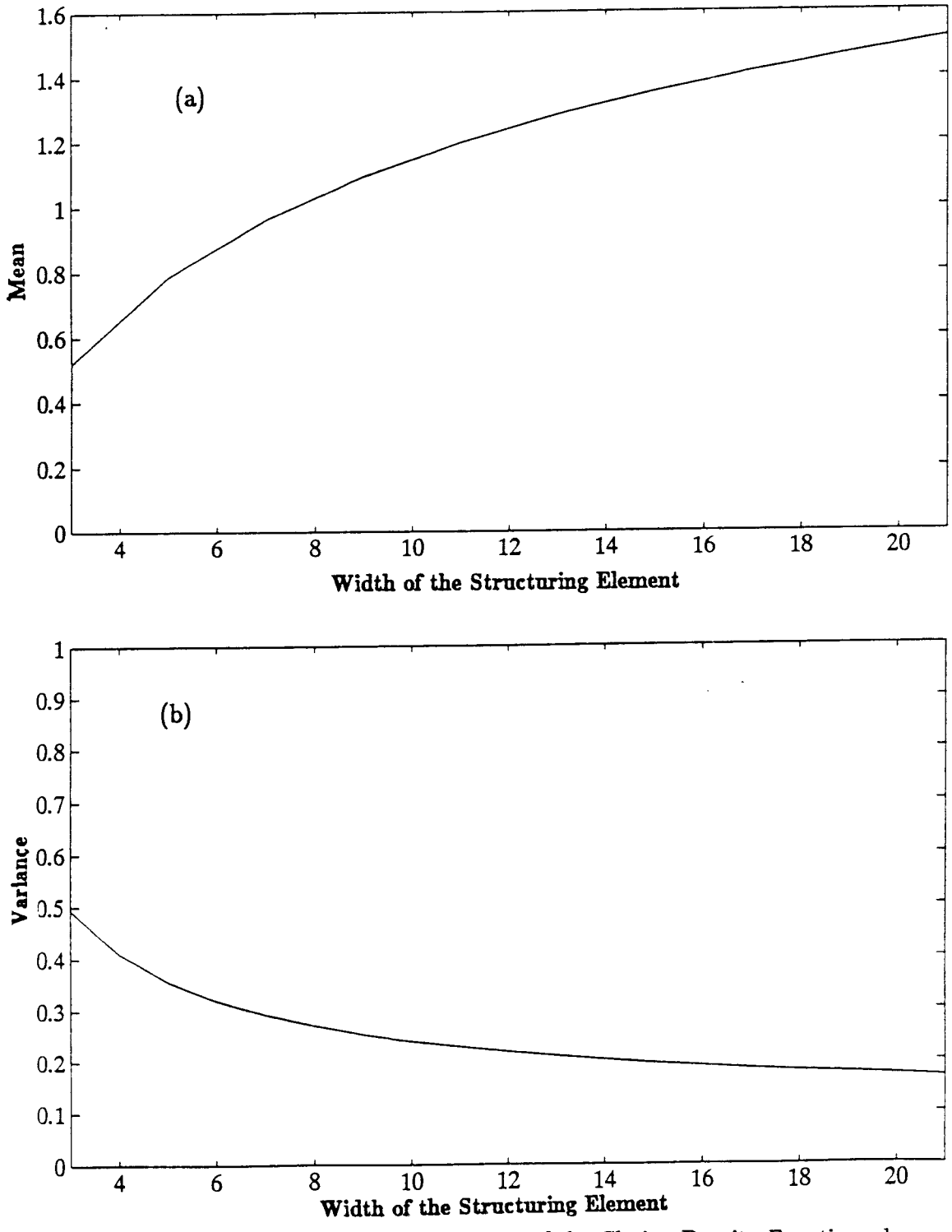

Figure 3.13 Mean, Variance and Skewness of the Closing Density Function when Input Signal has a Gaussian Density Function using a Flat Structuring Element

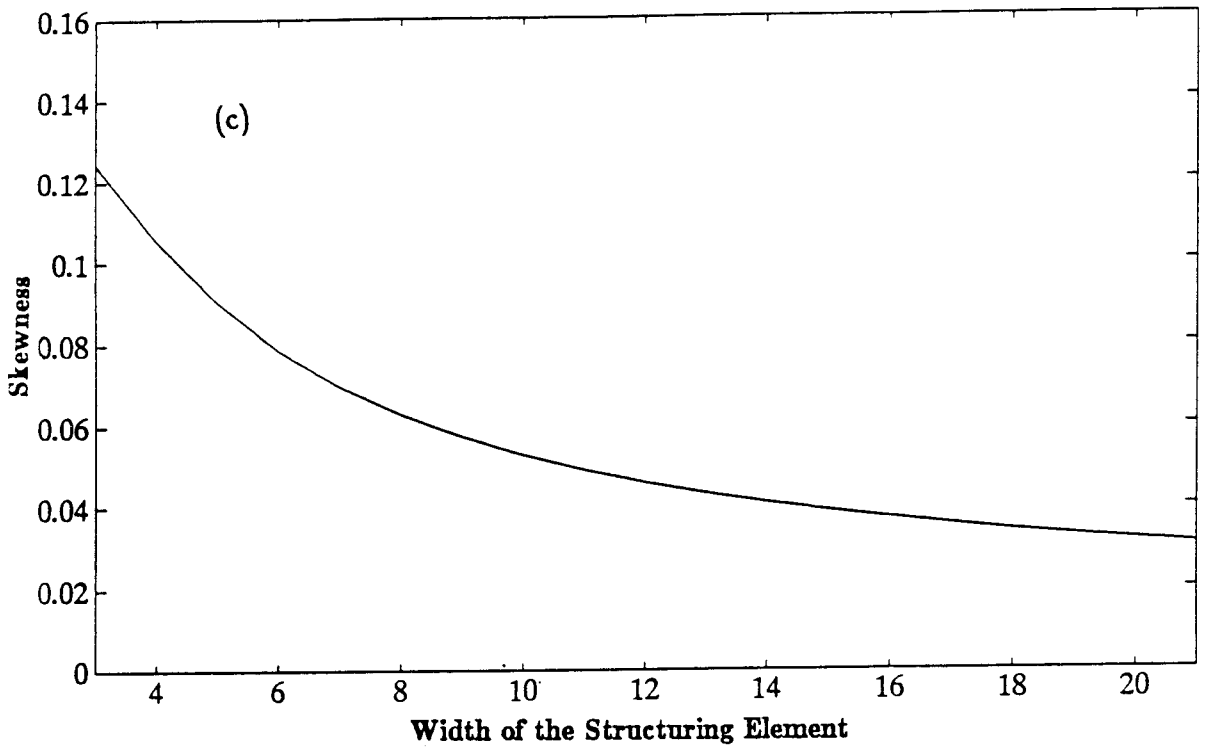

Figure 3.13 (Continued)

CHAPTER IV

MONTE CARLO SIMULATION OF MORPHOLOGICAL FILTERS

In the previous Chapter, the statistical expression for the dilation and erosion density function for a general shape structuring element has been derived utilizing the relationship between morphological filters and order statistics filters [44]. To extend the study of the morphological operations to other sequential stages such as closing, clos-erosion and clos-opening, Monte Carlo technique was used to estimate the processed signal density function. Monte Carlo simulation describes the statistical characteristics of the processed signal, overcoming the complexity that often arises in direct mathematical analysis due to statistical dependency of the results at different stages of morphological operations. In particular, we present the output density function of morphological filters when input signals have uniform, Gaussian and Rayleigh distributions. The simulated results and their statistics (mean, variance and skewness) present an interpretation of the noise suppression capability of morphological filters and their biasing effects.

4.1 Simulation Results

In this Chapter, the statistical properties of basic morphological operations are examined using structuring elements with different shapes applied to signals with different density functions. The structuring element is characterized by its shape, width and height. Using Monte Carlo simulation, we present the effect of these parameters and the output density functions at different stages of morphological operations when input signals have uniform, Gaussian and Rayleigh distributions. The Monte Carlo technique is used to avoid the difficulty of analyzing statistical dependency problems arising in the processed signal at different stages. Also, the mean, normalized variance (i.e., the ratio of output variance over input variance) and skewness is estimated for each of these density functions to present an interpretation of noise suppression capability of morphological filters and their biasing effects. To demonstrate the above objectives, simulation has been used to

process 300 input data sequences, each with a length of N=10000 samples. These sequences have been applied to a sequence of morphological operations, i.e., dilation, closing, clos-erosion and clos-opening using a flat structuring element, and a triangular structuring element representing a more general shape.

4.1.1 Results Using Flat Structuring Element. The dilation, closing, clos-erosion, and clos-opening density functions and their statistics (i.e., mean, normalized variance and skewness) when inputs are independent and identically distributed (iid), with uniform density functions (ranging between zero and one) and using flat structuring elements are shown in Figures 4.1 and 4.2. These figures indicate that dilation shifts the input signal toward the maximum values and the signal variance is reduced, resulting in a smooth operation. The closing operation (i.e., dilation followed by erosion) is a processing step toward recovering the original signal. Overall, the closing operation tunes down the bias caused by the dilation operation, and slightly increases the signal variance with respect to the dilation operation. The clos-opening operation results in further smoothing of the signal, where the signal variance, mean, and skewness are less than those of the closing signal. The mean of dilation, closing, clos-erosion and clos-opening is shifted to the right (see Figure 4.2a) due to the effect of dilation as a first operation in the sequence of the above operations. The differences in the skewness between dilation, closing, clos-erosion and clos-opening density functions decrease when the width of the flat structuring element is increased (see Figure 4.2c). Note that the height of the flat structuring element has no effect on the closing and clos-opening density function, but it shifts the dilation density function to the right and the clos-erosion density function to the left by a predictable value depending on the height. In general, the above figures indicate that by increasing the width of the flat structuring element the mean (bias) is increased and the variances and skewness of dilation, closing, clos-erosion and clos-opening output density functions are decreased. Furthermore, dilation has been found to be the most effective step in the smoothing operation. The effect of the other operations following dilation is rather small, especially when the width is increased.

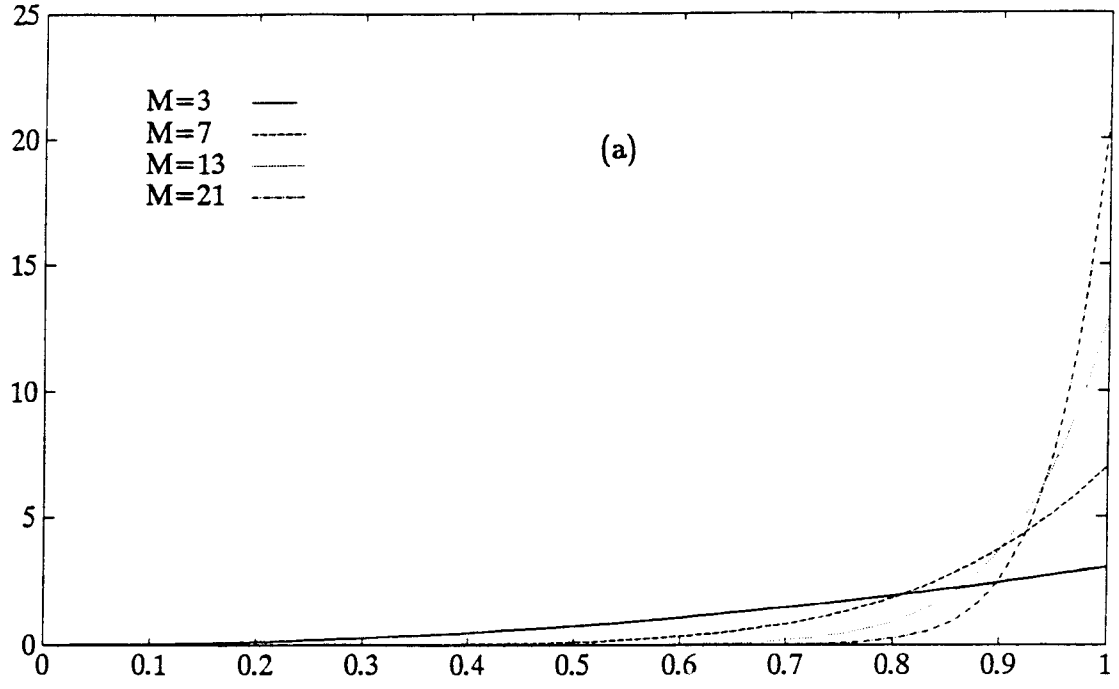

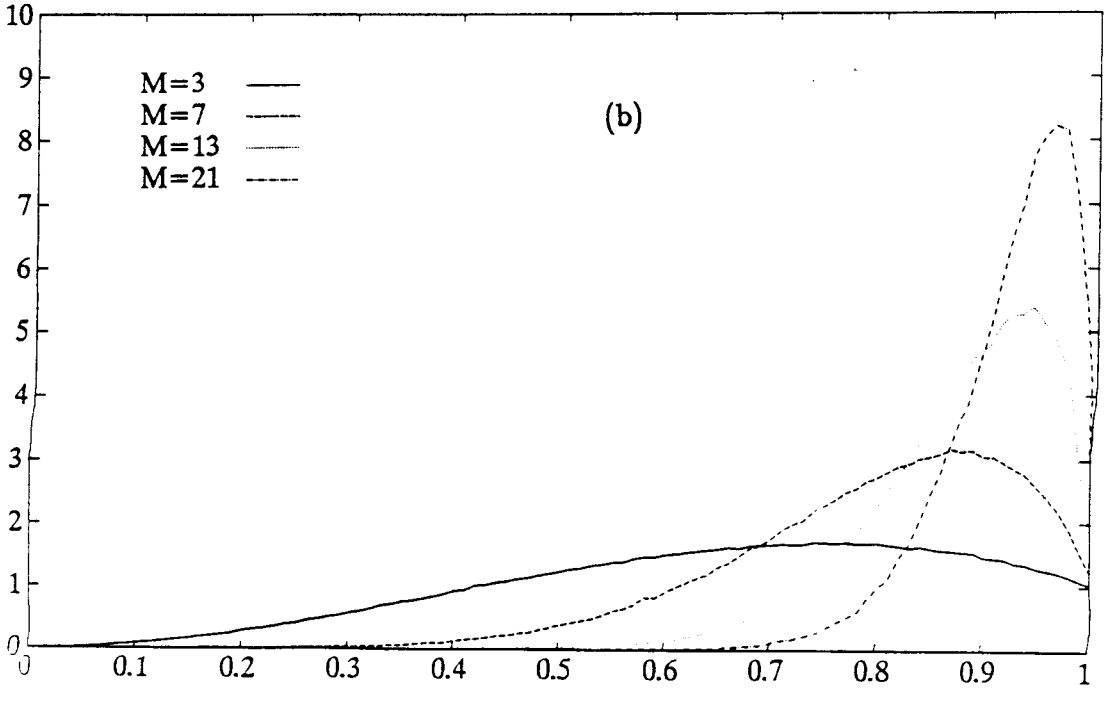

Figure 4.1 Output Density Function for a Flat Structuring Element when the Input Signal has a Uniform Density Function for:
(a) Dilation Operation (b) Closing Operation
(c) Clos-Erosion Operation (d) Clos-Opening Operation

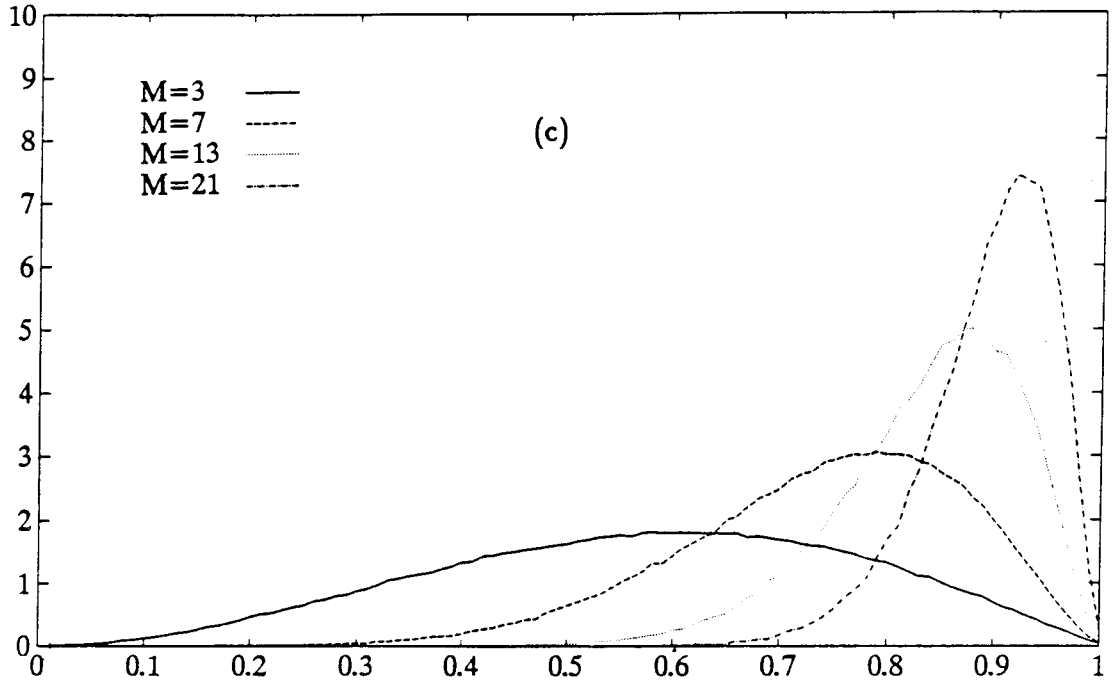

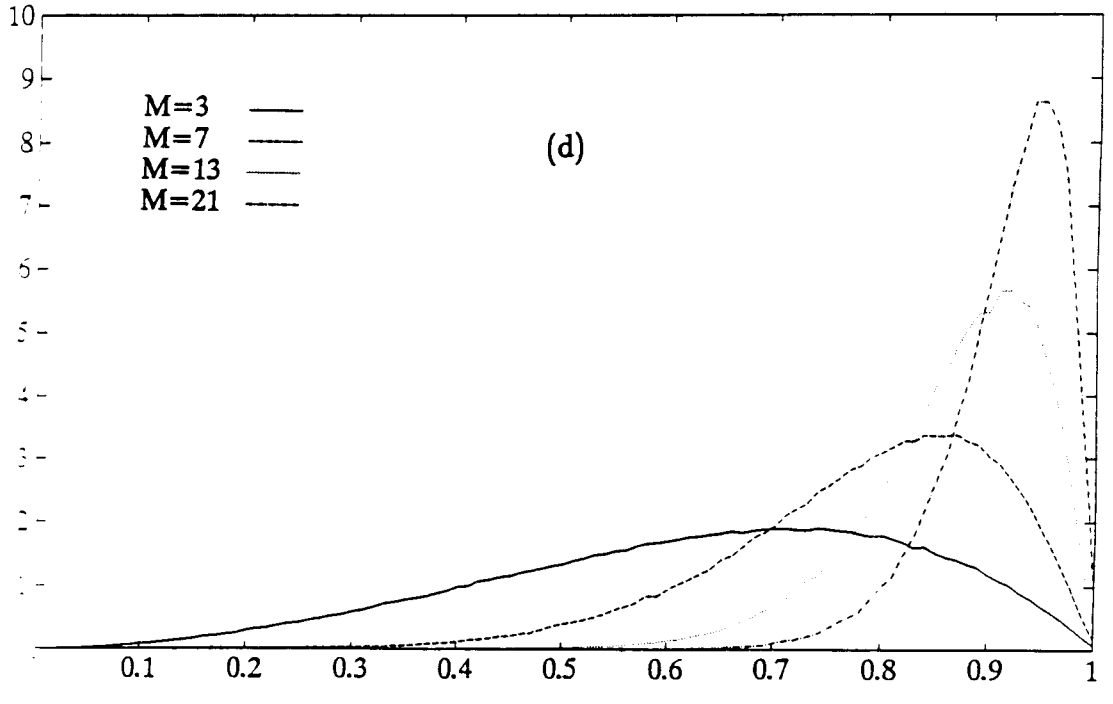

Figure 4.1 (Continued)

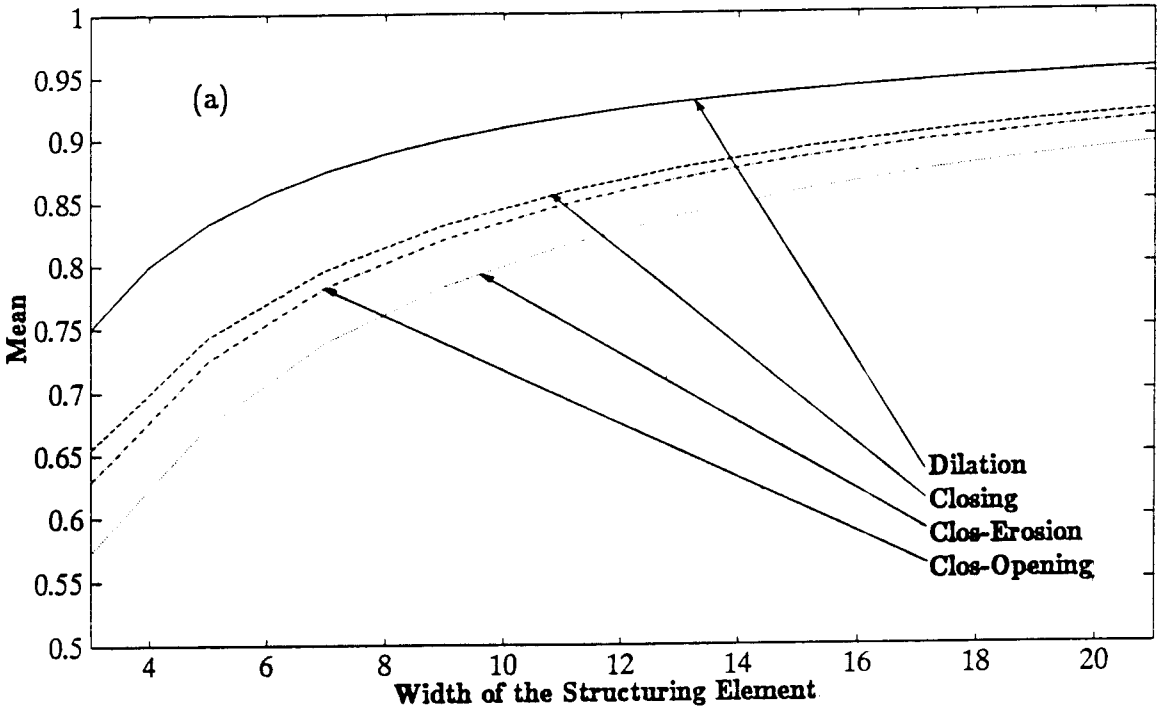

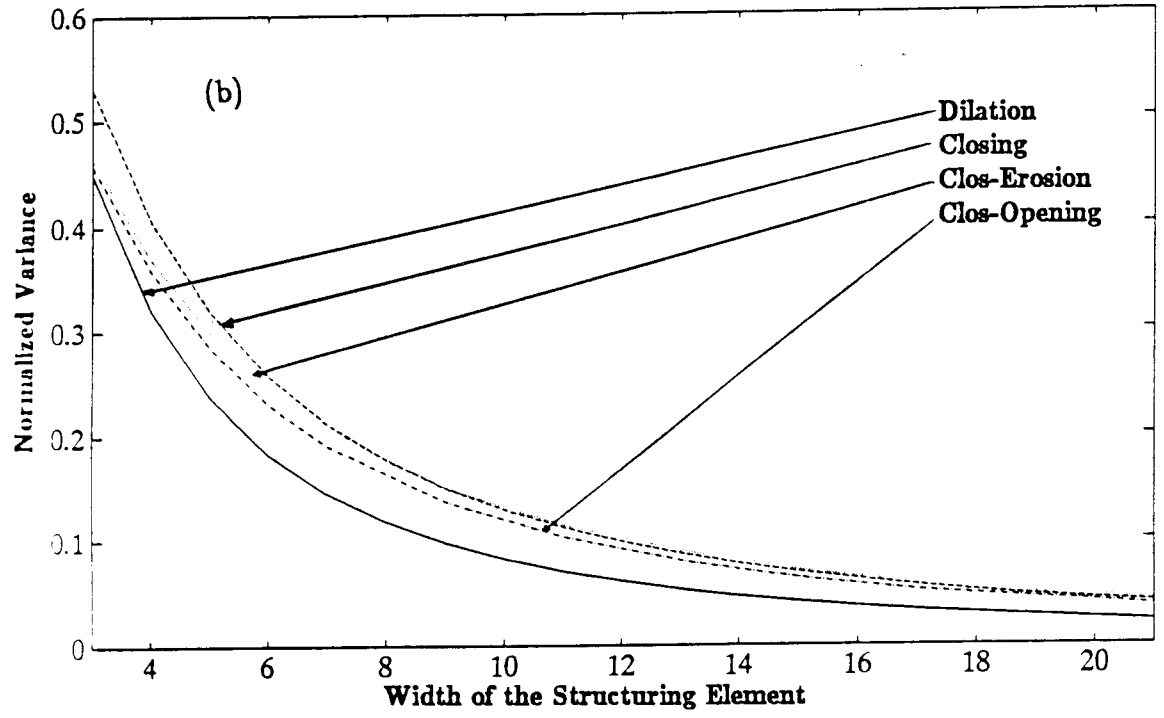

Figure 4.2 Mean, Normalized Variance and Skewness of Dilation, Closing, Clos-Erosion and Clos-Opening when the Input Signal has a Uniform Density Function using a Flat Structuring Element

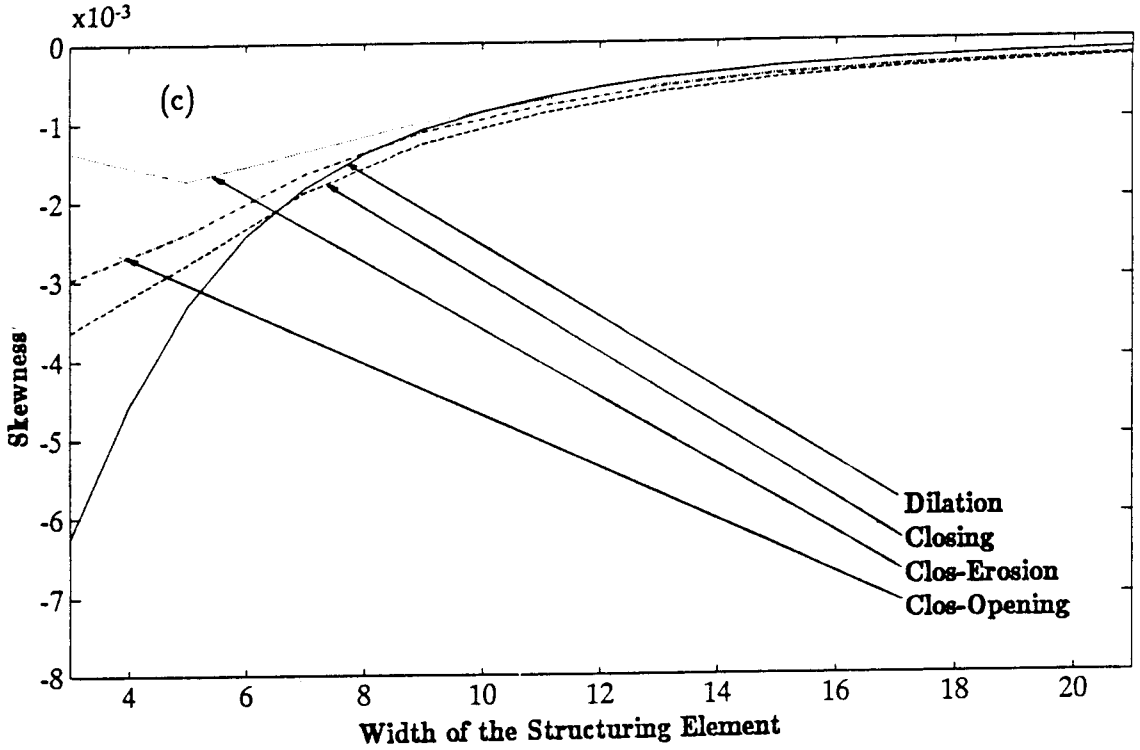

Figure 4.2 (Continued)

In this study, the statistical evaluation of morphological operations has been extended for input signals having iid Gaussian or Rayleigh density functions. Monte Carlo simulation is used to process the data sequence using the same procedure applied to the uniform density function. Figures 4.3 and 4.4 show the effect of flat structuring elements of different widths on dilation, closing, clos-erosion and clos-opening density functions when inputs are iid with a Gaussian density function (zero mean and variance equal to one) or a Rayleigh density function (with mean equal to $\sqrt{\pi/2}$ and variance $2(1 - \pi/4)$). Figures 4.5 and 4.6 show the mean, variance and skewness of dilation, closing, clos-erosion and clos-opening density functions versus the width of the flat structuring element, M, for Gaussian and Rayleigh density functions.

An inspection of Figures 4.3 - 4.6 suggests that the overall smoothing capability of the morphological filter applied to an input signal with a Gaussian or Rayleigh density function is similar to the results obtained for input signals with uniform distribution, although some differences can be noted.

The dilation density function has the least variance when input signals are uniformly distributed, although the clos-erosion density function has the smallest variance when input signals are Gaussian and Rayleigh distributed. The differences in the variance and skewness among dilation, closing, clos-erosion and clos-opening decrease as the width of the flat structuring element is increased when applied to input signals with a uniform density function. Contrary to this, the differences among dilation, closing, and clos-opening remain significant when the input signals have Gaussian or Rayleigh distributions. Therefore, the results describing the statistics of morphological filters applied to uniform density function can not be used to predict the performance associated with other types of density functions.

4.1.2 Results Using a Triangular Structuring Element Consideration of a triangular structuring element (representing a general shape) in the application of morphological filters offers the option to selectively interact with the shape of the

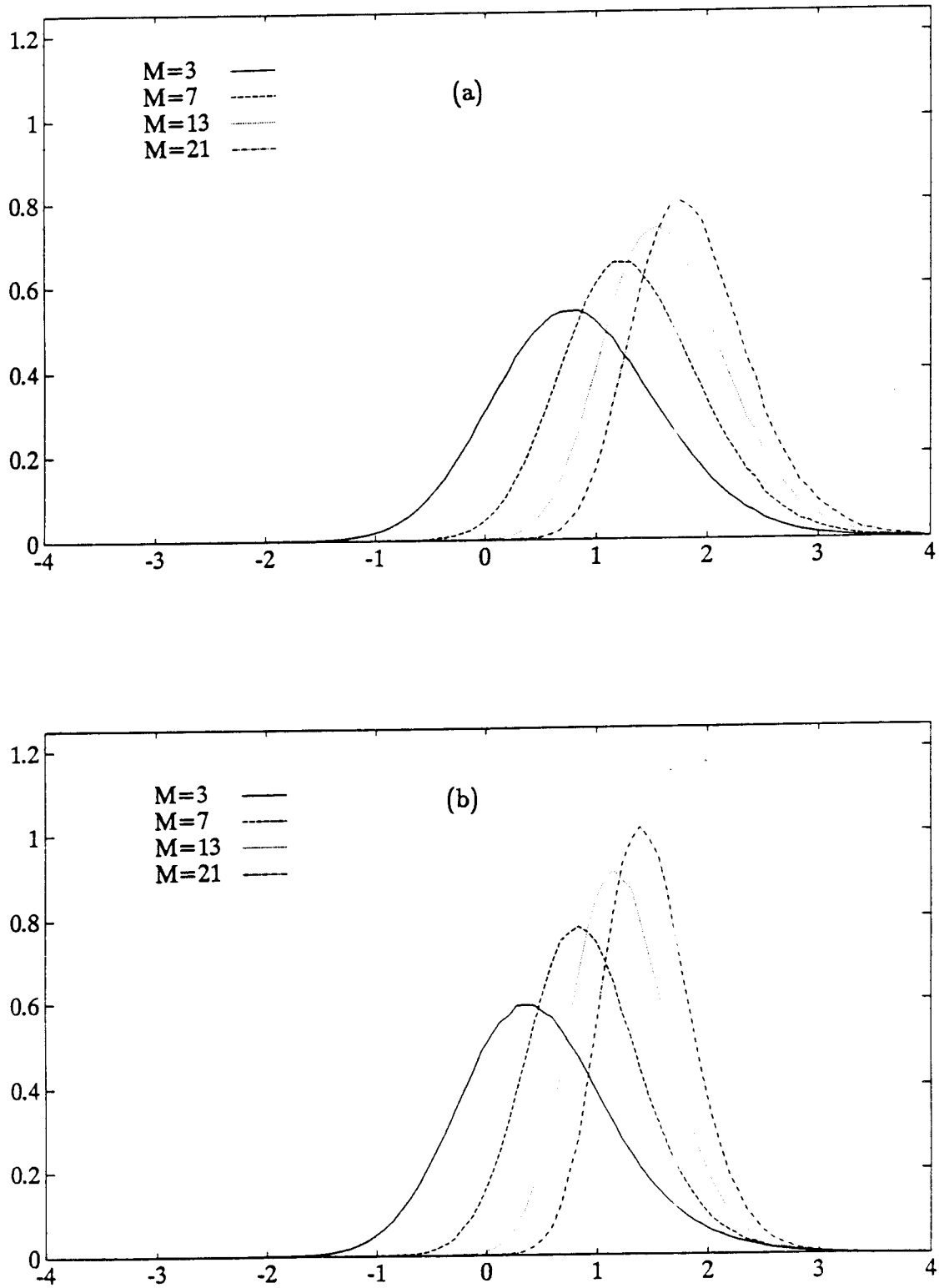

Figure 4.3 Output Density Function for a Flat Structuring Element when the Input Signal has a Gaussian Density Function for:
(a) Dilation Operation (b) Closing Operation
(c) Clos-Erosion Operation (d) Clos-Opening Operation

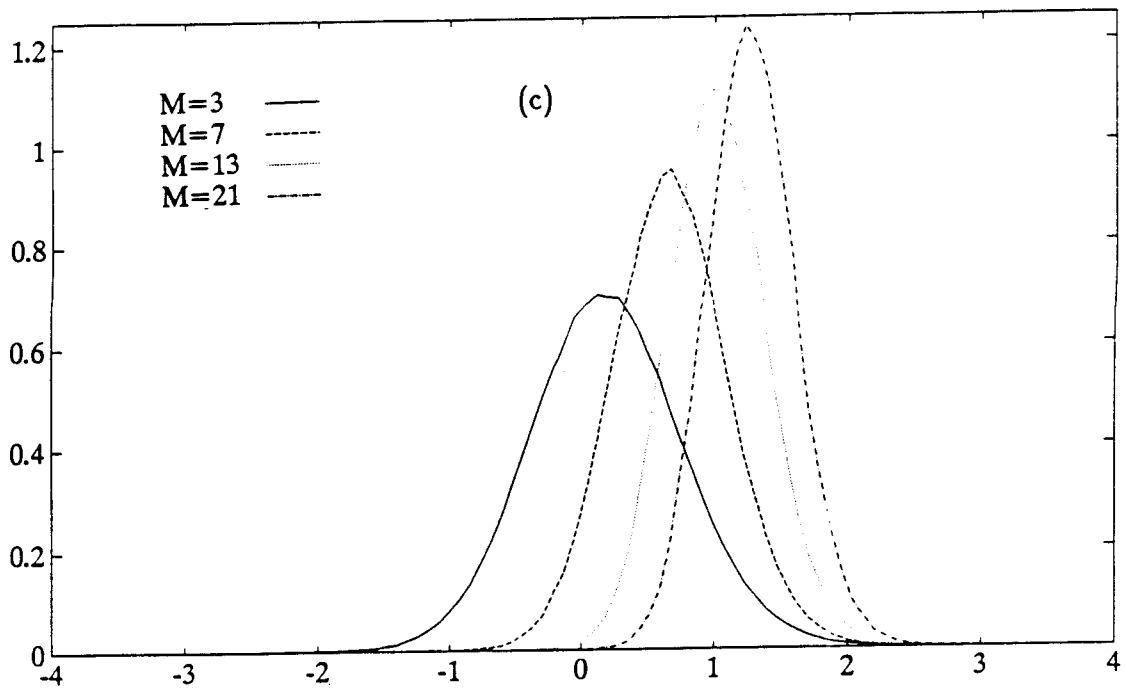

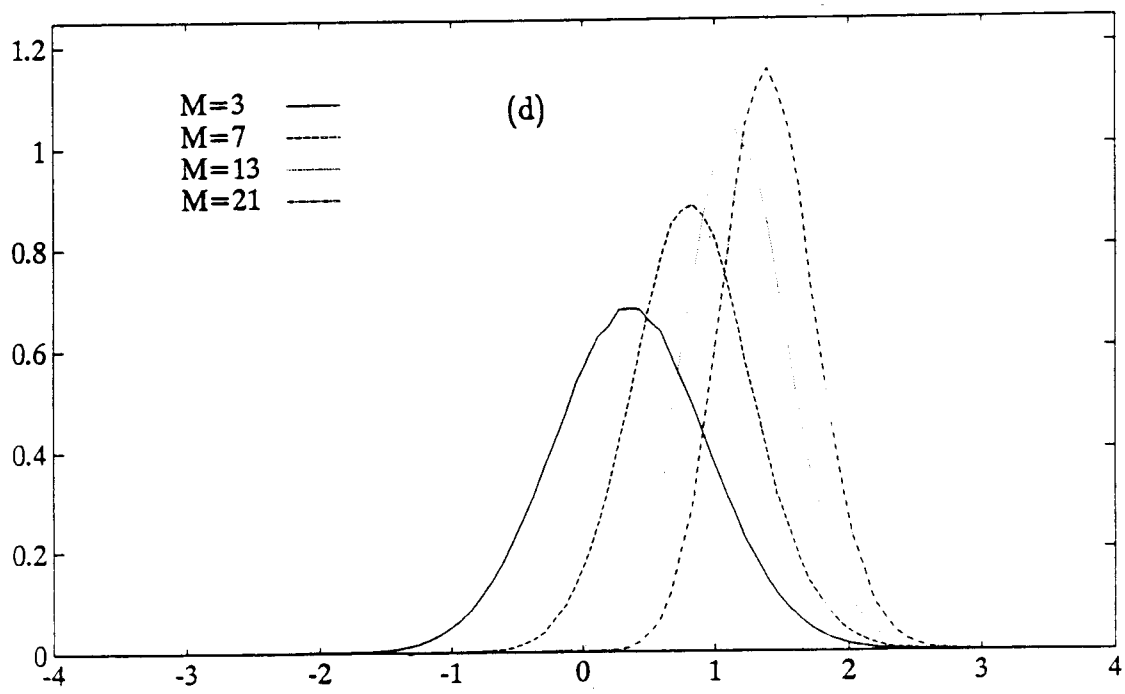

Figure 4.3 (Continued)

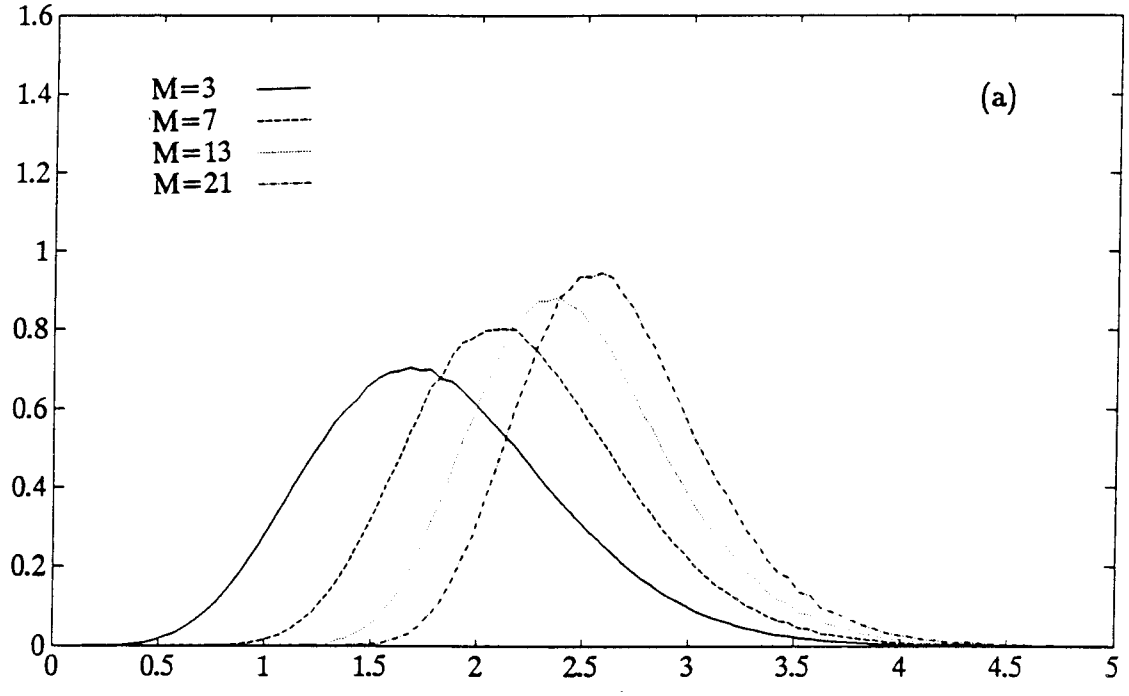

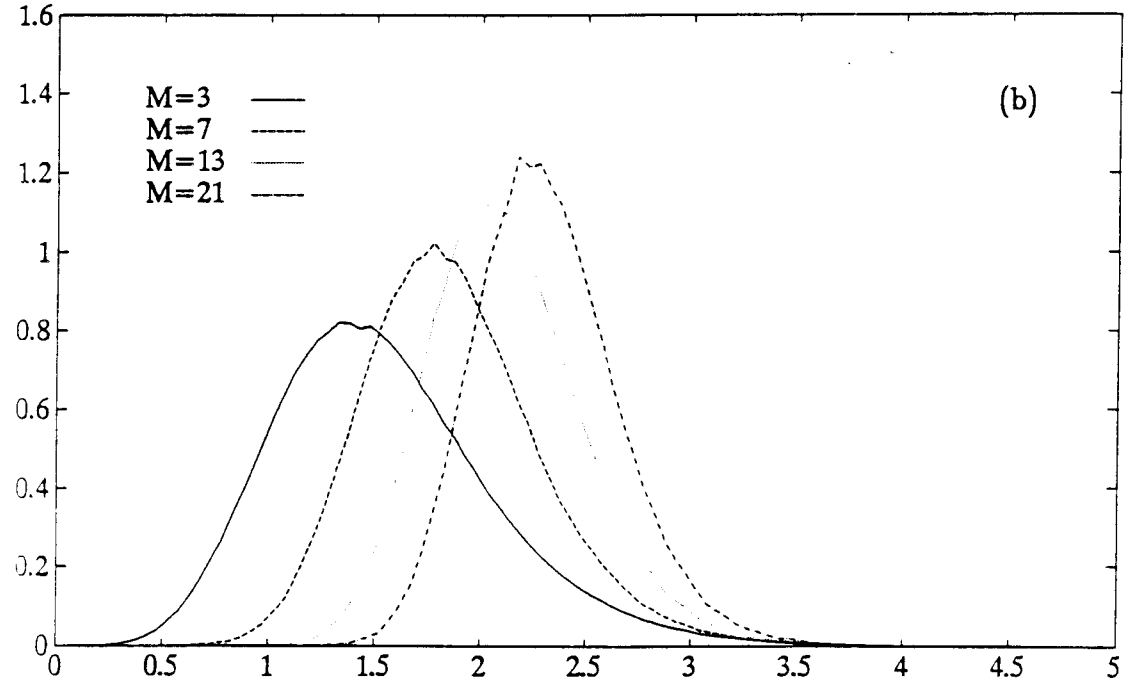

Figure 4.4 Output Density Function for a Flat Structuring Element when the Input Signal is Rayleigh Density Function for:
(a) Dilation Operation (b) Closing Operation
(c) Clos-Erosion Operation (d) Clos-Opening Operation

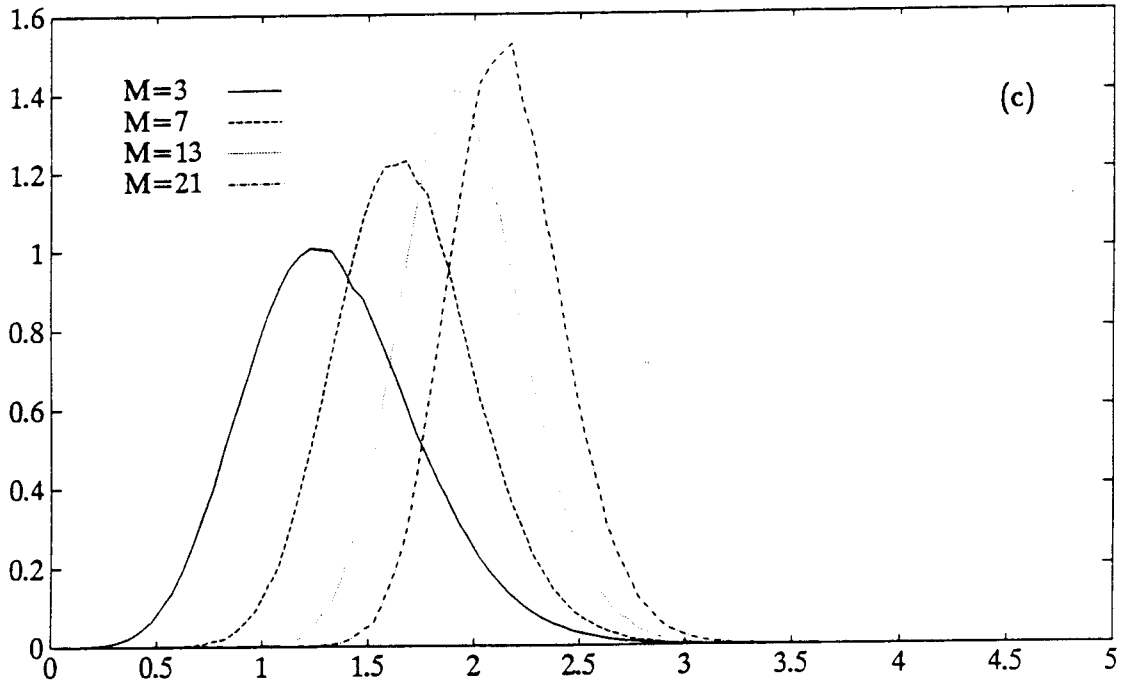

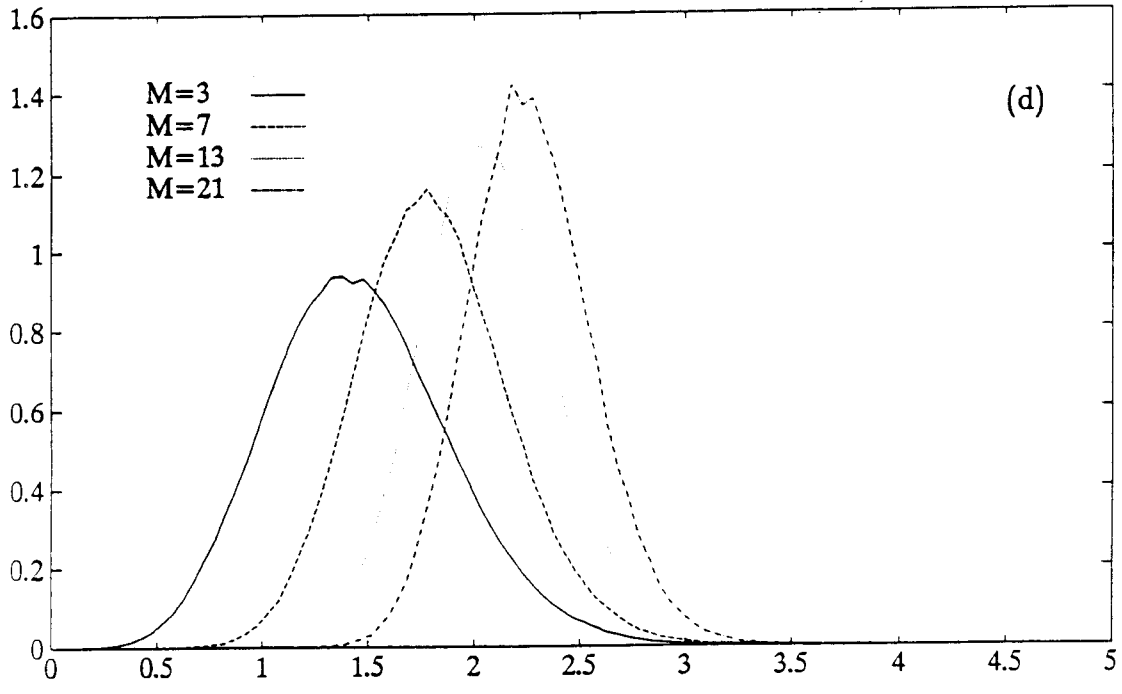

Figure 4.4 (Continued)

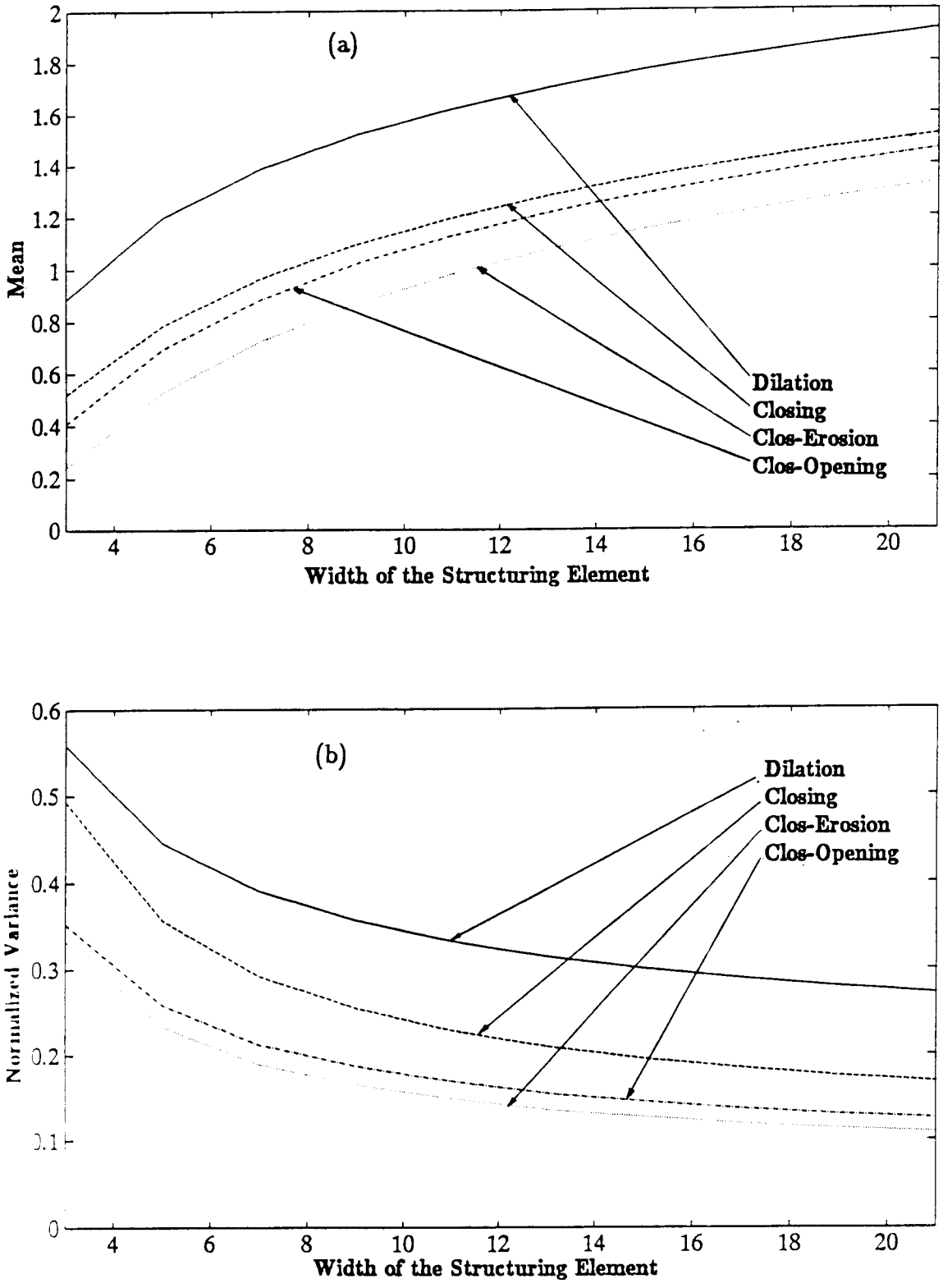

Figure 4.5 Mean, Normalized Variance and Skewness of Dilation, Closing, Clos-Erosion and Clos-Opening when the Input Signal has a Gaussian Density Function using a Flat Structuring Element

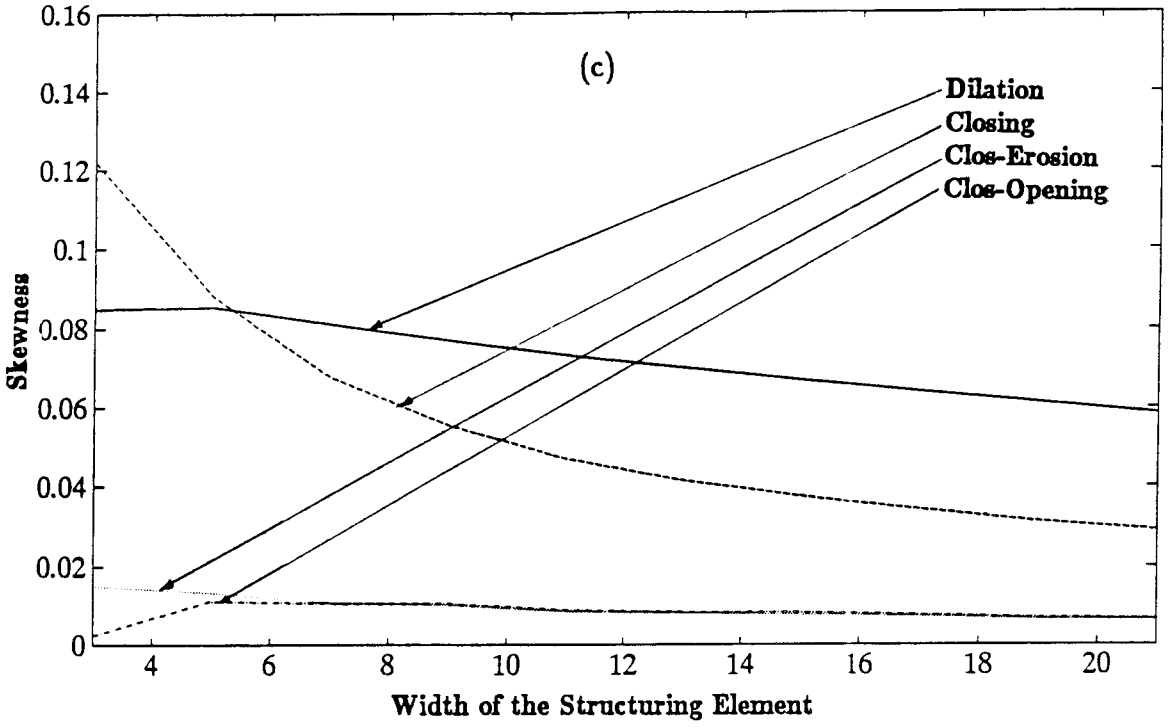

Figure 4.5 (Continued)

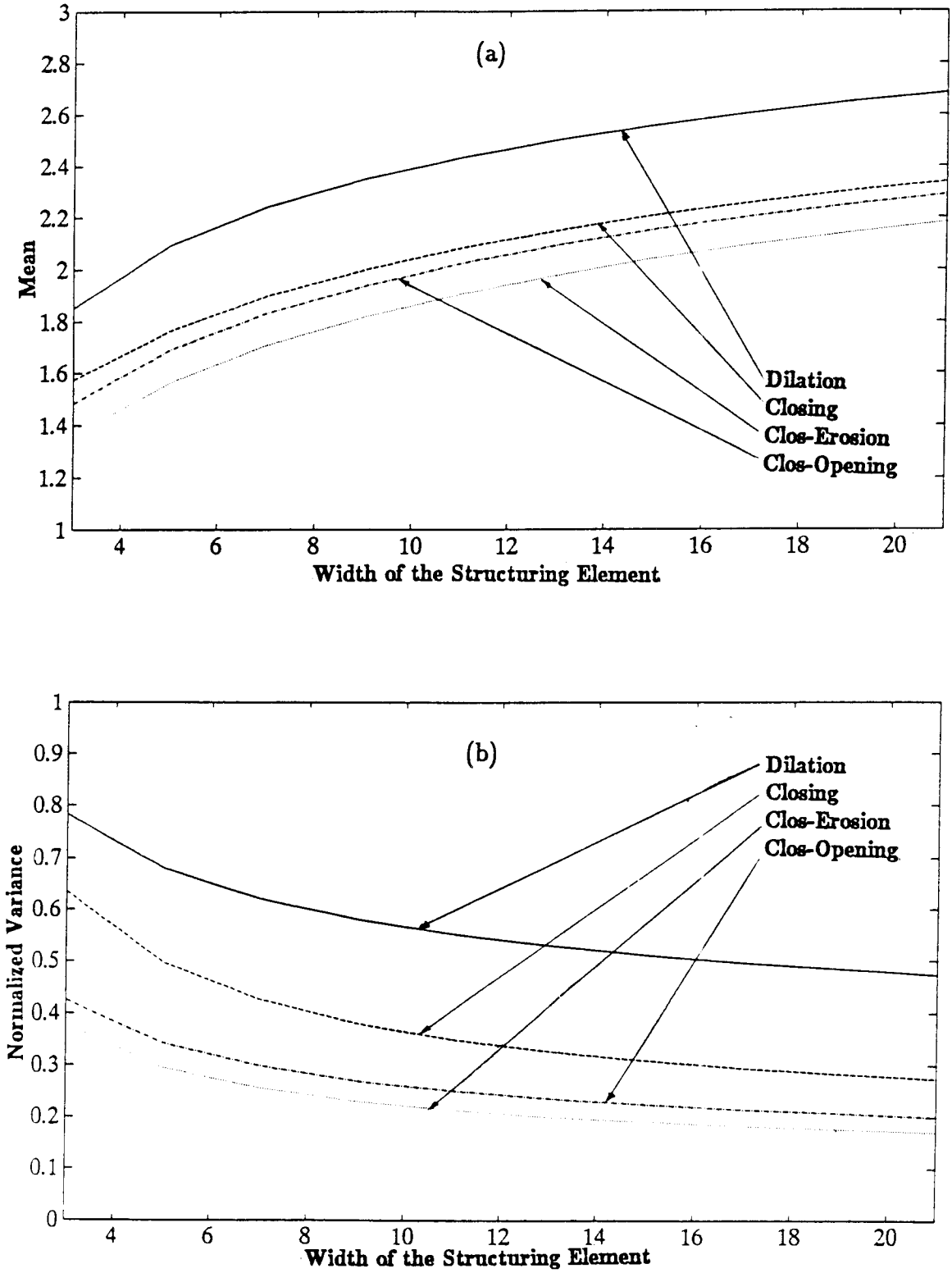

Figure 4.6 Mean, Normalized Variance and Skewness of Dilation, Closing, Clos-Erosion and Clos-Opening when the Input Signal has a Rayleigh Density Function using a Flat Structuring Element

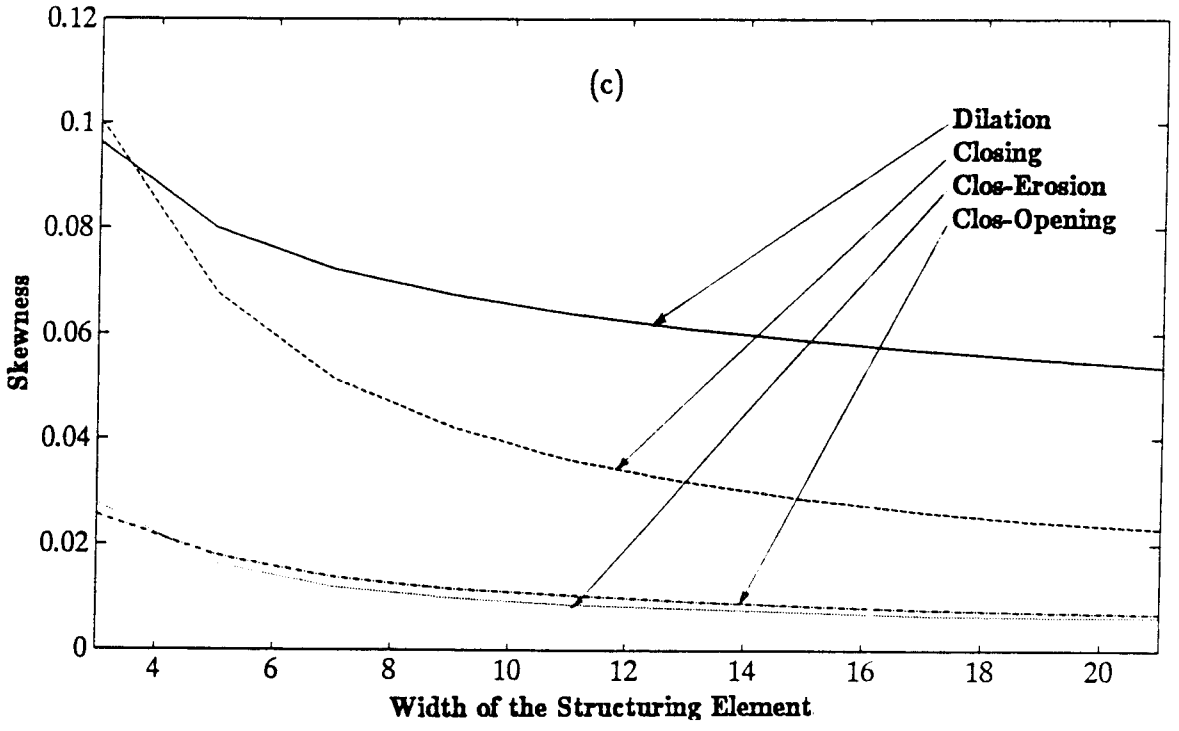

Figure 4.6 (Continued)

multilevel signal. In this study, the considered triangular structuring element is symmetrical with width M and height A. Figure 4.7 shows the output density function when: i) the input signals are iid uniformly distributed (range between zero and one), ii) the triangular structuring element has a different width, M, and height, A=0.2 (i.e., 20% of the dynamic range of the input signal), and iii) the processing operations are dilation, closing, clos-erosion and clos-opening). Monte Carlo simulation is used to obtain these results using the same data sequences as were simulated for a flat structuring element. Similar to the performance of the flat structuring element, the triangular structuring element smooths the signal, the variance decreases by increasing the width and the first stage, i.e., dilation is the most critical one in reducing of signal variance. Figures 4.8 - 4.10 show the mean, normalized variance and skewness of dilation, closing, clos-erosion and clos-opening using triangular structuring elements with different heights, A, and different widths, M. Inspection of these results suggests the following characteristics for morphological operations.

For the same width of a triangular structuring element, the mean (bias) of the dilation density function increases by increasing the height, i.e., the signal is biased to higher values while the mean of the closing, clos-erosion and clos-opening density function decreases by increasing the height. For a given height, A, the mean of dilation shows the largest value and the clos-erosion the lowest. For the same height A, the mean of dilation, closing, clos-erosion and clos-opening density functions increases by increasing the width of triangular structuring element while the variance decreases by increasing the width. For the same width, M, the variance of all density functions decreases by decreasing the height of the structuring element, i.e., the smoothing becomes more pronounced by increasing the width or decreasing the height of the triangular structuring element.

The closing density function has a slightly greater mean, variance and skewness than the clos-opening density function when the height, A=0.2 (i.e., A is 20% of the dynamic range of the input signal) but their statistics are almost equal when

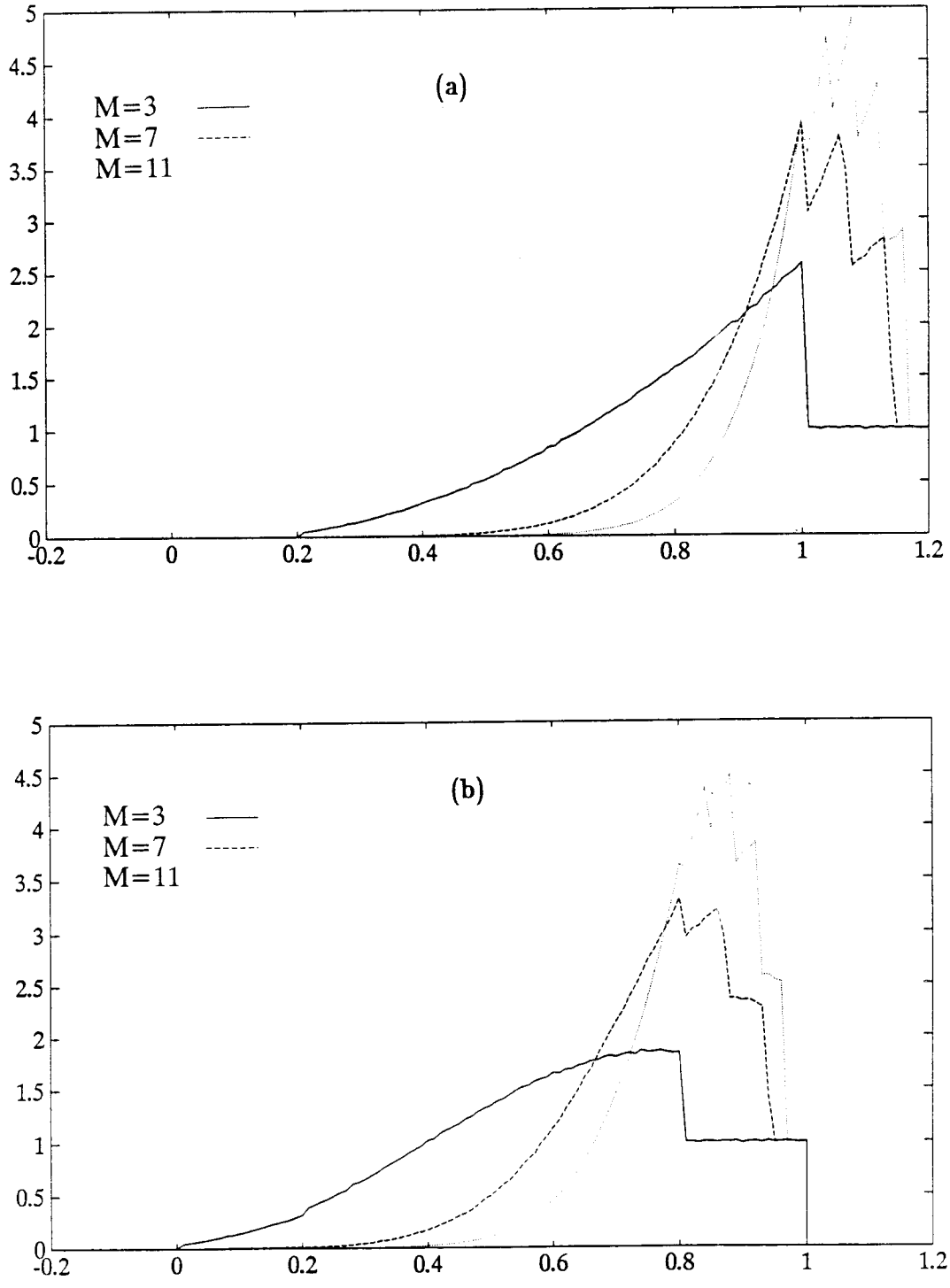

Figure 4.7 Output Density Function when the Input Signal has a Uniform Density Function for a Triangular Structuring Element with a Height A=20% of the Dynamic Range of the Input Signal for:
(a) Dilation Operation (b) Closing Operation
(c) Clos-erosion Operation (d) Clos-Opening Operation

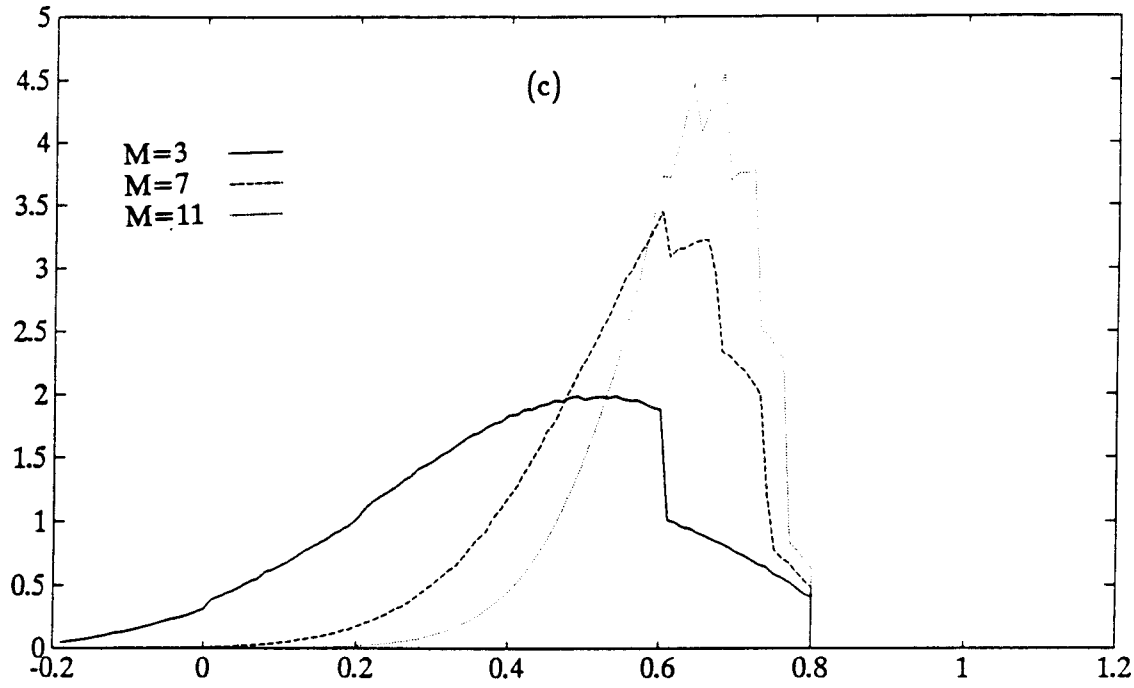

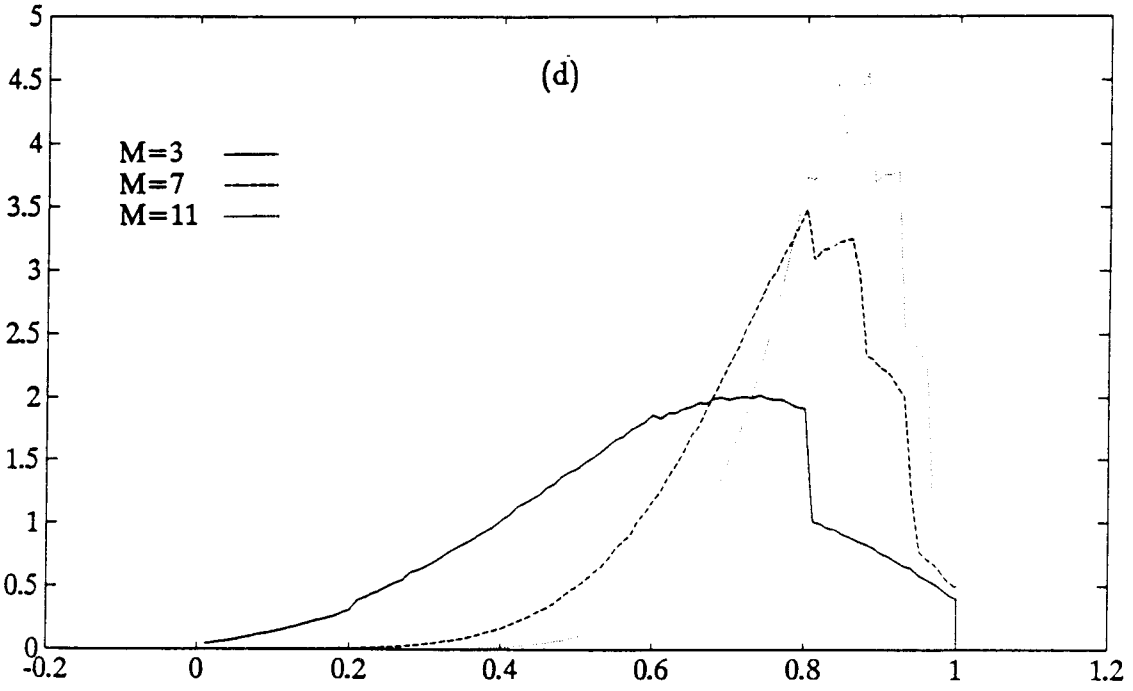

Figure 4.7 (Continued)

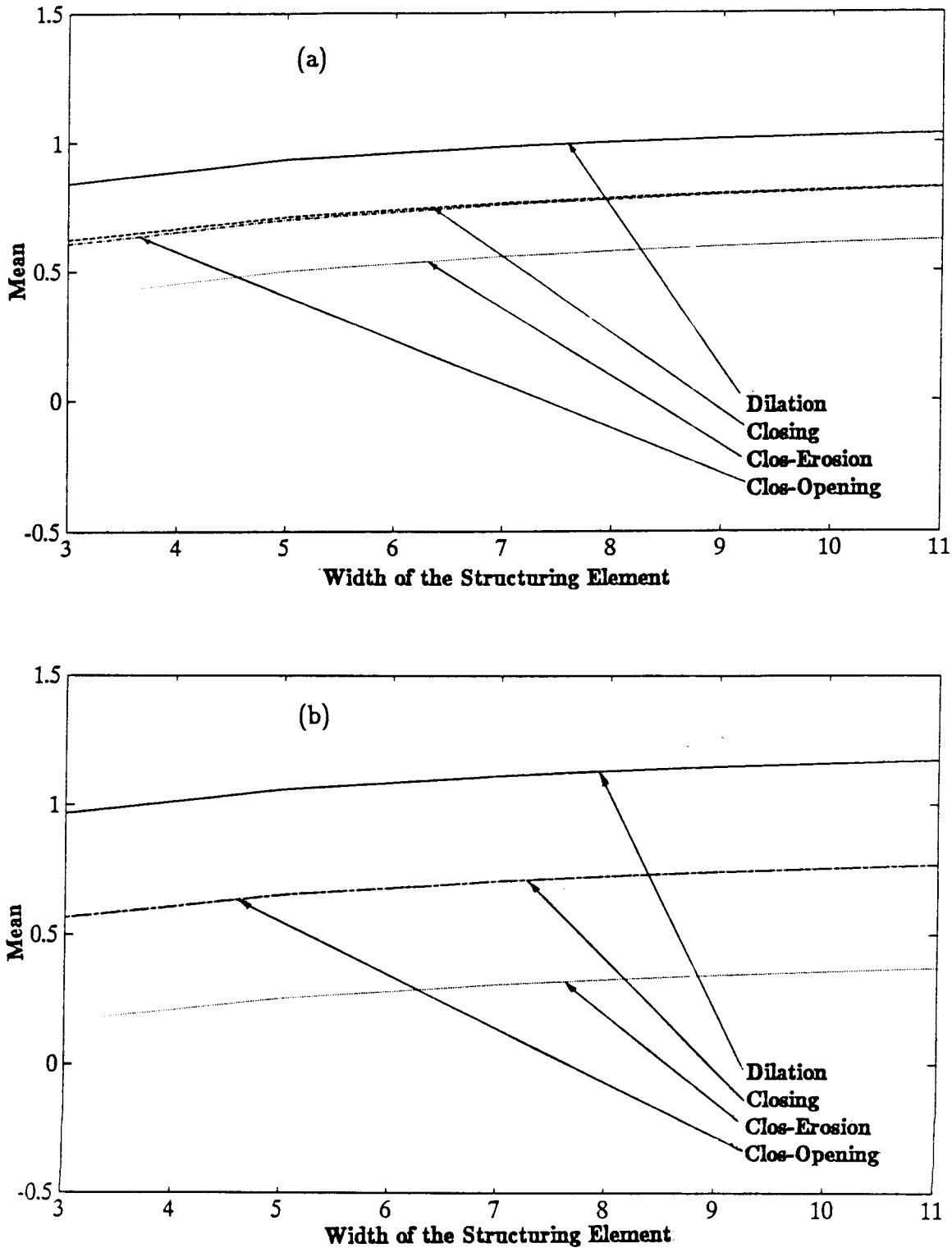

Figure 4.8 Mean of Dilation, Closing, Clos-Erosion and Clos-Opening when the Input has a Uniform Density Function using a Triangular Structuring Element with a Height A :

(a) A=0.2 (b) A=0.4

(c) A=0.6 (d) A=0.8

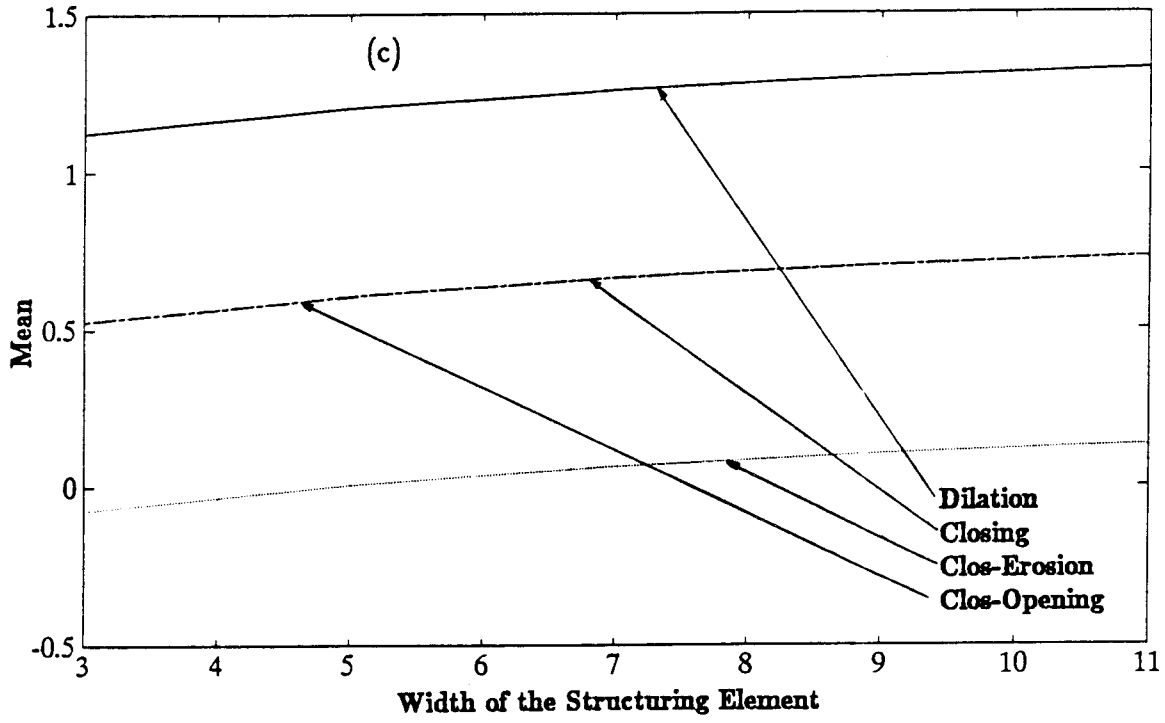

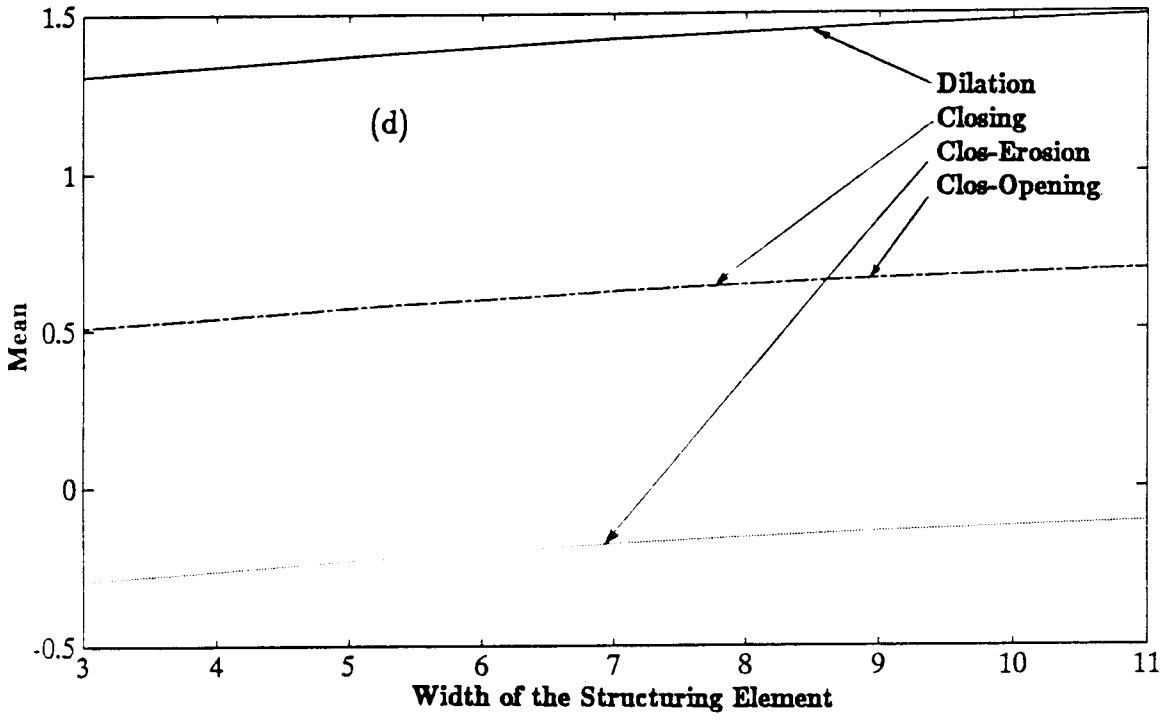

Figure 4.8 (Continued)

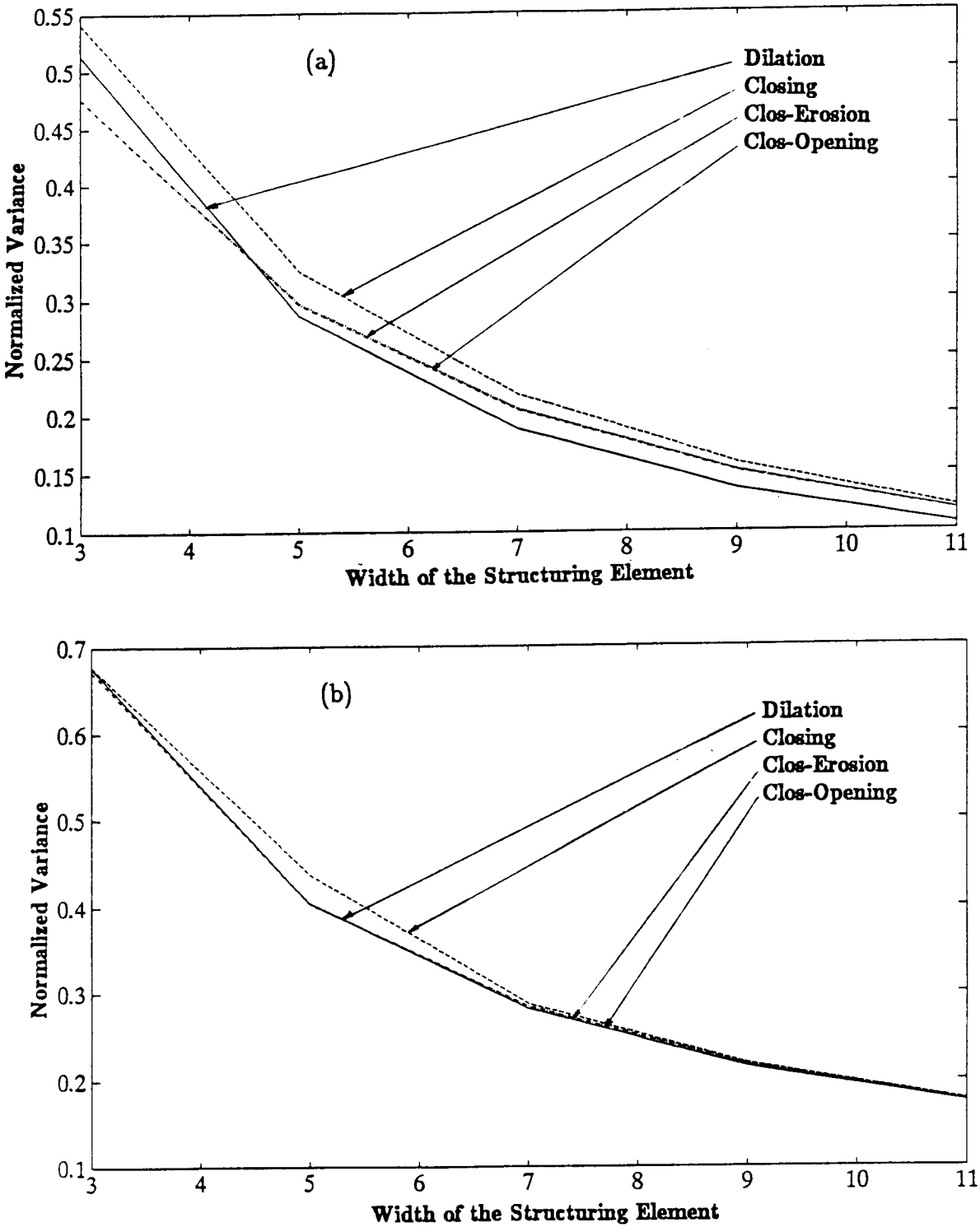

Figure 4.9 Normalized Variance of Dilation, Closing, Clos-Erosion and Clos-Opening when the Input Signal has a Uniform Density Function using a Triangular Structuring Element with a Height A :
(a) A=0.2 (b) A=0.4
(c) A=0.6 (d) A=0.8

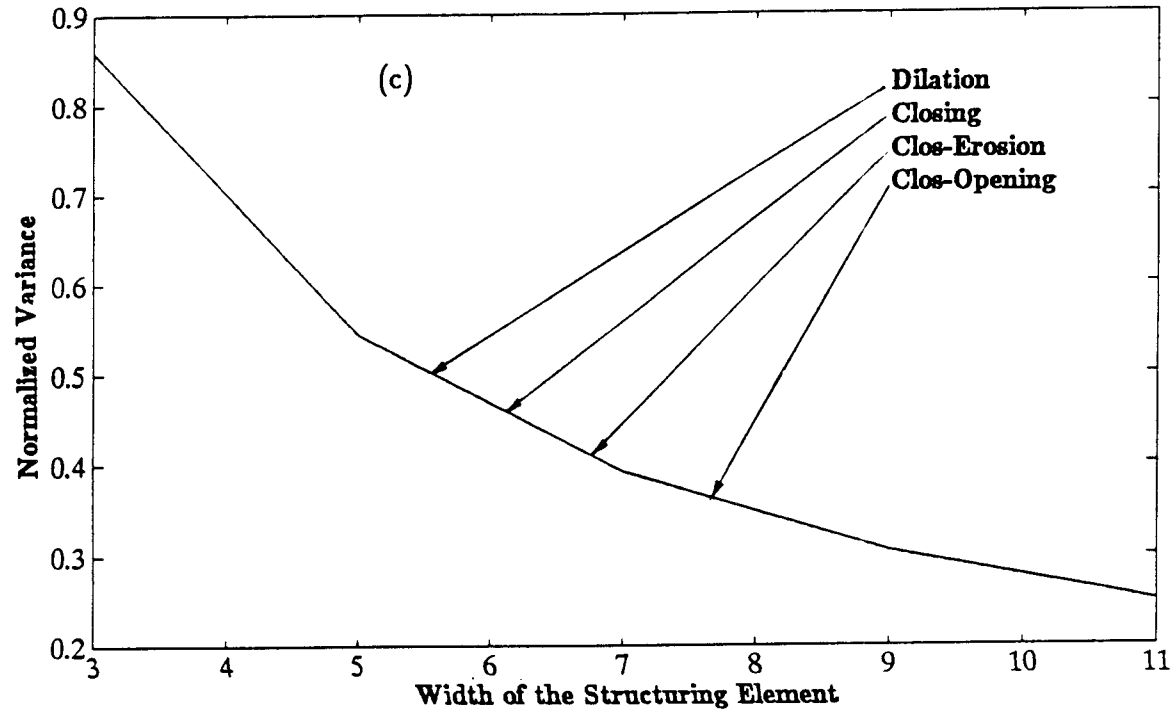

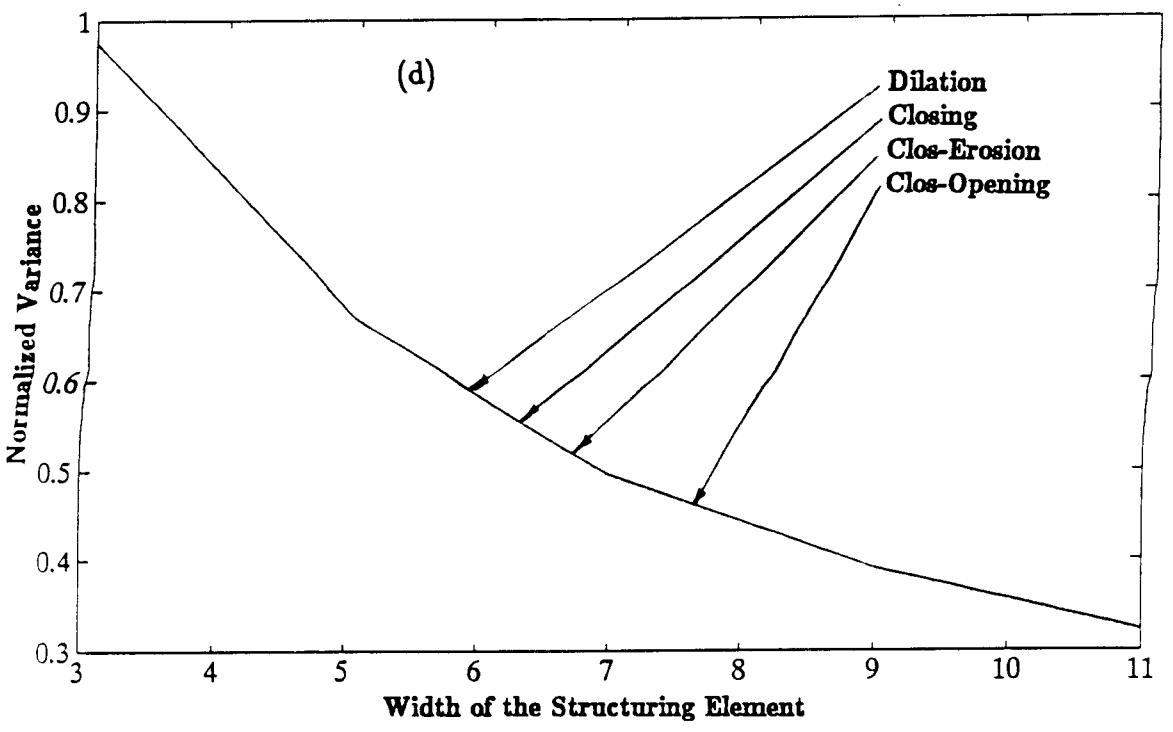

Figure 4.9 (Continued)

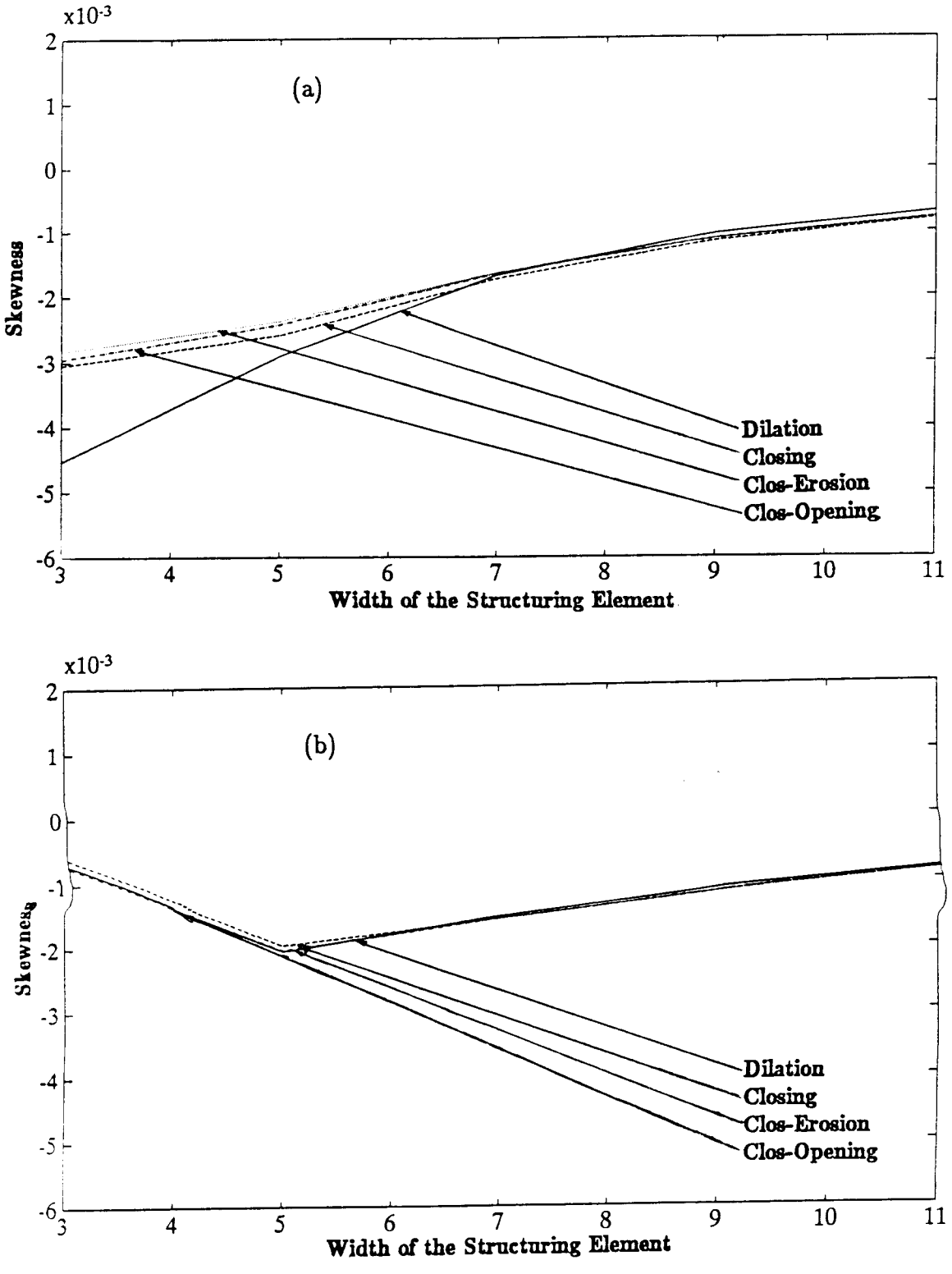

Figure 4.10 Skewness of Dilation, Closing, Clos-Erosion and Clos-Opening when the Input Signal has a Uniform Density Function using a Triangular Structuring Element with a Height A :
(a) A=0.2 (b) A=0.4
(c) A=0.6 (d) A=0.8

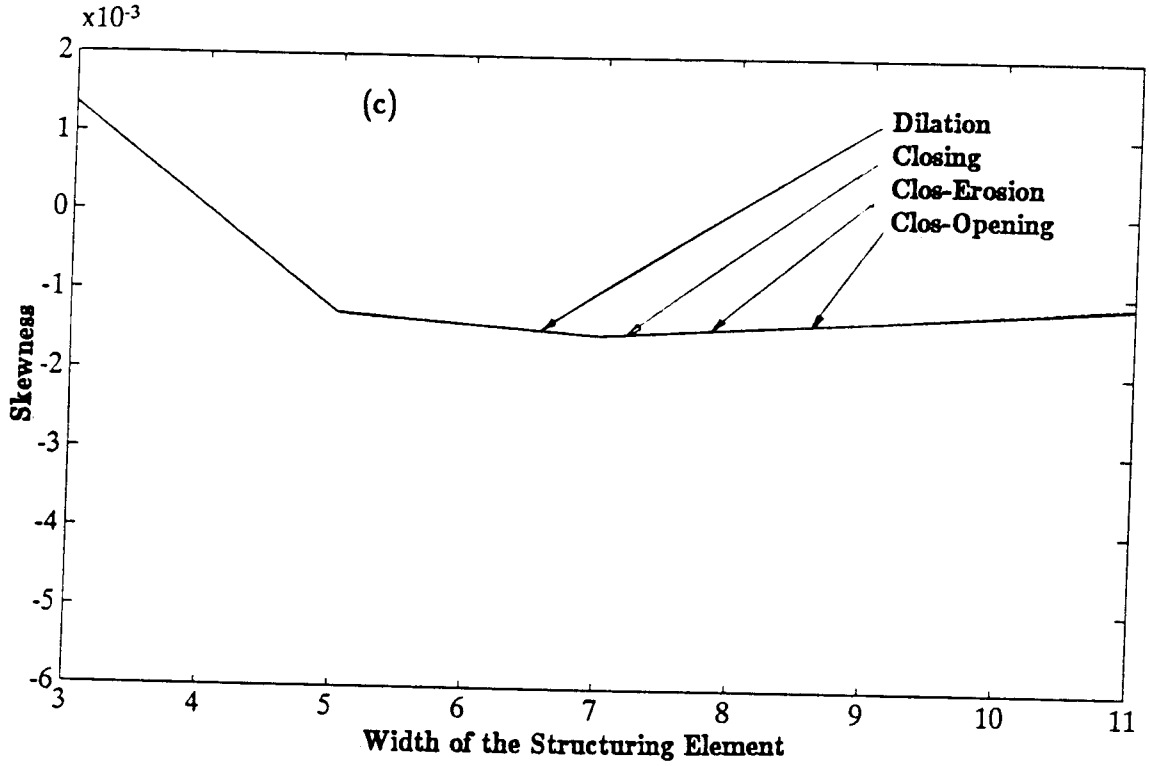

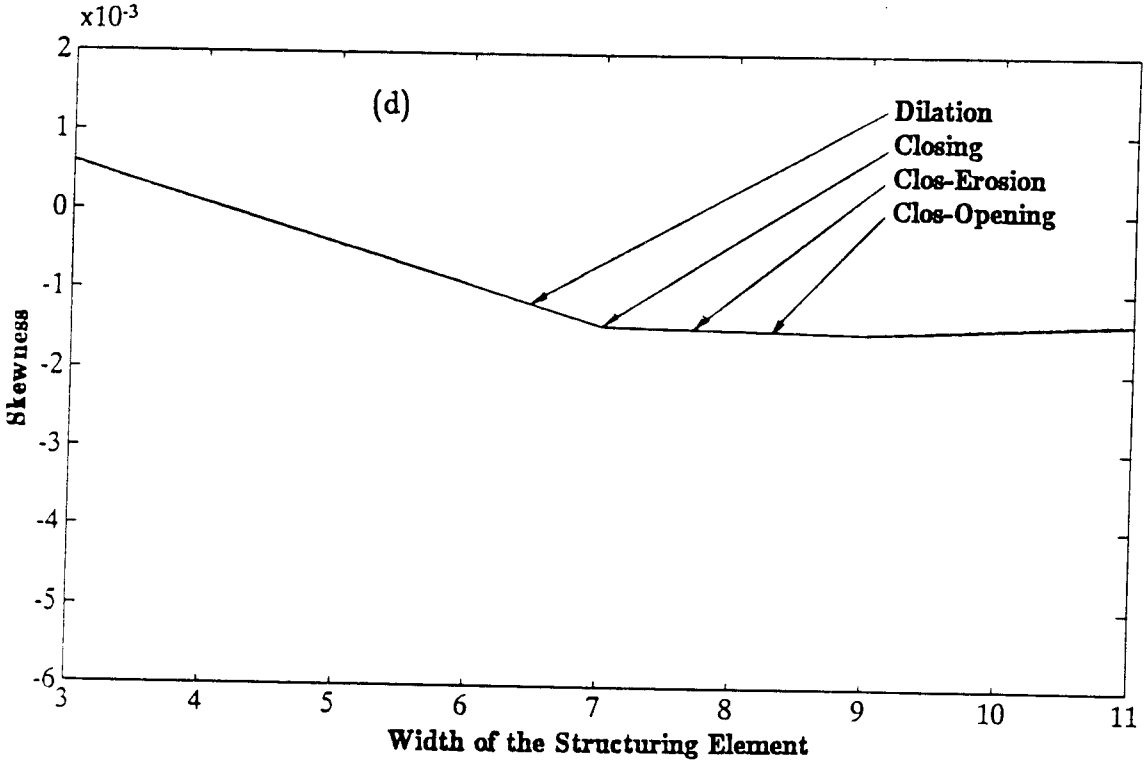

Figure 4.10 (Continued)

the height , A≥0.6 (i.e., the similarity in shape between closing and clos-opening density functions increases by increasing the height of the triangular structuring element). Moreover, when the height A≥0.6 the closing density function is exactly equal to the shifted dilation density function by a constant A, and the closing and clos-opening have exactly the same density functions. Also, when the height A≥0.6, the clos-erosion density function is equal to the closing density function shifted by value A. This means that the root of the signal is found after the first stage (i.e., dilation). Therefore, if operations are repeated after dilation, only the density function is shifted to the right or left depending on the operation (dilation or erosion). An example of the performance of a triangular structuring element when the input has a uniform density function {0,1} is shown in Figure 4.11. The input has 200 samples and the structuring element has a width M=7 and a height A=0.6. This Figure indicates that the closing signal is similar to the dilated signal except that there is an offest equal to 0.6. The differences in the variance and in skewness between dilation, closing, clos-erosion and clos-opening density functions decrease when the height of the structuring element is increased.

A comparison between the output density function of closing for the uniform density function using a flat structuring element with a width M=7 and triangular structuring element with a width M=7 and different heights is shown in Figure 4.12. Figure 4.13 shows the variance of a closing density function for a flat and triangular structuring element with different heights. These figures show that to obtain the same variance equal to 0.03, a flat structuring element with a width of M=5, a triangular structuring element with a width of M=7 and height of A=0.4, or one with a width of M=9 and height of A=0.6 can be used. This suggests that, to obtain the same output variance, we can use a flat structuring element with a smaller width than a triangular structuring element. Also, if the width of the triangular structuring element decreases, the height must be decreased to maintain the same variance.

The statistical analysis of a triangular structuring element has also been

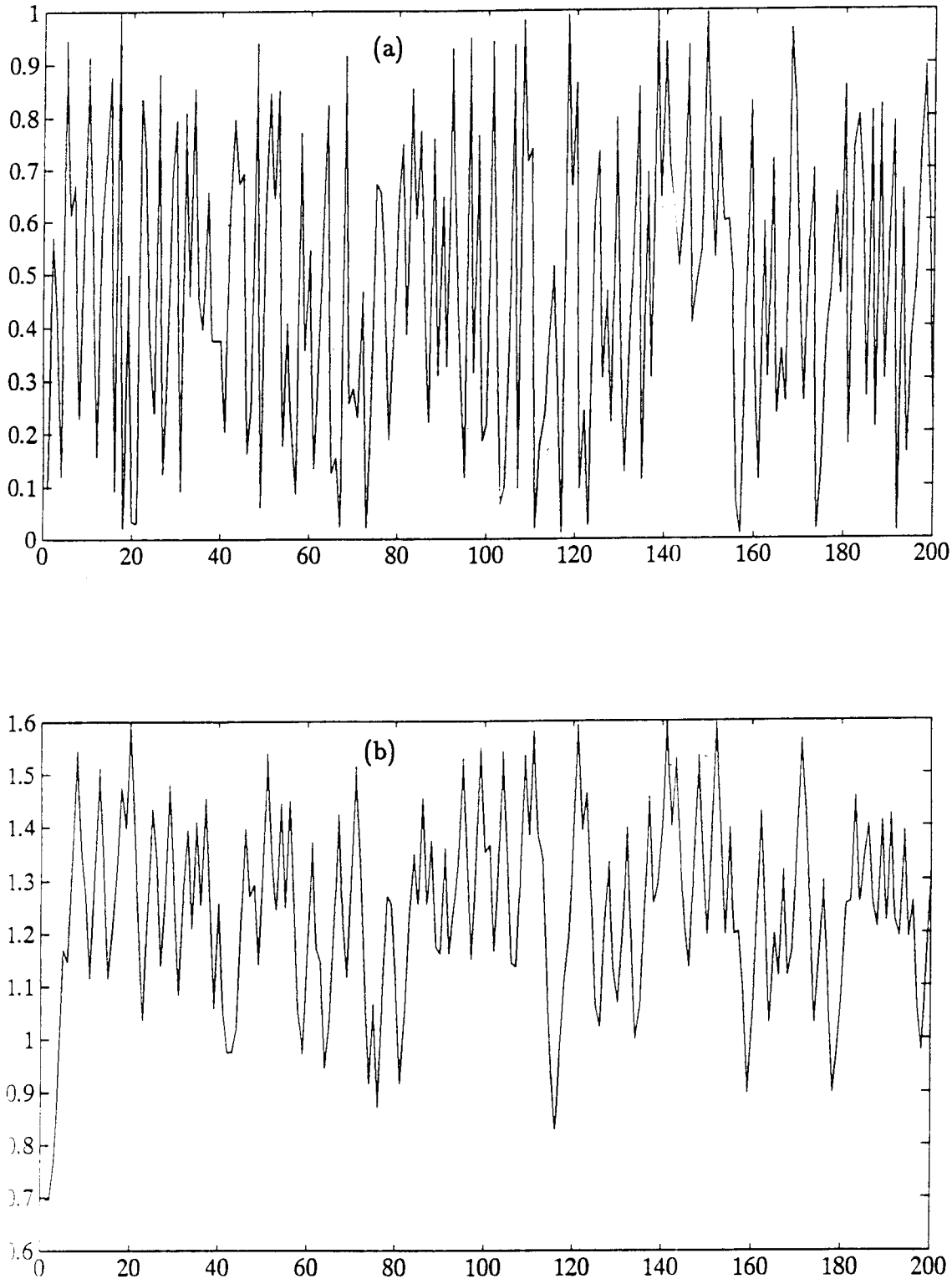

Figure 4.11 (a) Input Signal with a Uniform Density Function
(b) The Dilated Signal using Triangular Structuring Element
(c) The Closed Signal using Triangular Structuring Element

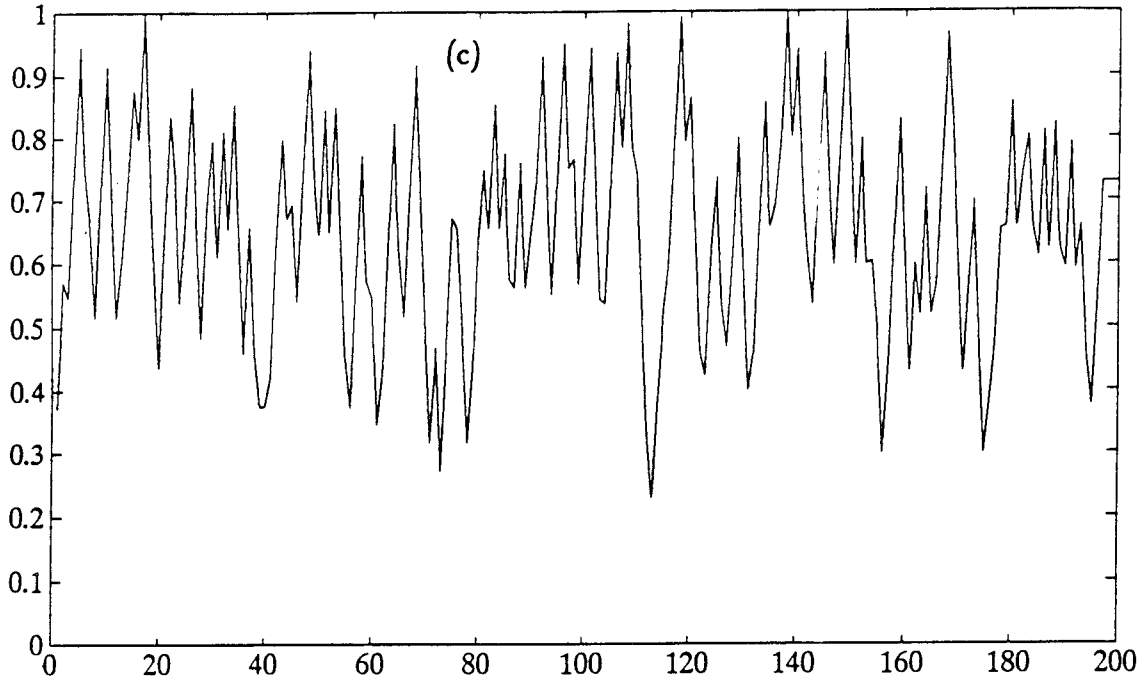

Figure 4.11 (Continued)

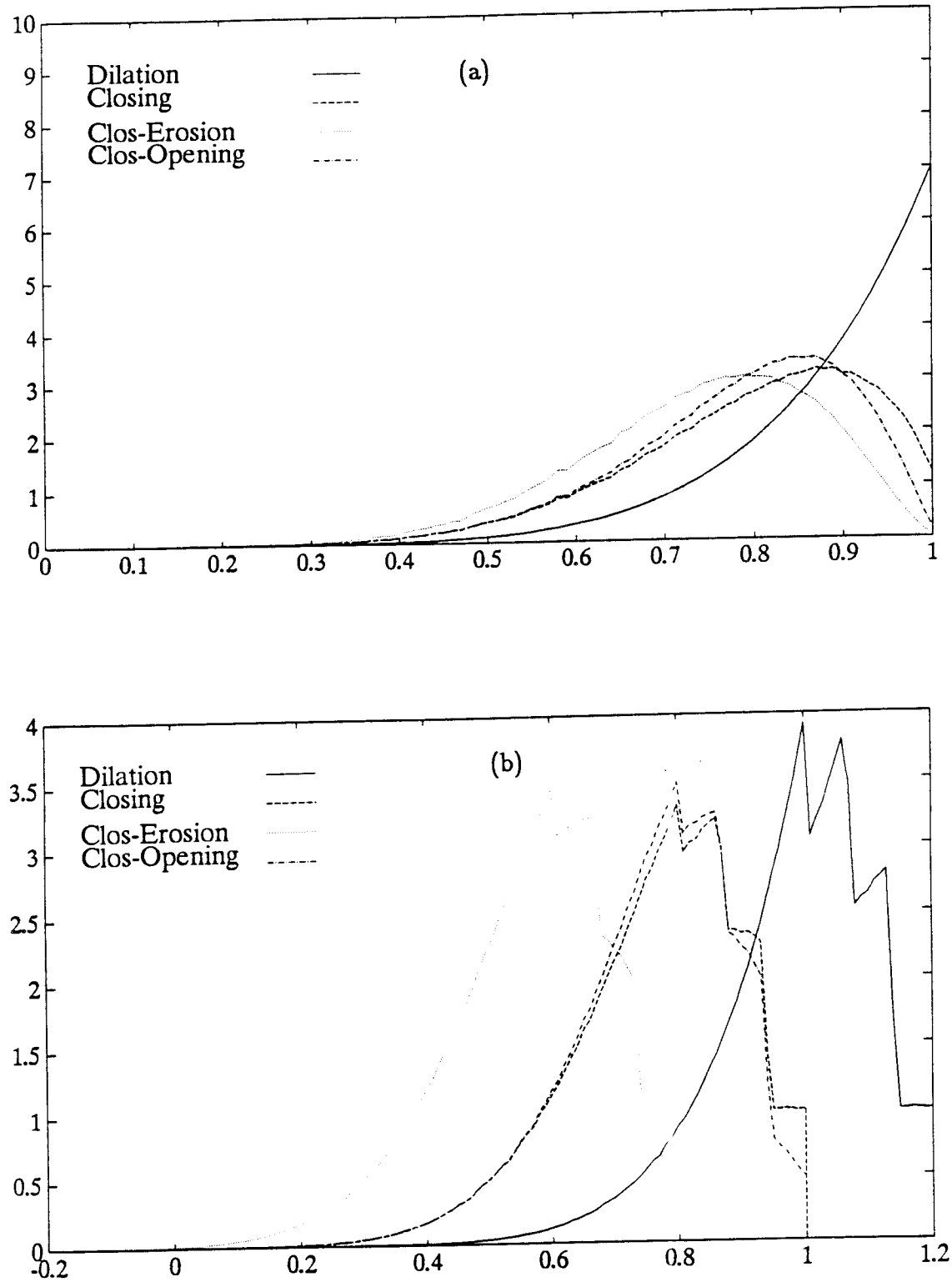

Figure 4.12 A Comparison between Dilation, Closing, Clos-Erosion, and Clos-Opening for:
(a) Flat Structuring Element with a Width M=7
(b) Triangular Structuring Element with a Width M=7 and a Height A=0.2

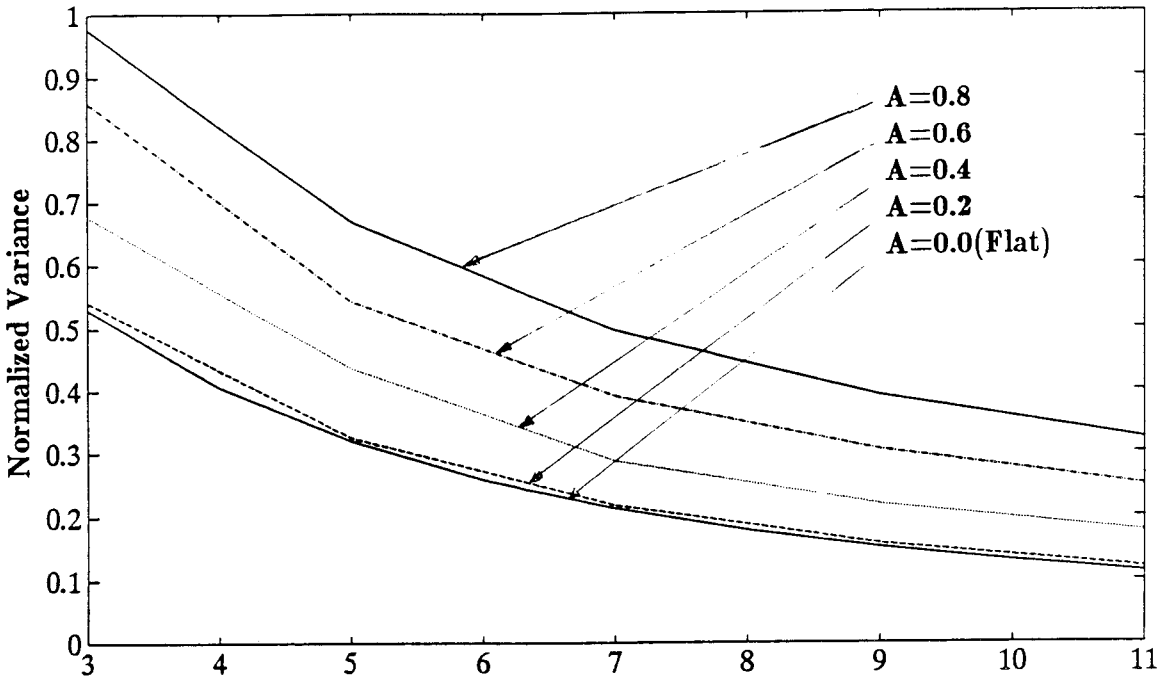

Figure 4.13 A Comparison between the Variance of a Closing Density Function for Uniform Density Function using a Flat and Triangular Structuring Element

extended to input signals with Gaussian or Rayleigh distributions. The dilation, closing, clos-erosion and clos-opening output density functions are shown in Figures 4.14 and 4.15 when inputs are iid with a Gaussian density function (zero mean and variance equal to one) and a Rayleigh density function (with a mean equal to $\sqrt{\pi/2}$ and a variance $2(1 - \pi/4)$). The triangular structuring elements have different widths M and a height A=20% of the dynamic range of the input signal. The mean, variance and skewness of the above density function are shown in Figures 4.16 - 4.21 for different widths, M, and heights, A, of the triangular structuring element.

Inspection of these results indicates that the statistical outcome of morphological filters using a triangular structuring element is very similar to a flat structuring element with a few noticeable differences. For the same height of a triangular structuring element, the skewness of dilation, closing, clos-erosion and clos-opening decreases by increasing the width when the inputs are Gaussian or Rayleigh ($M \geq 5$) distributed. However, when the inputs are uniformly distributed, the change in the skewness is irregular and not predictable (For clarification see Figure 4.1)

A comparison between the performance of a flat and a triangular structuring element for Gaussian density function is shown in Figure 4.22. This figure with the above figures indicates that, for the same width of a triangular structuring element, the variance of all density functions decreases when the height of the triangular structuring element is increased. When the height approaches zero, the statistical properties of the triangular structuring element become very similar to the properties of the flat structuring element. This means that flat structuring elements smooth the signal more effectively than triangular structuring elements , although this may be at the expense of destroying certain desired features of the original signal.

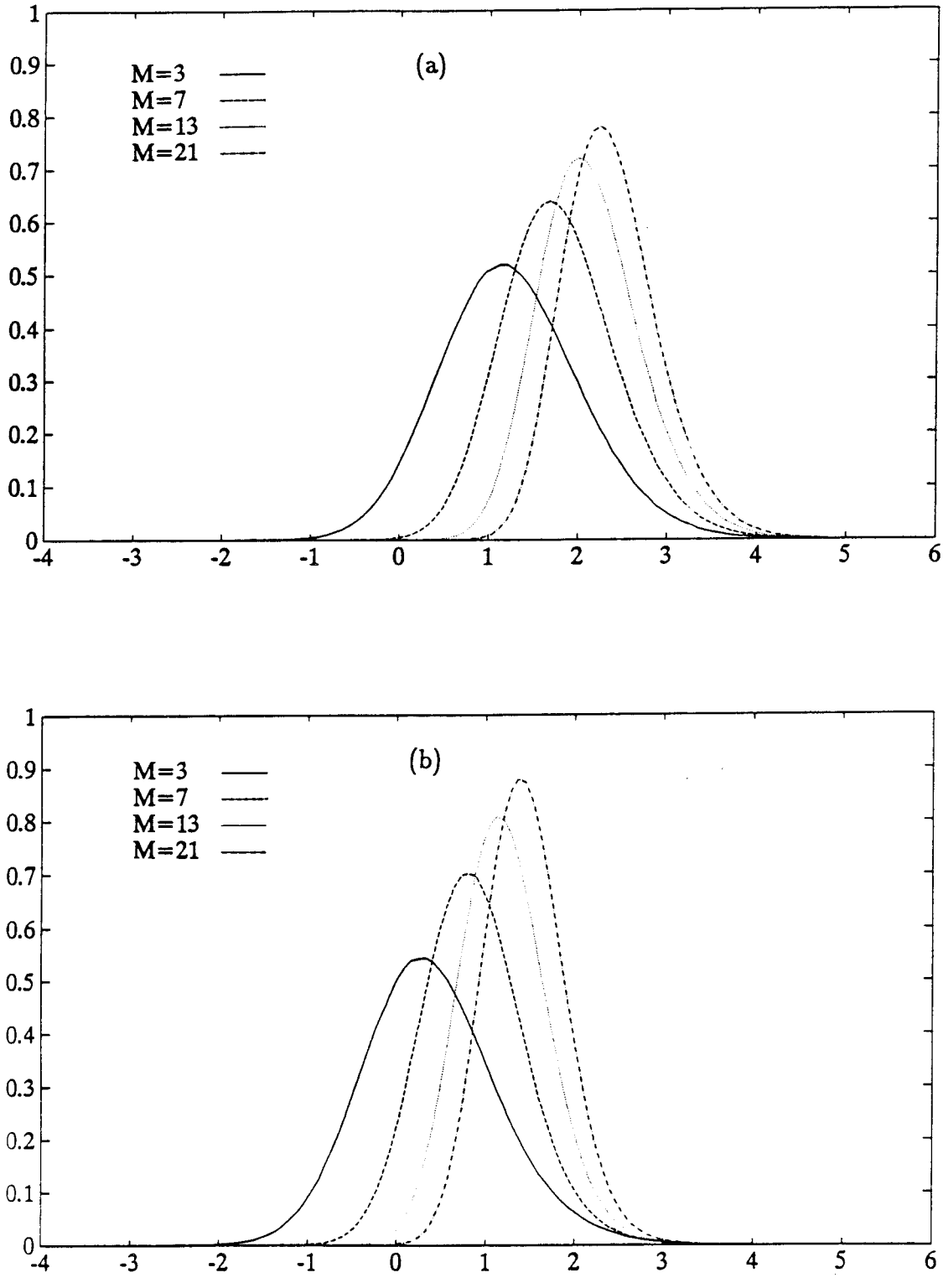

Figure 4.14 Output Density Function when the Input Signal has a Gaussian Density Function using a Triangular Structuring Element with a Height A=20% of the Dynamic Range of the Input Signal for:
(a) Dilation Operation (b) Closing Operation
(c) Clos-Erosion Operation (d) Clos-Opening Operation

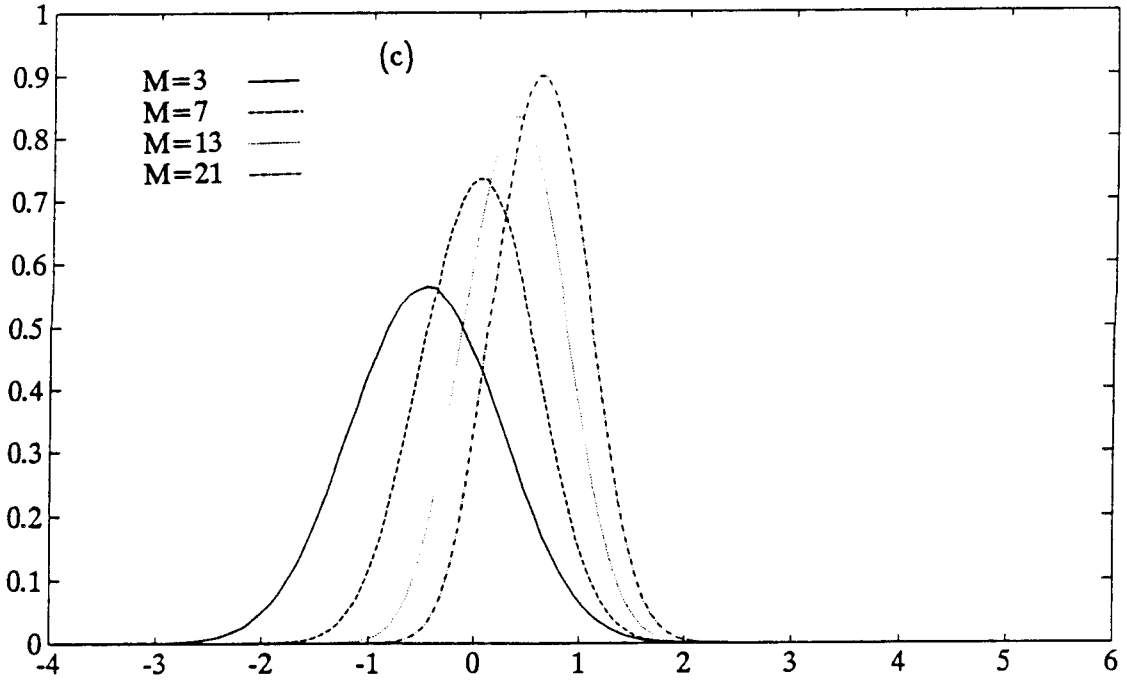

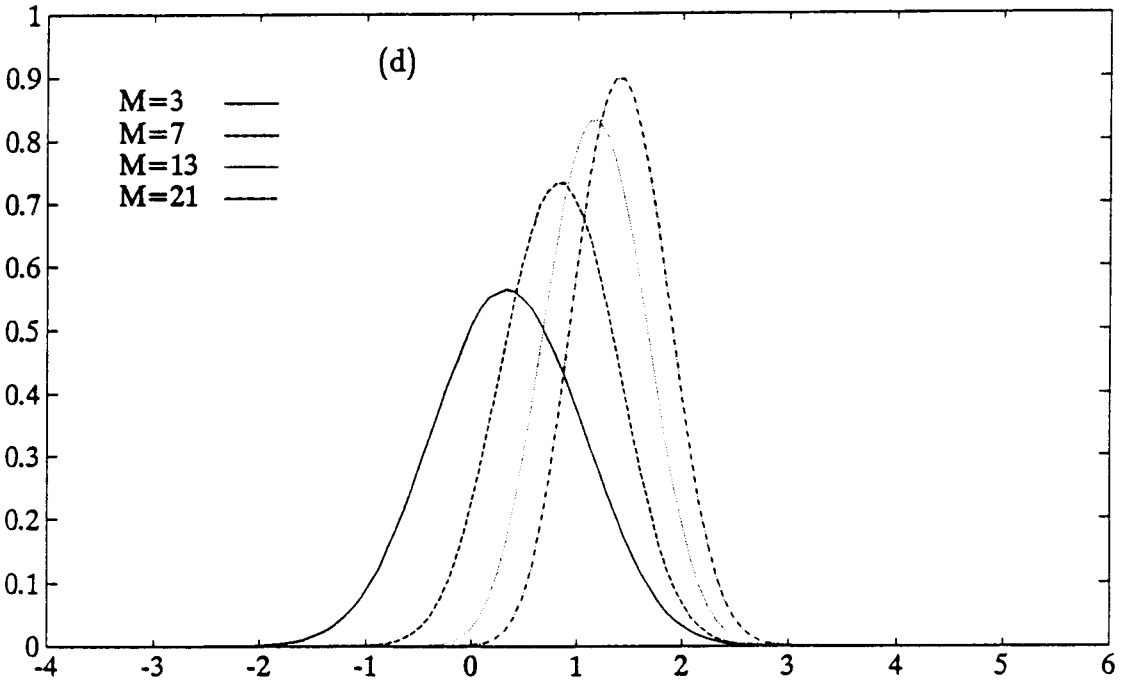

Figure 4.14 (Continued)

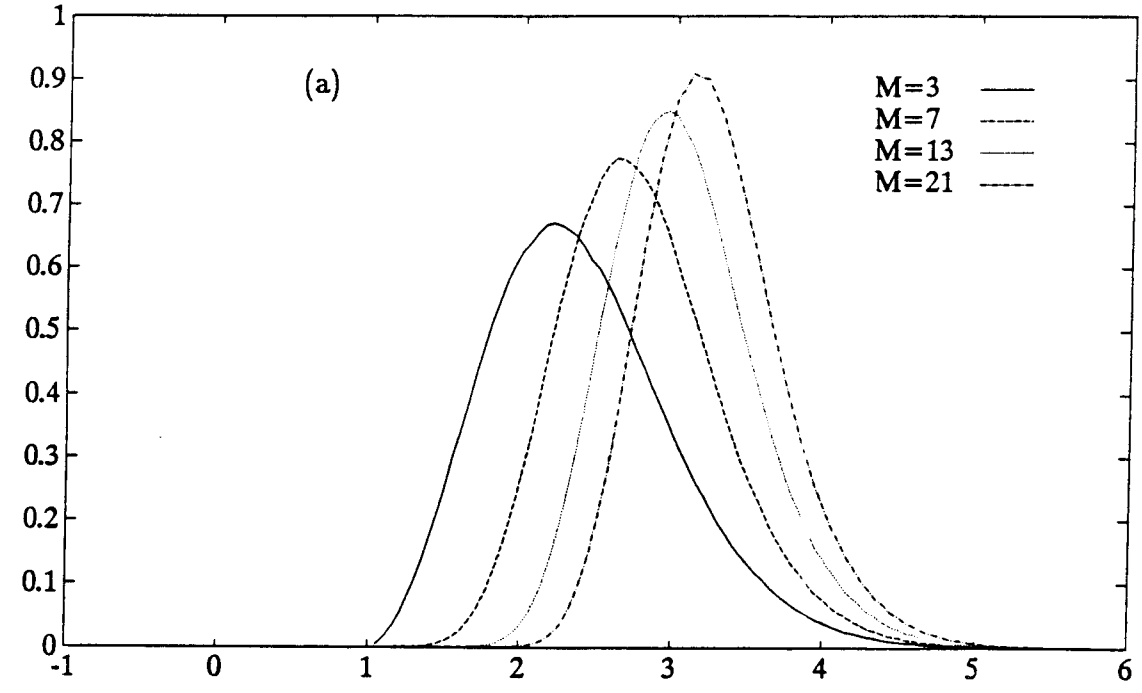

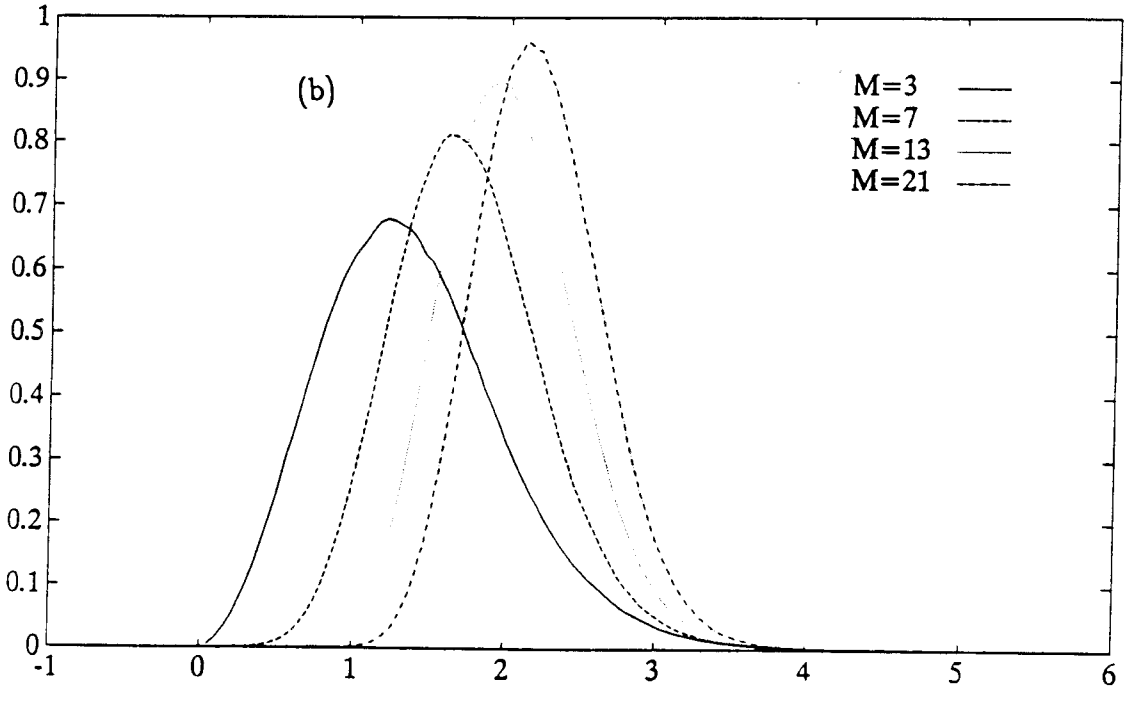

Figure 4.15 Output Density Function when the Input Signal has a Rayleigh Density Function using a Triangular Structuring Element with a Height A=20% of the Dynamic Range of the Input Signal for:
(a) Dilation Operation (b) Closing Operation
(c) Clos-Erosion Operation (d) Clos-Opening Operation

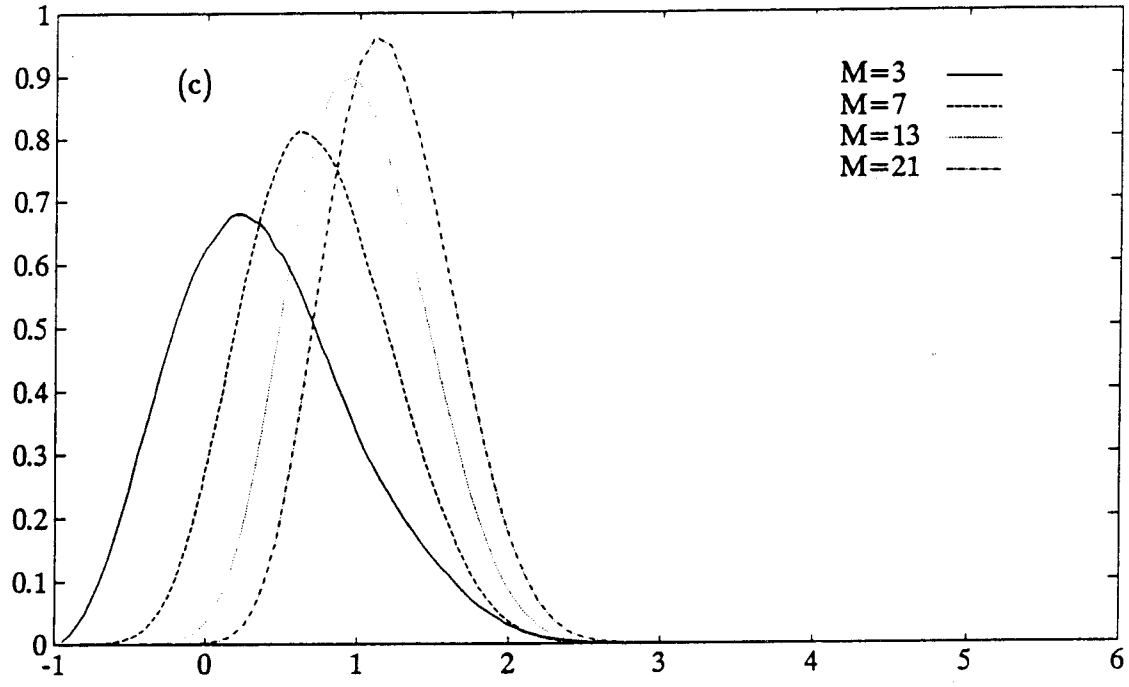

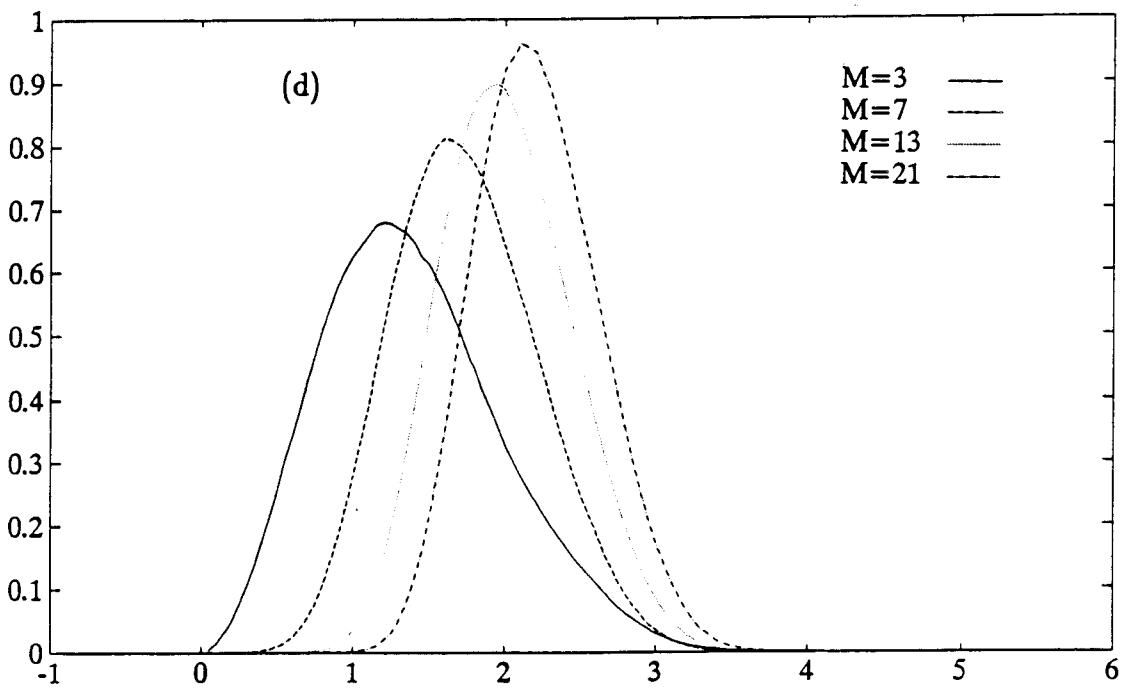

Figure 4.15 (Continued)

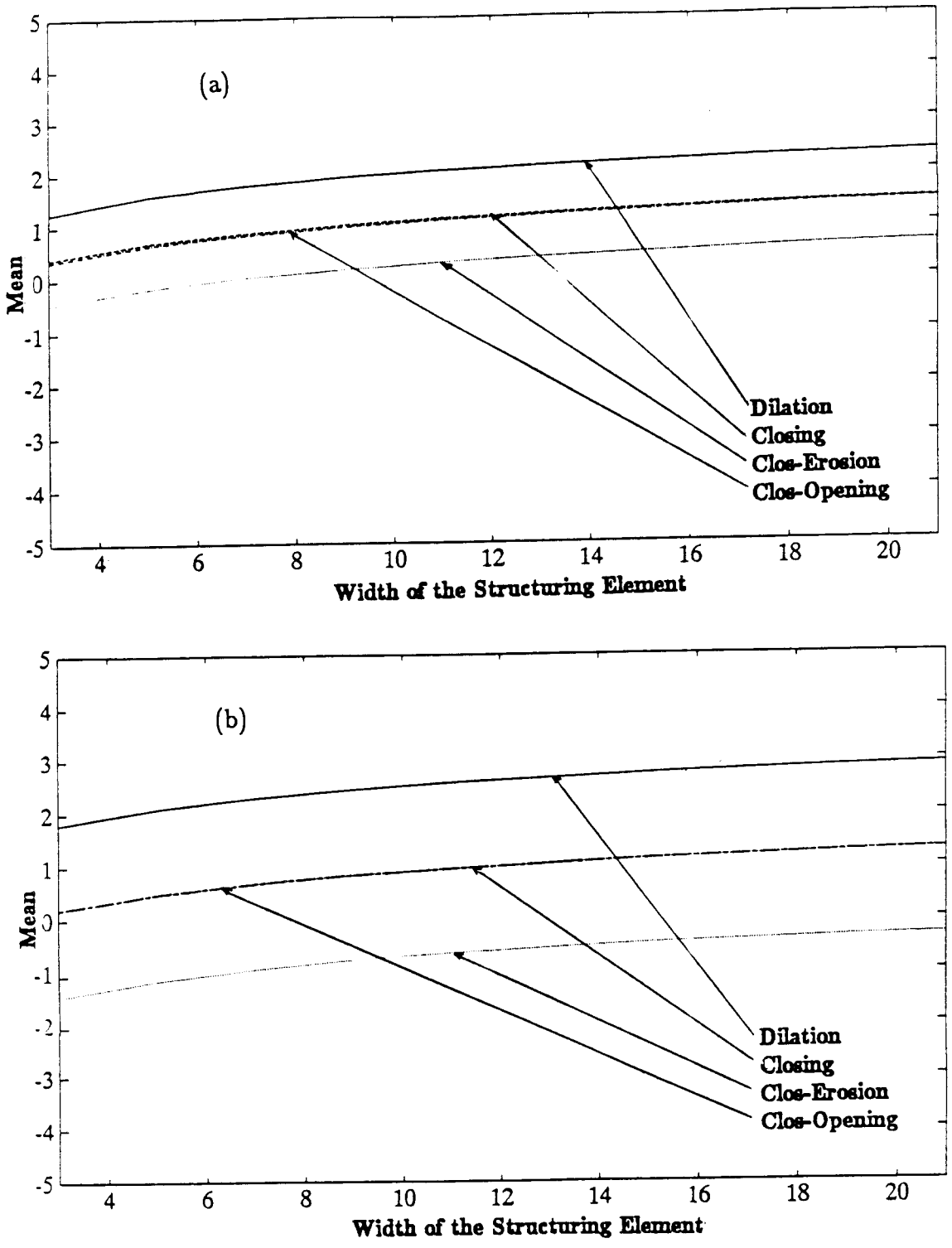

Figure 4.16 Mean of Dilation, Closing, Clos-Erosion and Clos-Opening when the Input Signal has a Gaussian Density Function using a Triangular Structuring Element with Height A :

(a) A=0.2 (b) A=0.4
(c) A=0.6 (d) A=0.8

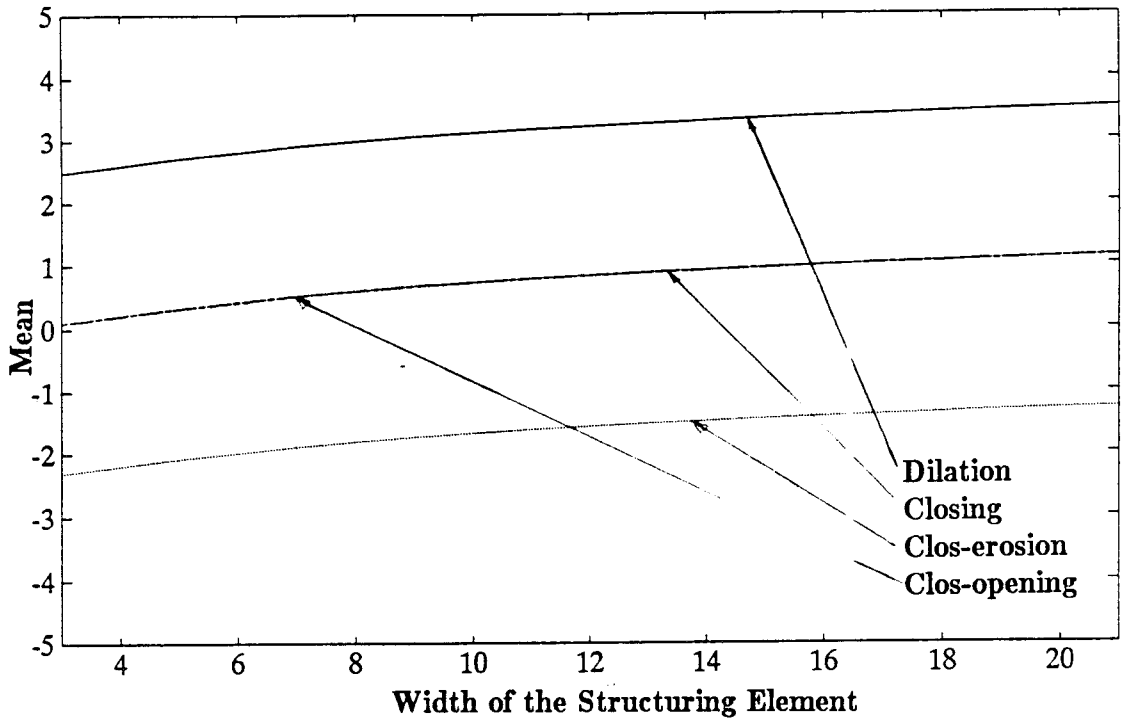

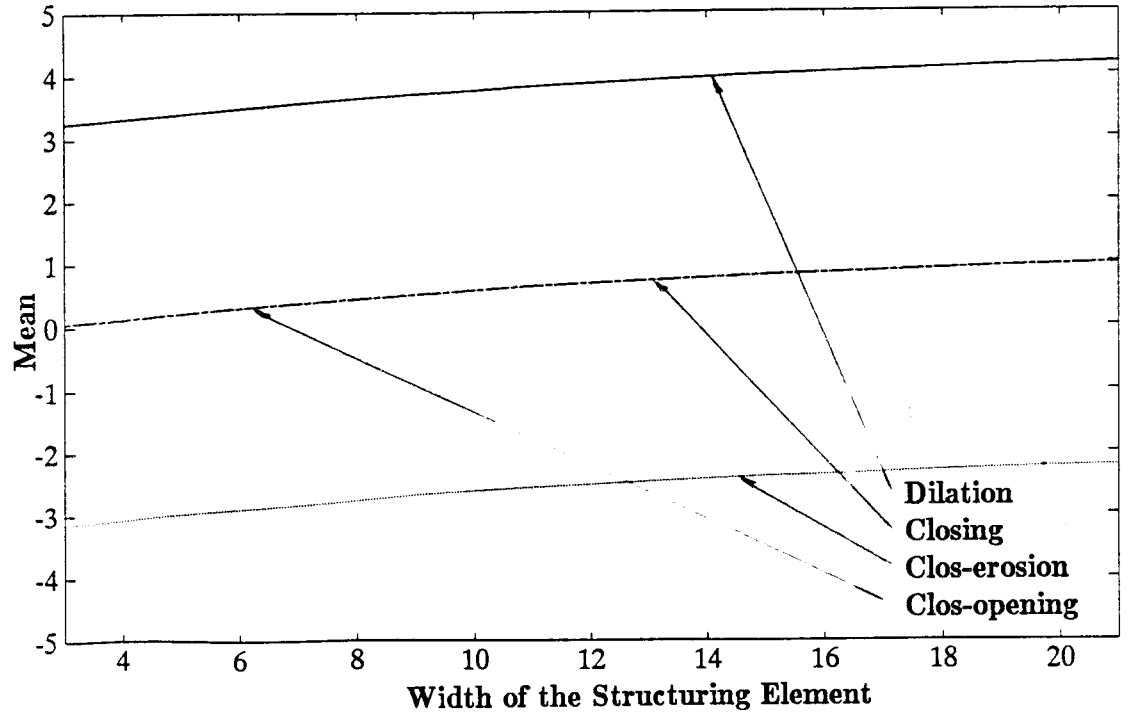

Figure 4.16 (Continued)

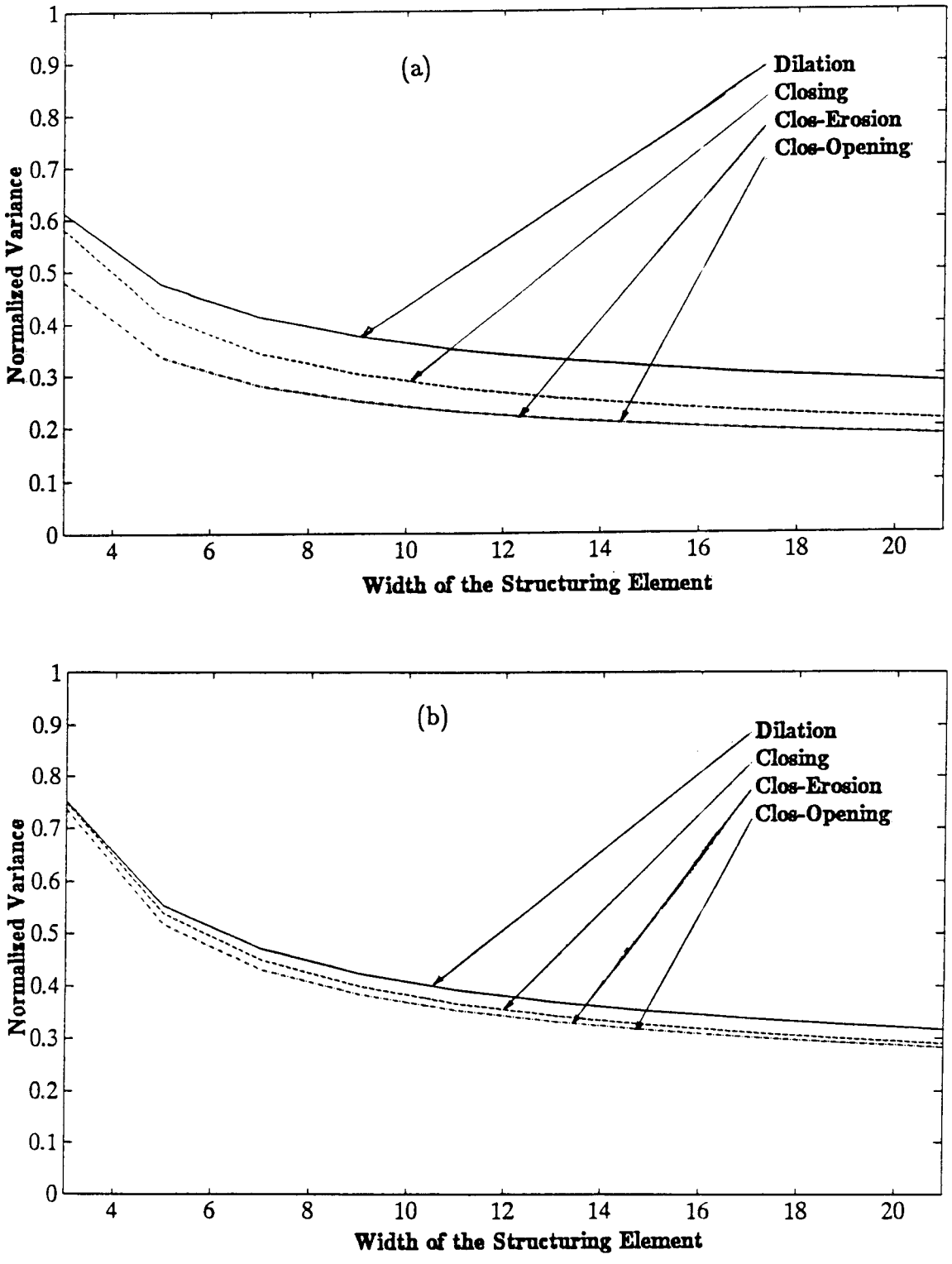

Figure 4.17 Normalized Variance of Dilation, Closing, Clos-Erosion and Clos-Opening when the Input Signal has a Gaussian Density Function using a Triangular Structuring Element with a Height A :
(a) A=0.2 (b) A=0.4
(c) A=0.6 (d) A=0.8

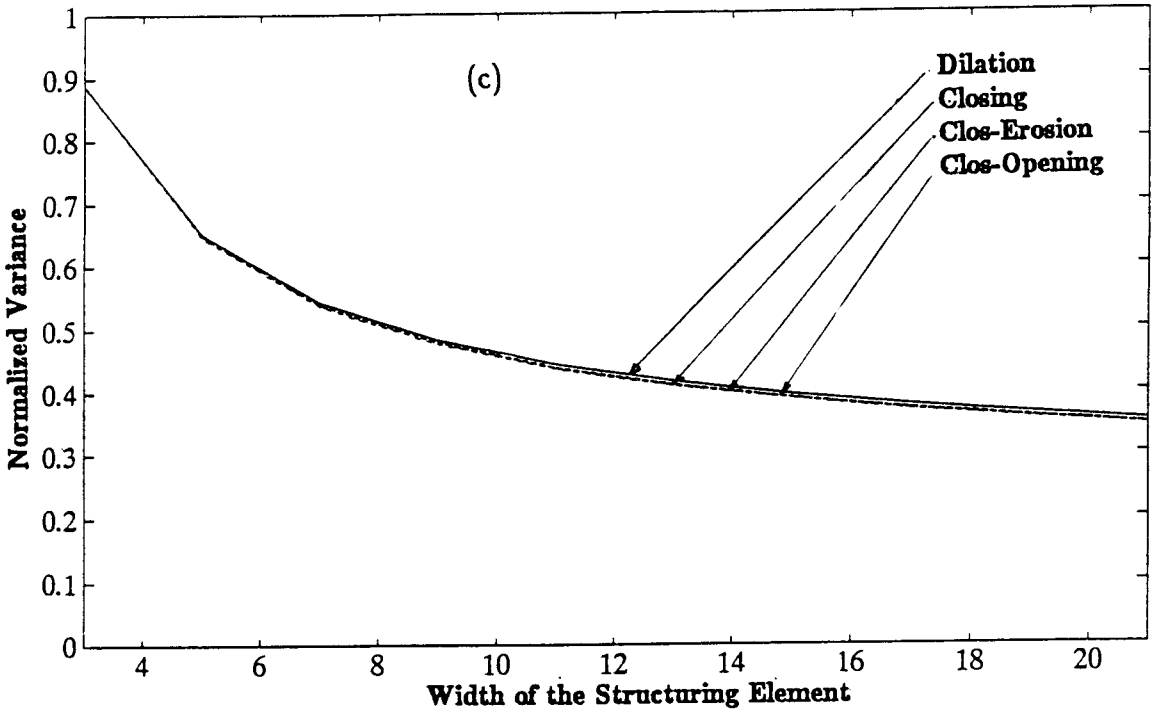

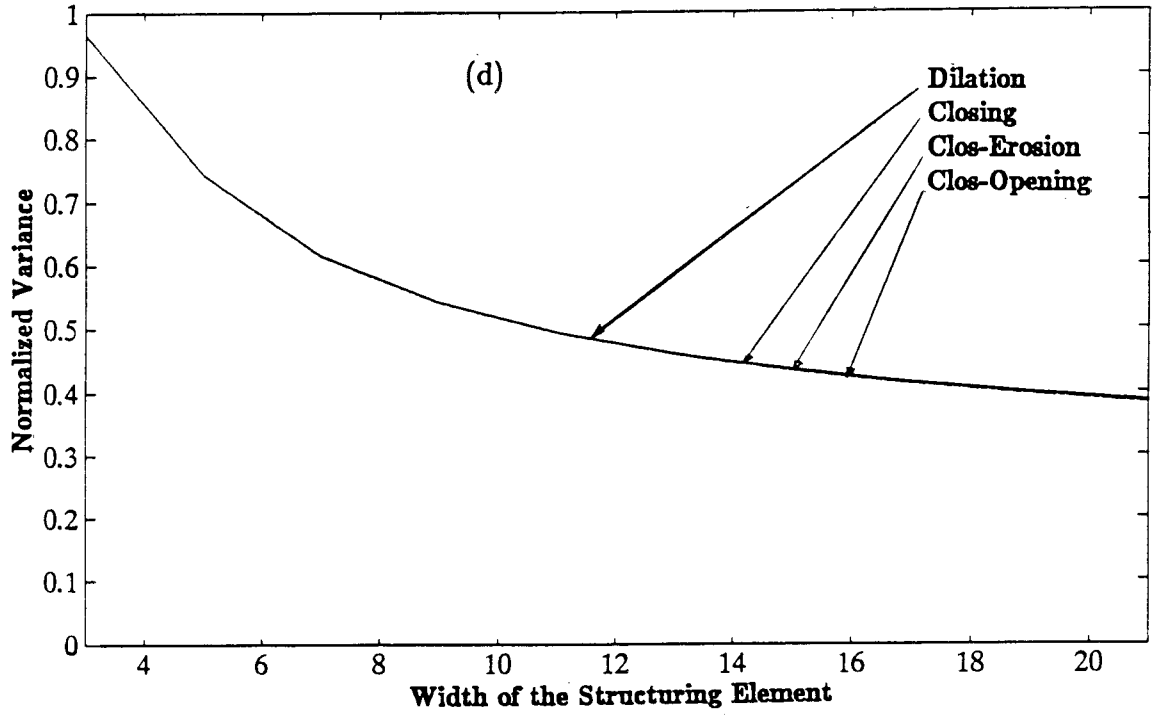

Figure 4.17 (Continued)

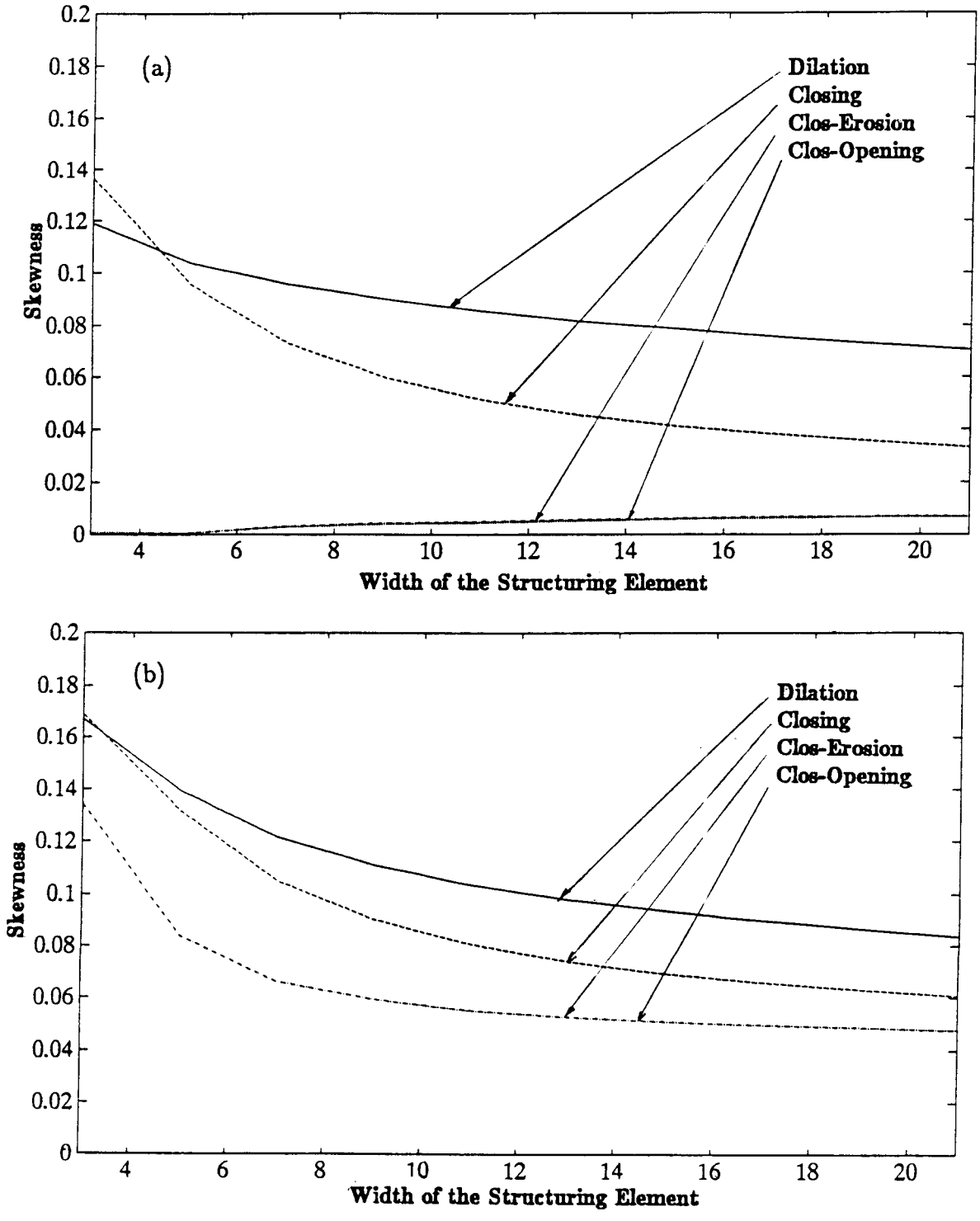

Figure 4.18 Skewness of Dilation, Closing, Clos-Erosion and Clos-Opening when the Input Signal has a Gaussian Density Function using a Triangular structuring Element with a Height A :
(a) A=0.2 (b) A=0.4
(c) A=0.6 (d) A=0.8

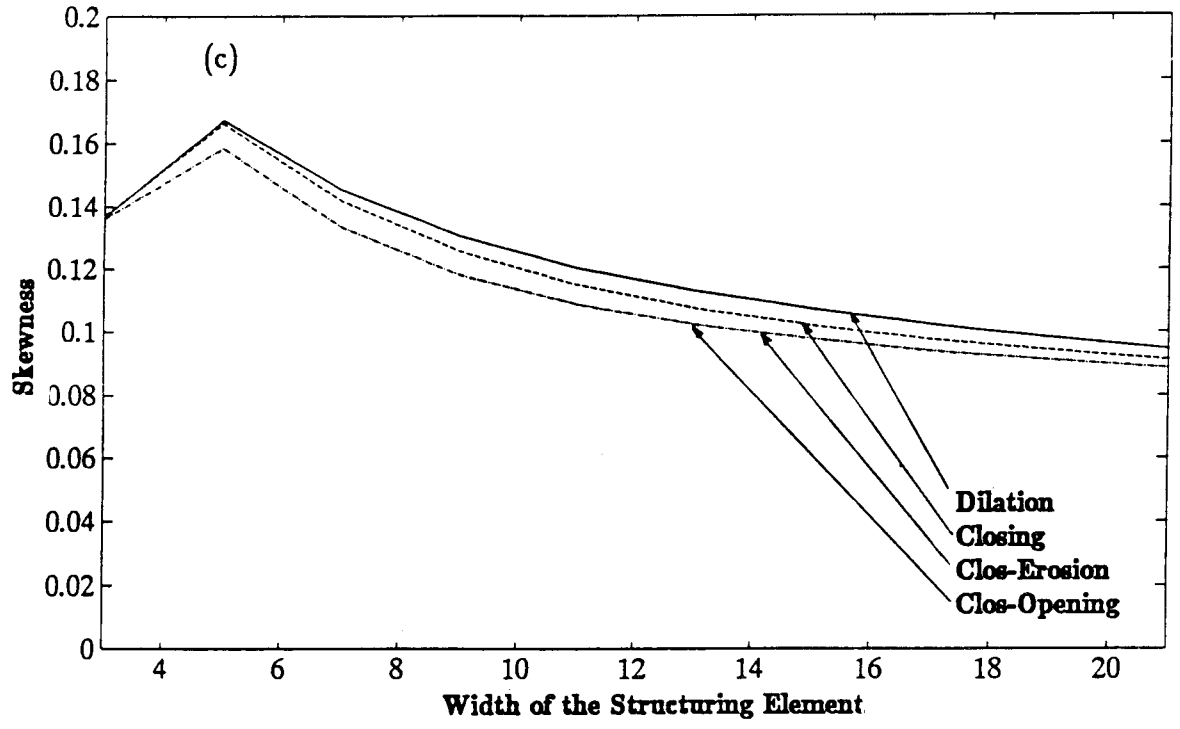

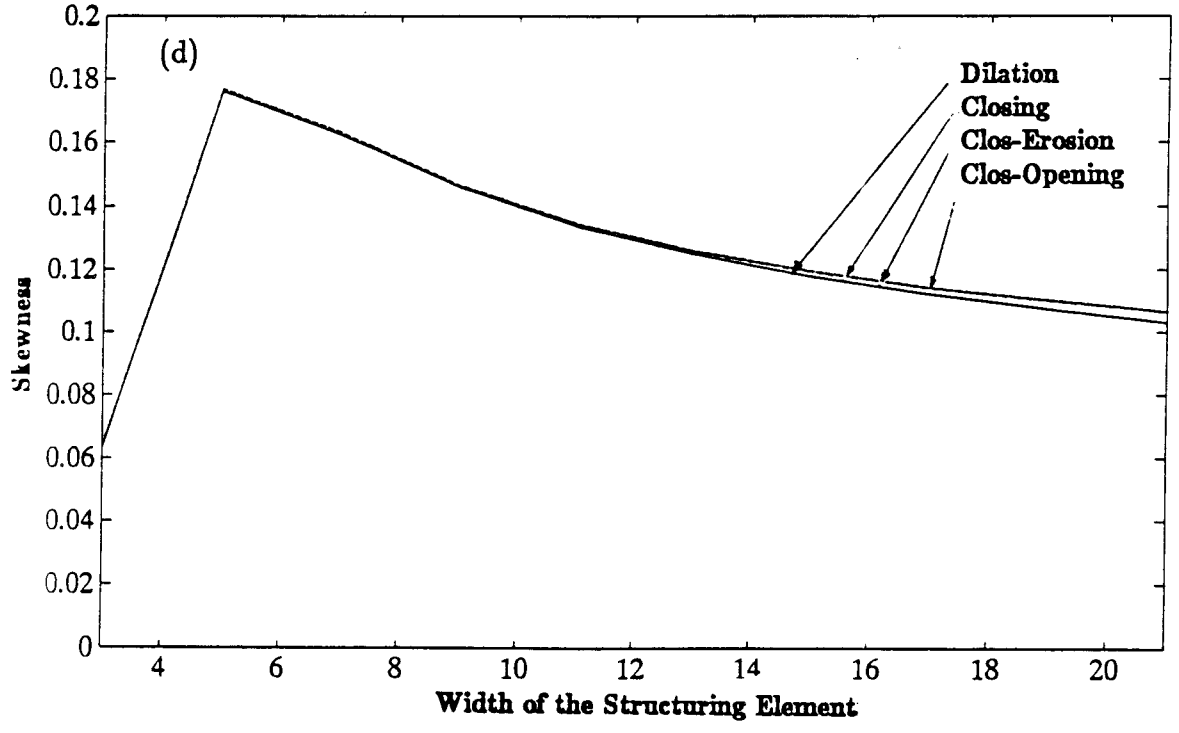

Figure 4.18 (Continued)

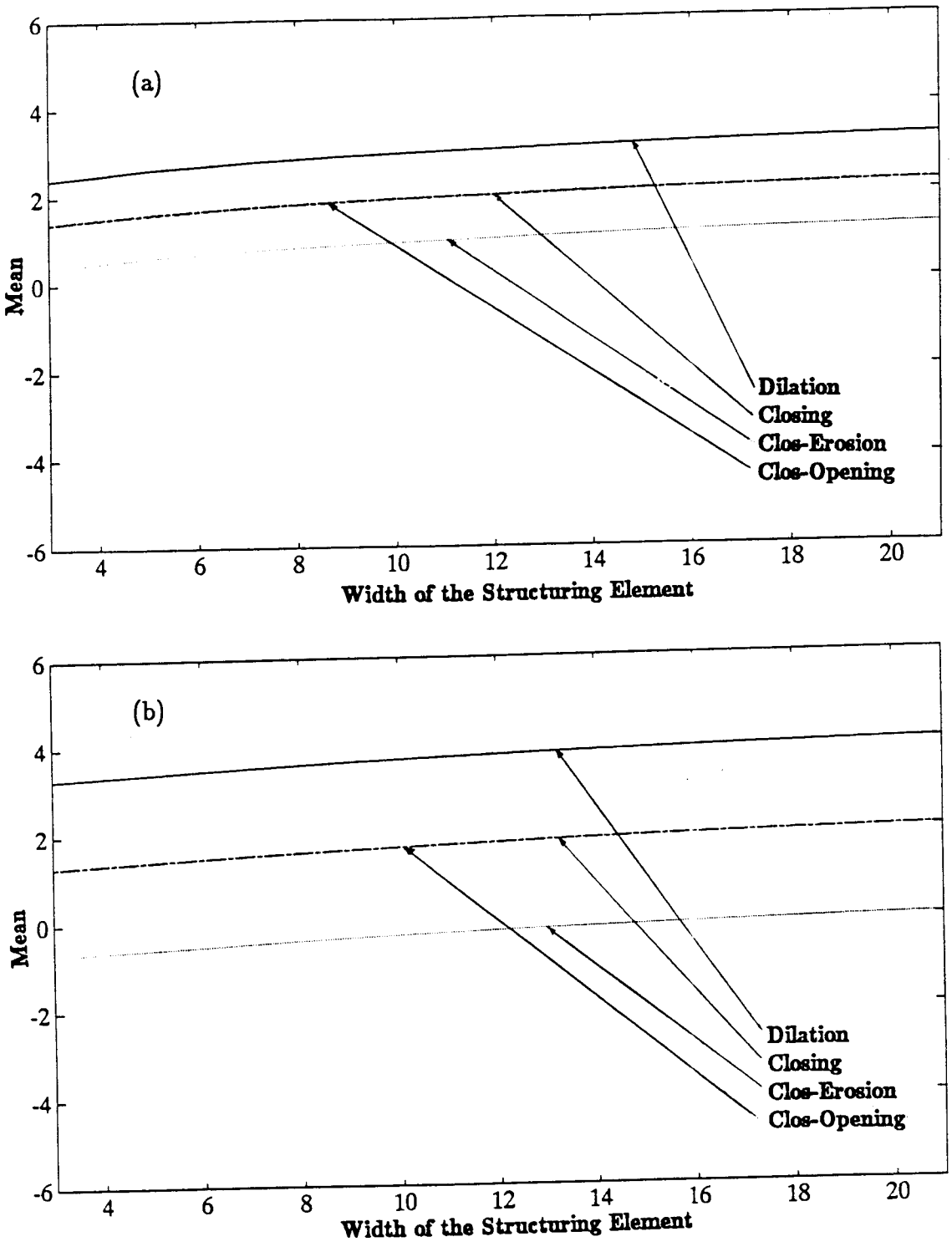

Figure 4.19 Mean of Dilation, Closing, Clos-Erosion and Clos-Opening when the Input Signal has a Rayleigh Density Function using a Triangular Structuring Element with a Height A :
(a) A=0.2 (b) A=0.4
(c) A=0.6 (d) A=0.8

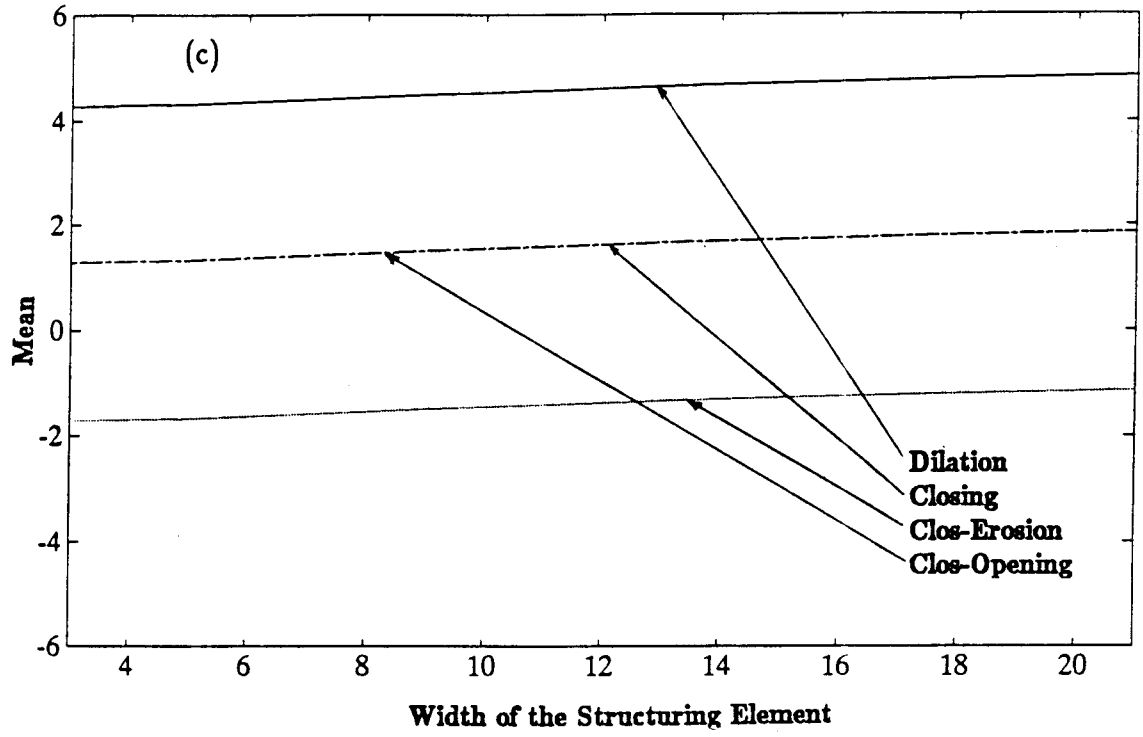

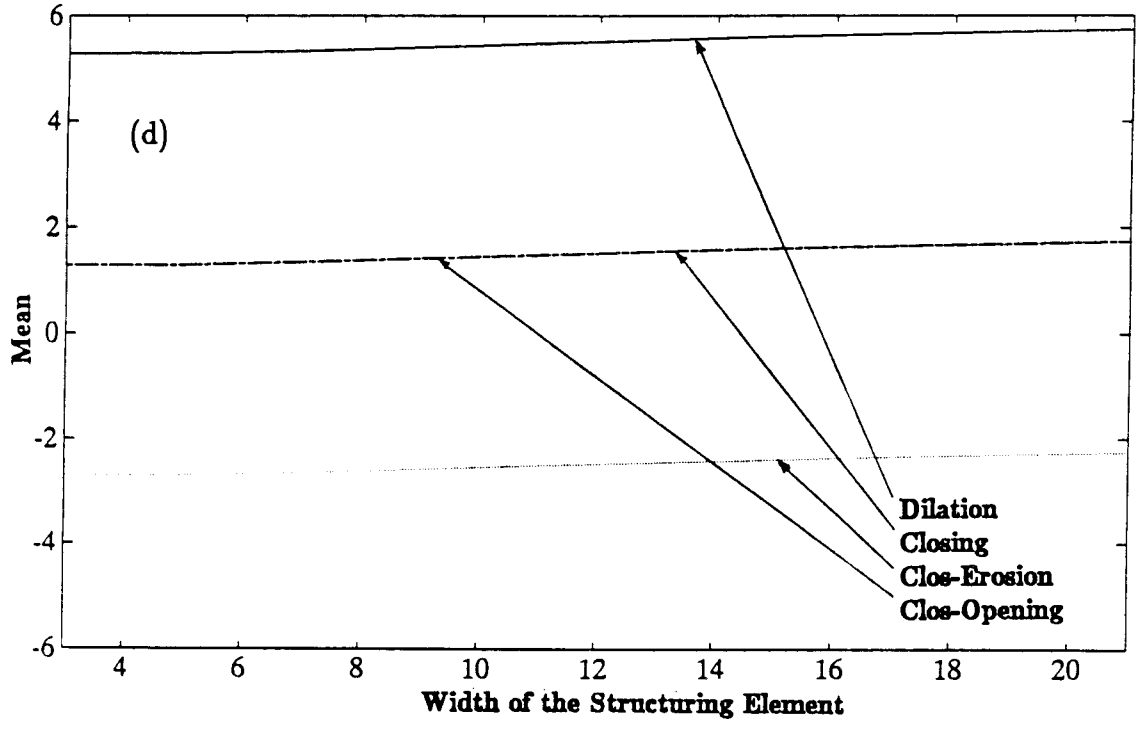

Figure 4.19 (Continued)

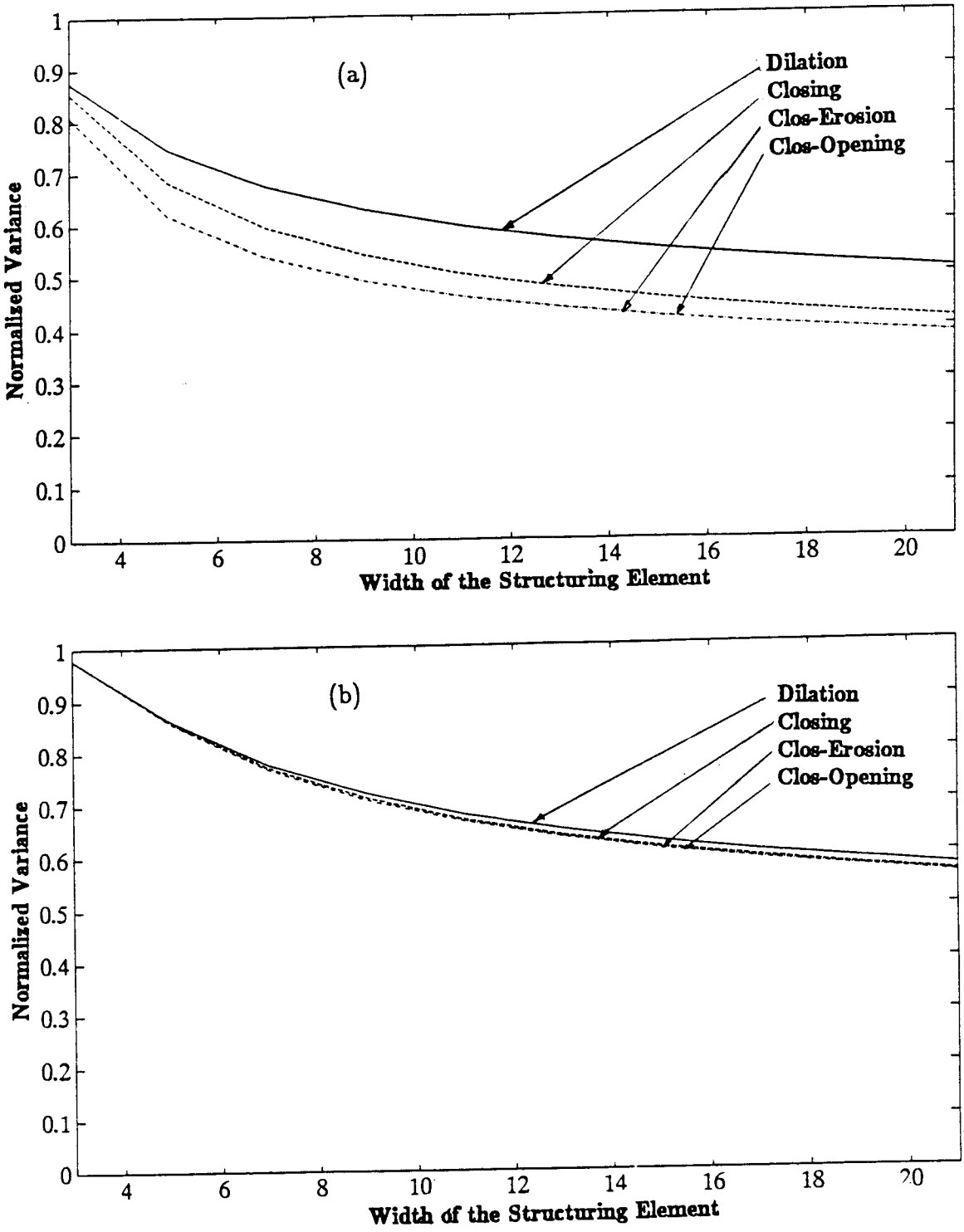

Figure 4.20 Normalized Variance of Dilation, Closing, Clos-Erosion and Clos-Opening when the Input Signal has a Rayleigh Density Function using a Triangular Structuring Element with a Height A :
(a) A=0.2 (b) A=0.4
(c) A=0.6 (d) A=0.8

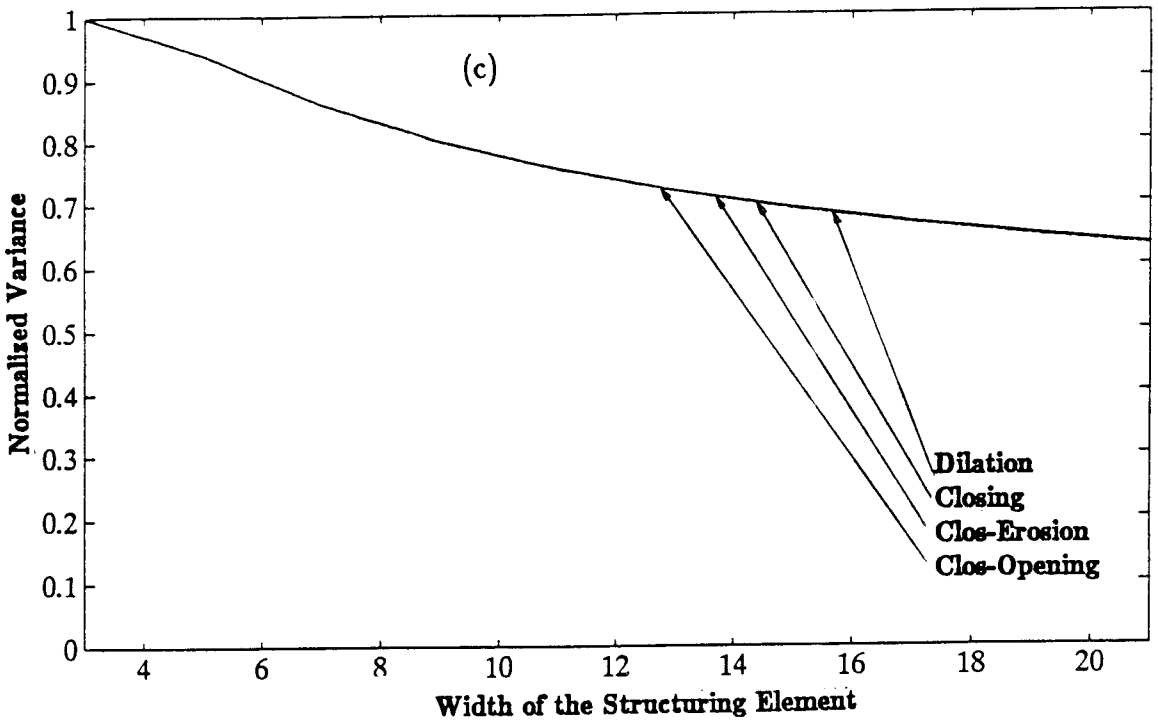

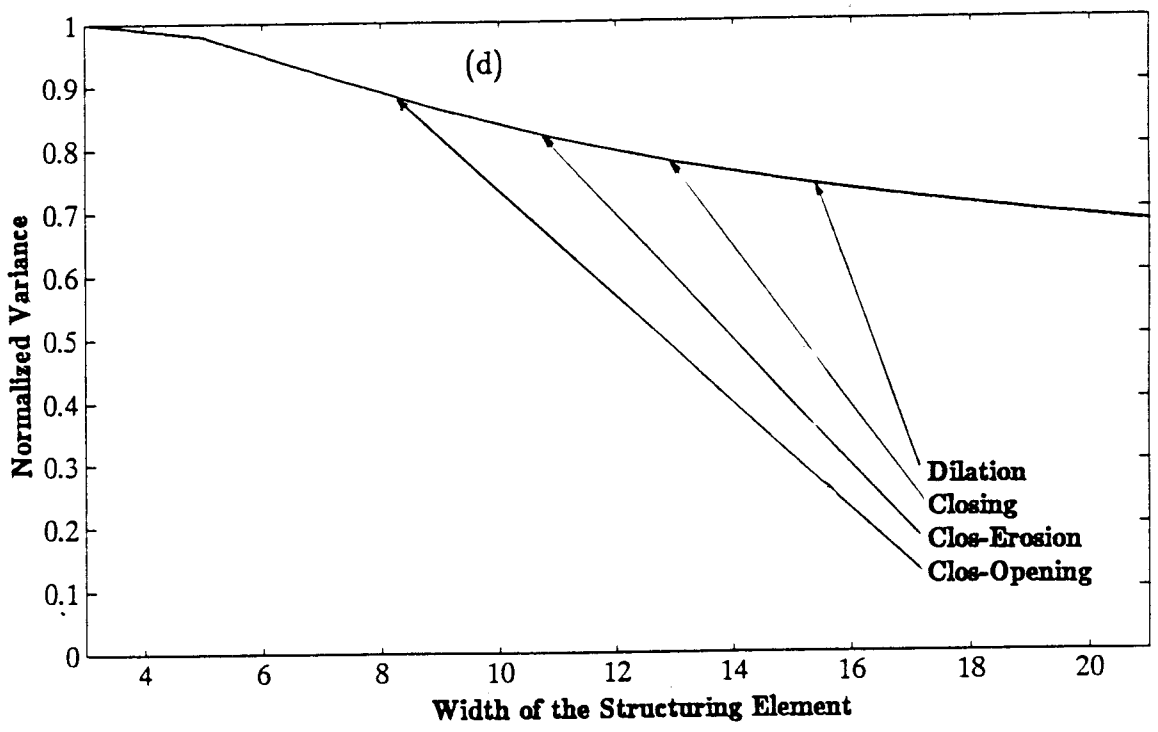

Figure 4.20 (Continued)

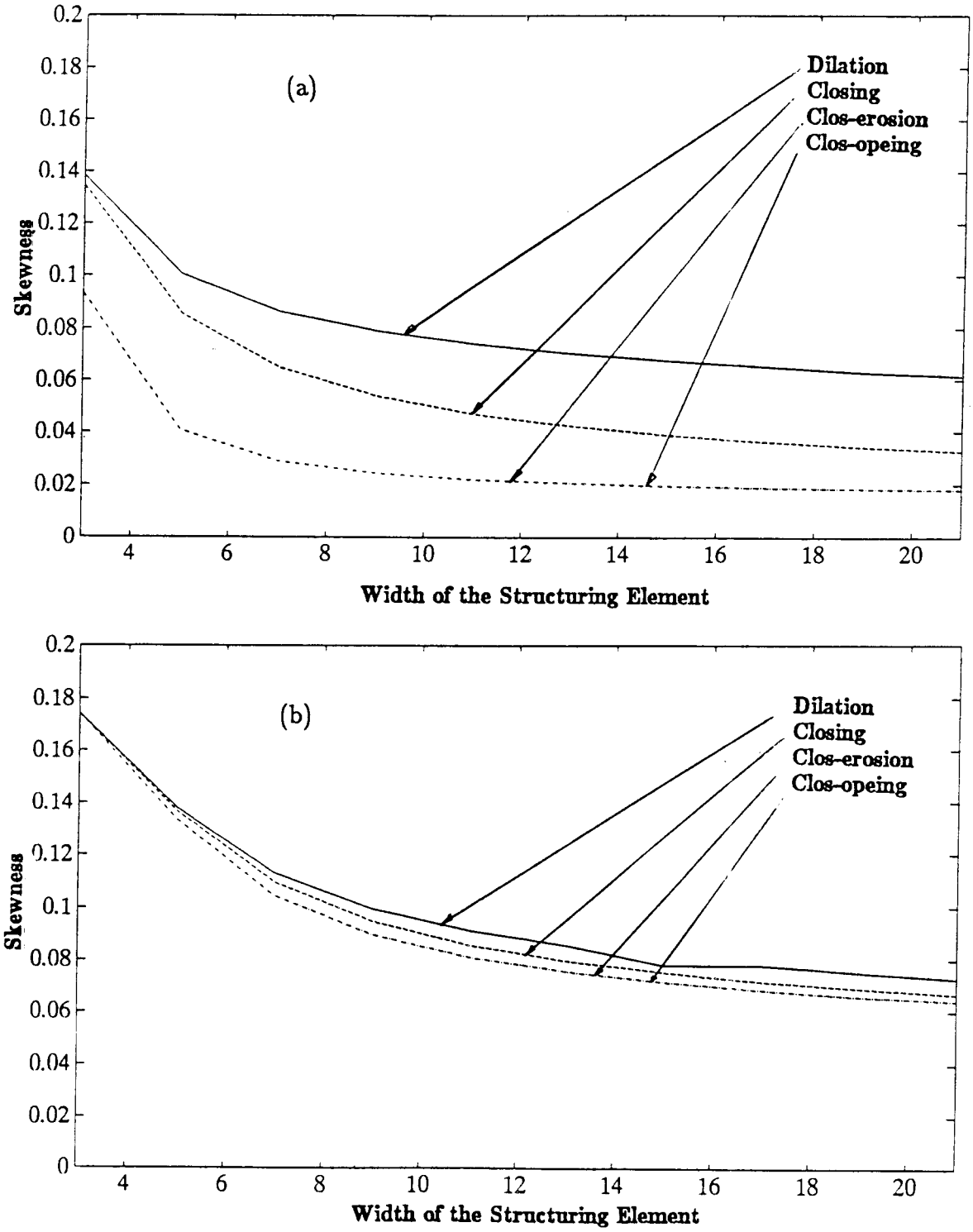

Figure 4.21 Skewness of Dilation, Closing, Clos-Erosion and Clos-Opening when the Input Signal has a Rayleigh Density Function using a Triangular Structuring Element with a Height A :
(a) A=0.2 (b) A=0.4
(c) A=0.6 (d) A=0.8

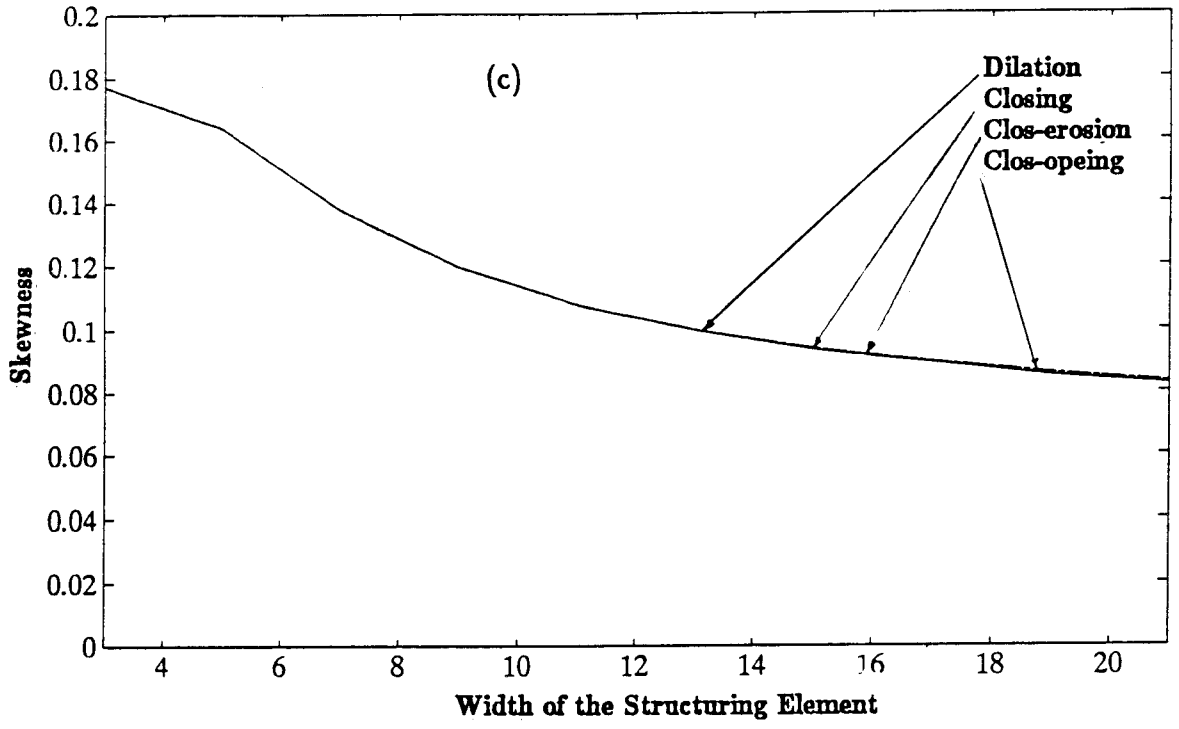

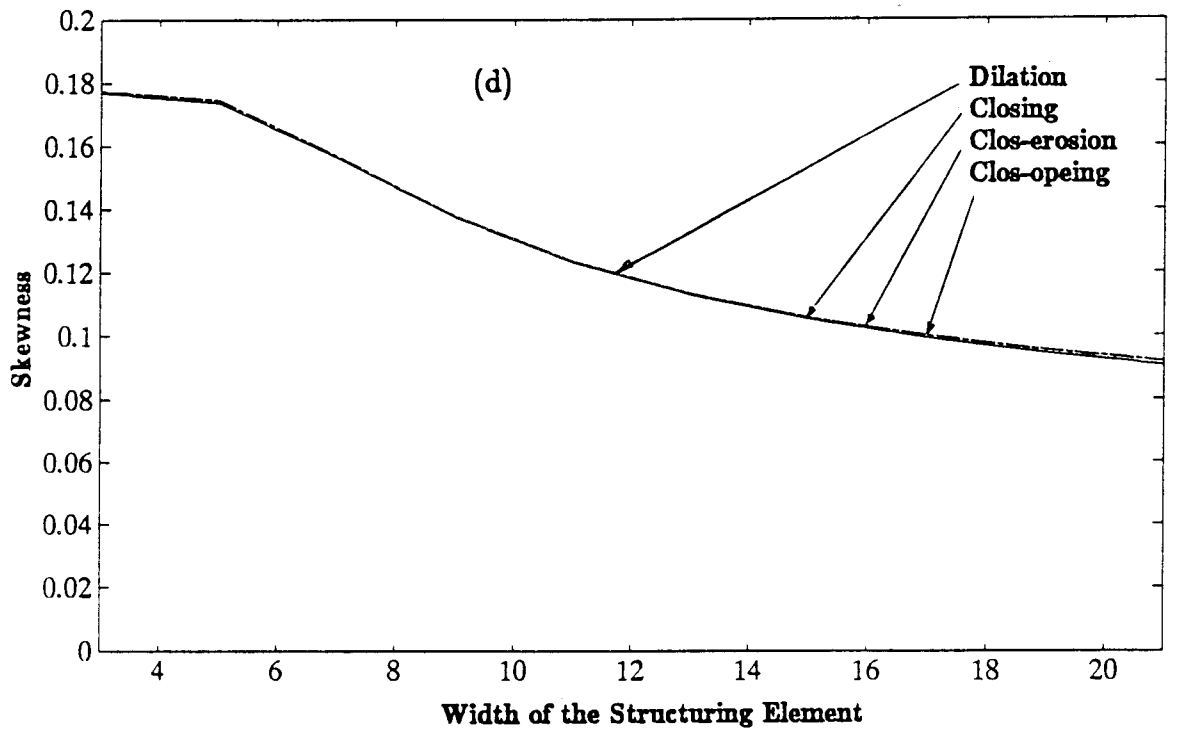

Figure 4.21 (Continued)

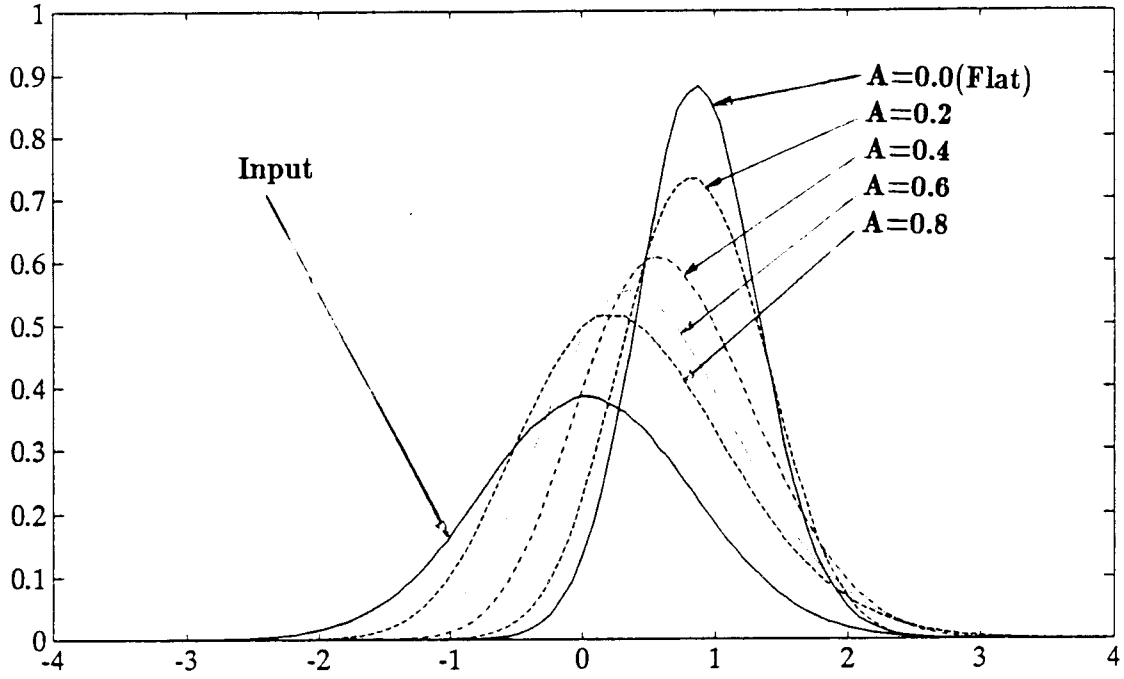

Figure 4.22 A Comparison between Clos-Opening Density Functions when the Input Signal has a Gaussian Density Function using Flat and Triangular Structuring Elements with Different Heights.

4.2 Conclusion

In this Chapter, we examined the statistical properties of sequential morphological operations using different shapes of structuring elements applied to signals with uniform, Gaussian, and Rayleigh density functions. The effect of the parameters of the structuring elements are evaluated using Monte Carlo simulation. The simulated results indicate that by increasing the width of the flat structuring element the mean (bias) is increased and the variance and skewness of dilation, closing, clos-erosion and clos-opening density functions are decreased. Also, dilation is the most effective step in the smoothing operation. The effect of other operations following dilation is rather small, especially, when the width of the structuring element is increased. It has been shown that, for a certain height of the triangular structuring element and input signal with uniform density function, the dilated signal is a root signal, i.e., becoming invariant to any proceeding morphological operations using the same structuring element. For the same width of structuring element, the flat structuring element has better noise suppression (less variance) than the triangular structuring element, although a triangular structuring element similar to certain patterns of the input signal may be desirable in preserving these patterns.

CHAPTER V

DETERMINISTIC PROPERTIES OF MORPHOLOGICAL FILTERS

In order to evaluate the behavior of morphological filters in time domain when applied to certain signals, the deterministic properties of morphological filters are studied using different structuring elements. In this Chapter, the effect of shape, width and height of structuring elements is examined on the output signal through a sequence of opening and closing operations. In particular, the capability of morphological filters for noise suppression and signal filtering is investigated by introducing different classes of morphological operations.

5.1 Noise Suppression Using Morphological Operations

In this section, simulation results are presented which illustrate the performance of morphological filters for noise suppression and echo detection. The signal to be processed is a sum of two components: an ultrasonic echo, u(n), backscattered from a single reflector and a random noise, ν (n), i.e.,

$$r(n)=u(n) + \nu(n) \tag{5.1}$$

where the ultrasonic echo is assumed to have a Gaussian envelope and is modeled as:

$$u(n)=e^{-\alpha n^2} cos(2\pi \frac{f_c}{f_s} n) \tag{5.2}$$

The Gaussian envelope echo is often used in many detection problems such as radar, sonar or ultrasound. The term f_c is the center frequency, f_s is the sampling rate, and α is a constant proportional to the bandwidth of the echo and f_s. In this simulation α =0.0002, f_c =1.25 MHz and f_s =100 MHz (i.e., the number of samples per cycle of the ultrasonic echo is 80). The term $\nu(n)$ is a random impulsive noise with amplitude = 0.5, and a width =7 samples is added to the echo signal. The echo signal, and the echo signal contaminated by impulsive noise

is shown in Figures 5.1a and 5.1b respectively. The above signal (Figure 5.1b) is processed using an open-closing operation with a flat structuring element. The flat structuring element has a width =8 samples. The opening operation is used to suppress the positive impulses while the closing operation suppresses the negative impulses. Figures 5.1c and 5.1d show the recovered signal and the error (difference) between the actual echo signal and the recovered signal respectively. These figures show the ability of an open-closing operation for suppressing positive and negative impulsive noise and recovering the original echo signal.

To evaluate the performance of morphological filters for noise suppression of random noise with a uniform density function, the Gaussian envelope echo, u(n), is contaminated by a random noise, $\nu(n)$, with a uniform density function between $\{-\frac{1}{2}, \frac{1}{2}\}$ resulting in a signal to noise power ratio of 5.54 dB. An estimate of the output signal is obtained by processing the input signal using an open-closing operation. A second estimate of the output signal is formed by processing the input signal using a clos-opening operation. Then the output signal is the average of these two estimates. The average of the two signals is used to minimize the bias caused by the extensiveness properties of opening and closing. A block diagram of the above morphological operations is shown in Figure 5.2. The echo signal and the echo signal contaminated by noise are shown in Figures 5.3a and 5.3b respectively. Figures 5.3c - 5.3f represent the processed results using sinusoidal structuring elements with different widths (M=5, 11, 17, and 23 samples) and a height A=0.1. The sinusoidal structuring element is a half cycle of a sinusoidal signal and is shown in Figure 5.4. The processed signal shows the effectiveness of the algorithm in suppressing the noise with uniform density function and preserving the original echo. Also, the noise suppression increases by increasing the width of the structuring element, but the echo signal is attenuated when M>17. Figure 5.5a shows a comparison between the original signal with the processed output signal for a width M=23 and a height A=0.1. The error of the recovered signal is shown in Figure 5.5b. The signal-to-noise power ratio after processing is

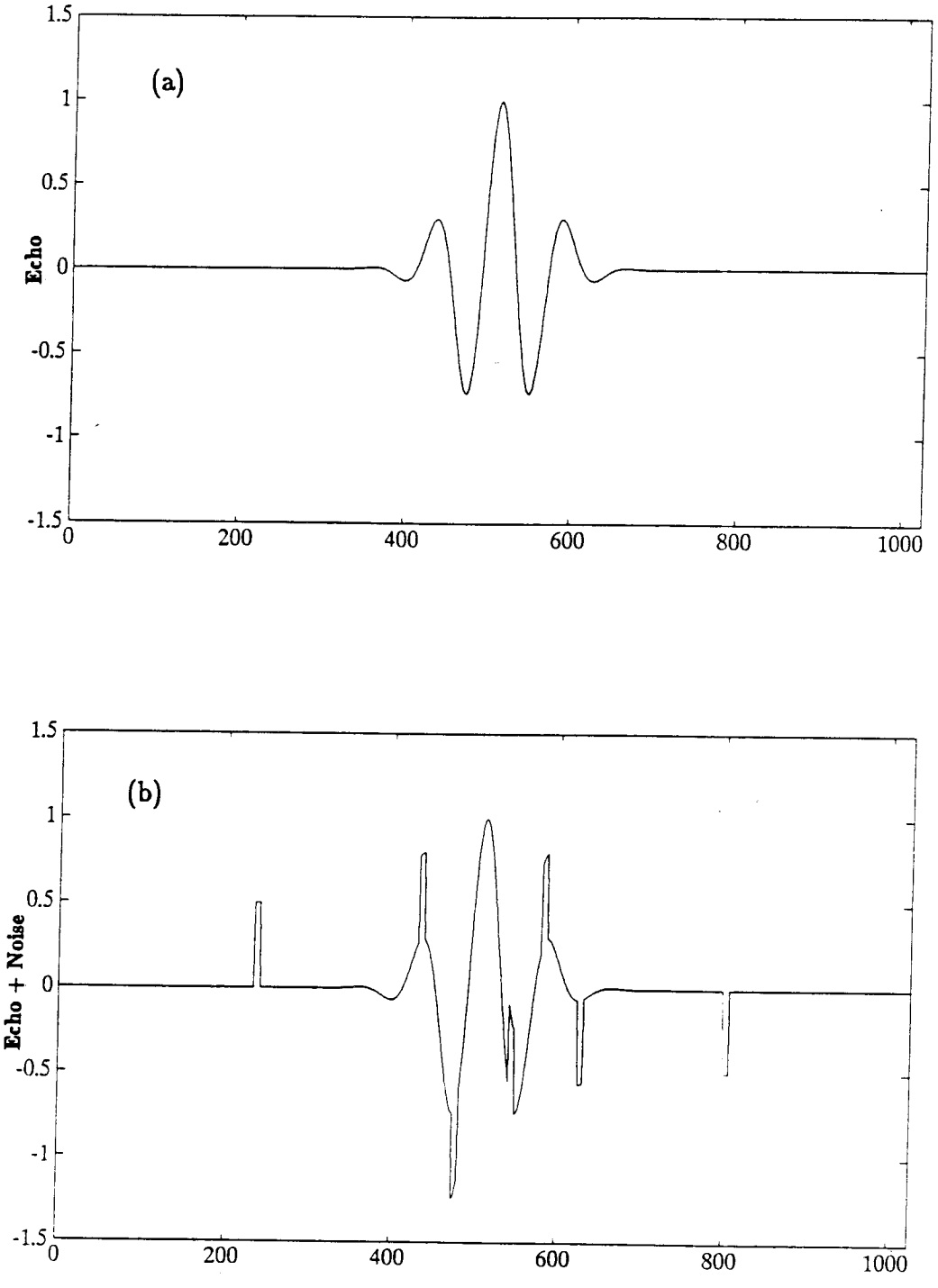

Figure 5.1 Impulsive Noise Suppression using Morphological Open-Closing Operation
(a) Simulated Ultrasonic Echo
(b) Echo Contaminated by Random Impulsive Noise
(c) Recovered Signal using Open-Closing Operation
(d) Error Signal

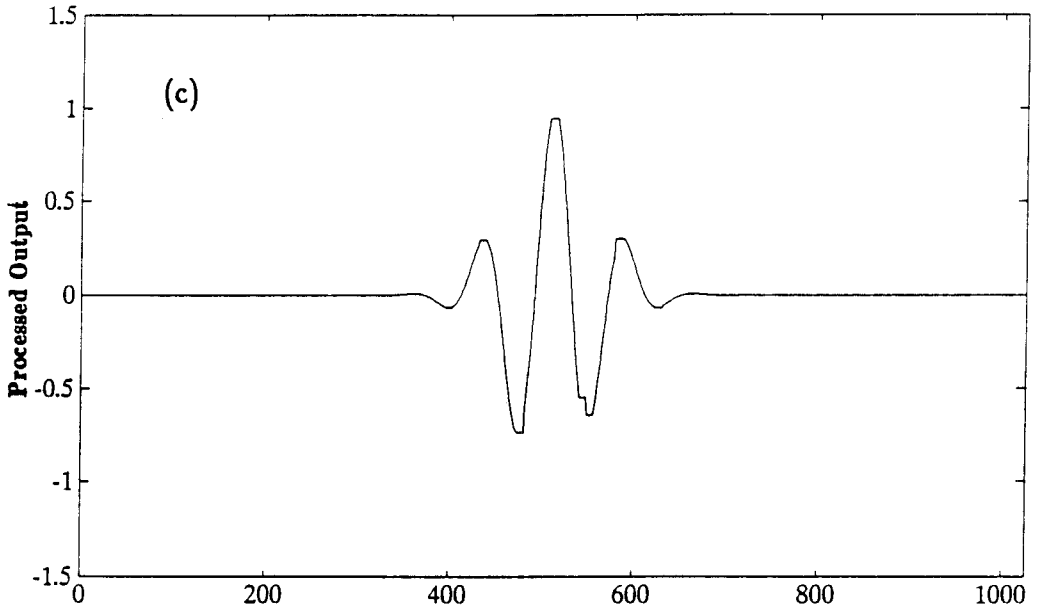

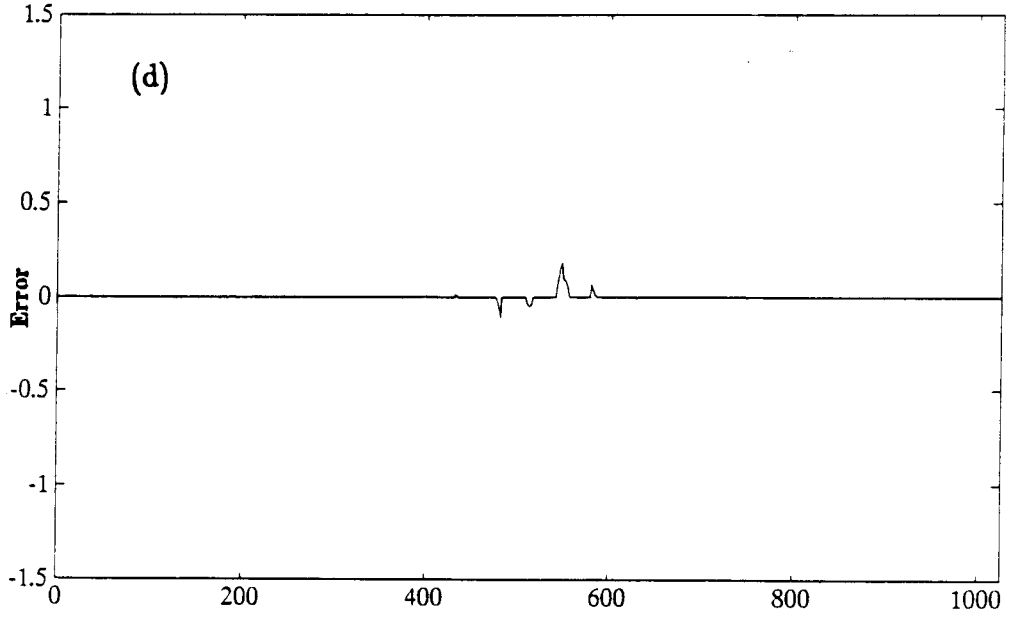

Figure 5.1 (Continued)

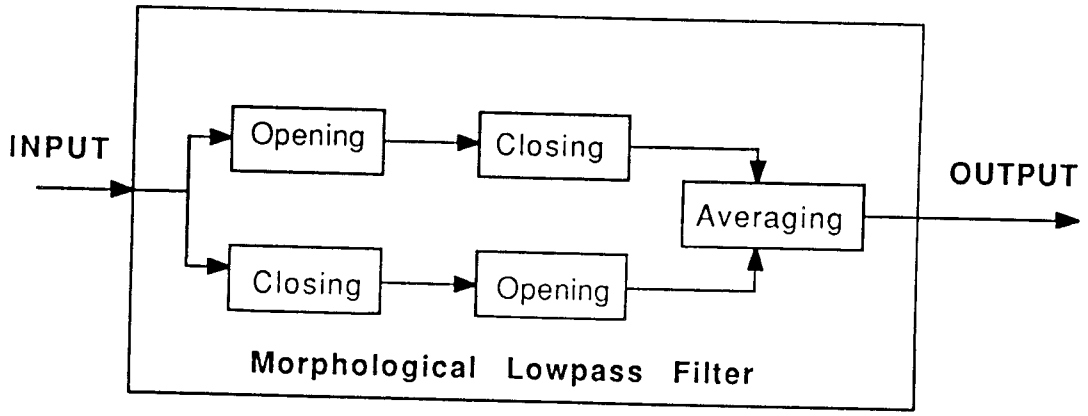

Figure 5.2 Block Diagram of Morphological Operations for Noise Suppression

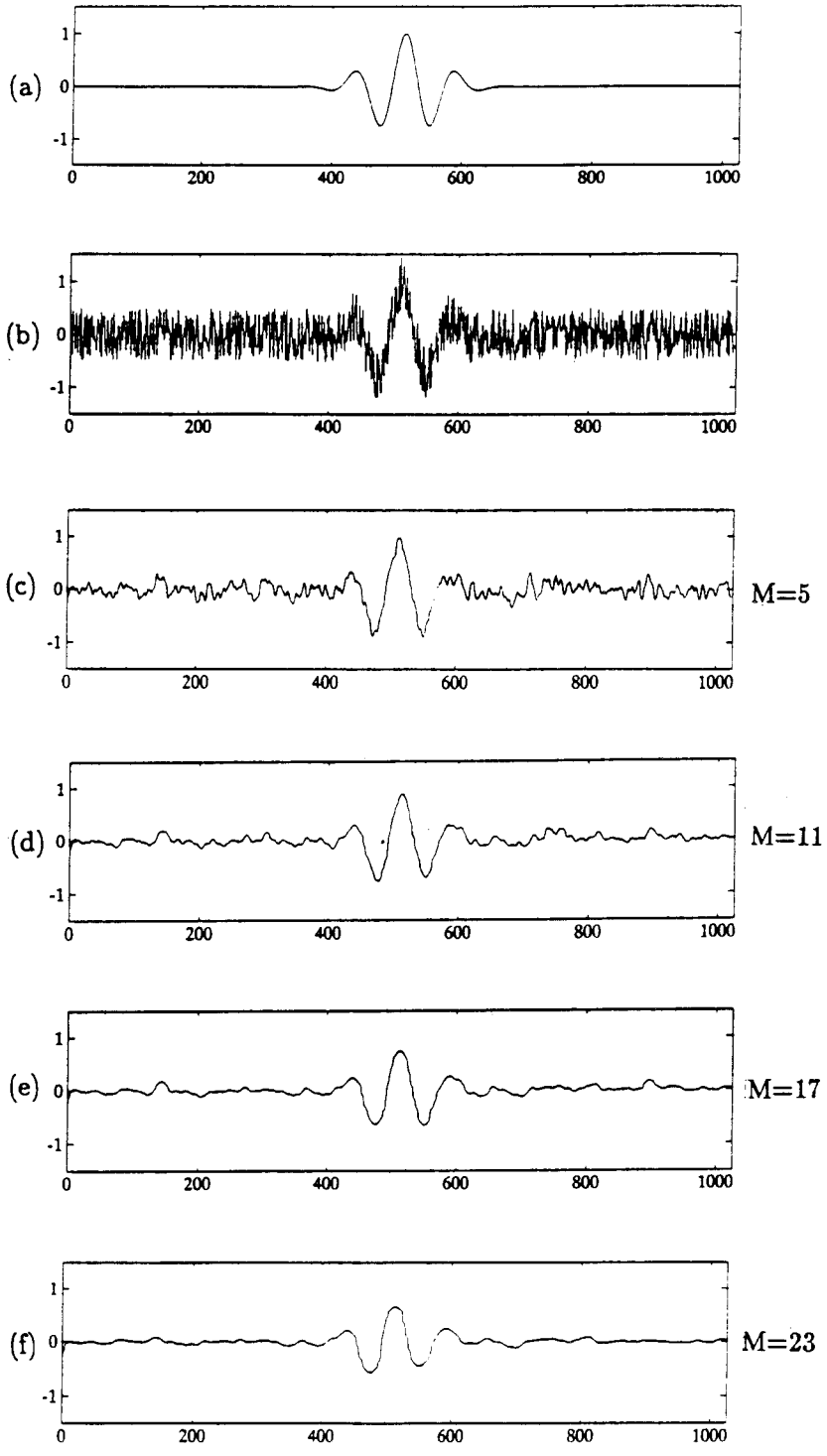

Figure 5.3 Noise Suppression and Echo Detection using a Morphological filter

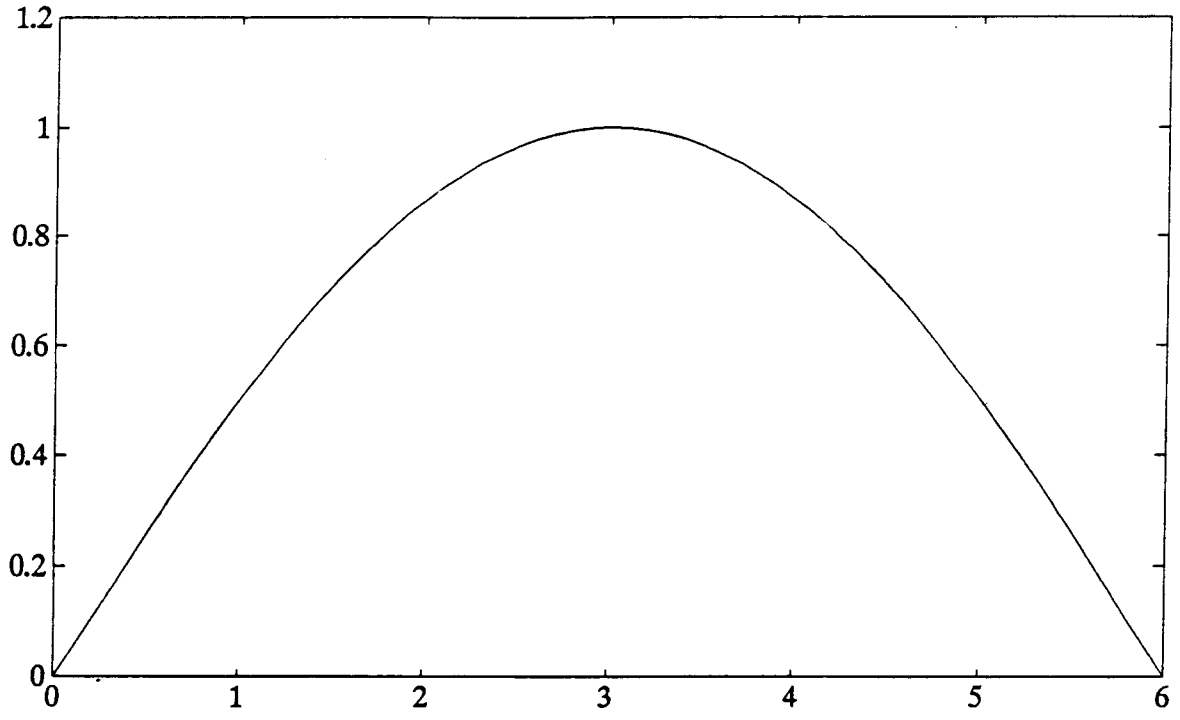

Figure 5.4 A Sinusoidal Structuring Element with a Width M=7 and a Height A=1

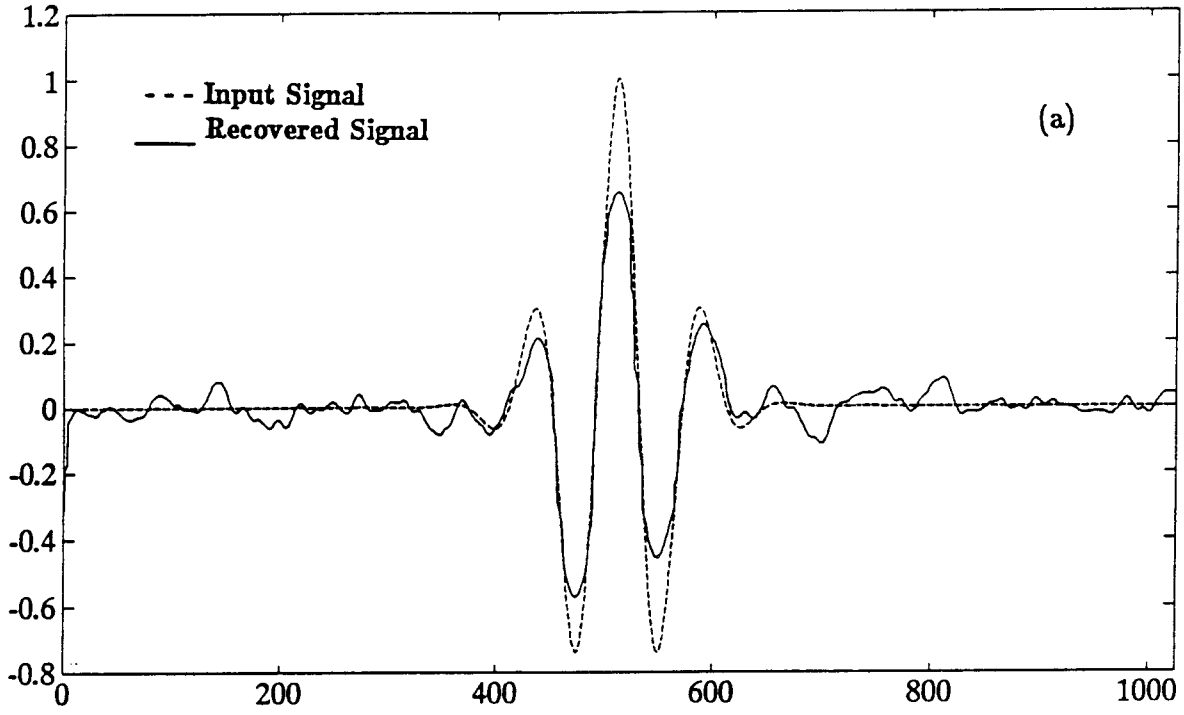

Figure 5.5a Comparison between the Input Echo Signal and Recovered Echo

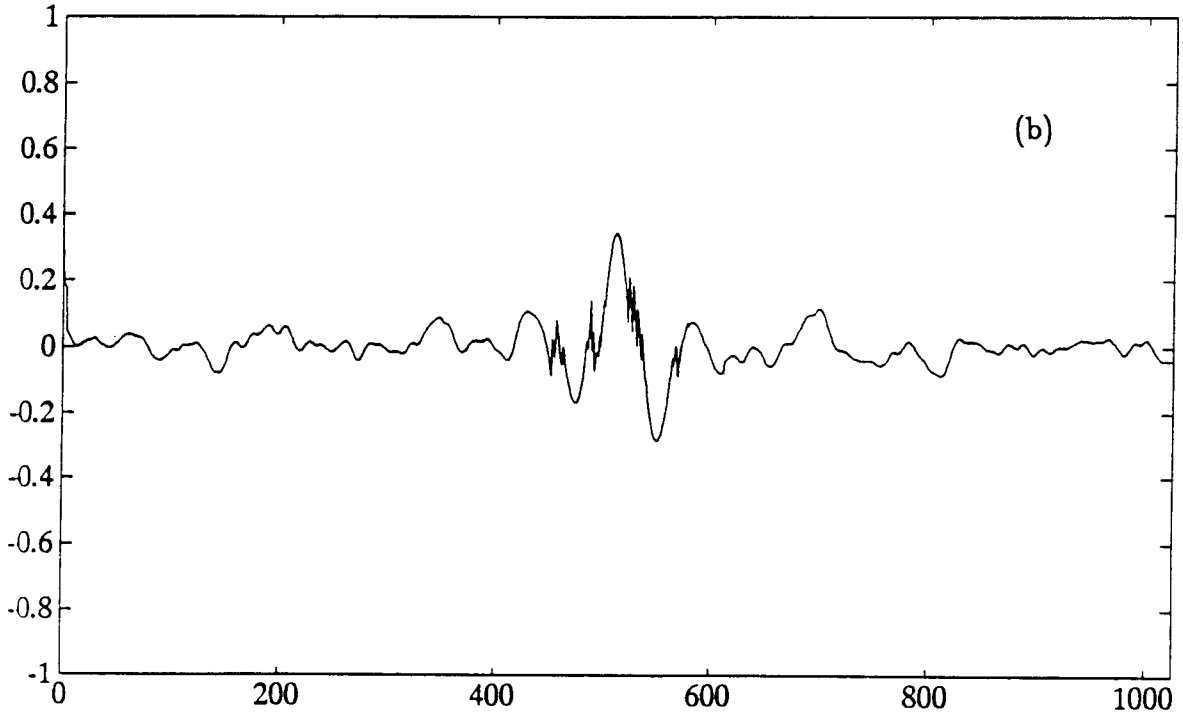

Figure 5.5b The Error Signal

18.65 dB. This means that the morphological filter improved the signal-to-noise ratio by 13.11 dB.

5.2 Filter Classification

In general, various types of morphological filters can be designed using a combination of basic morphological operations with different structuring elements. By varying the structuring element one can extract different types of information from the signal. In this section, the effect of the parameters of the structuring element on the output signal are examined through a sequence of opening and closing operations. Also, different types of filters are constructed using a sequence of morphological operations in parallel and series.

To demonstrate the effect of the parameters of the structuring elements, the Gaussian envelope echo (see Equation (5.1)) was used as an input. This signal is processed using the same sequence of the morphological operations shown in Figure 5.2. Figure 5.6 shows the processed signal using a flat structuring element. The flat element has a width M and a constant height equal to zero. The output signal is processed for different values of M. When $M \geq 7$, the output signal begins to attenuate with small distortion until M=21. When $M \geq 21$ the output echo becomes very small in value and the shape suffers severe distortion. Therefore, we recommend using a structuring element with a width less than half the period of the cosine cycle to preserve the original shape without severe distortion. Figure 5.7 shows the result of applying the single echo to the same block diagram with a sinusoidal structuring element. This figure shows that the output echo is less distorted than the output echo with a flat structuring element of the same width and height. This results because the sinusoidal structuring element has a shape similar to the original signal which allows the sinusoidal structuring element to penetrate inside the peaks or valleys of the input signal. Therefore, the surface of the output takes the shape of the structuring element.

From the above discussion, it is shown that both the shape and width of the

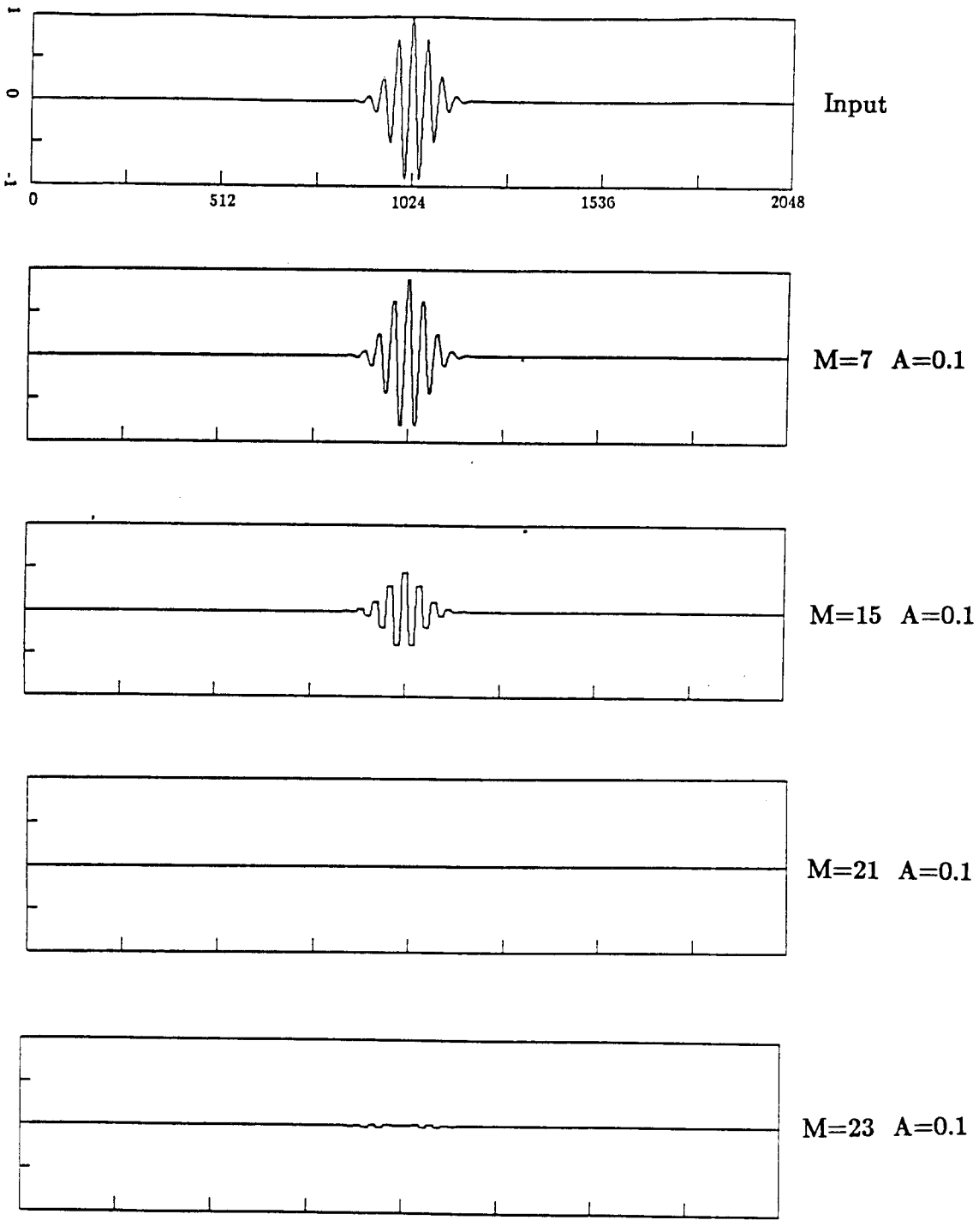

Figure 5.6 The Output Echo using a Flat Structuring Element

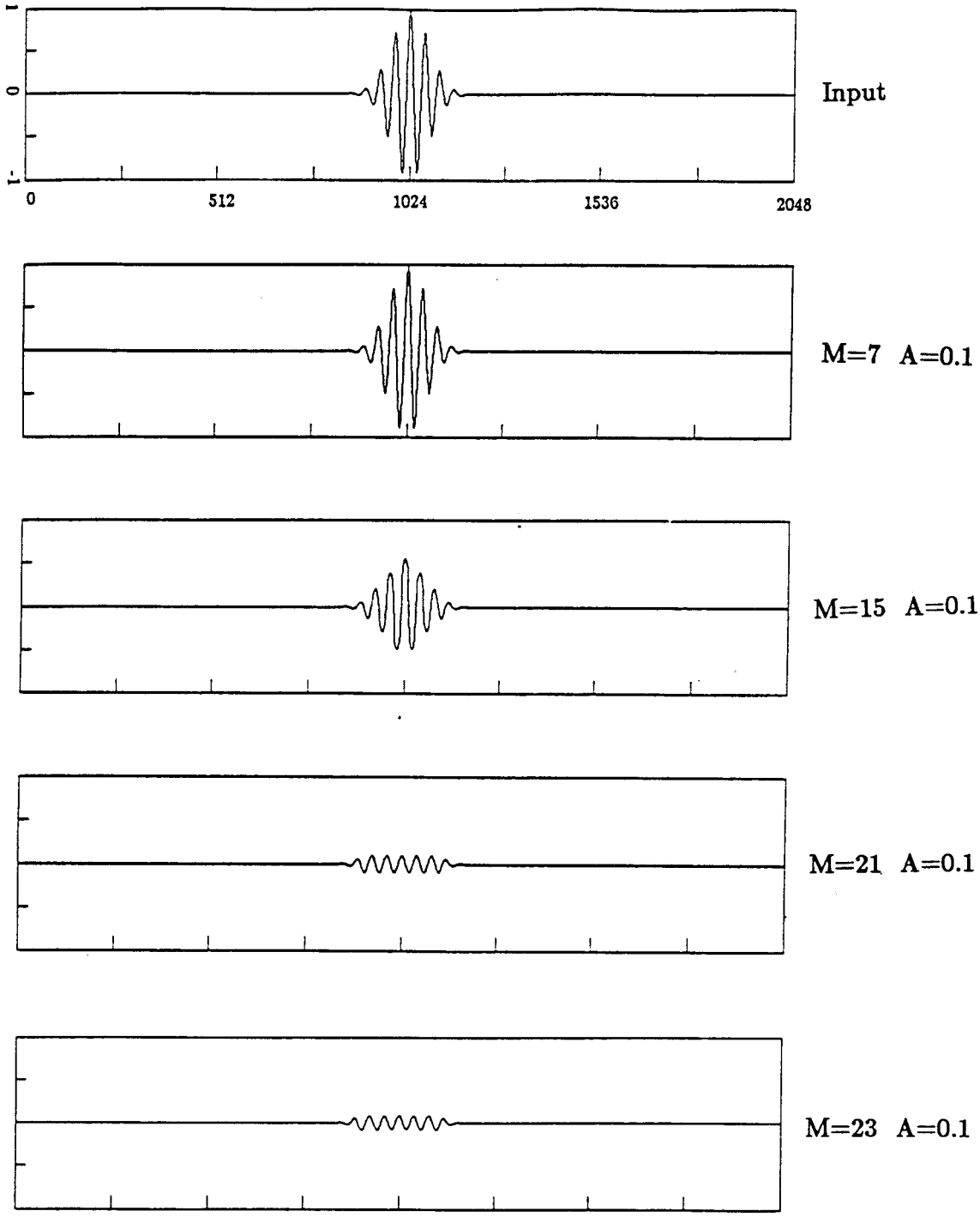

Figure 5.7 The Output Echo using a Sinusodial Structuring Element

structuring elements affect the output. Height is another factor which affects the output. Figure 5.8 shows the effect of the height of a sinusoidal structuring element on input consists of three echoes. These echoes are Gaussian envelope cosine functions with frequencies 5/3, 5/2 and 5 MHz (i.e., 60, 40, and 20 samples/cycle). The width of the structuring element is equal to 11. It can be seen that the output tends to keep the original echoes by increasing the height of the structuring element. The height is more effective when the echo frequency is increased. The output is almost unaffected by the height when the number of samples/cycle is large with respect to the width of the structuring element (60 sample/cycle and width=11). This helps us determine when to keep a certain signal and discard another.

It is well known, if a sinusoidal signal with a certain frequency is unmodified, any signals with a lower frequency will also be unmodified [25]. It is also well known that sequentially alternating the application of opening and closing with the same structuring element removes details of the signal which are small relative to this structuring element. Using classical terminology, we can denote these alternating sequential filters as morphological low-pass filters. The filters are low-pass because the high-frequency fluctuation is attenuated in the output signal [18]. Therefore, we will use this idea to build different types of filters:

- The **low-pass filter** is defined as the average of **open-closing+clos-opening.**
- The **high-pass filter** is defined as the original signal minus the average of **open-closing+clos-opening.**
- The **band-pass filter** is defined as the difference of two averages of **open-closing+clos-opening** with two different structuring elements.

The block diagrams of the high-pass and band-pass filters are shown in Figures 5.9 - 5.10. Also, examples of low-pass, high-pass and band-pass filters are shown in Figures 5.11 - 5.13 respectively for three echoes with different structuring elements. These figures indicate that the parameters of the structuring element with morphological and simple mathematical operations like addition and subtraction determine what frequencies of the signal are affected by the filtering.

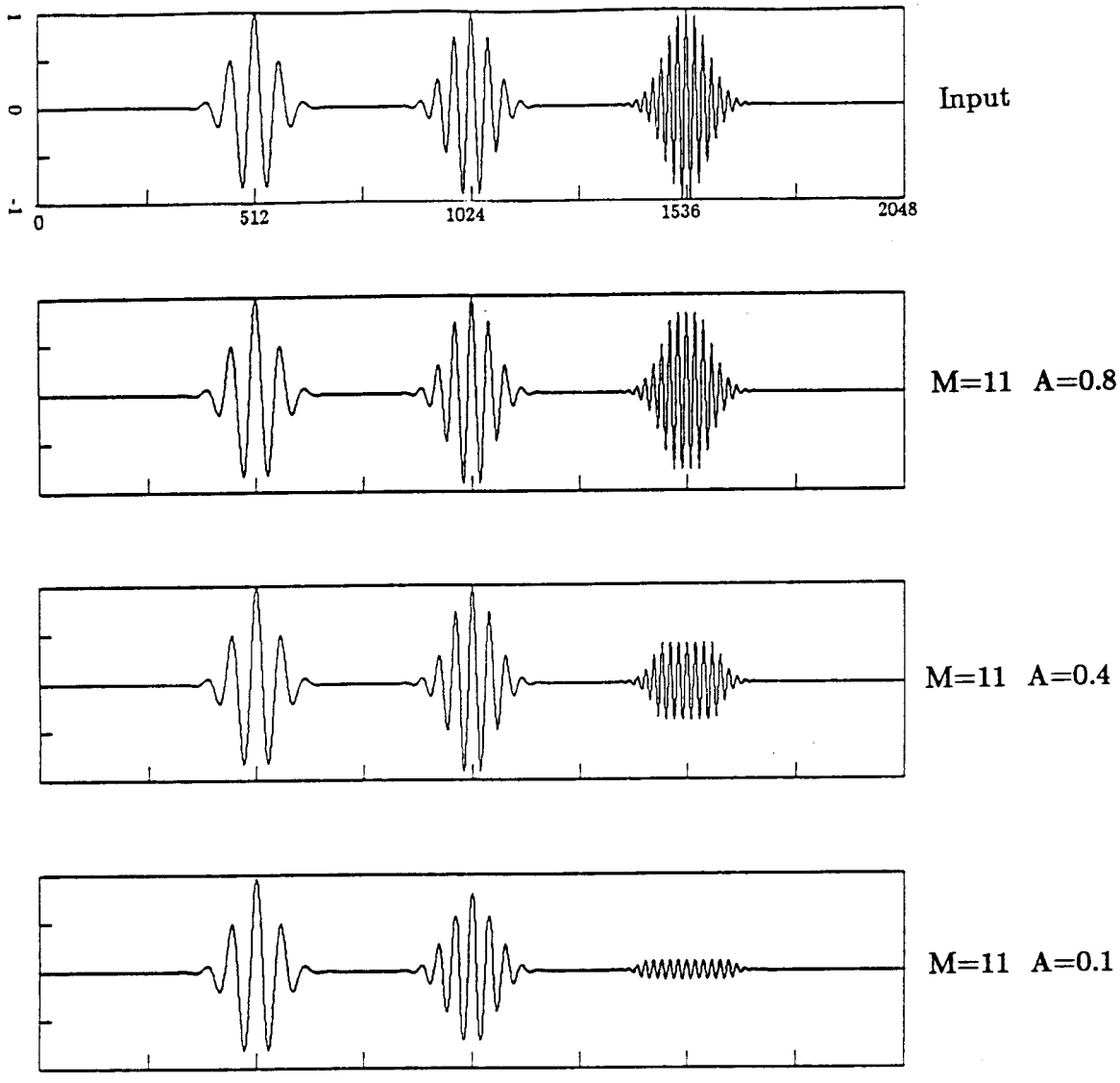

Figure 5.8 The Effect of Height when using a Sinusodial Structuring Element

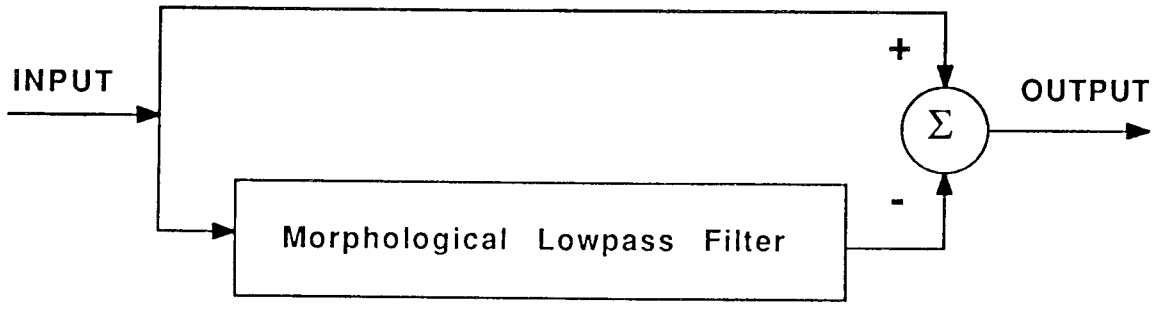

Figure 5.9 Block Diagram of a Highpass Morphological Filter

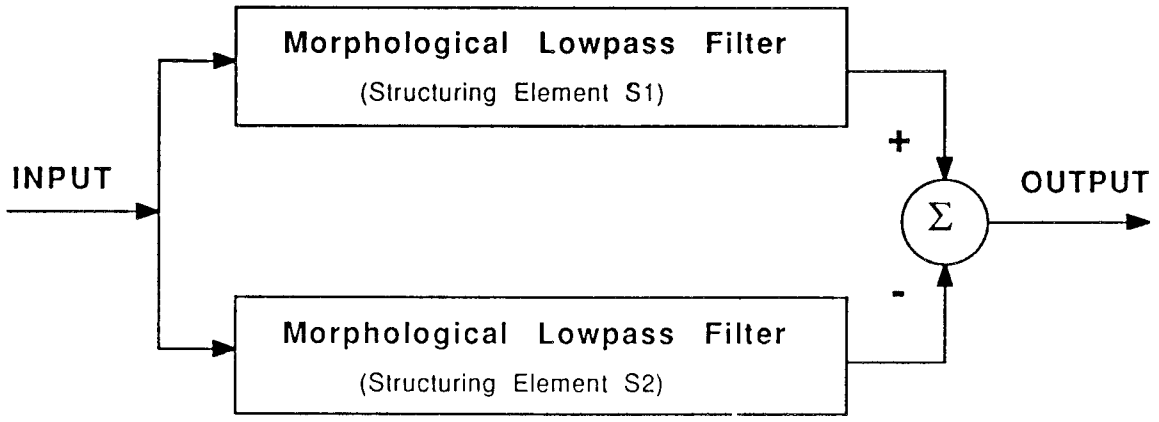

Figure 5.10 Block Diagram of a Bandpass Morphological Filter

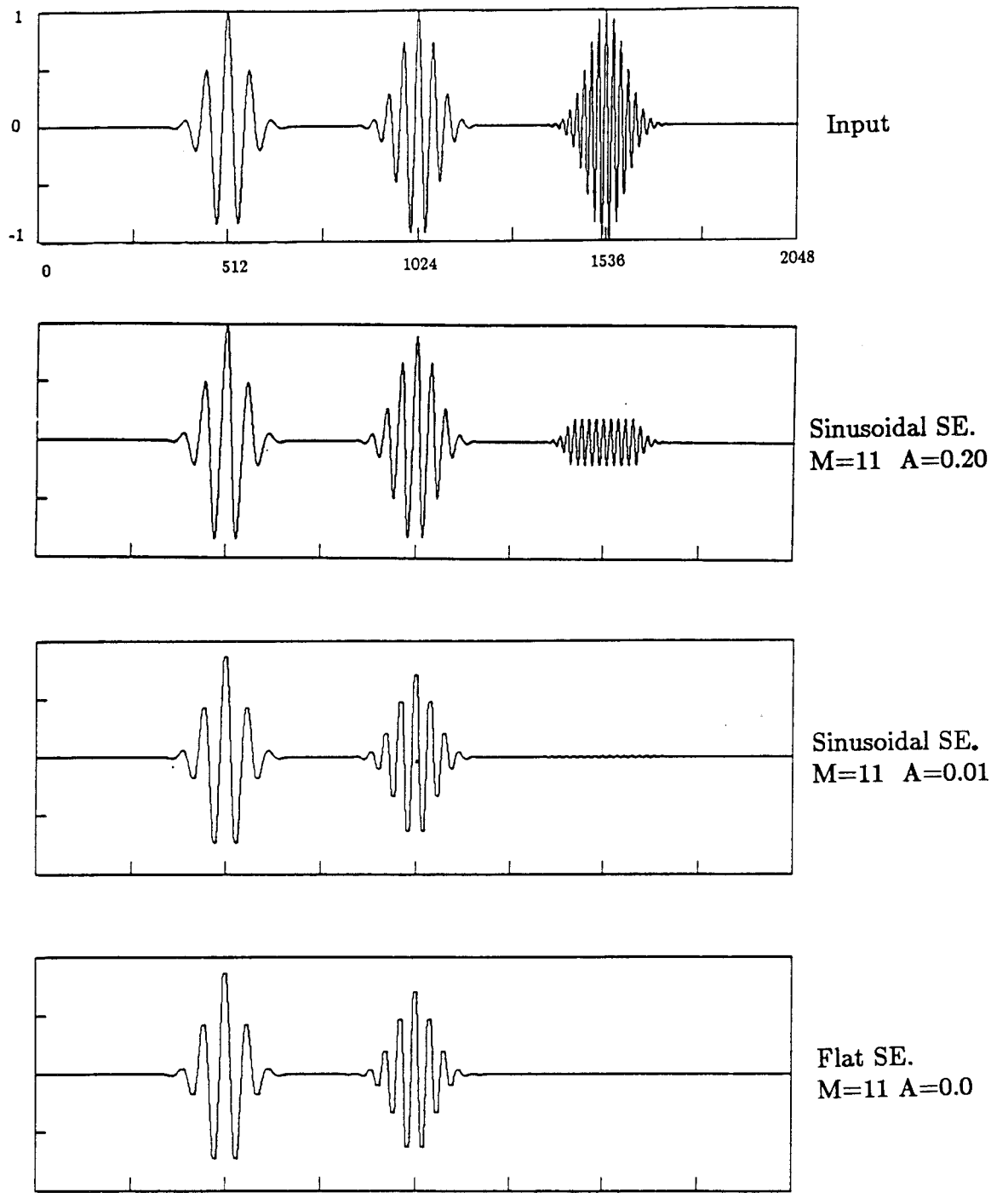

Figure 5.11 Examples of Lowpass Characteristics of Morphological Filters

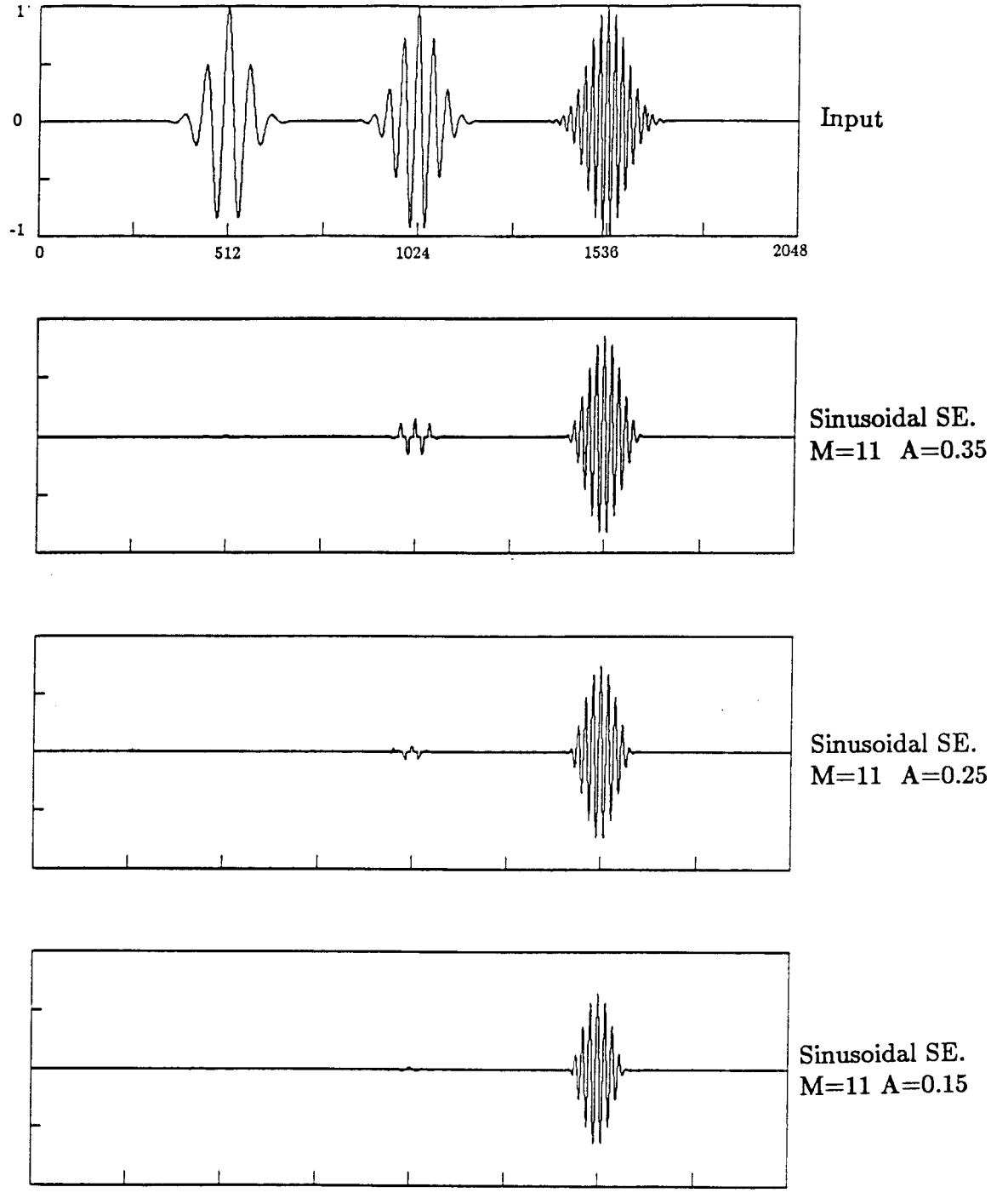

Figure 5.12 Examples of Highpass Characteristics of Morphological Filters

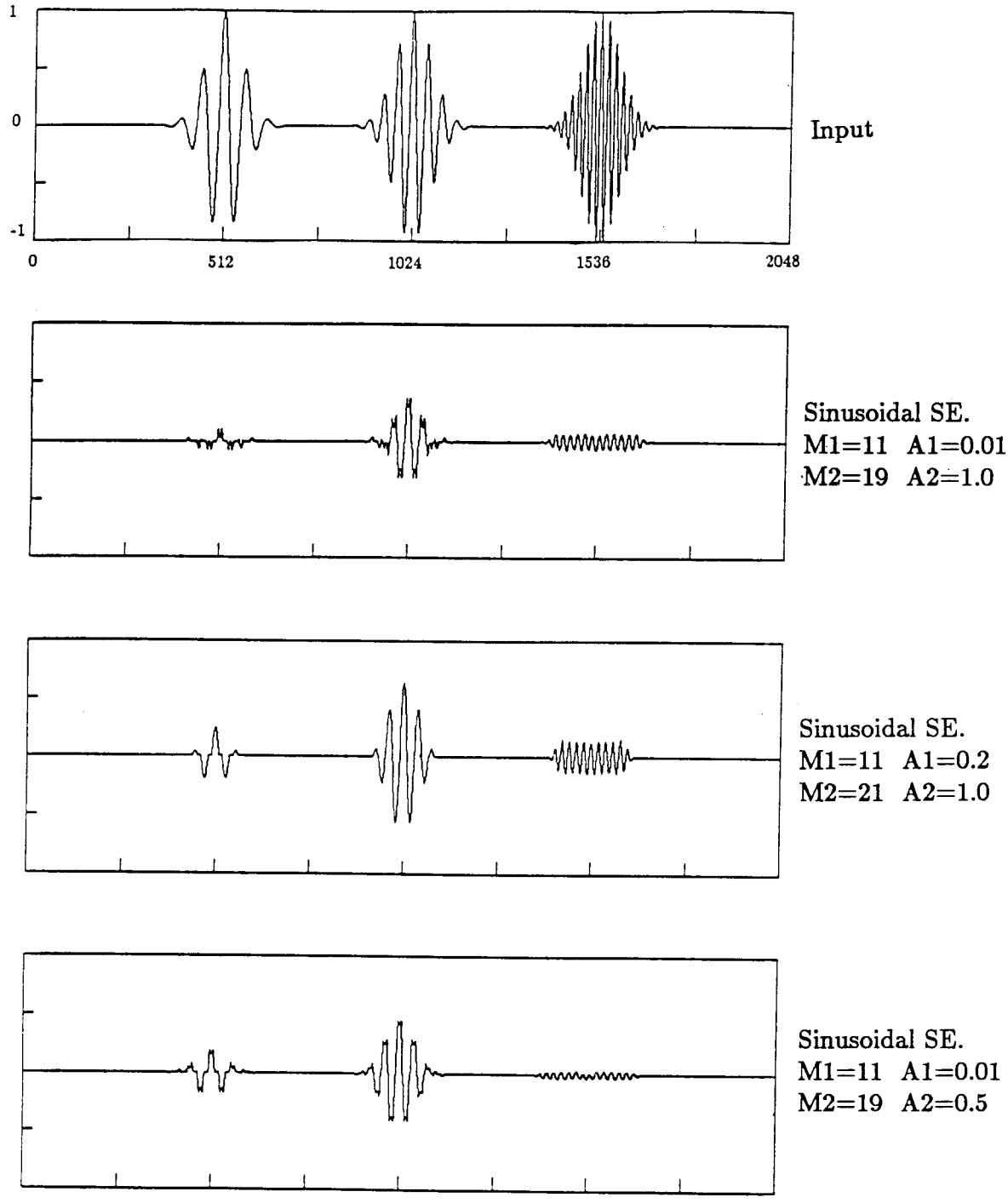

Figure 5.13 Examples of Bandpass Characteristics of Morphological Filters

In general, nonlinear filtering cannot be analyzed in terms of frequency response. Linear filtering, via the superposition principle, allows frequency response analysis by decomposing the input and output into a sum of sinusoidals. The superposition principle does not apply to nonlinear filters, hence "bandwidth" is a meaningless quantity. This study indicates that the filtering process depends on the input signal as well as the parameters of structuring elements.

CHAPTER VI

MORPHOLOGICAL FILTERS FOR ULTRASONIC FLAW DETECTION

6.1 Introduction

Ultrasonic flaw detection is an important application of morphological filters. The goal in detection is to isolate the flaw echo from its background noise (e.g., speckles or microstructure scattering echoes) and to estimate its exact location. In this Chapter, morphological filters have been applied to enhance the features of ultrasonic signals (A-Scan or B-Scan) when they have been contaminated by multiple interfering echoes with random amplitudes and phases. These interfering echoes often become significant to the point that the detection of flaw echoes becomes very difficult. We have used the information content of ultrasonic signals to design a suitable structuring element to enhance flaw-to-clutter ratio. Also, the performance of morphological filters is compared with other techniques such as recursive median filters and frequency diverse rank order statistic filters. This Chapter is organized as follows. In Section 6.2, experimental results are presented which illustrate objectively the performance of morphological filters to detect flaw and improve flaw-to-clutter ratio. Then, a comparison between the performance of morphological and recursive median filters when applied to ultrasonic signals is presented in Section 6.3. In Section 6.4, the performance of morphological filters is compared with frequency diverse rank order statistic filters. Finally, the performance of morphological filters for improving flaw detection and resolution when applied to experimental ultrasonic images (B-Scan) is evaluated in Section 6.5.

6.2 Experimental Results for Noise Suppression and Flaw Detection

This section focuses on the selection of morphological filters to detect flaw (i.e., target) in the ultrasonic imaging of complex structures with high scattering noise (clutter). To illustrate the effectiveness of the parameters of the structuring

element in ultrasonic flaw detection a broadband transducer was used to test a simulated flaw embedded within a steel block. Measurements were accomplished using the contact technique and data was acquired with a 100 MHz sampling frequency. An experimental measurement of a broadband signal with its amplitude spectrum is shown in Figure 6.1. This signal was processed by the same sequence of opening and closing operations discussed in the previous chapter (see Figure 5.2). Processed results are shown in Figure 6.2 for a flat structuring element with different widths (M=4, 5, 6, 7, and 8 samples). These results indicate that morphological filters are capable of detecting targets while suppressing clutter.

In order to achieve an optimal performance of morphological filters for noise suppression and flaw detection, the effect of the width of the flat structuring element in detecting ultrasonic signals was examined using the flaw-to-clutter ratio (FCR) of the output signal and an evaluation of the zero crossing of the input signal. The FCR of the output signal as a function of the width of a flat structuring element is shown in Figure 6.3. This figure shows that the FCR increases as the width approaches the optimal value (M_{op}= 6). The FCR of the output signal at M_{op}=6 is 1.6 times (i.e., 2.05 dB) better than the FCR of the input signal.

To further achieve a better selection of morphological filters, the number of zero crossings of the processed output signal is calculated as a function of the width of the flat structuring element. The result is shown in Figure 6.4 which indicates that the number of zero crossings decreases when the width of a flat structuring element is increased. This simply implies that the smoothing process becomes more effective when the width of the structuring element is increased, although excessive smoothing may eliminate flaw echoes. Therefore, an evaluation of a zero crossing can lead to an estimation of the optimal width of the structuring element. Since microstructure echoes represent the dominating information, hence properly removing them requires a structuring element with a width larger than the duration of zero crossing of the measured signal. The average width estimated

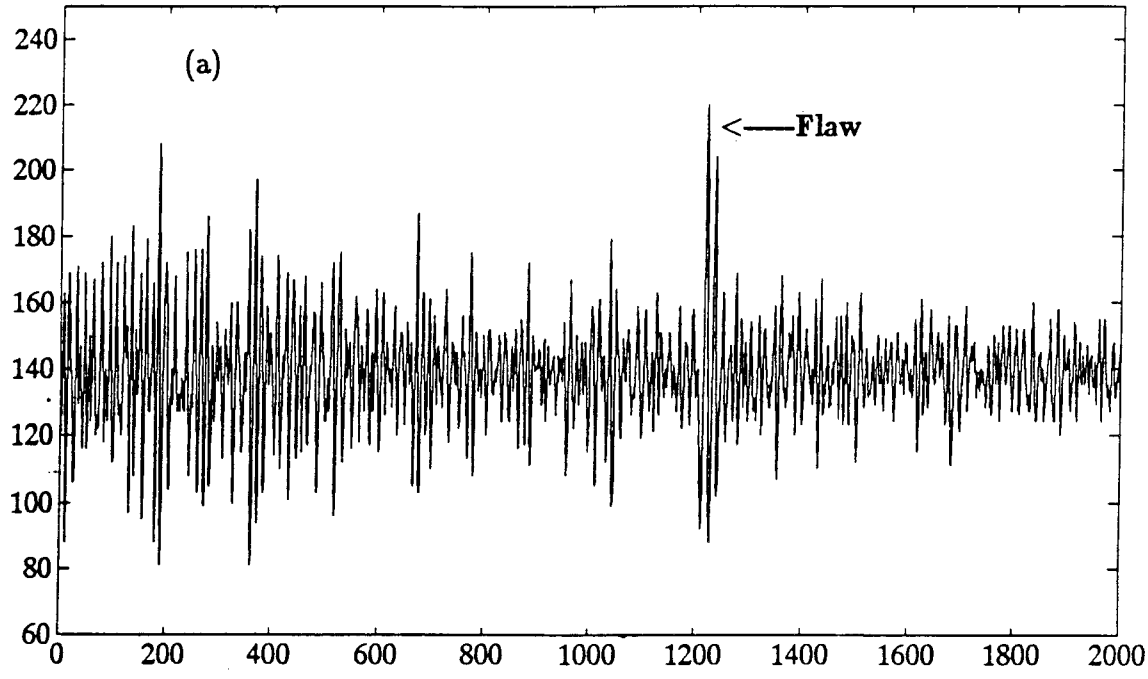

Figure 6.1a An Ultrasonic Backscattered Flaw Signal

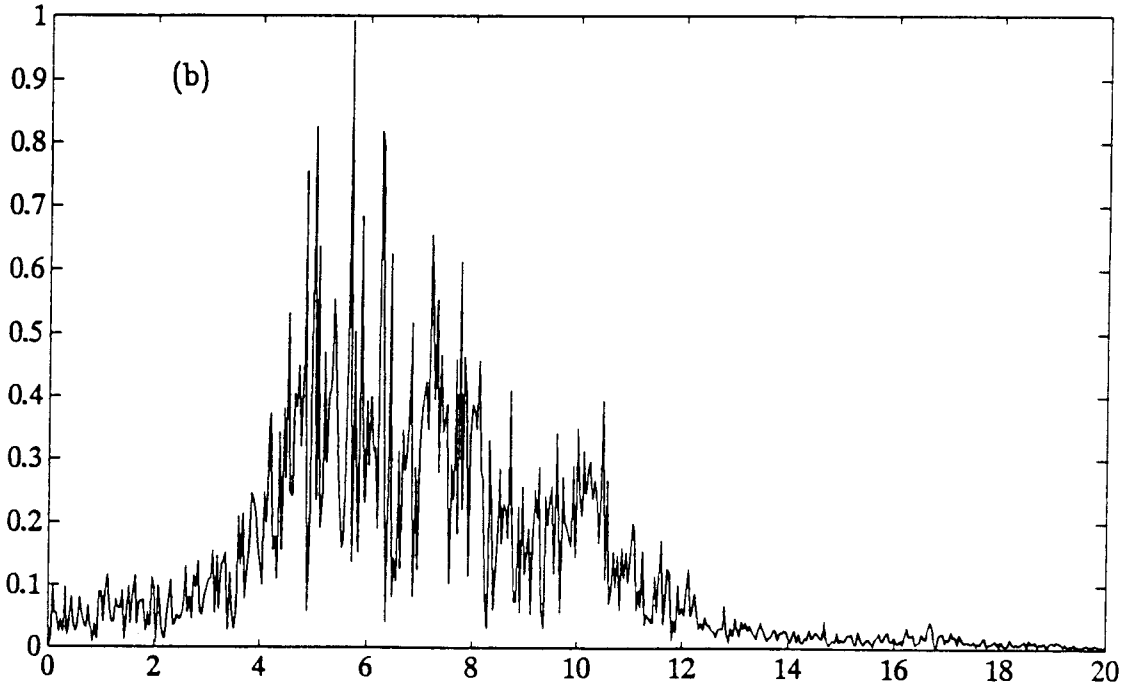

Figure 6.1b Amplitude Spectrum of the Signal

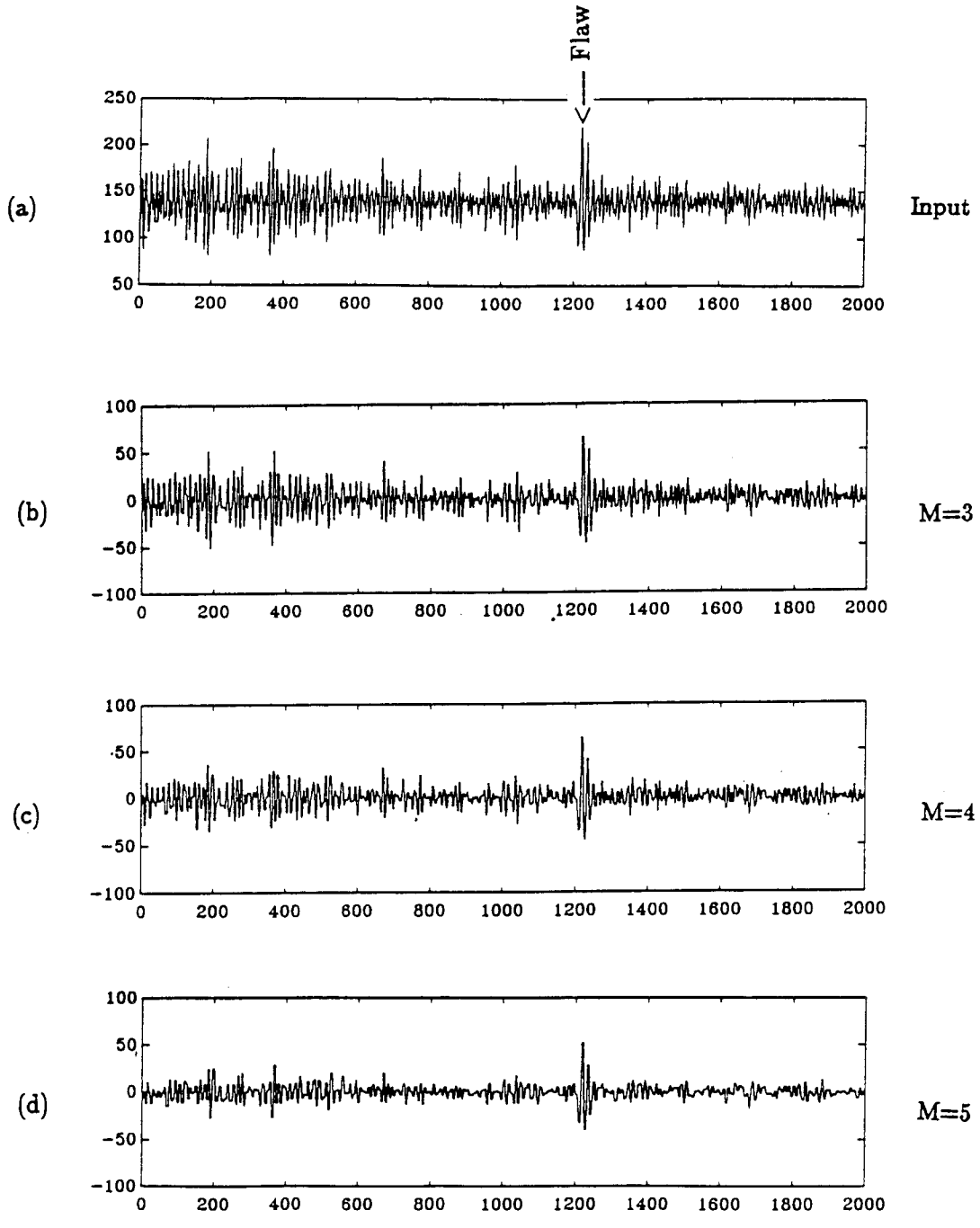

Figure 6.2 Flaw Echo Detection and Clutter Suppression using Morphological Filters with Flat Structuring Elements. The Flat Structuring Elements have Different Widths (M). Figure (a) is the Original Measured Signal

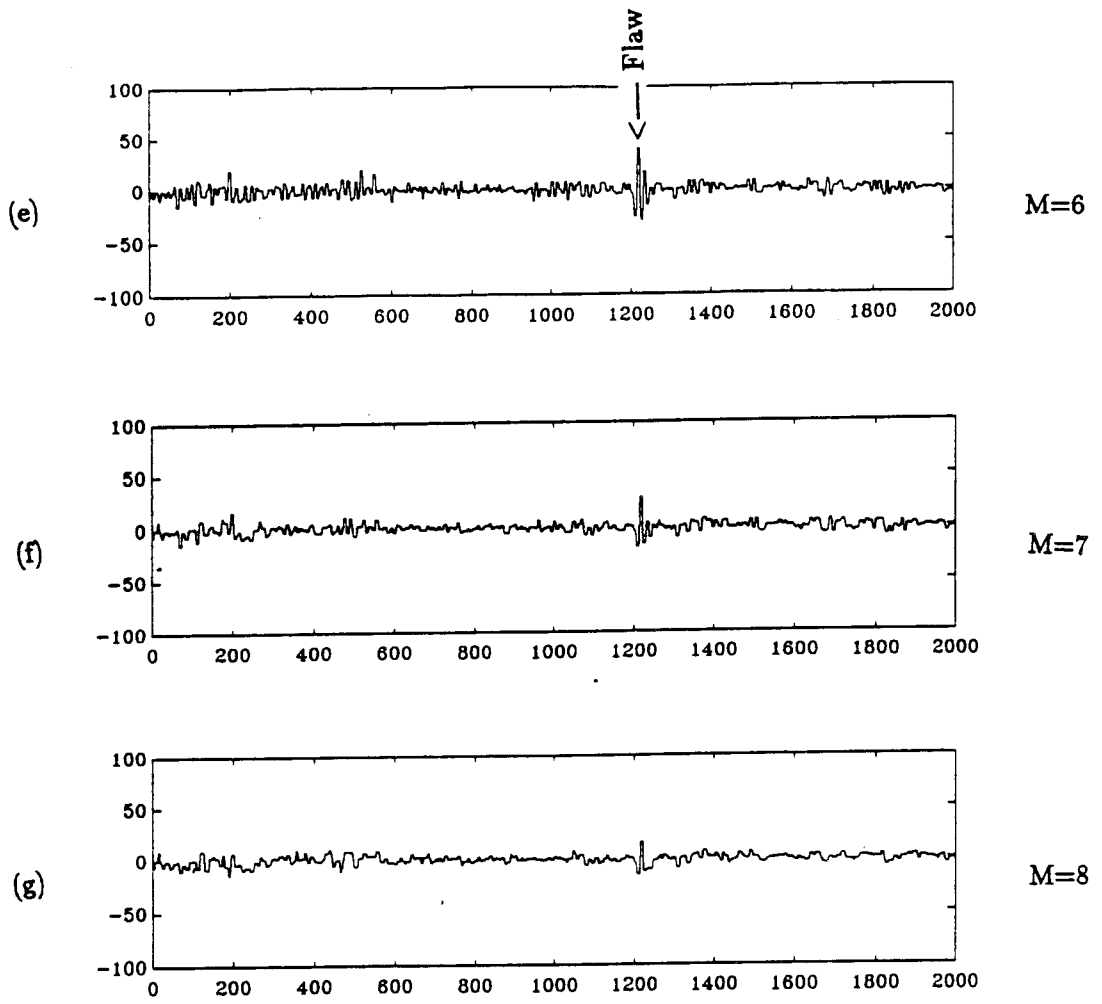

Figure 6.2 (Continued)

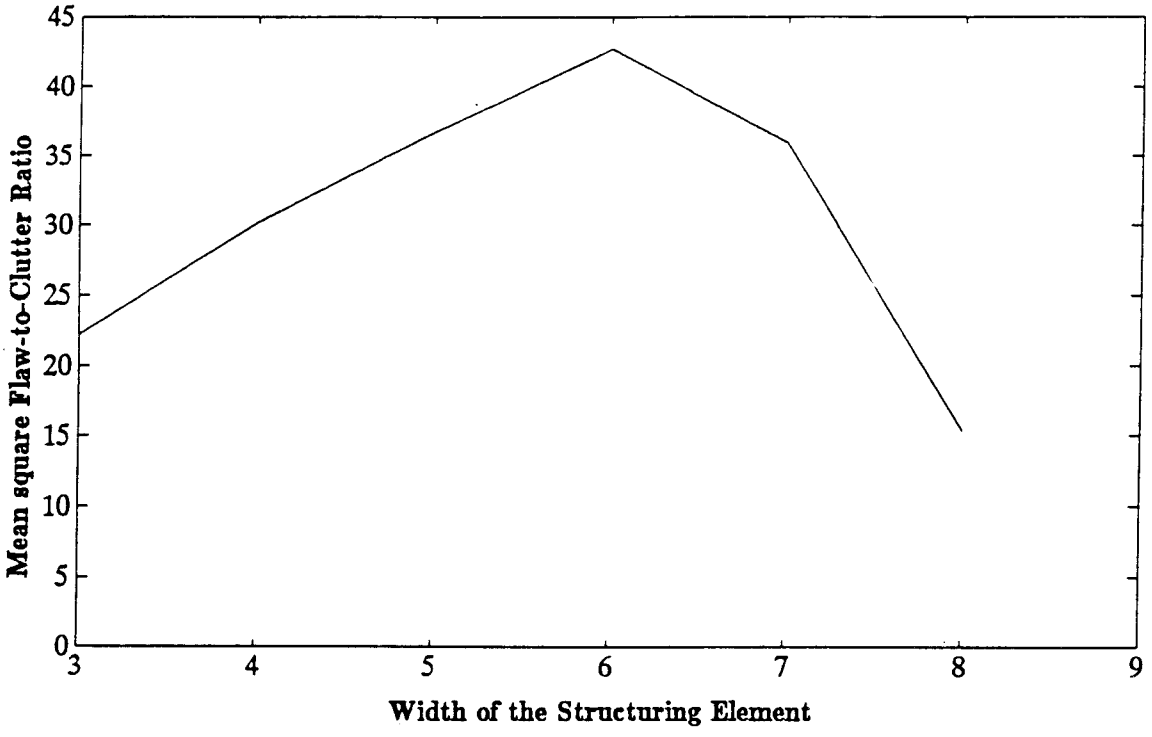

Figure 6.3 Flaw-to-Clutter Ratio of the Output Signal as a Function of the Width of the Flat Structuring Element

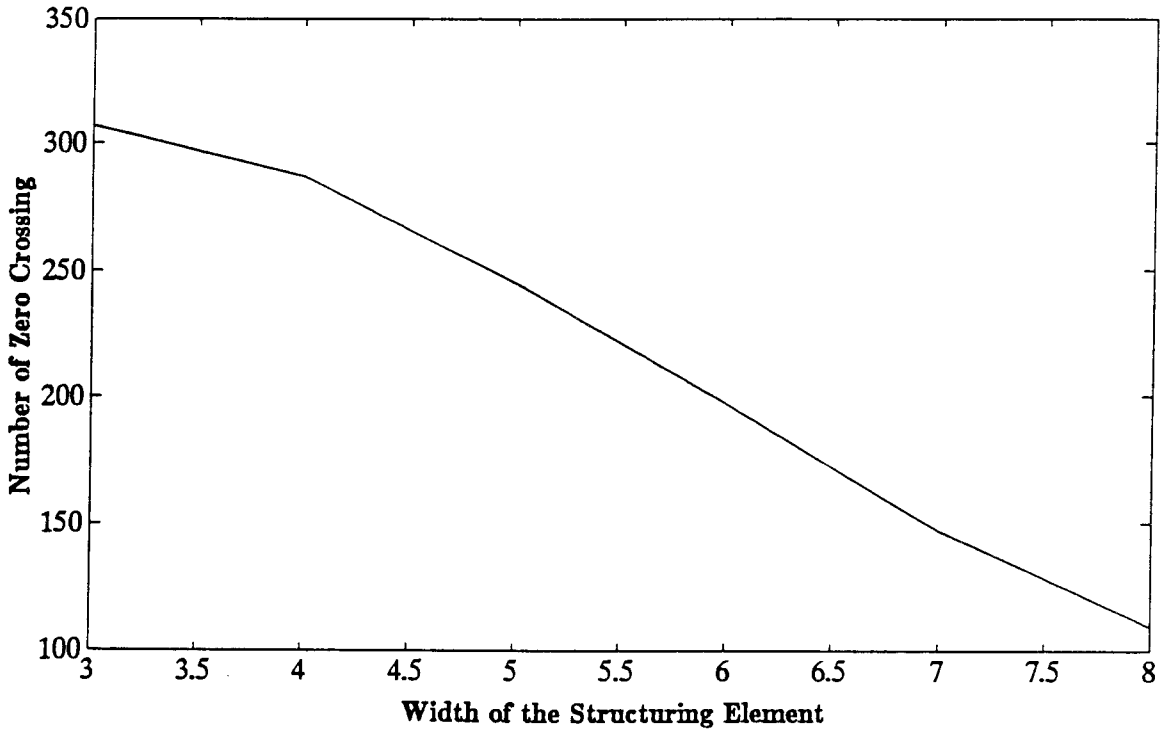

Figure 6.4 Zero Crossing of the Output Signal as a Function of the Width

with a zero crossing for the measured signal is 5.14 which is very close to the optimal width, M_{op}=6, of the flat structuring element.

The strength of morphological filters lies in their natural coupling between the shape of the signal and the structuring element. To illustrate the effectiveness of the parameters of the structuring element in detection, an experimental measurement of an ultrasonic signal contaminated by microstructure scattering noise has been used as an input (Figure 6.1). A comparison between the performance of a flat and sinusoidal structuring element with the same width (M = 5 samples) and height (A=2.0) for a segment of the processed signal, i.e., (1140 - 1300 samples) is shown in Figure 6.5. This figure indicates that the sinusoidal structuring element preserves the original shape of the signal better than the flat structuring element because the surface of the processed signal takes the shape of the structuring element. However, the flat structuring element smooths the signal more effectively than the sinusoidal structuring element of the same width. Note that the height of the flat structuring element does not effect the processed results when a closing or opening operation is performed.

A comparison of the FCR between the flat and sinusoidal structuring elements of the processed signal is shown in Figure 6.6. This figure shows that the FCR increases as the width approaches the optimal value (M_{op}=6 for a flat structuring element and M_{op}=7 for a sinusoidal structuring element). In general, these results indicate that the application of a flat structuring element results in better FCR while a sinusoidal structuring element has better syntactical performance in preserving the details of the original signal.

To further improve the resolution and FCR ratio for flaw detection, it is effective to estimate the background echoes (clutter) and then subtract this estimate from the preprocessed signal. This technique is a band-pass filtering operation and can be represented as

$$\hat{y}(n)=y(n)-[(y(n)os_2)\bullet s_2+(y(n)\bullet s_2)os_2]/2 \qquad (6.1)$$

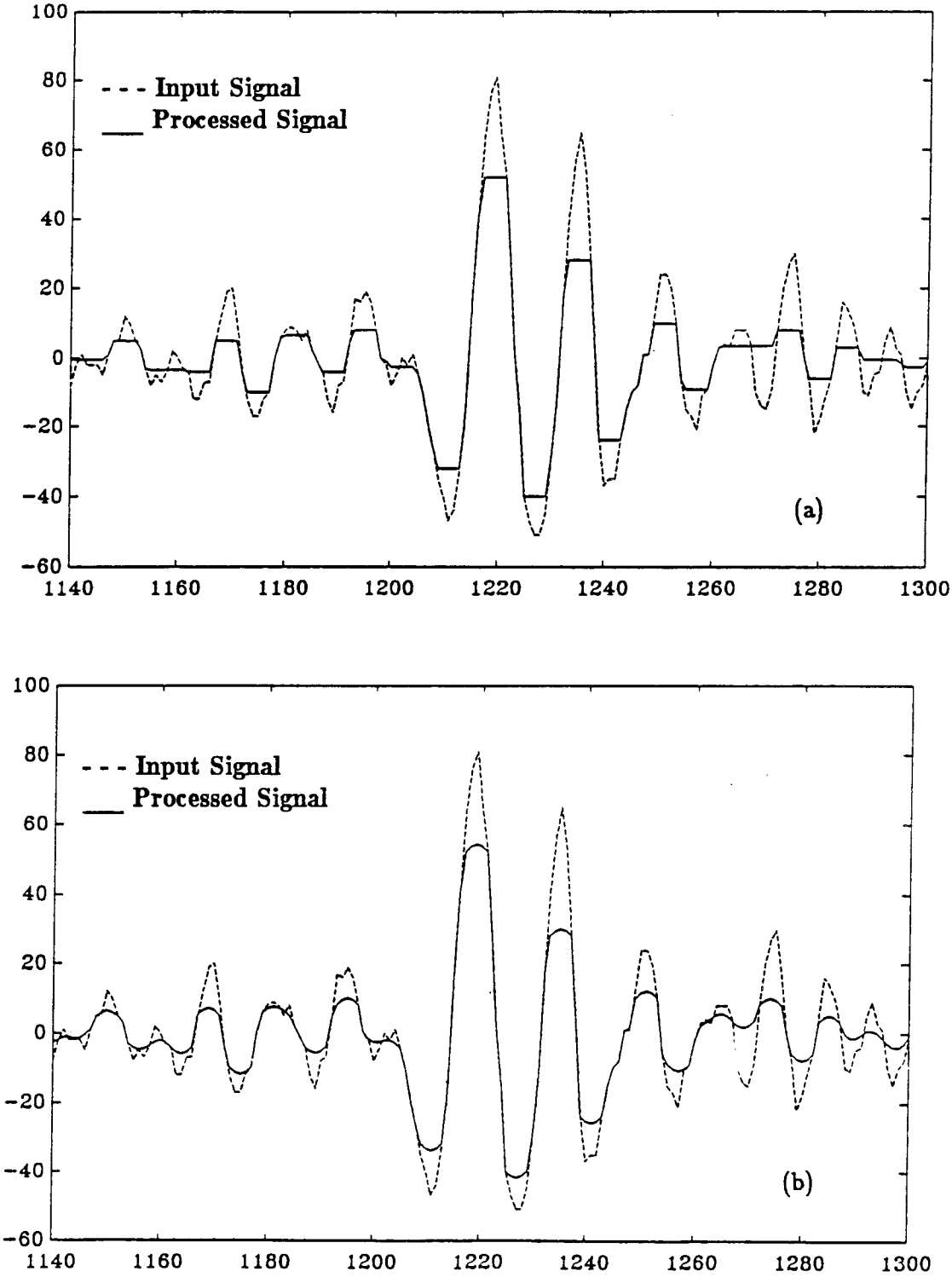

Figure 6.5 The Effect of Structuring Elements on the Processed Ultrasonic Signals using
(a) Flat Structuring Element with a Width M=5
(b) Sinusoidal Structuring Element.

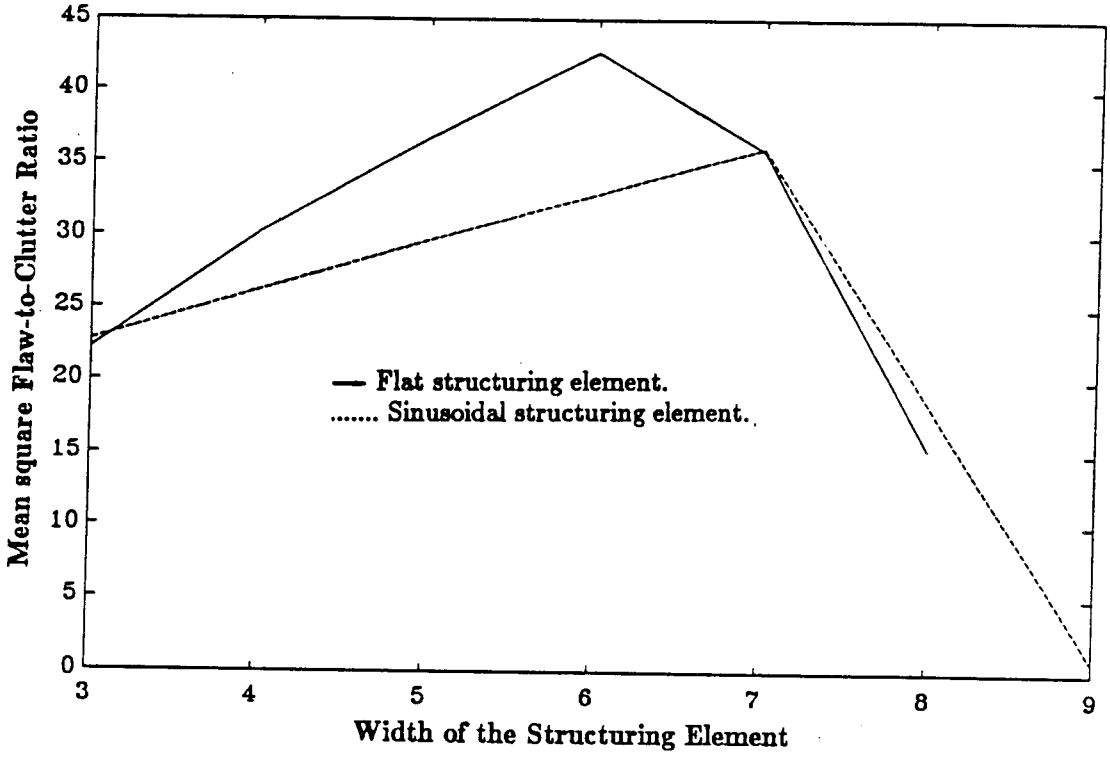

Figure 6.6 Flaw-to-Clutter Ratio of the Output Signal as a Function of the Width using
(a) Flat Structuring Element
(b) Sinusoidal Structuring Element with a Height A=2.0

where

$$y(n)=[(x(n)\ o\ s_1)\bullet s_1 + (x(n)\bullet s_1)\ o\ s_1]/2, \qquad (6.2)$$

x(n) is the input signal, and s_1 and s_2 are flat structuring elements with lengths of 8 and 10 respectively. Processed results are shown in Figure 6.7. This result shows that the background noise is tremendously reduced, while the resolution is enhanced. The FCR is also improved by 5.66 dB.

Morphological filters can be used as a replacement for ensemble averaging which requires numerous measurements. Ensemble averaging is also impractical because it can not eliminate interfering echoes resulting from stationary scatterers. A typical measured ultrasonic signal with poor FCR is shown in Figure 6.8a. This signal is processed using morphological filters (Figure 5.2) and the result is shown in Figure 6.8b. Figure 6.8c shows the same signal processed using an ensemble averaging of 500 measurements. The ability of each method to smooth the signal is comparable, although morphological filtering is far more practical and efficient.

6.3 Comparison of Morphological and Median Filters

In this section, the performance of morphological filters for flaw detection using different shapes of structuring elements, is compared with the performance of recursive median filters with different lengths (widths). A median filter is a special case of rank order filters whose output is the median of the samples inside certain window with a length (M=2N+1). Median filtering is an efficient point estimation technique which has a low-pass effect yet preserves important signal structures such as edges [35]. The recursive median filter is a modification of the standard median filter which results in the output being the median of the last N outputs and the last N+1 inputs [45]. If {x(.)} and {y(.)} are the input and output of a recursive median filter with window size M=2N+1, respectively, then y(.) is given by

$$y(m) = median\ [\ y(m-N),\ ...,\ y(m-1),\ x(m),\ x(m+1),\ ...,x(m+N)\ ] \qquad (6.3)$$

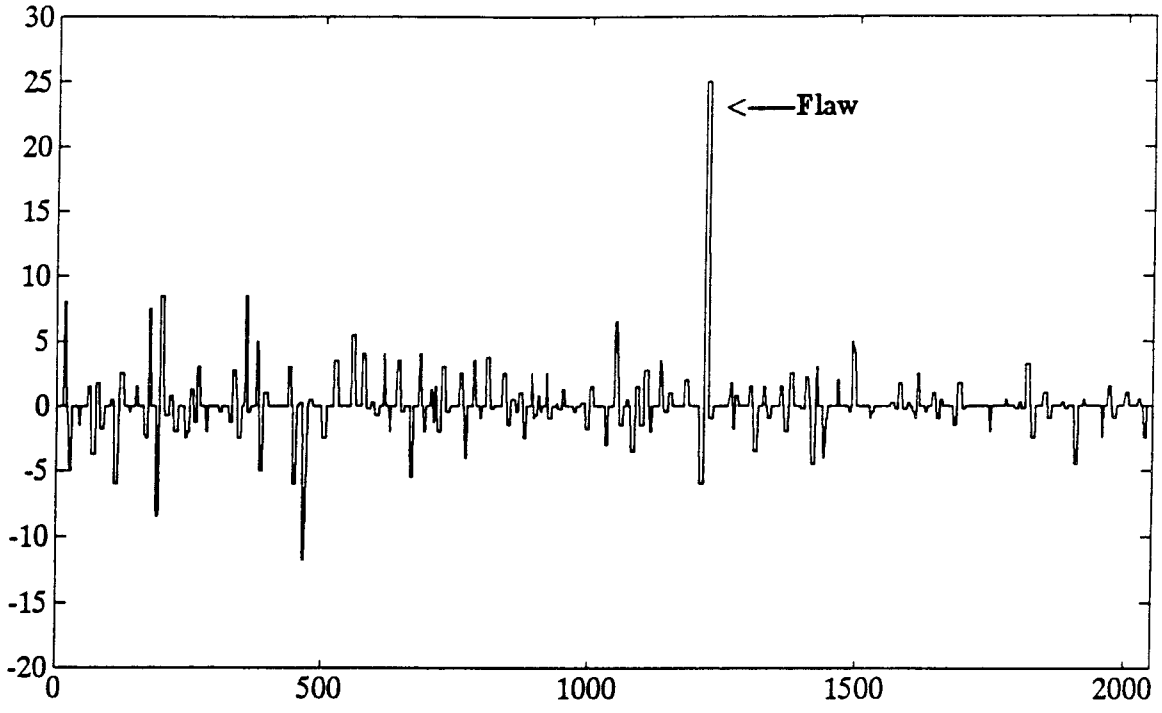

Figure 6.7 Processed Backscattered Flaw Signal using a Morphological Bandpass Filter

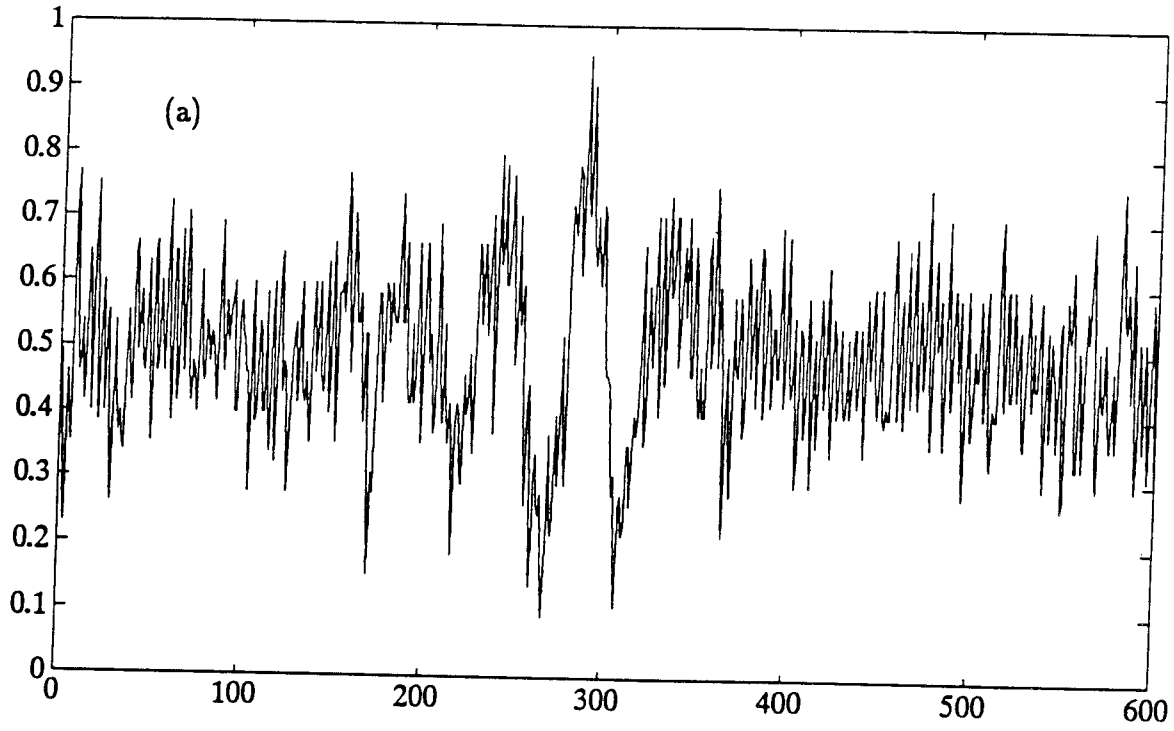

Figure 6.8a A Typical Measured Ultrasonic Echo with Poor Flaw-to-Clutter Ratio

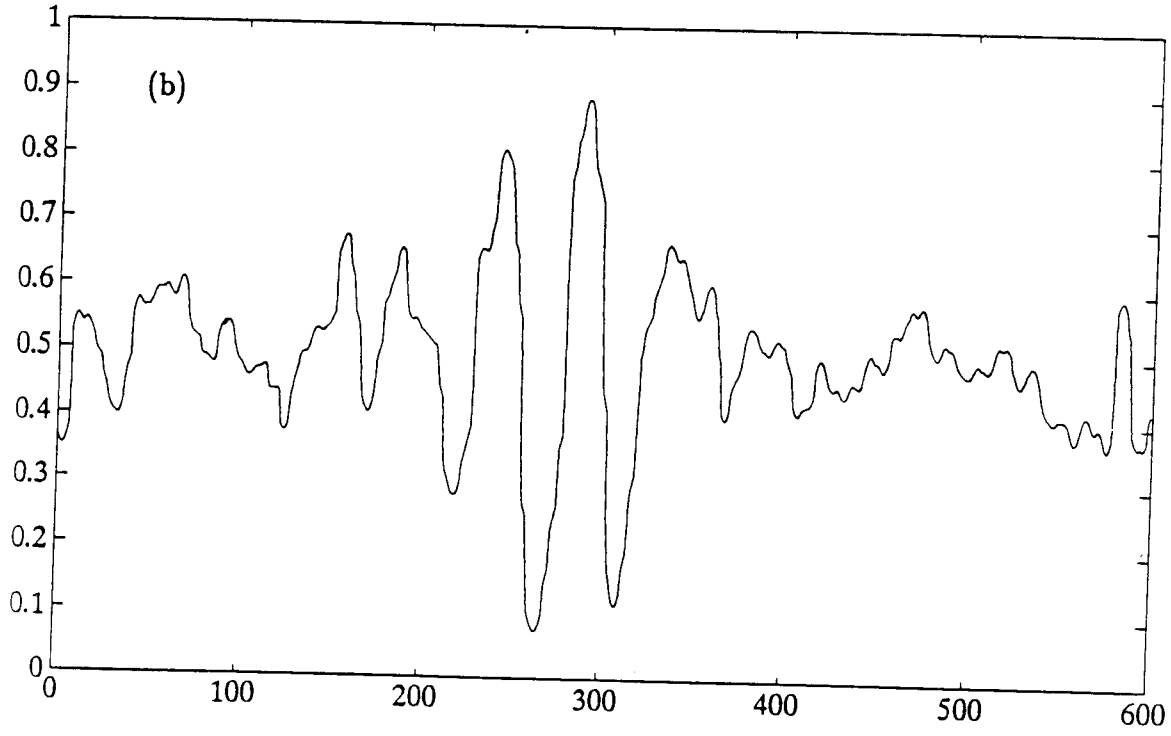

Figure 6.8b The Processed Echo using a Morphological Filter

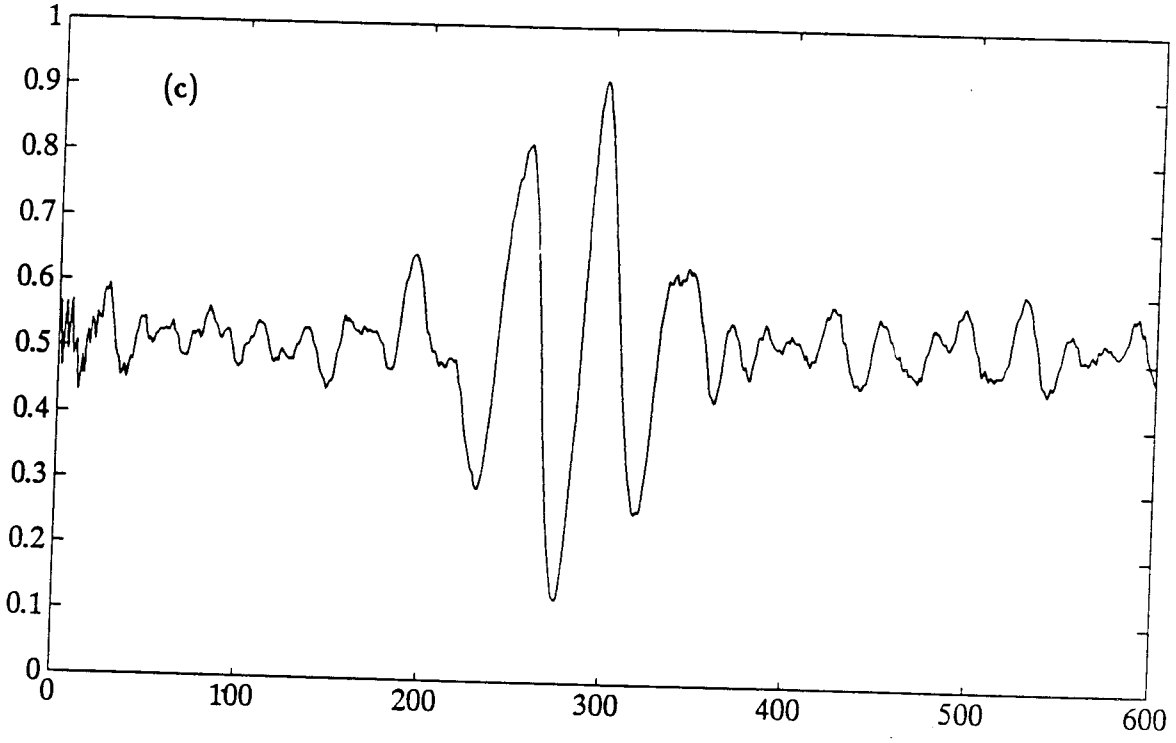

Figure 6.8c Ensemble Averaging of the Echo using 500 Measurements

It important to point out that the recursive operation generates a root with only a single pass through the data, where a root is an invariant signal to the filter.

A connection between median filters and morphological operations with flat structuring elements was made by Maragos [36]. In particular, a signal is a median root if it is the root of both the opening and closing. Moreover, medians and their iterations are bounded below by the opening and above by closing, while the median root is bounded below by the open-closing and above by clos-opening.

The performance of recursive median filters with different widths (M=3, 5, 7, 9, 11, 13, and 15 samples) when applied to the same input ultrasonic signal (see Figure 6.1) is shown in Figure 6.9. This figure shows that the recursive median filter can detect flaw echoes and suppress backscattered noise. Note that morphological filters have better syntactical performance in preserving the details of the signal when compared to recursive median filters since they have a flexibility in changing the shape of their structuring elements to match a particular pattern of the original signal.

6.4 Comparison of Morphological and Rank Order Filters

In the previous sections, both morphological and recursive median filtering have been applied in a time domain for flaw detection and FCR enhancement. Frequency analysis is a useful alternative in which certain features hidden in the time domain can be displayed. In particular, split-spectrum processing combined with rank order statistic filters has been used for flaw detection [46, 47]. In this section, a comparison between morphological filters with frequency diverse rank order statistic filters is presented.

In split-spectrum processing the backscattered signal is divided into several narrow-band channels. The observations from the output of these channels are normalized with respect to the power in order to obtain the equally-powered output signals (see Figure 6.10). These sets of signals represent uncorrelated

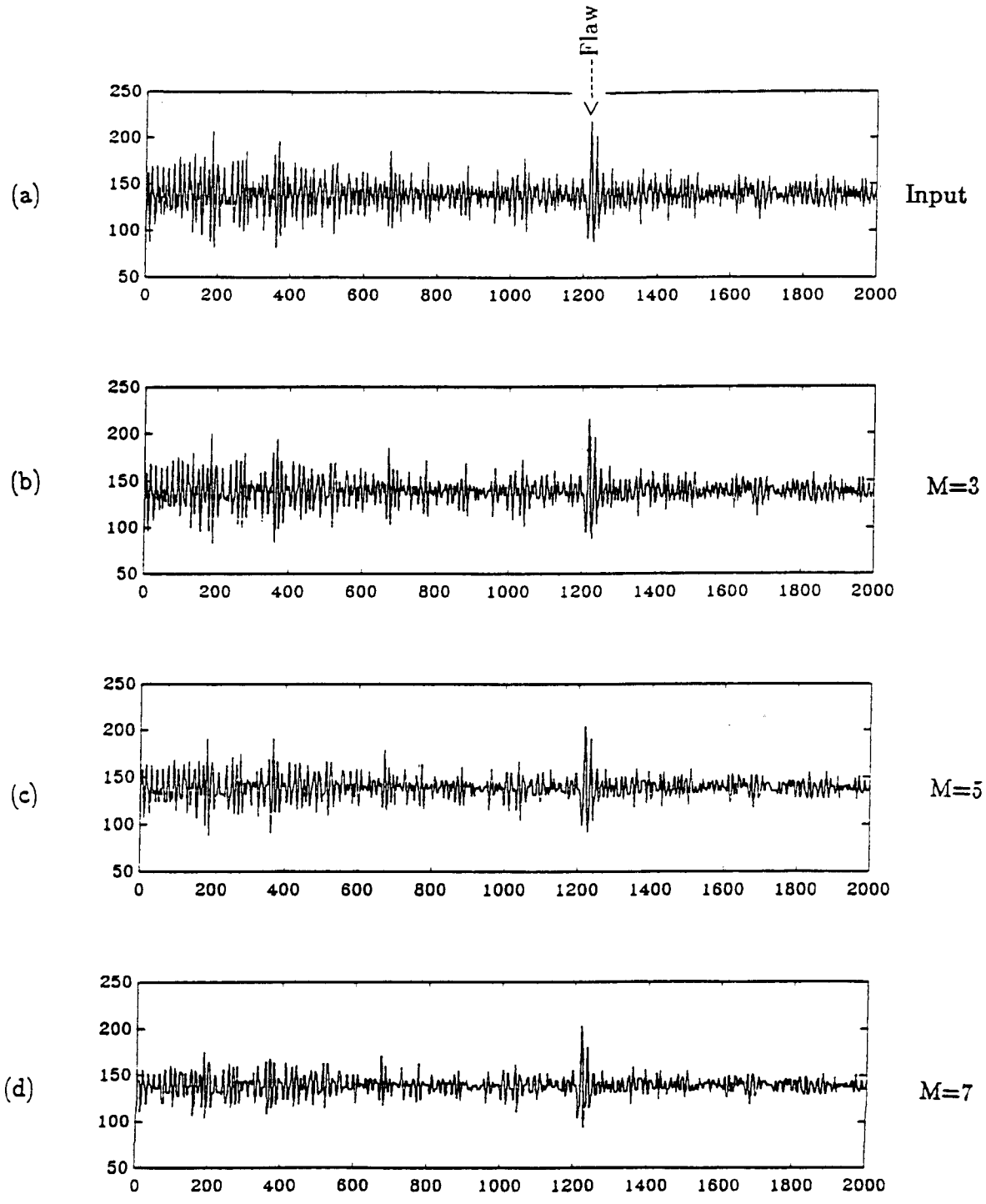

Figure 6.9 Flaw Echo Detection and Clutter Suppression using Recursive Median Filters with Different Widths. Figure (a) is the Original Measured Signal

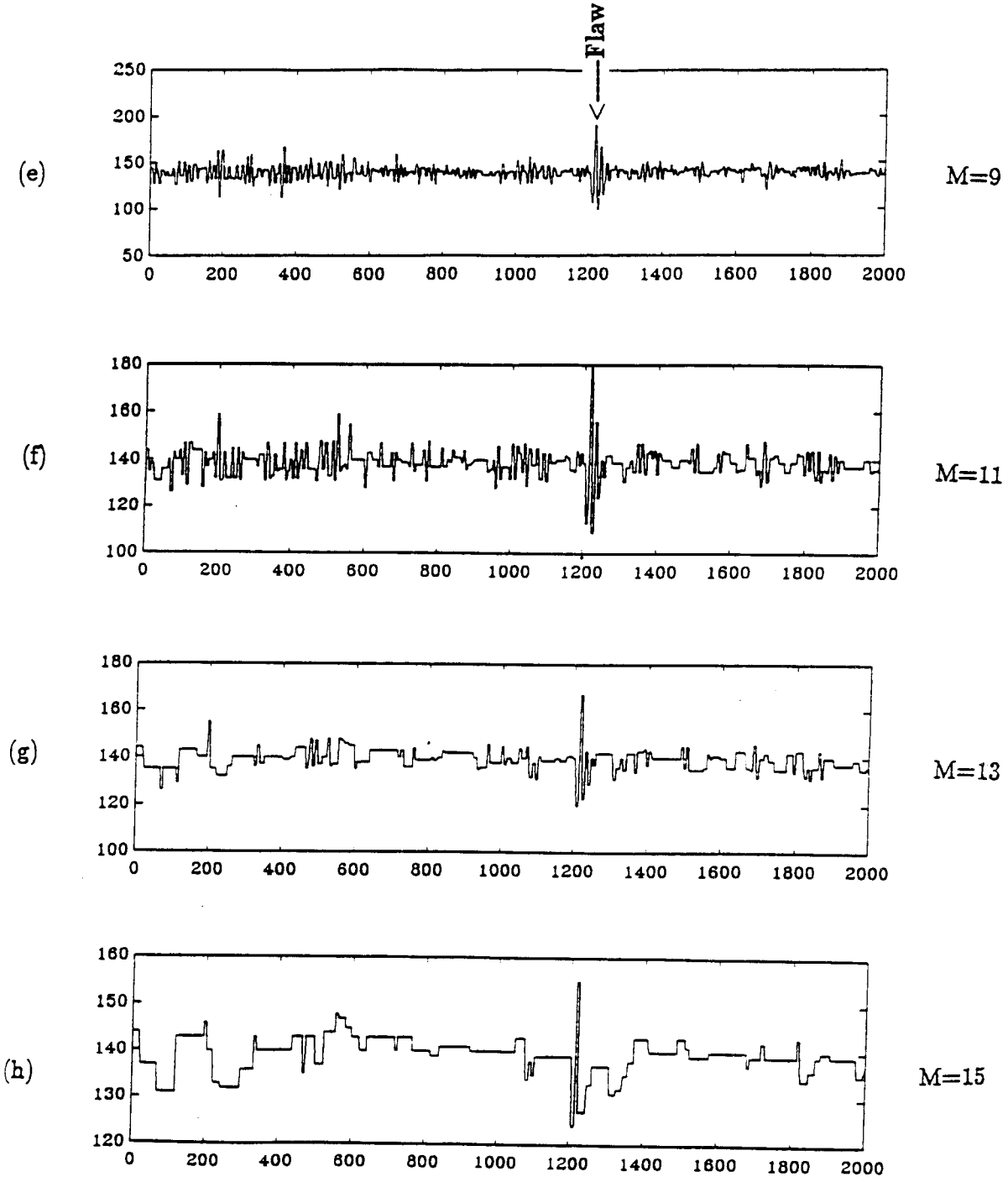

Figure 6.9 (Continued)

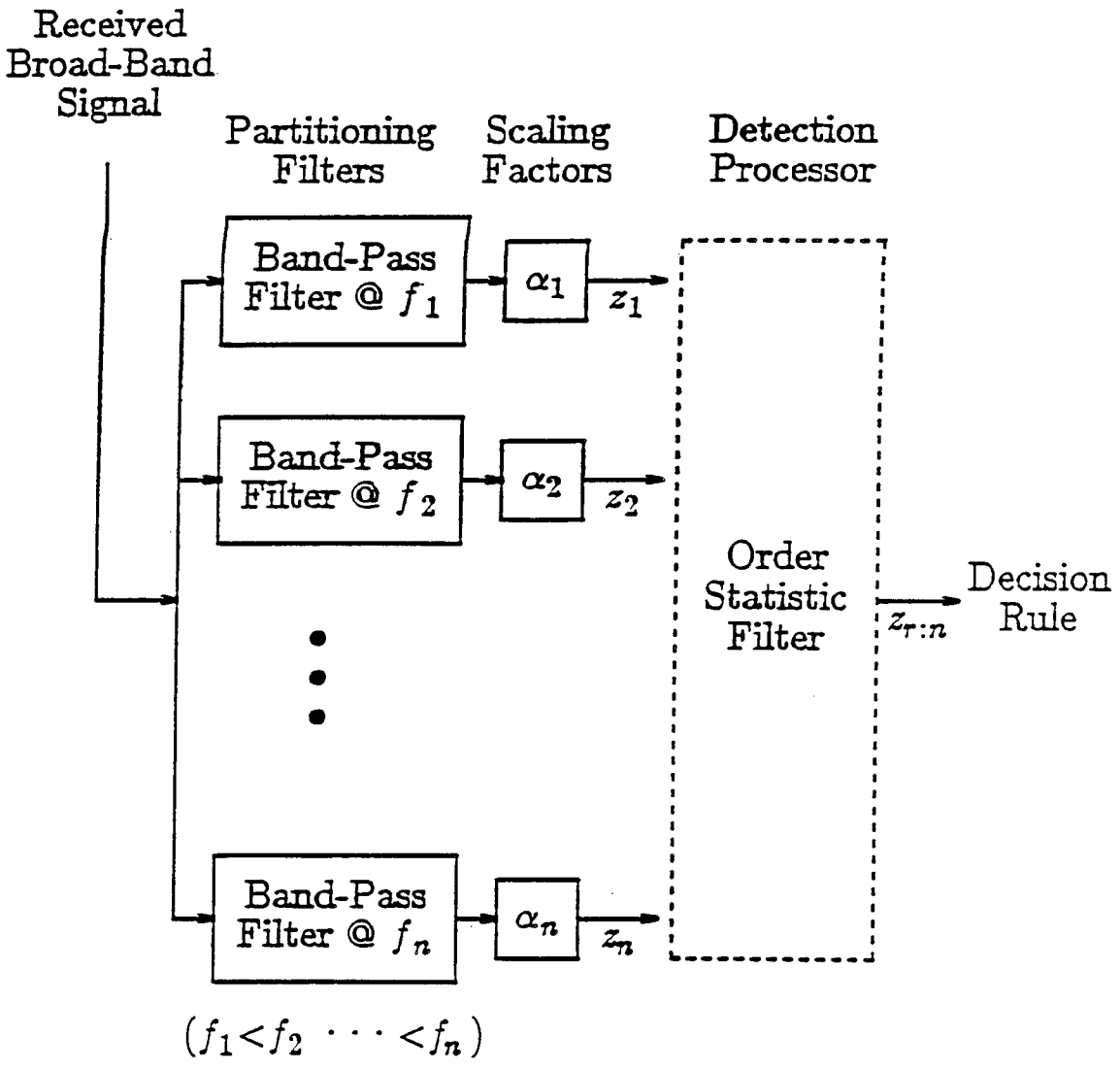

Figure 6.10 Split-Spectrum Processor Coupled with Rank Order Filters

microstructure noise. The filtered outputs are passed to a detection processor consisting of a rank order statistic filter for flaw detection. The filtered outputs are ordered in ascending values with respect to their magnitudes. The split-spectrum technique is applied to the same input ultrasonic signal (see Figure 6.11) using 11 bandpass filters with a 3-dB bandwidth of 1.04 MHz, and 1.2 MHz spacing between adjacent filters covering a frequency range of 0 - 12.8 MHz. The ranked outputs corresponding to each frequency band are shown in Figure 6.11. The higher ranked outputs (i.e., ranks 7 - 11) show an improvement in flaw visibility in contrast to the lower ranks (i.e., ranks 1 - 6). Figure 6.12 is another example of the same broad band ultrasonic signal processed using eleven filters with a 3-dB bandwidth of 1.2 MHz, and 0.6 MHz spacing between adjacent filters covering a frequency range of 0 - 6.8 MHz. All the ranked outputs show a noticeable improvement in flaw visibility. It must be noted that the performance of split-spectrum processing with rank order statistic filters depends on the number of subbands, correlation between each subband signal and statistical information about the target in each frequency band of the signal [46, 47].

In general, the results indicate the ability of the above techniques in detecting flaw echoes and improving the flaw-to-clutter ratio. However, morphological and recursive median filters have an advantage over split-spectrum processing combined with rank order statistic filters because they are more computationally efficient. Moreover, morphological filters have better performance in preserving the character of the signal because of their flexibility in changing the shape of the structuring elements to preserve certain patterns of the original signal.

6.5 Morphological Processing of Ultrasonic Images.

In this Section, the evaluation of morphological filtering has been extended from A-Scans to B-Scans. A B-Scan experimental measurement is shown in Figure 6.13. This image has 512x512 points. A 5 MHz broadband transducer was used to test a flat bottom hole (0.067") embedded within a steel block as a simulated flaw. This image is processed using Figure 5.2 with a flat structuring

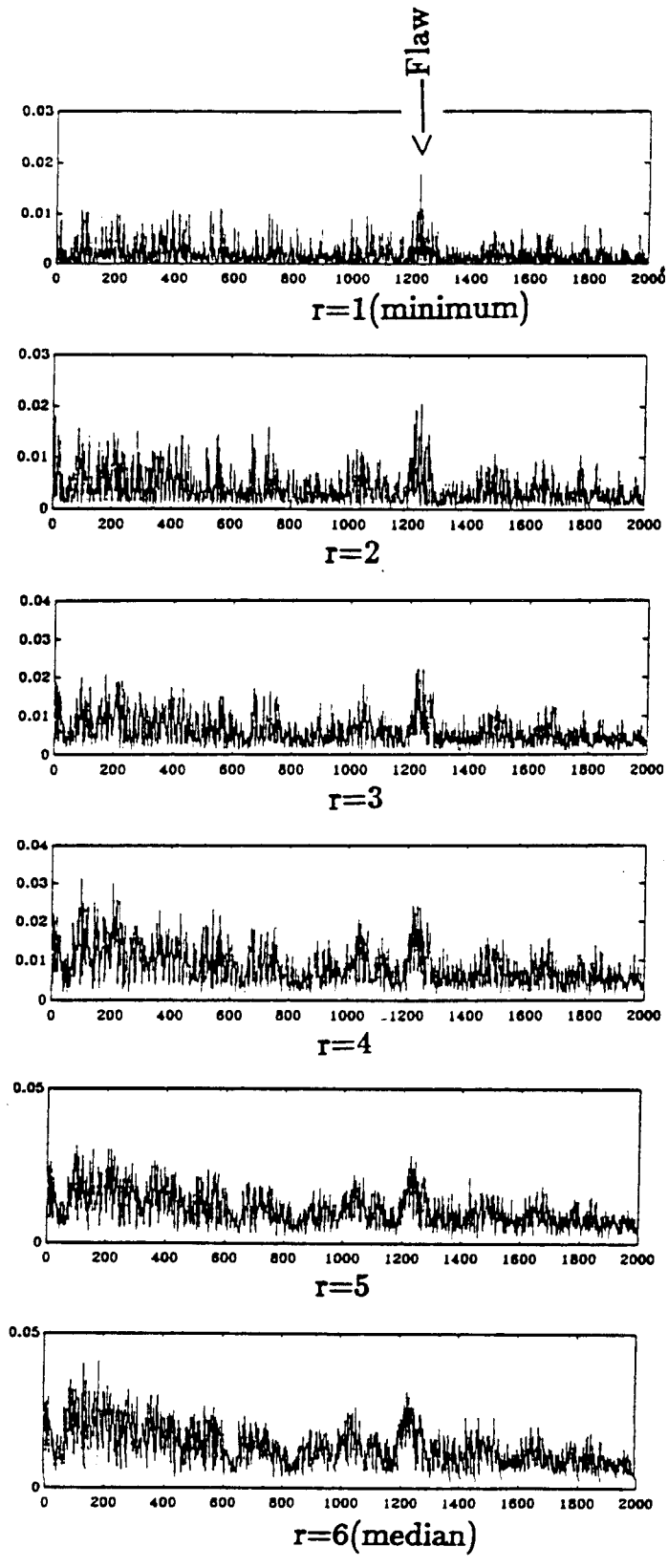

Figure 6.11 Ranked Outputs of Order Statistic Filters for 0-12.8 MHz Frequency Information

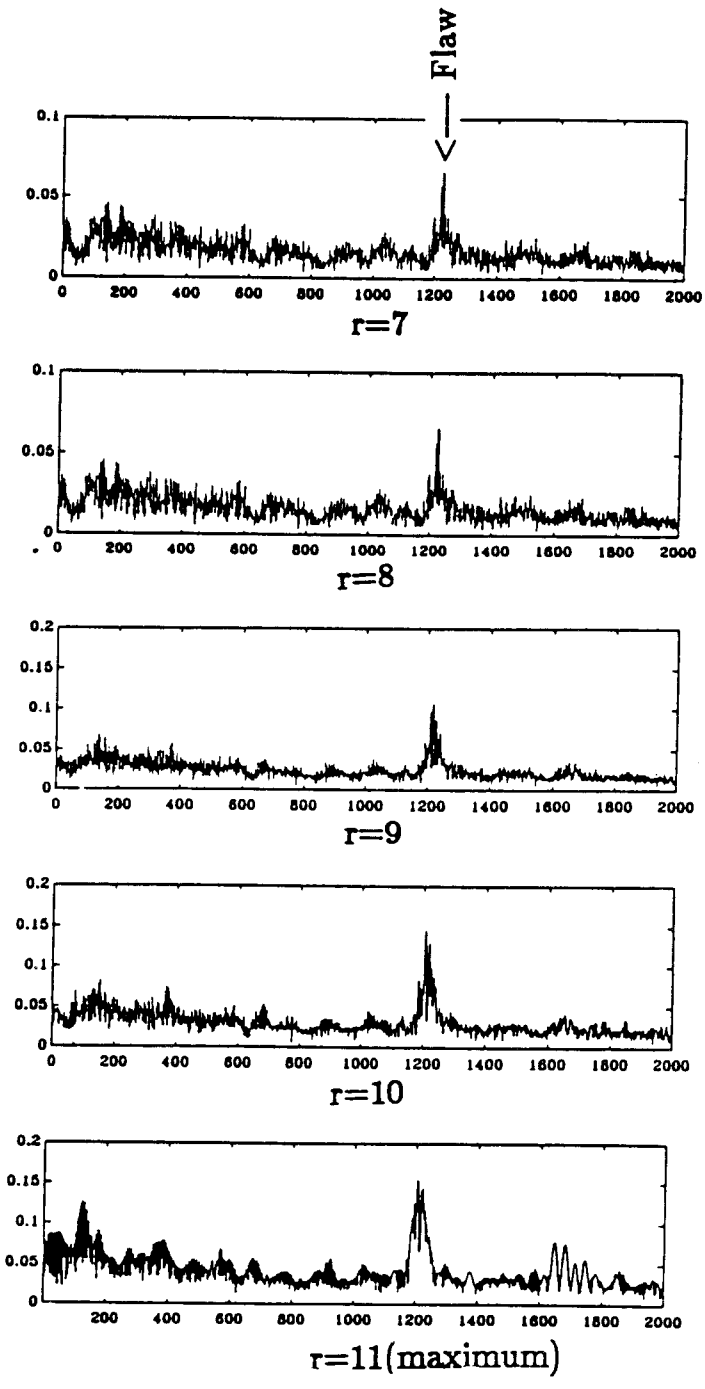

Figure 6.11 (Continued)

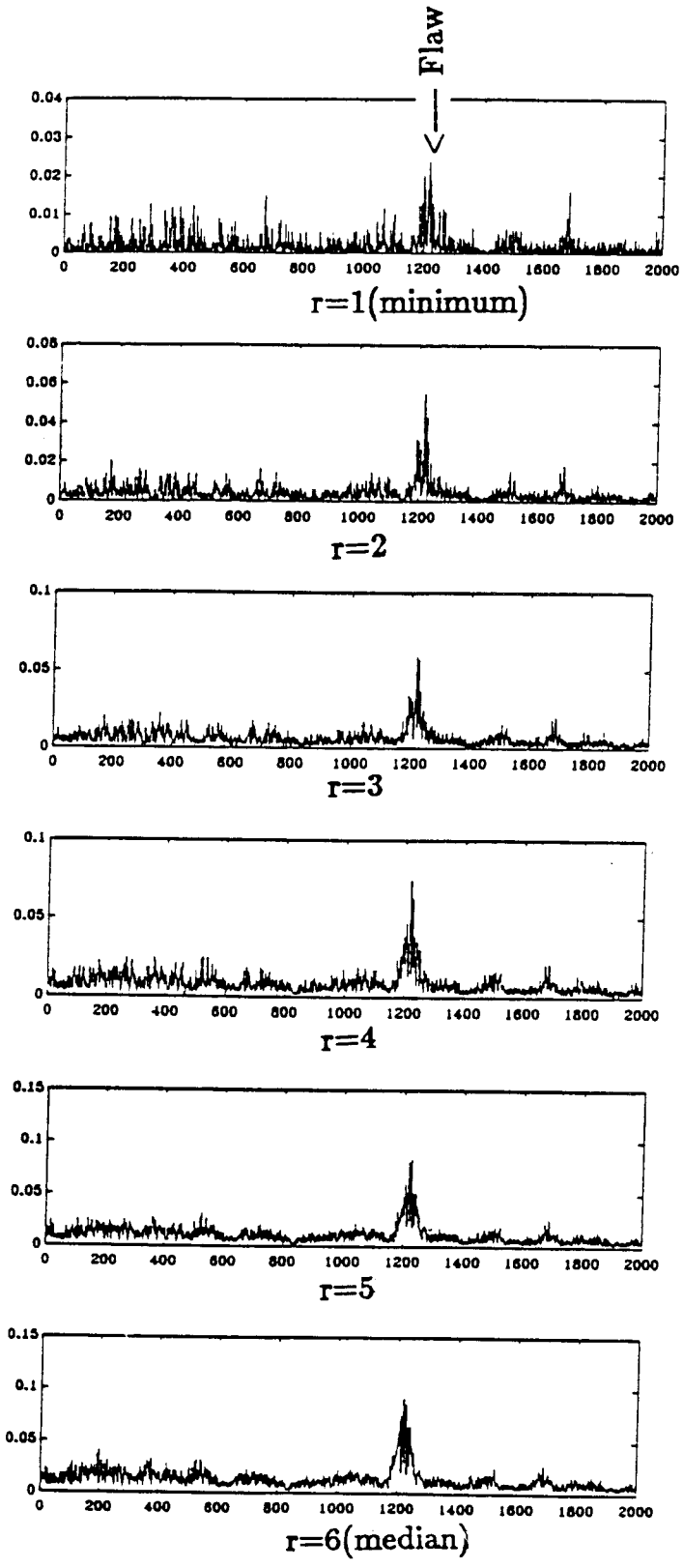

Figure 6.12 Ranked Outputs of Order Statistic Filters for 0-6.8 MHz Frequency Information

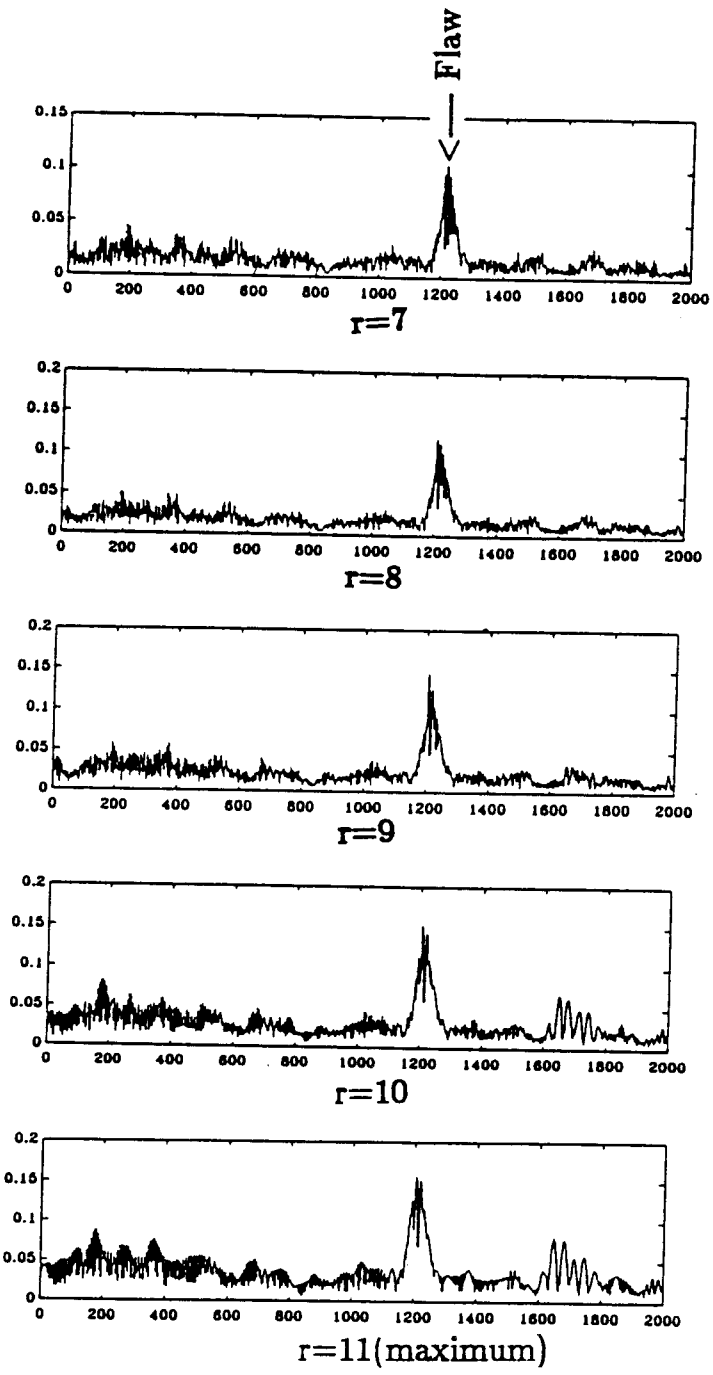

Figure 6.12 (Continued)

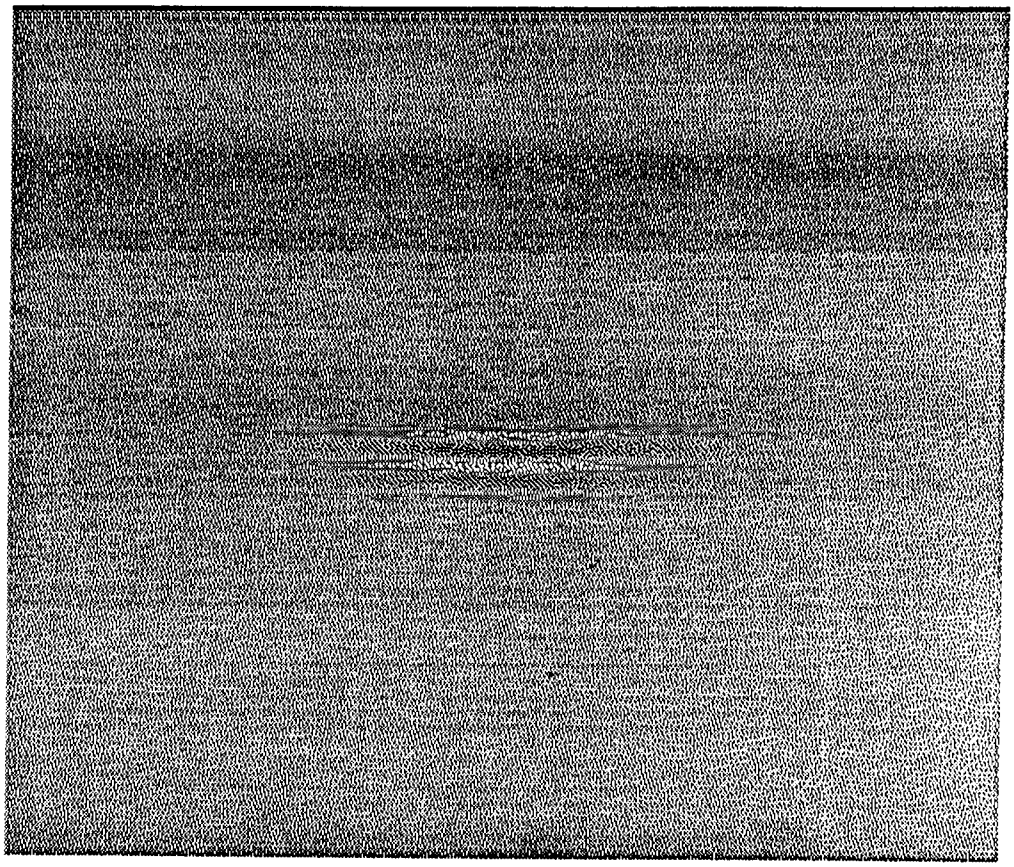

Figure 6.13 An Experimental B-Scan Image

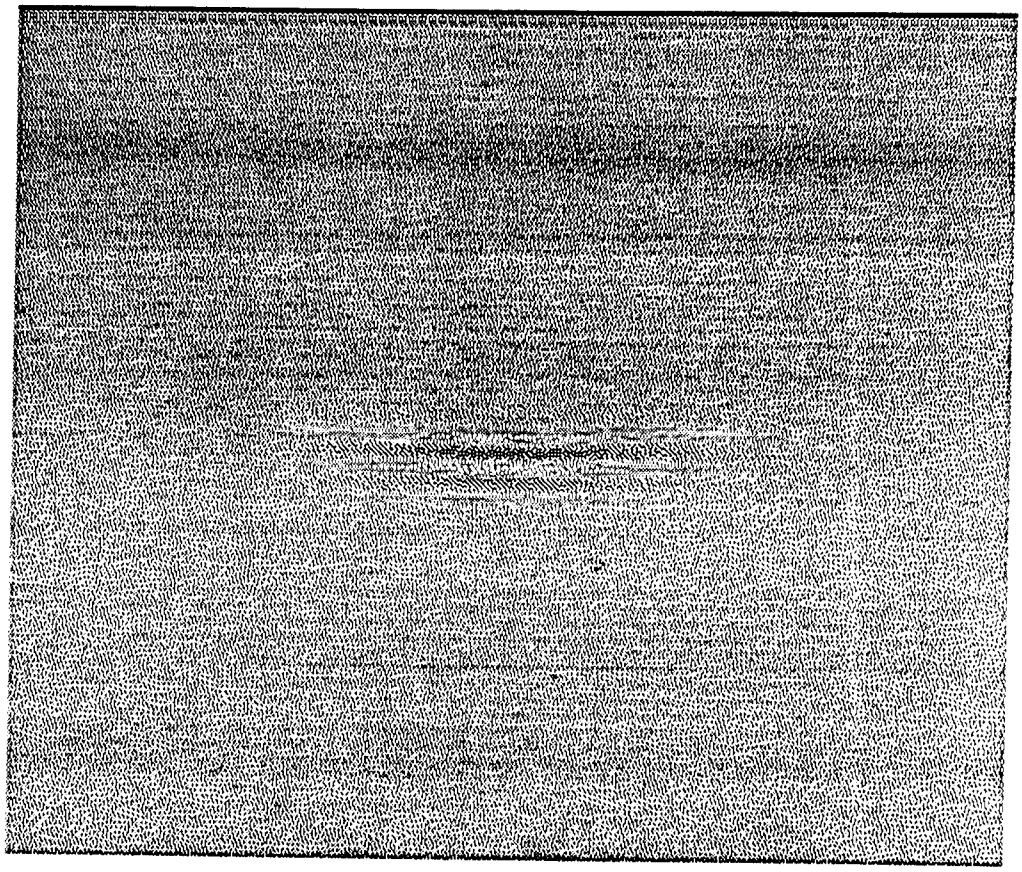

Figure 6.13 An Experimental B-Scan Image

element. The information content of the image has been used to design a suitable flat structuring element with an optimal performance. The average duration of the zero crossing of the B-Scan image is 8.08. Therefore, the flat structuring element with a width of 9 samples was chosen for noise removal. The result of the processed image is shown in Figure 6.14 indicating that morphological filters are capable of reducing noise and improving resolution. Further improvement in detection resolution is obtained using the bandpass morphological filter (see Equation 6.1). s_1 and s_2 are flat structuring elements with lengths 9 and 13 respectively. The processed image is shown in Figure 6.15. The processed results show that morphological filters are capable of improving the detection resolution and image quality.

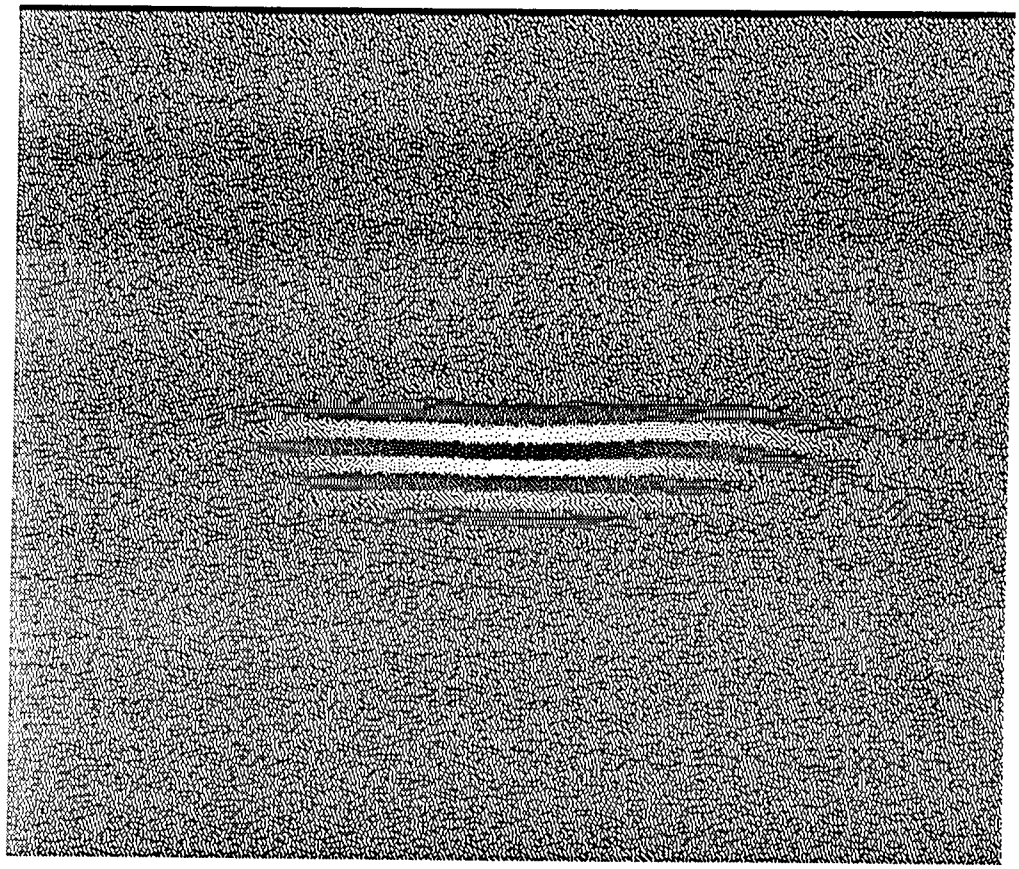

Figure 6.14 The Processed B-Scan Image using a Lowpass Morphological Filter

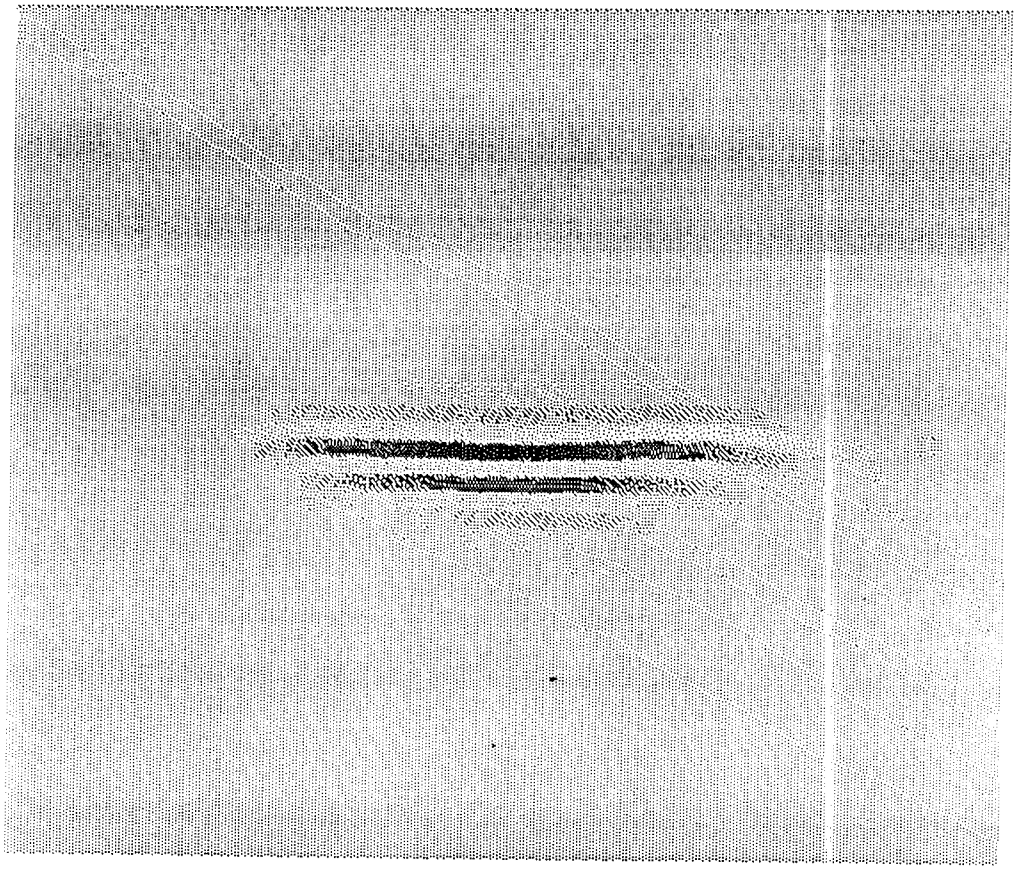

Figure 6.15 Processed B-Scan Image using a Bandpass Morphological Filter

CHAPTER VII

MORPHOLOGICAL FILTERS AND DECONVOLUTION

7.1 Introduction

The resolution of ultrasonic signals is limited by the bandwidth of the transducer and the presence of noise. In ultrasonic imaging systems, resolution of detection can be improved using broad band transducers with higher frequencies. However, higher frequency signals become attenuated, making difficult to penetrate deep into the material. Deconvolution can improve the detection resolution, but only at the expense of increasing undesired microstructural noise (i.e., echoes caused by dense scatterers or grains) and the additive impulsive noise caused by the instrument. An improvement in signal-to-noise ratio (SNR) can be obtained, to some extent, by performing ensemble averaging of numerous measurements. This method is impractical and can not eliminate interfering echoes resulting from stationary scatterers. Contrary to averaging, morphological filters are capable of eliminating impulsive noise, moderately reducing grain echoes and improving the overall signal quality while selectively preserving certain signal features.

In this Chapter, an effective solution to the above problem is introduced by coupling deconvolution with morphological filters in tandem (i.e., deconvolution before or after morphological operations). The performance of these algorithms to improve resolution and SNR is evaluated. Also, the design of the deconvolution kernel and the structuring element of morphological filters is included using experimental results.

7.2 Deconvolution

Deconvolution is a method which unravels the effects of a convolution between a system and a signal. An approach to improve detection resolution is deconvolution (inverse filtering) with a linear system whose transfer function is the

reciprocal of the Fourier transform of the measuring system. This method is only useful when signal-to-noise ratio (SNR) is high and the echo waveshape (the impulse response of the measuring system) is known. One type of inverse filtering that has been extensively used because of its mathematical simplicity is or the Wiener filter [48]. Deconvolution based on the Wiener theory requires knowledge of the characteristics of the noise process in terms of its spectral density.

Suppose a measured data r(n) is related to the input, (i.e., the ultrasonic wavelet) u(n), noise, ν(n), and the desired unknown target impulse response y(n) as follows:

$$r(n) = u(n) * y(n) + \nu(n) \tag{7.1}$$

One must now estimate the target impulse response, $\hat{y}$(n), which is subject to the following mean square error,

$$\epsilon = <(y(n) - \hat{y}(n))^2> \tag{7.2}$$

A solution for y(n) can be obtained by performing a linear operation, h(n), on the measured data sequence (i.e., Wiener filter). This means that the output of the estimator h(n):

$$\hat{y}(n) = r(n) * h(n) \tag{7.3}$$

is subject to the minimization of Equation (7.2). The optimum discrete Fourier transform of h(n), is obtained by solving [48],

$$H(k) = \frac{1}{U(k)} W(k) \tag{7.4}$$

where

$$W(k) = \frac{|U(k)|^2}{|U(k)|^2 + \Phi} \tag{7.5}$$

and Φ, the noise-to-signal ratio, is approximated by a suitable constant. The output of such a filter is the optimal estimate of the target impulse response.

$$\hat{Y}(k)=\frac{R(k)}{U(k)}W(k) \tag{7.6}$$

The frequency weighting function W(k) has a very desirable behavior. When $|U(k)|^2$ is much greater than zero and naturally greater than Φ, W(k) approaches one which implies that the ratio of $\frac{R(k)}{U(k)}$ is reliable and needs minimal correction. On the other hand, in the frequency region of poor signal-to-noise ratio, W(k) approaches zero thus reducing the value of $\hat{Y}$(k) significantly.

7.3 Simulation Results

This section illustrates the performance of deconvolution and morphological filters when connected in tandem for noise suppression and echo detection. The signal to be processed is a sum of two components: an ultrasonic echo, u(n), backscattered from a single reflector, δ(n), and uniformly distributed noise, ν(n), i.e.,

$$r(n)=u(n)*\delta(n)+\nu(n) \tag{7.7}$$

where the ultrasonic echo is assumed to have a Gaussian envelope and is modeled as:

$$u(n)=e^{-\alpha n^2}\cos(2\pi\frac{f_c}{f_s}n) \tag{7.8}$$

The term f_c is the center frequency, f_s is the sampling rate, and α is a constant proportional to the bandwidth of the echo and f_c. In this simulation α=0.0002, f_c=1.25 MHz and f_s=100 MHz. The noise ν(n) is a sequence of independent, identically distributed random signals with a uniform density function {-0.5, 0.5} resulting in an average signal power to average noise power ratio of 3.58 (SNR=5.54 dB). The echo signal and the echo signal contaminated by noise are shown in Figures 7.1a and 7.1b respectively. The above signal (Equation 7.7) is processed using a morphological filter followed by deconvolution (Method I) and the results are compared with the processed signal using deconvolution first and then a morphological filter (Method II). Note that Methods I and II are not

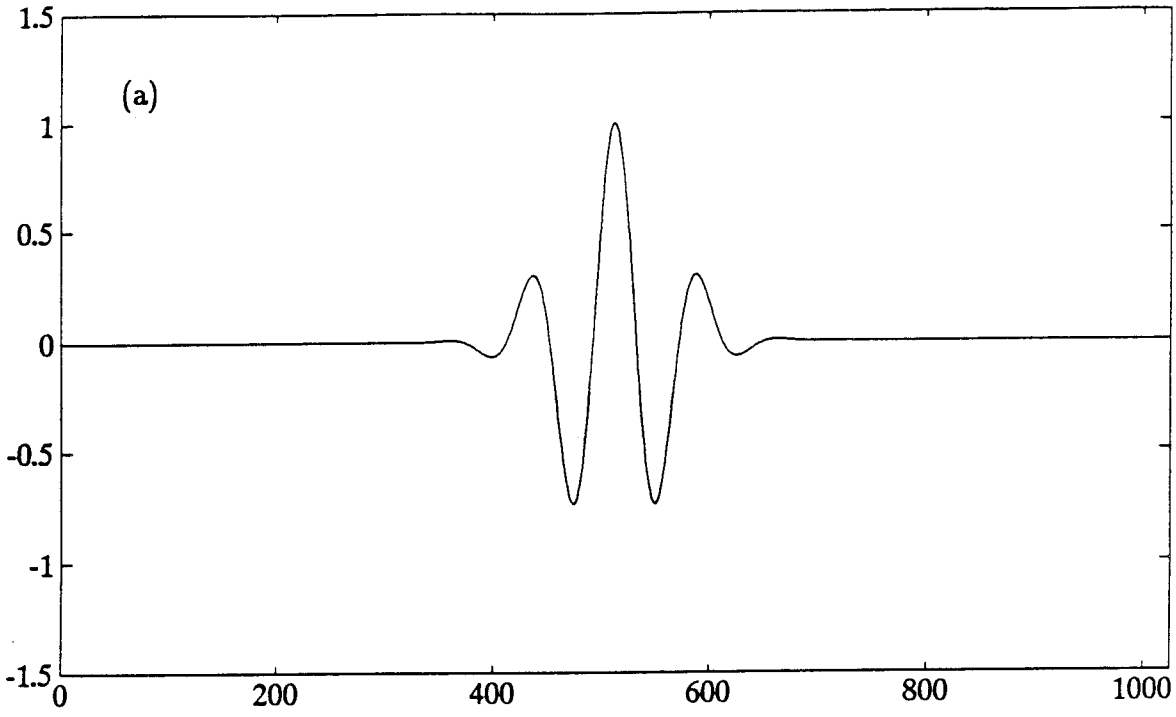

Figure 7.1a Simulated Ultrasonic Echo

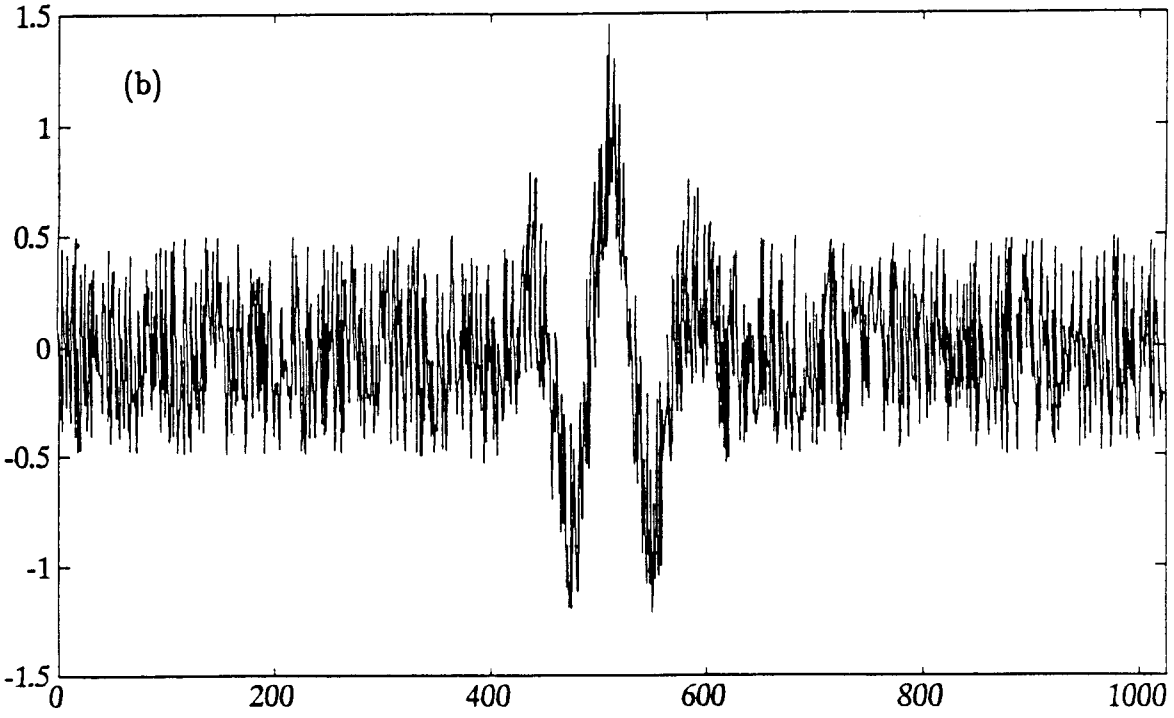

Figure 7.1b Echo Contaminated by Uniformly Distributed Noise

equivalent since they include morphological filters which are nonlinear processors. Figures 7.2 and 7.3 show the processed signals of Methods I and II respectively, using a half period sinusoidal structuring element for morphological filters, and Gaussian shape spectrum for deconvolution. The sinusoidal structuring element has a width = 23 samples and a constant height = 0.1. In order to eliminate both the very high and very low frequencies, the frequency response of the output of deconvolution processing (Equation 7.6) is modified by the following form:

$$\hat{\hat{Y}}(k)=\frac{R(k)}{|\hat{U}(k)|}\hat{W}(k) \tag{7.9}$$

where $|\hat{U}(k)|=|U(k)|+\Psi$ and $\hat{W}(k)$ is the frequency window defined as

$$\hat{W}(k)=1 \text{ for } k1<k<k2 \quad \text{and} \quad \hat{W}(k)=0 \quad \textit{otherwise} \tag{7.10}$$

In this simulation k1=7, k2=25, (corresponding to frequency range of 0.68-2.5 MHz) and Ψ (i.e., a factor for reducing the effect of noise in the passband region) is one-seventh of the peak value of |U(k)|. Processed signals using Methods I and II demonstrate the effectiveness of these methods for suppressing noise and preserving the original echo. A comparison between the average signal power to average noise power for the above methods is presented in Table 7.1. These results indicate that a morphological filter without deconvolution offers the best SNR. Also, in both Methods, the processed signals show some oscillation resulting from limited bandwidth of the filter defined in Equation (7.10).

7.4 Experimental Results

To illustrate the effectiveness of morphological filtering coupled with deconvolution to improve the SNR and resolution in detection, a typical ultrasonic signal (A-Scan) contaminated by microstructure scattering noise has been used (Figure 6-1). This signal was processed using deconvolution and morphological filtering in tandem (i.e., deconvolution before and after morphological operations, i.e., Methods I and II). The processed results are shown in Figures 7.4 and 7.5, respectively, using a flat structuring element for morphological filtering (Figure

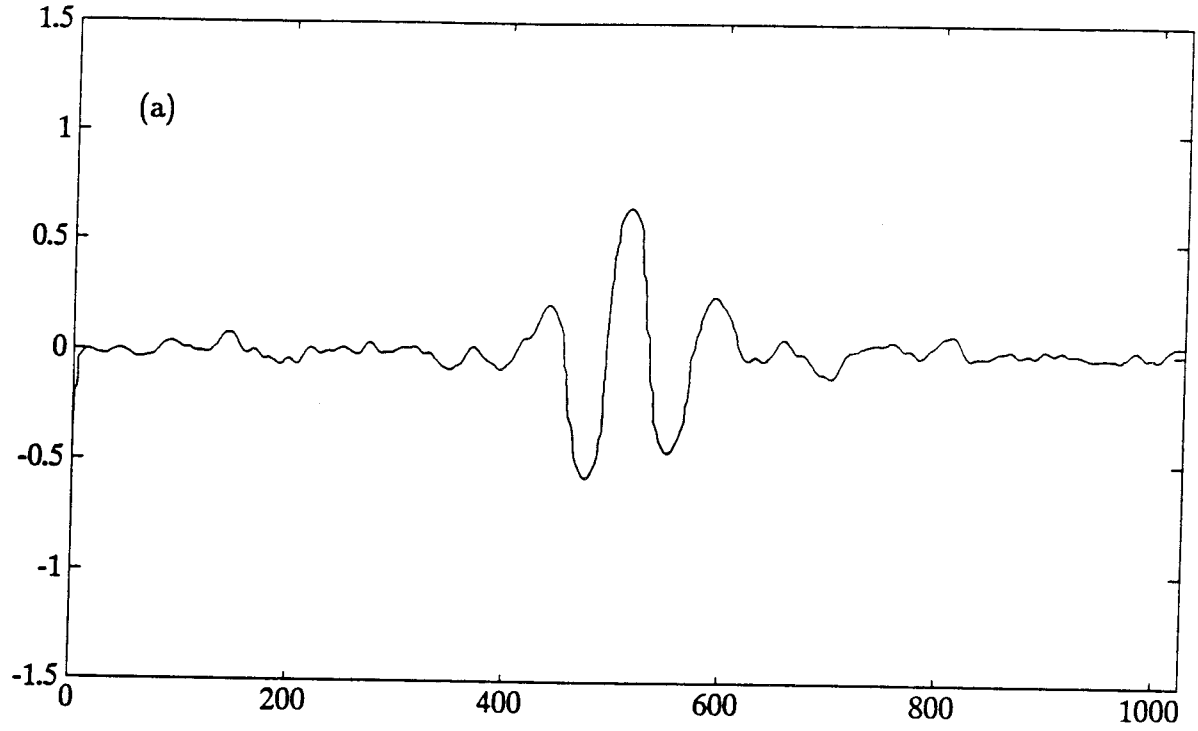

Figure 7.2a Processed Echo using a Morphological Filter

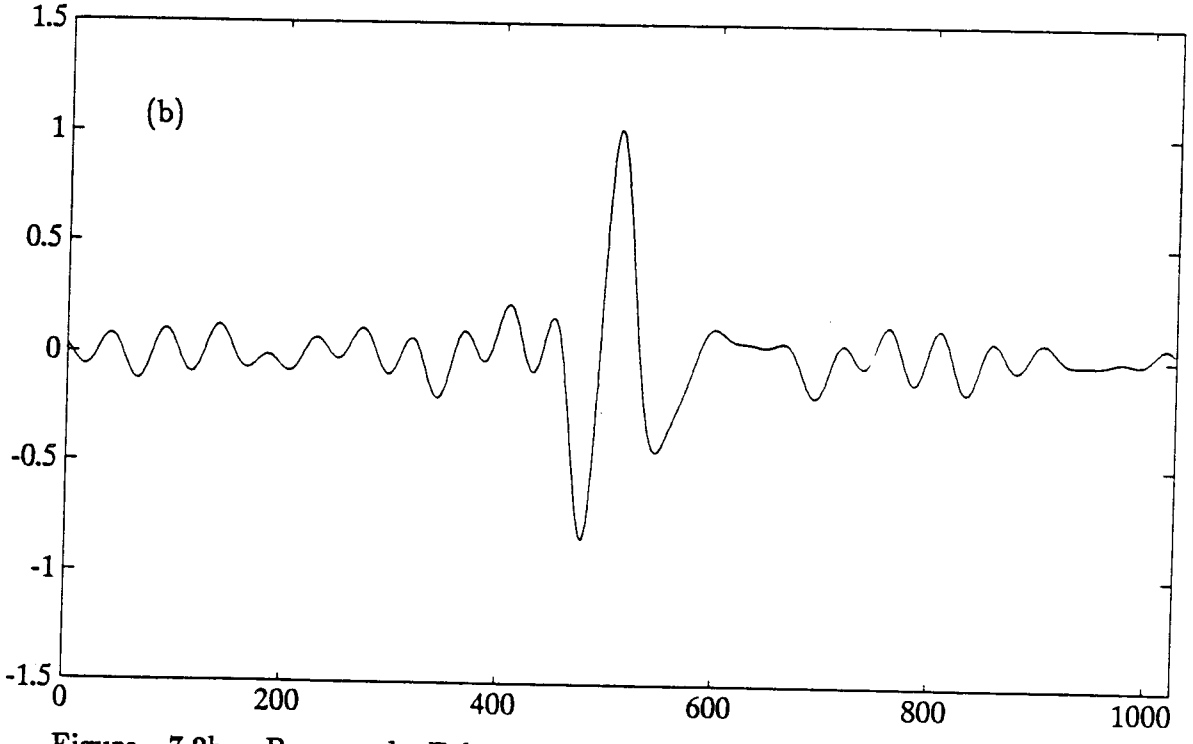

Figure 7.2b Processed Echo using a Morphological Filter Followed by Deconvolution

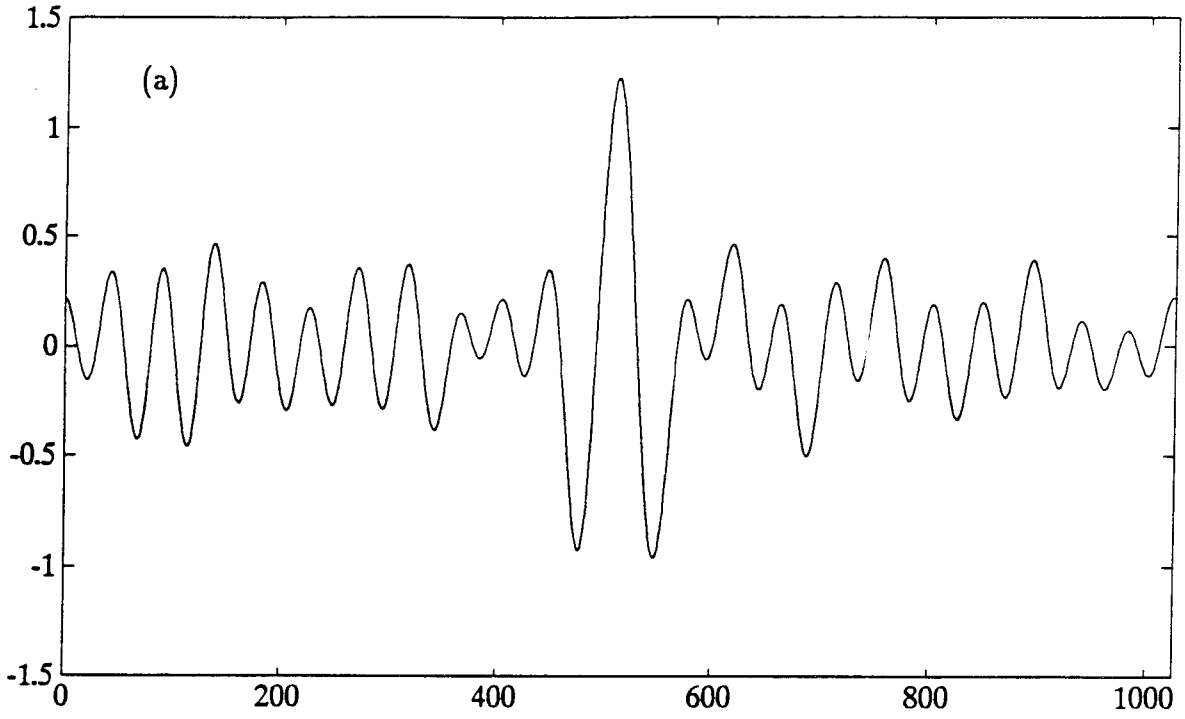

Figure 7.3a Processed Echo using Deconvolution

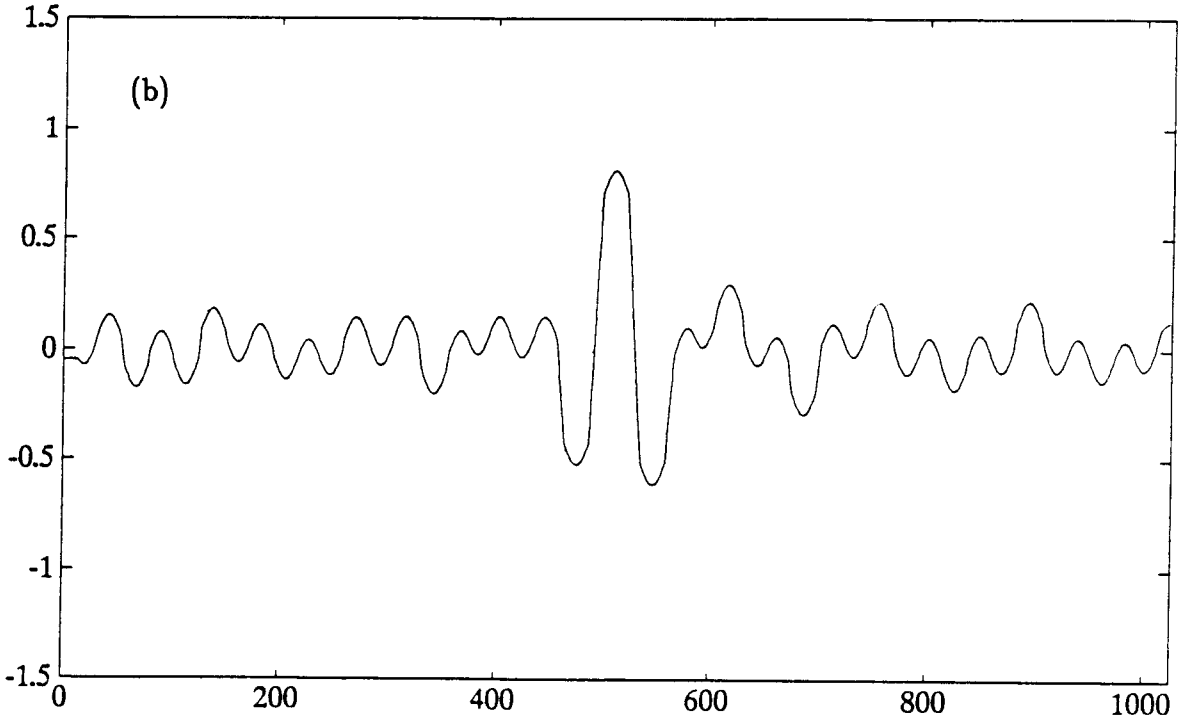

Figure 7.3b Processed Echo using Deconvolution Followed by a Morphological Filter

Table 7.1 Comparison of SNR for different types of processing.

The input SNR is 5.54 dB.

Operation	SNR
Morphological filter	18.65 dB.
Morphological filter followed by deconvolution	14.91 dB.
Deconvolution	7.97 dB.
Deconvolution followed by morphological filter	11.16 dB.

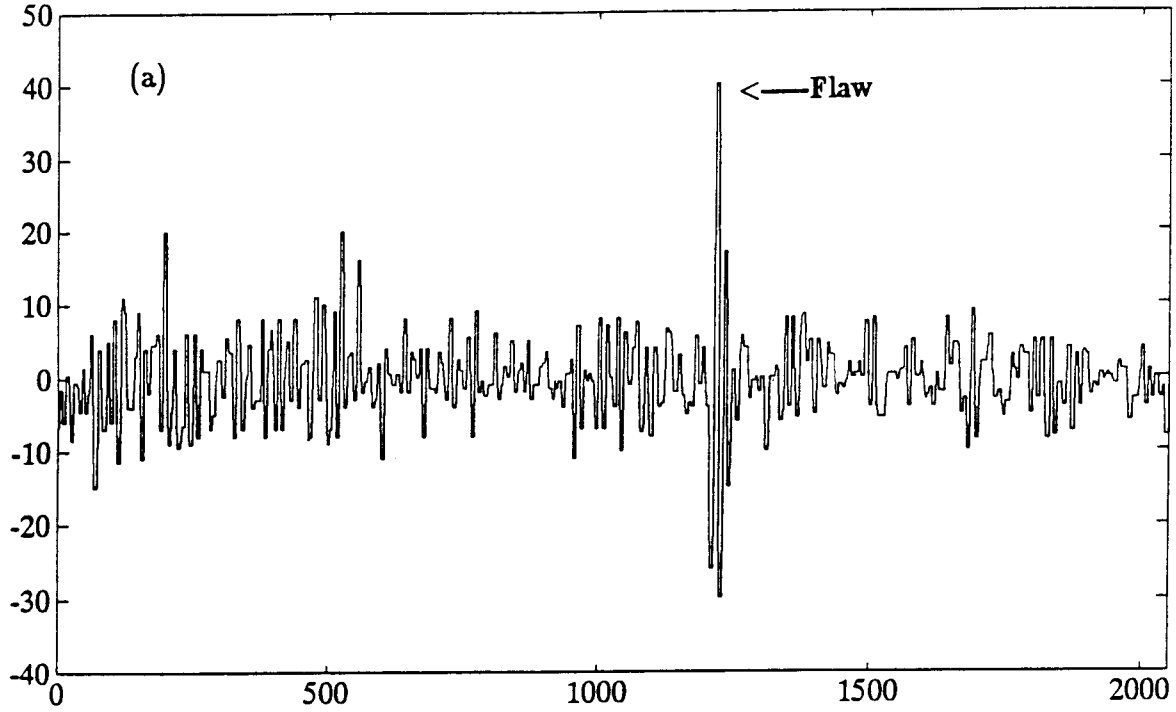

Figure 7.4a Processed Backscattered Flaw Signal using a Morphological Filter

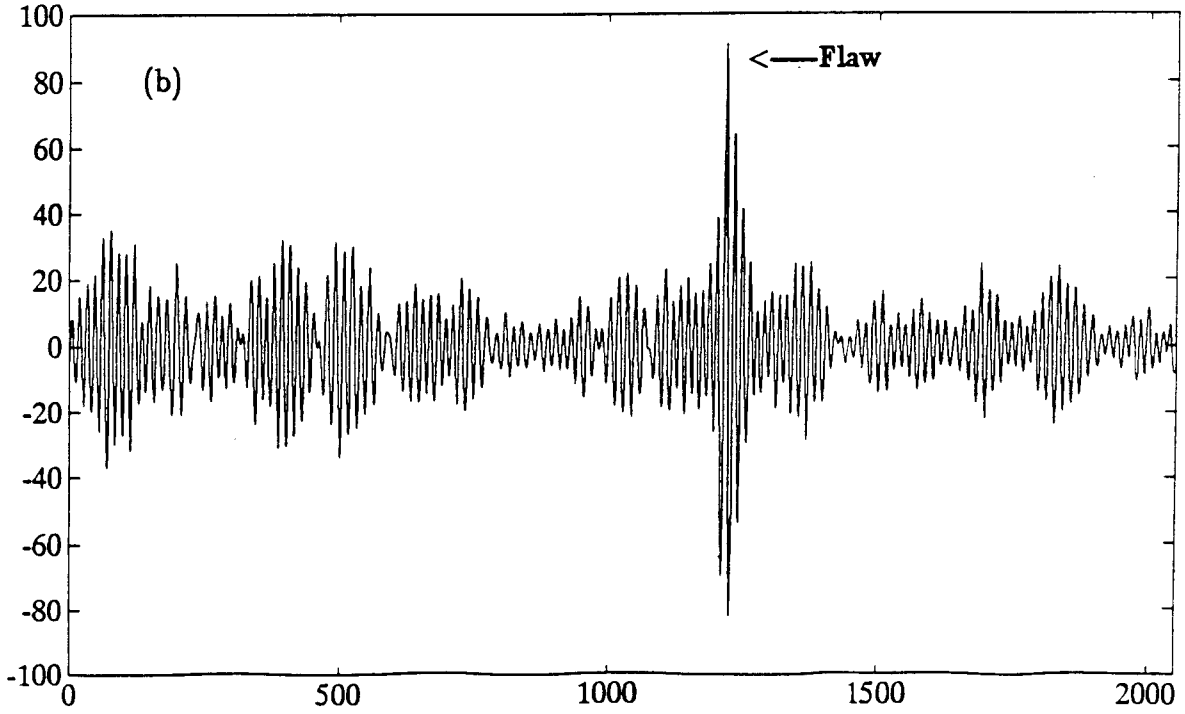

Figure 7.4b Processed Backscattered Flaw Signal using a Morphological Filter Followed by Deconvolution

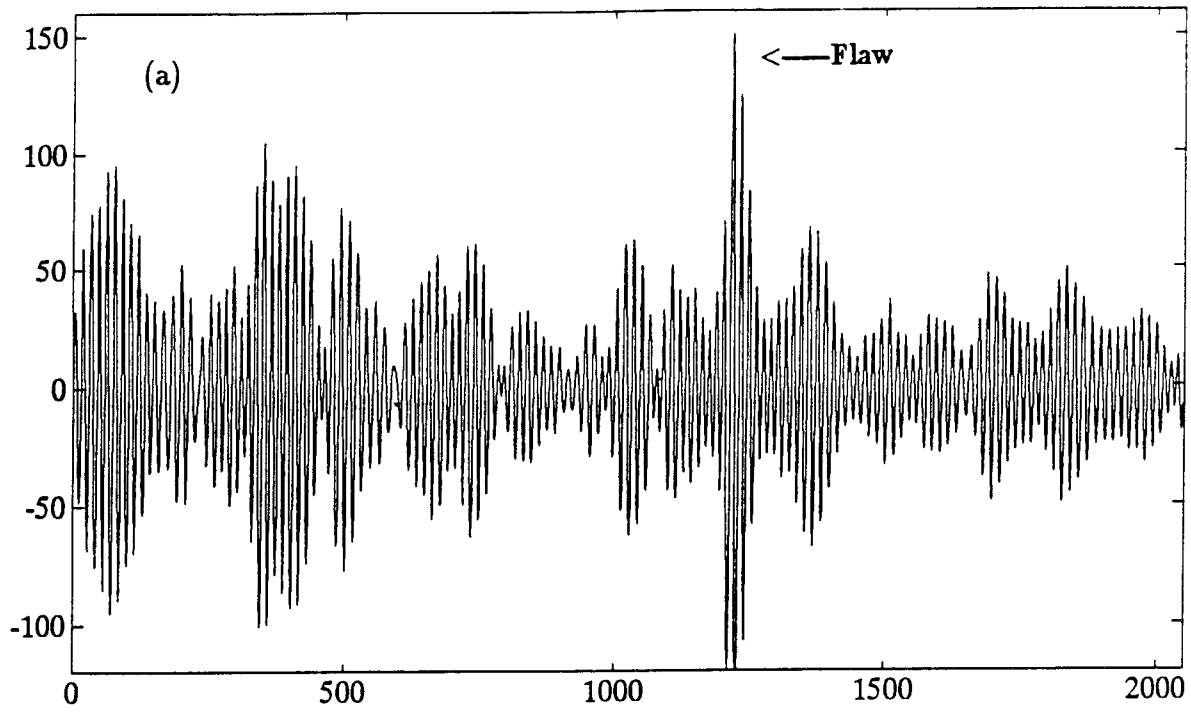

Figure 7.5a Processed Backscattered Flaw Signal using Deconvolution

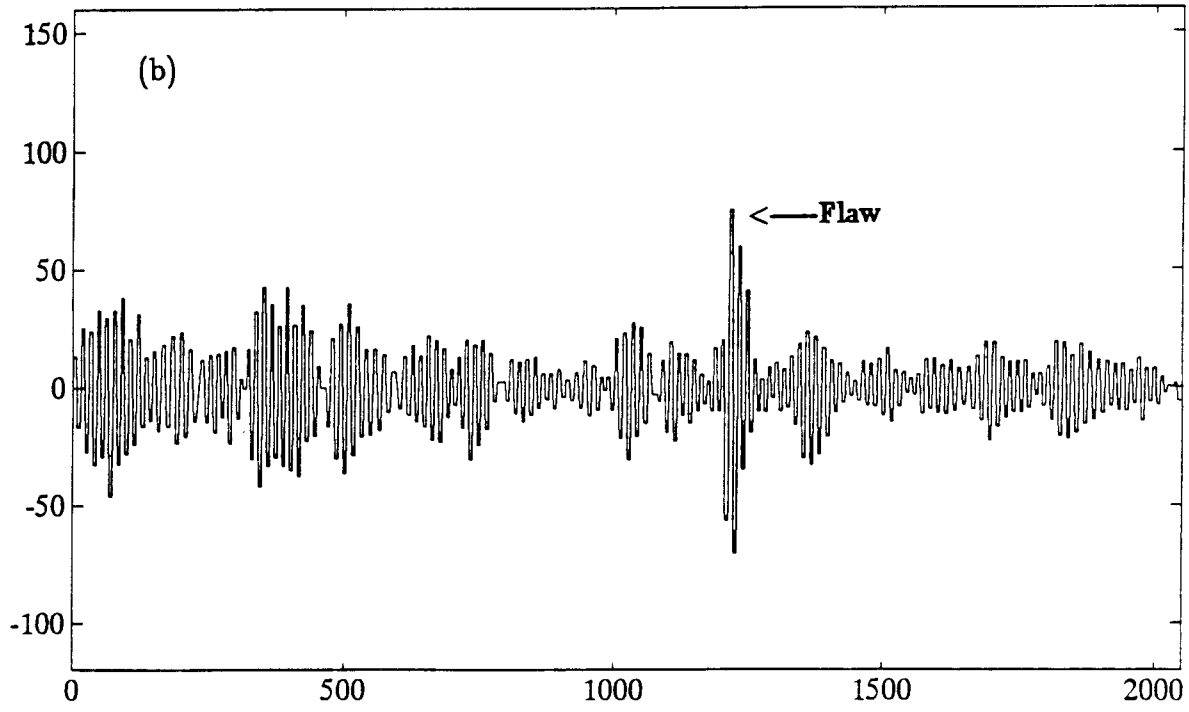

Figure 7.5b Processed Backscattered Flaw Signal using Deconvolution Followed by a Morphological Filter

5.2) and a Gaussian shape kernel for deconvolution (Equation 7.9). The flat structuring element has a width = 6 samples. The frequency response of the kernel of deconvolution is estimated from the envelope of the frequency response of the signal before deconvolution. Then, the output of the deconvolution operation is calculated using Equation 7.9. In this processing, the parameters are k1=50, k2=150, (corresponding to frequency range of 2.44-7.32 MHz)), and Ψ is one-tenth of the peak value of |U(k)|.

A comparison between SNR for the above methods is shown in Table 7.2. The input SNR is 8.86 dB. These results indicate that both Methods I and II are able to improve SNR. However, Method I shows a slightly better performance than Method II. With each method the improvement depends on the design parameters of inverse filtering. A further improvement of SNR can be achieved by coupling morphological filters with band-pass filters rather than deconvolution since the flaw echo has frequency range different than the microstructure noise [47]. Figure 7.6 shows an example of the processed signal using morphological filtering followed by bandpass filtering. These results are processed using a flat structuring element with a width = 6 samples and a ideal bandpass filter with a frequency range of 2.44-7.32 MHz. The results indicate that the average output SNR is equal to 14.73. It must be mentioned that coupling a morphological filter with an ideal band pass filter has better SNR than the SNR of the proposed morphological bandpass filter discussed in Chapter (6).

7.5 Conclusion

In this chapter, the performance of deconvolution and morphological filters has been evaluated to improve the detection resolution and SNR of A-Scan signals. The results presented indicate that by combining of morphological operations and deconvolution filtering microstructure noise is reduced and resolution is improved. It has been shown that coupling bandpass filtering with morphological filtering provides the best performance in regard to SNR and resolution.

Table 7.2 Comparison of SNR for different types of processing.

The input SNR is 8.86 dB.

Operation	SNR
Morphological filter	13.70 dB.
Morphological filter followed by deconvolution	12.09 dB.
Deconvolution	9.04 dB.
Deconvolution followed by morphological filter	10.35 dB.

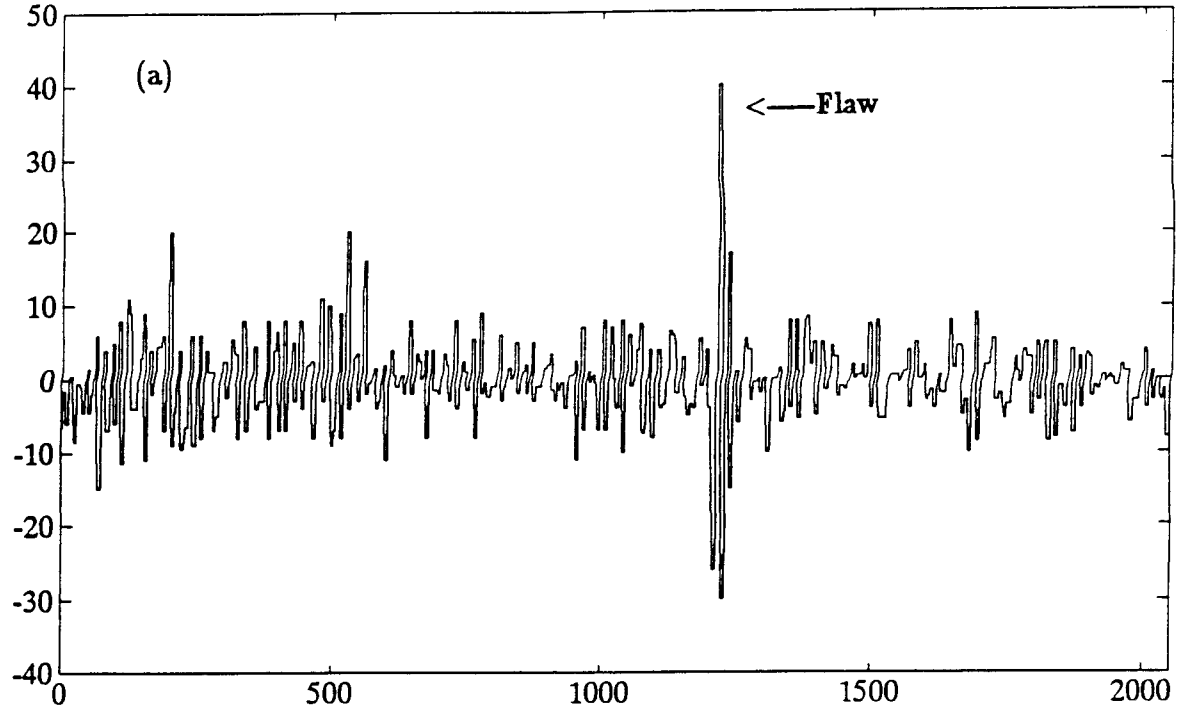

Figure 7.6a Processed Backscattered Flaw Signal using a Morphological Filter

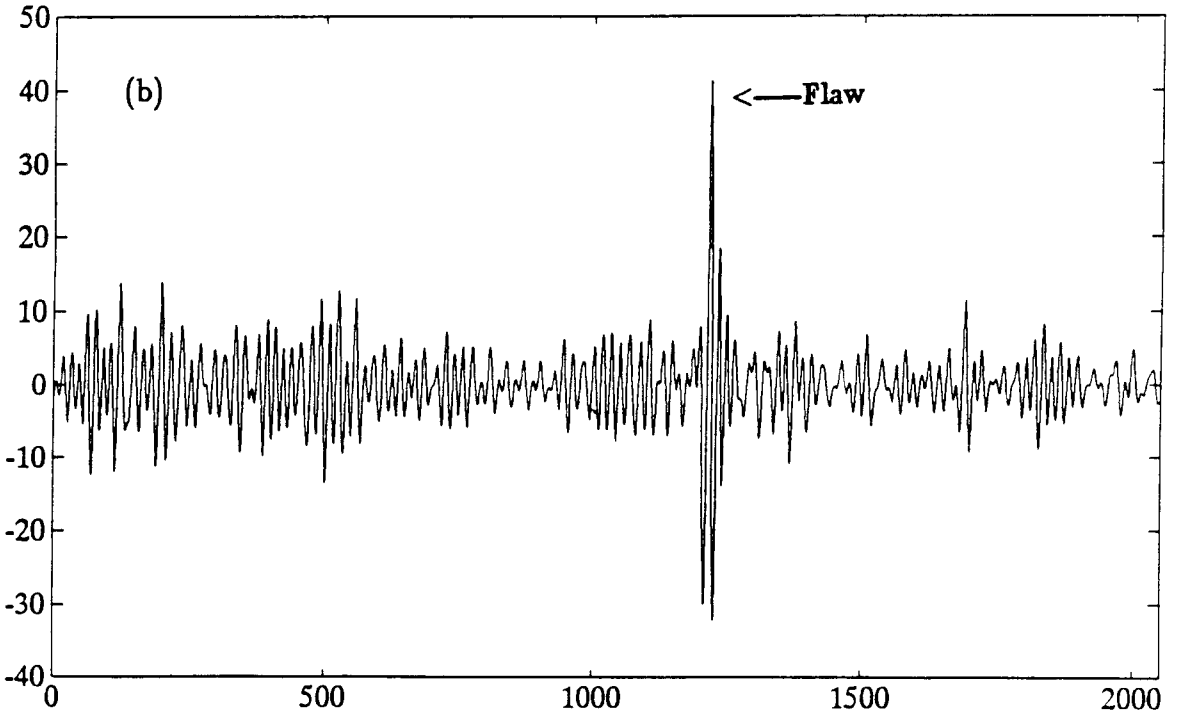

Figure 7.6b Processed Backscattered Flaw Signal using a Morphological Filter Followed by a Bandpass Filter

CHAPTER VIII

CONCLUSION

This thesis has dealt with the properties of morphological filters and their applications for improving the flaw-to-clutter ratio of ultrasonic signals (A-Scan or B-Scan). Our study has focused on the deterministic and stochastic properties of morphological filters using different structuring elements. Structuring elements are characterized by their width, height and shape. From both a deterministic and a stochastic point of view, it has been shown that the filtering process depends on the input signal as well as the parameters of the structuring element.

A mathematical expression for the dilation and erosion density function of independent and identically distributed (iid) inputs has been derived using the statistical properties of order statistics filters. Also, a statistical expression for the closing density function is derived when inputs are (iid) for any density function. This expression is derived by utilizing probabilistic mappings between input and output signals. This expression is restricted to FSP morphological filters (i.e., flat structuring elements) since the main tool of analysis is threshold decomposition. Furthermore, the statistical properties of sequential morphological operations (i.e., dilation, closing, clos-erosion and clos-opening) are examined using different shapes of structuring elements applied to signals with uniform, Gaussian, and Rayleigh density functions.

The effect of the parameters of the structuring elements are evaluated using Monte Carlo simulation. This technique is advantageous in that it can be used with input signals with any type of statistical characteristics, and differently shaped structuring elements. The simulated results indicate that by increasing the width of the flat structuring element the mean (bias) is increased and the variance and skewness of dilation, closing, clos-erosion and clos-opening density functions are decreased. Also, dilation is the most effective step in the smoothing operation.

The effect of other operations following dilation is rather small, especially when the width of the structuring element is increased. It has been shown that, for a certain height of the triangular structuring element and input signal with uniform density function, the dilated signal is a root signal, i.e., becoming invariant to any proceeding morphological operation using the same structuring element. For the same width of a structuring element, the flat structuring element has better noise suppression (less variance) than the triangular structuring element, although, a triangular structuring element similar to certain patterns of the input signal may be desirable in preserving these patterns.

Morphological filters have been applied to detect flaw echoes in ultrasonic signals contaminated by grain scattering noise. Also, the evaluation of morphological filtering for flaw detection has been extended from A-Scans (one dimension) to B-Scans (two dimensions). The processed experimental results show that morphological filters can detect flaw echoes while suppressing microstructure noise. It has been shown that morphological filters can replace ensemble averaging which requires numerous measurements.

In this study, a recursive median filter has been introduced as effective method to enhance the FCR of ultrasonic signals. Morphological and recursive median filters have been compared with the split-spectrum technique combined with rank order statistic filters. The results indicate that morphological and recursive median filters have an advantage over split-spectrum processing combined with rank order statistic filters because they are more computationally efficient. Moreover, morphological filters have better performance in preserving the character of the signal because of their flexibility in changing the shape of the structuring elements to preserve certain patterns of the original signal.

In this thesis, the performance of deconvolution and morphological filters has been evaluated to improve the detection resolution and FCR of A-Scan signals. The results presented indicate that by combining morphological operations with deconvolution filtering microstructure noise is reduced and resolution is improved.

It has been shown that coupling bandpass filtering with morphological filtering provides the best performance in regard to FCR and resolution.

REFERENCES

[1] C. R. Giardina and E. R. Dougherty, *Morphological Methods in Image and Signal Processing,* Prentice - Hall, Inc., 1988.

[2] G. Matheron, *Random Sets and Integral Geometry,* New York, Wiley, 1975.

[3] J. Serra, *Image Analysis and Mathematical Morphology,* London, Academic, 1982.

[4] S. R. Sternberg, "Biomedical Image Processing," *IEEE Comput. Mag.,* pp. 22 - 34, Jan. 1983.

[5] S. R. Sternberg and E. S. Sternberg, "Industrial Inspection by Morphological Virtual Gauging," *in Proc. IEEE Workshop Comput. Archit. Pattern Anal. Image Database Manag.,* Pasadena, CA, pp. 237 - 247, Oct. 1983.

[6] I. Pitas and A. N. Venetsanopoulos, "Morphological Shape Decomposition," *Pattern Anal. Machine Intell.,* Vol. PAMI-12, No. 1, pp. 38 - 45, Jan. 1990.

[7] P. A. Maragos and R. W. Schafer, "Morphological Skeleton Representation and Coding of Binary Image," *IEEE Trans. Acoust., Speech, Signal Processing,* Vol. ASSP - 34, pp. 1228 - 1244, oct. 1986.

[8] C. H. Richardson and R. W. Schafer, "Application of Mathematical Morphology to FLIR Images," SPIE Vol. 845 *Visual Communications and Image Processing ll,* pp. 249 - 252, 1987.

[9] P. Maragos, "Tutorial on Advances in Morphological Image Processing and Analysis," *Optical Eng.,* Vol. 26, pp. 623 - 632, Jul. 1987.

[10] V. Goetcherian, "From Binary to Grey Tone Image Processing Using Fuzzy Logic Concepts," *Pattern Recognition,* Vol. 12, pp. 7 - 15, 1980.

[11] F. K. Sun and S. L. Rubin, "Algorithm Development for Autonomous Image Analysis based on Mathematical Morphology," SPIE Vol. 845, *Visual Communications and Image Processing ll,* pp. 216 - 226, 1987.

[12] T. R. Esselman and J. G. Verly, "Some Applications of Mathematical Morphology to Range Imagery," *Proc. ICASSP,* pp. 245 - 248, 1987.

[13] P. A. Maragos and R. W. Schafer, "Applications of Morphological Filtering to Image Analysis and Processing," *Proc. ICASSP,* pp. 2067 - 2070, 1986.

[14] T. R. Crimmins and W. M. Brown, "Image Algebra and Automatic Shape Recognition," *IEEE Trans. Aerospace and Electronic Systems,* Vol. AES-21, No. 1, pp. 60 - 69, 1985.

[15] S. A. Rajala, H. A. Peterson, and E. J. Delp, "Binary Morphological Coding of Grayscale Images," *Proc. ISCAS,* pp. 2807 - 2811, 1988.

[16] F. Meyer, "Feature Extraction by Mathematical Morphology in the Field of Quantitative Cytology," *Lecture Notes in Medical Informatics,* ed. by D. A. B. Lindberg and P. L. Reichertz, pp. 56 - 65, 1980.

[17] R. J. Feehs and G. R. Arce, "Multidimensional Morphological Edge Detection," SPIE Vol. 845, *Visual Communications and Image Processing II,* pp. 285 - 292, 1987.

[18] A. Toet, "A Morphological Pyramidal Image Decomposition," *Pattern Recognition letters 9, North Holland,* pp. 255 - 261, 1989.

[19] R. M. Haralick, Xinhua Zhuang, Charlotte Lin, and James Lee, "The Digital Morphological Sampling Theorem," *Proc. ISCAS,* pp. 2789 - 2793, 1988.

[20] L. Shapiro, R. MacDonald and S. Sternberg, "Ordered Structural Shape Matching with Primitive Extraction by Mathematical Morphology," *Pattern Recognition,* Vol. 20, No. 1, pp. 75 - 90, 1987.

[21] J. F. Bronskill and A. N. Venetsanopoulos, "Multidimensional Shape Description and Recognition Using Mathematical Morphology," *J. Intelligent and Robotic Systems,* Vol. 1, pp. 117 - 143, 1988.

[22] P. A. Maragos, and R.W. Schafer, "Morphological Filters-Part I: Their Set-Theoretic Analysis and Relations to Linear Shift-Invariant Filters," *IEEE Trans. Acoust., Speech, Signal Processing,* Vol. ASSP-35, pp. 1153 - 1169, Aug. 1987.

[23] E. J. Coyle, "The Theory and VLSI Implementation of Stack Filters," *in VLSI Signal Processing II,* New York, IEEE Press, pp. 141 - 151, 1986.

[24] C. H. G. Wright, E. J. Delp, and N. C. Gallagher, "Nonlinear Target Enchancement for The Hostile Nuclear Environment," *IEEE Trans. on Aerospace and Electronic Systems* Vol. 26, No. 1, pp. 122 - 145, Jan. 1990.

[25] C. H. Chu and E. J. Delp, "Impulsive Noise Suppression and Background Normalization of Electrocardiogram Signals Using Morphological Operators," *IEEE Trans .on Biomedical Eng.,* Vol. BME-36, pp. 262 - 273, Feb. 1989.

[26] R. M. Haralick, S. R. Sternberg, and X. Zhuang, "Image Analysis Using Mathematical Morphology," *IEEE Trans. Pattern Anal. Mach. Intell.,* Vol. PAMI-9, pp. 532 - 550, Jul. 1987.

[27] J.B .T.M. Roerdink and H.J .A.M. Heijmans, "Mathematical Morphology for Structures without Translation Symmetry," *Signal Processing, North Holland,* pp. 271 - 277, 1988.

[28] J. Song, R. Stevenson and E. J. Delp, "The Use of Mathematical Morphology in Image Enhancement," *Proceedings of the 32nd Midwest Symposium on Circuits and Systems,* pp. 67 - 70, Aug., 1989.

[29] J. P. Fitch, E. J. Coyle, and N. C. Gallager, Jr., "Median Filtering by Threshold Decomposition," *IEEE Trans. Acoust., Speech, Signal Proc.* Vol., ASSP-32, pp. 1183 - 1188, Dec., 1984.

[30] S. R. Sternberg, "Grayscale Morphology," *Comput. Vision, Graphics, Image Process.*, Vol. 35, No 3, pp. 333 - 355, 1986.

[31] F. Y. Shin, and O. R. Mitchell, " Threshold Decomposition of Gray-Scale Morphology into Binary Morphology," *IEEE Trans. Pattern Anal. Mach. Intell.*, Vol. PAMI-11, pp. 31 - 42, Jan. 1989.

[32] R. M. Haralick, S. R. Sternberg, and X. Zhuang, "Grayscale Morphology," *IEEE Conference On Computer Vision and Pattern Recognition*, pp. 543 - 550, 1986.

[33] P. A. Maragos, "A Unified Theory of Translation-Invariant Systems with Applications to Morphological Analysis and Coding of Images," *Ph.D. dissertation, School Elec. Eng., Georgia Inst. Technol.*, Atlanta, GA, July 1985.

[34] R. L. Stevenson and G. R. Arce, "Morphological Filters: Statistics and Further Syntactic Properties," *IEEE Trans. Circuits and Systems*, Vol. CAS-34, No. 11, pp. 1292 - 1305, Nov. 1987.

[35] N. C. Gallagher, JR., and G. L. Wise, "A Theoretical Analysis of Median Filters," *IEEE trans. Acoust., Speech, Signal Processing*, Vol. ASSP-29, pp. 1136 - 1141, Dec. 1981.

[36] P. A. Maragos, and R. W. Schafer, "Morphological Filters-Part II: Their Set-Theoretic Analysis and Relations to Linear Shift-Invariant Filters," *IEEE Trans. Acoust., Speech, Signal Processing*, Vol. ASSP-35, pp. 1170 - 1184, Aug. 1987.

[37] P. A. Maragos and R. W. Schafer, "A Unification of Linear, Median, Order Statistics and Morphological Filters Under Mathematical Morphology," *Proc., ICASSP*, pp. 1329 - 1332, 1985.

[38] L. Koskinen, J. Astola, and Y. Neuvo, "Statistical Properties of Discrete Morphological Filters," *IEEE Symposium on Circuits and Systems*, pp. 1219 - 1222, May, 1990.

[39] L. Koskinen, J. Astola, and Y. Neuvo, "Analysis of Noise Attenuation in Morphological Image Processing," *Nonlinear Image Processing*, pp. 102 - 113, Feb. 1991.

[40] H. A. David, *Order Statistics*, New York, Wiley, 1981.

[41] R. J. Vaughan and W. N. Venables, "Permanent Expressions for Order Statistic Densities," *J. R. Statist. Soc.* 34, pp. 308 - 310, 1972.

[42] A. C. Aitken, *"Determinants and Matrices,"* Edinburgh, Oliver and Boyd, pp. 30, 1939.

[43] H. L. Harter, *Order Statistics and Their Use in Testing and Estimation*, US Government Printing Office, Washington D.C., 1970.

[44] M.A. Mohamed and J. Saniie "Application of Morphological Filters in Ultrasonic Flaw Detection," *IEEE Ultrasonic Symposium Proceedings,* pp. 1157 - 1161, 1990.

[45] I. Pitas and A. N. Venetsanopoulos, Nonlinear Digital Filters : Principles and Applications, 1990.

[46] J. Saniie, D.T. Nagle and K.D. Donohue, "Analysis of Order Statistic Filters Applied to Ultrasonic Flaw Detection Using Split Spectrum Processing," *IEEE Trans. Ultrasonics, Ferroelectrics and Frequency Control,* Vol. 38, pp. 133 - 140, Mar. 1991.

[47] J. Saniie and D.T. Nagle, "Robust Ultrasonic Flaw CFAR Detection using Order Statistic Threshold Estimators," *IEEE Ultrasonics Proceedings,* pp. 785 - 789, 1991.

[48] A. Papoulis, *Signal Analysis,* McGraw-Hill, New York, 1977.